GEOTRACK

# PLATYPUS-1 AND DUNTROON-1 WELLS, DUNTROON BASIN, OFFSHORE SOUTH AUSTRALIA

## THERMAL HISTORY RECONSTRUCTION USING APATITE FISSION TRACK ANALYSIS AND VITRINITE REFLECTANCE



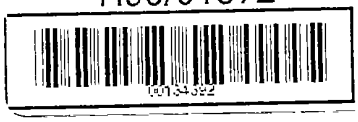

Telephone:

National (03) 344 7214
International 613 344 7214

Facsimile 612 347 5932

Telex AA35185 UNIMEL

Geotrack International Pty Ltd
PO Box 4120
Melbourne University
Victoria 3052
Australia

Samples to:

Room 225
Earth Sciences Bldg
University of Melbourne
Cnr Swanston and Elgin St
Carlton Victoria 3052
Australia

GEOTRACK

# PLATYPUS-1 AND DUNTROON-1 WELLS, DUNTROON BASIN, OFFSHORE SOUTH AUSTRALIA

## THERMAL HISTORY RECONSTRUCTION USING APATITE FISSION TRACK ANALYSIS AND VITRINITE REFLECTANCE

## GEOTRACK REPORT #589

**A report prepared for BHP Petroleum, Melbourne**


| | |
|---|---|
| Report prepared by: | I. R. Duddy |
| AFTA determinations by: | M. E. Moore |
| Vitrinite determinations by: | Keiraville Konsultants |


**February 1996**


Geotrack International Pty Ltd
A C N 006 821 209
PO Box 4120
Melbourne University
Victoria 3052 Australia

Telephone 61+3 9344 7214
Facsimile 61+3 9347 5938

Samples to:
Room 225 Earth Sciences Bldg
University of Melbourne
Cnr Swanston and Elgin St
Carlton Victoria 3052
Australia

# PLATYPUS-1 AND DUNTROON-1 WELLS, DUNTROON BASIN, OFFSHORE SOUTH AUSTRALIA

## THERMAL HISTORY RECONSTRUCTION USING APATITE FISSION TRACK ANALYSIS AND VITRINITE REFLECTANCE

*CONTENTS*

## *TABLES*

## *FIGURES*

# PLATYPUS-1 AND DUNTROON-1 WELLS, DUNTROON BASIN, OFFSHORE SOUTH AUSTRALIA

## THERMAL HISTORY RECONSTRUCTION USING APATITE FISSION TRACK ANALYSIS AND VITRINITE REFLECTANCE

## EXECUTIVE SUMMARY

### Aims and Objectives

This study was commissioned by **BHP Petroleum,** Melbourne, and was completed in February 1996. Principal objectives of the study were to apply Geotrack's THR methodology to determine the timing and nature of any episodes of heating and cooling affecting the Platypus-1 and Duntroon-1 well sites, and to integrate the THR results with those from other wells in the region. The report provides a thermal history framework for understanding the history of potential hydrocarbon occurrence in the vicinity of the **Platypus-1 and Duntroon-1 wells, Offshore South Australia.**

### Technical Results

Technical results are summarised in Tables i & ii, while schematic illustrations of the main features of the thermal history reconstruction are presented in Figures i & ii. Full details of the interpretation, including discussion of reconstructed burial histories and maturation histories are given in Sections 2 to 4.

### Conclusions

1. Thermal History Reconstruction clearly reveals that the drilled Tertiary to Early Cretaceous section in both wells is **currently at maximum temperatures**, with no direct evidence for any periods of post-depositional heating or cooling.

2. The thermal history at the Platypus-1 and Duntroon-1 well sites has been reconstructed by incorporating regional information on the occurrence of a period of high heat flow in the Early Cretaceous. Paleogeothermal gradients during the Early Cretaceous have been

constrained previously by THR in the Duntroon Basin (Geotrack Report #569) to 60°C/km in the Vivonne-1 well , and a very similar paleogeothermal gradient can be inferred from open file VR data available for Echidna-1 (internal assessment, Geotrack International).

3. Predictions based on this regional history reveal that a significant thickness of Cretaceous and deeper section at the Platypus-1 (~4000 m) and Duntroon-1 (~3000 m) locations was actively generating hydrocarbons during the period from ~50 Ma (Platypus-1) and 25 Ma (Duntroon-1) to the present-day. This occurred at both locations despite an early phase of hydrocarbon generation from the Early Cretaceous and deeper section prior to regional Mid-Cretaceous cooling ~95 Ma (Geotrack Report #569).

4. There is very tentative evidence in Duntroon-1 for post Miocene-Pliocene transient heating within the Nullarbor Limestone section, that may have resulted from localised hot fluid flow.

5. The fission track age patterns and broad apatite chlorine distributions in samples from the Early Cretaceous section in both wells provide clear evidence of derivation of most detritus from contemporaneous explosive volcanic activity as seen previously in the Duntroon Basin (Geotrack Report #569). In the case of Platypus-1 and Duntroon-1, however, the data also suggest significant reworking of the Early Cretaceous detritus into the Late Cretaceous sequence, presumably as a consequence of nearby Mid-Cretaceous uplift and erosion. This reworking will potentially have an effect on the quality of Late Cretaceous reservoir sands.

## Recommendations

1. *Early Cretaceous high heat flow:* Previous work (Geotrack Report #569) has shown conclusively the occurrence of highly elevated Early Cretaceous heat flow in the Duntroon Basin. It is recommended that AFTA and selected VR data be collected on the Echidna-1 well to more fully document the elevated heat-flow event and its effect on regional source rock maturation patterns.

2. *Late Tertiary to Recent hot fluids:* Existing VR data from the Nullarbor Limestone section in Duntroon-1 suggest a transient lateral heating episode has affected the section. This event has not been specifically investigated with new samples in this study, but the problem could be addressed using a combined AFTA, VR and fluid inclusion approach.

**Table i: Paleotemperature analysis summary - AFTA and VR samples from Platypus-1, Duntroon Basin (Geotrack Report #589)**

| Sample number*1 GC | Average depth (TVD) (m) | Stratigraphic age (Ma) | Present temperature*2 (°C) | Maximum paleotemperature*3 (°C) |
|---|---|---|---|---|
| 589-1.1 | 1598 | 33-0 | 54 | 96 |
| 589-2.1 | 1800 | 50-33 | 60 | 59 |
| 589-3.1 | 1910 | 73-65 | 63 | 75 |
| 589-3 | 1950 | 73-65 | 64 | <66 |
| 589-4.1 | 2151 | 73-65 | 71 | 71 |
| 589-5.1 | 2211 | 85-73 | 75 | 71 |
| 589-5 | 2250 | 85-73 | 74 | <74 |
| 589-6.1 | 2401 | 85-73 | 78 | 70 |
| 589-7.1 | 2501 | 85-73 | 81 | 71 |
| 589-8 | 2600 | 85-73 | 85 | <85 |
| 589-8.1 | 2602 | 85-73 | 85 | 78 |
| BHP-1 | 2649 | 85-73 | 80 | 69 |
| BHP-2 | 2835 | 85-73 | 92 | 81 |
| 589-9.1 | 2901 | 85-73 | 94 | 86 |
| 589-9 | 2910 | 85-73 | 94 | <94 |
| 589-10.1 | 3010 | 96-85 | 97 | 88 |
| 589-10 | 3040 | 96-85 | 98 | <100 |
| 589-11.1 | 3198 | 96-85 | 103 | 93 |
| BHP-3 | 3200 | 96-85 | 103 | 84 |
| 589-12.1 | 3400 | 100-96 | 109 | 104 |
| 589-12 | 3440 | 100-96 | 110 | <110 |
| 589-13.1 | 3501 | 100-96 | 112 | 93 |
| 589-14.1 | 3601 | 100-96 | 115 | 93 |
| 589-15.1 | 3699 | 100-96 | 118 | 98 |
| 589-16.1 | 3812 | 115-100 | 122 | 114 |
| BHP-4 | 3888 | 115-100 | 124 | 124 |
| 589-17.1 | 3888 | 115-100 | 124 | 105 |

*1 AFTA samples numbered 589-N; new VR samples numbered 589-N.1; Selected supplied VR samples numbered BHP-N.

*2 See Appendix A for details of present temperature calculation.

*3 AFTA shows that the sampled section is at maximum temperatures at the present day; AFTA samples give estimates of maximum possible paleotemperature while VR estimates are point estimates; both calculated using a heating rate of 1°C/Ma.

## Table ii: Paleotemperature analysis summary - AFTA and VR samples from Duntroon-1, Duntroon Basin (Geotrack Report #589)

| Sample number*1 GC | Average depth (TVD) (m) | Stratigraphic age (Ma) | Present temperature*2 (°C) | Maximum paleotemperature*3 (°C) |
|---|---|---|---|---|
| 8622-40 | 1500 | 55-50 | 53 | No apatite |
| 589-18.1 | 1603 | 55-50 | 57 | 54 |
| 8622-41 | 1630 | 65-60 | 58 | <90 |
| 589-19.1 | 1683 | 65-60 | 60 | 82 |
| 8622-42 | 1800 | 65-60 | 63 | <? |
| 589-20.1 | 1813 | 65-60 | 63 | 60 |
| 589-21.1 | 1903 | 73-65 | 66 | 65 |
| 589-22.1 | 2053 | 73-65 | 71 | 68 |
| BHP-5 | 2065 | 73-65 | 72 | 82 |
| 8622-43 | 2100 | 85-73 | 73 | <90 |
| 589-23.1 | 2153 | 85-73 | 74 | 79 |
| 589-24.1 | 2303 | 85-73 | 80 | 85 |
| 589-25.1 | 2503 | 85-73 | 86 | 89 |
| 8622-45 | 2507 | 85-73 | 86 | <95 |
| 589-26.1 | 2603 | 100-96 | 89 | 95 |
| 8622-46 | 2700 | 100-96 | 92 | <92 |
| BHP-6 | 2754 | 100-96 | 94 | 68 |
| 589-27.1 | 2853 | 100-96 | 97 | 100 |
| 589-28.1 | 2953 | 119-100 | 100 | 97 |
| BHP-7 | 3000 | 119-100 | 102 | 63 |
| 8622-47 | 3000 | 119-100 | 102 | <102 |
| 589-29.1 | 3053 | 119-100 | 103 | 88 |
| 589-30.1 | 3353 | 119-100 | 114 | 97 |
| 589-31.1 | 3453 | 119-100 | 117 | 114 |
| 589-32.1 | 3508 | 119-100 | 119 | 125 |
| BHP-8 | 3500 | 119-100 | 119 | 105 |
| 8622-49 | 3510 | 119-100 | 119 | <119 |

*1 AFTA samples numbered 8622-N; new VR samples numbered 589-N.1; supplied VR samples number ed BHP-N.

*2 See Appendix A for details of present temperature calculation.

*3 AFTA shows that the sampled section is at maximum temperatures at the present day; AFTA samples give estimates of maximum possible paleotemperature while VR estimates are point estimates; both calculated using a heating rate of 1°C/Ma.

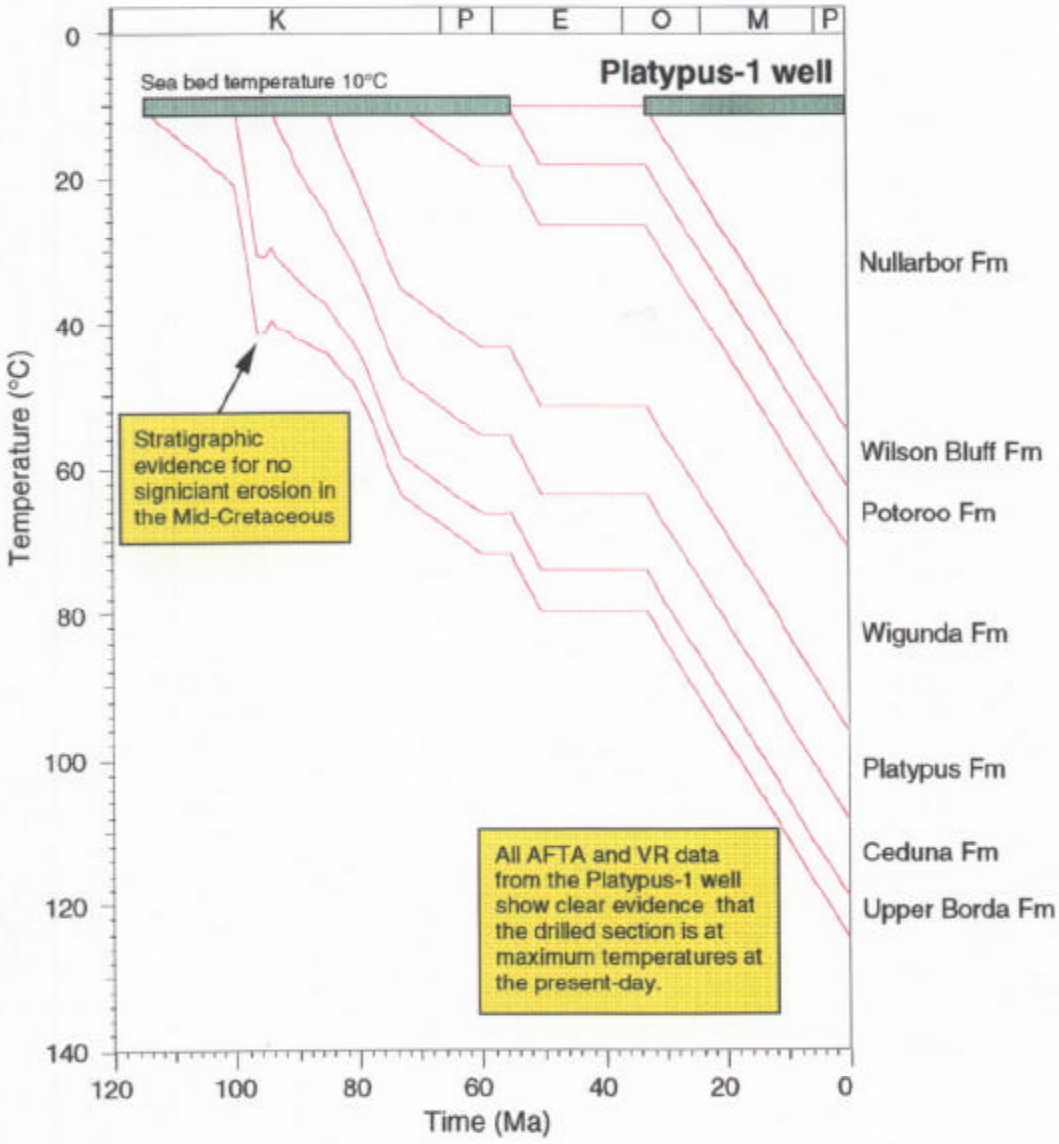


**Figure i:** Schematic illustration of the preferred thermal history interpretation for AFTA and VR data from the **Platypus-1 well, Duntroon Basin.**

The main conclusion of this study is that the drilled section at Platypus-1 is currently at maximum temperatures, and that as a consequence, a significant thickness (~4000 m+) of Cretaceous and deeper section became mature for oil and gas generation during the period from ~50 Ma to the present-day - see text.

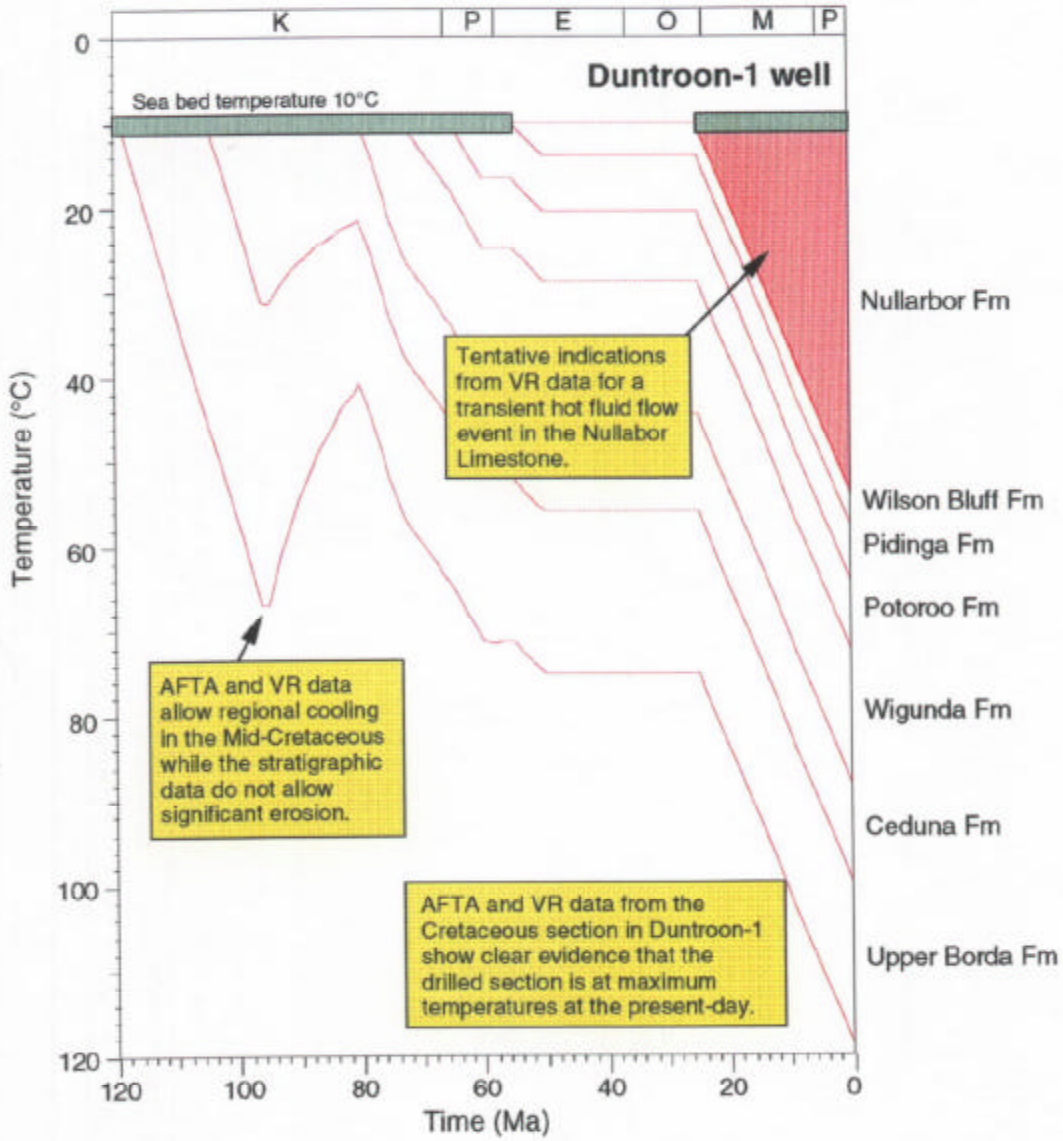


**Figure ii:** Schematic illustration of the preferred thermal history interpretation for AFTA and VR data from the **Duntroon-1 well, Duntroon Basin.**

The main conclusion of this study is that the drilled section at Duntroon-1 is currently at maximum temperatures, and that as a consequence, a significant thickness (~3000 m) of Early Cretaceous and deeper section became mature for oil and gas generation during the period from ~25 Ma to the present-day - see text.

# 1. Introduction

## 1.1 Background and objectives of this report

This report describes the results of a study designed to provide a thermal history framework for understanding the structural and hydrocarbon generation history in the vicinity of the **Platypus-1 and Duntroon-1 wells, Duntroon Basin, South Australia.** The study was commissioned by **BHP Petroleum,** with key results provided in January 1996 and the full report completed in February 1996.

The study involves Thermal History Reconstruction (THR) using Apatite Fission Track Analysis (AFTA®) and Vitrinite Reflectance (VR). Six AFTA samples and 17 vitrinite reflectance samples were provided from the collections of **AGSO** and **MESA** for the **Platypus-1 well.** Eight existing open-file AFTA samples from the **Duntroon-1 well** were recounted and reprocessed using Geotrack's newest modelling technology, supplemented with 15 new vitrinite reflectance samples. Additional VR data on 33 samples from Platypus-1 and 34 samples from Duntroon-1 were provided by BHPP.

AFTA is used to identify any episodes of elevated paleotemperatures which have affected the region, to estimate the timing and magnitude of maximum paleotemperatures and to place constraints on any subsequent episodes of heating and cooling. VR data are also used to provide estimates of maximum paleotemperatures, the timing of which is interpreted on the basis of information provided by AFTA. Paleotemperature constraints from AFTA and VR are then integrated into a coherent thermal history synthesis.

Estimates of maximum paleotemperature from AFTA and VR over a range of depths are used to constrain paleogeothermal gradients, which are used to infer the origins of the various episodes of heating and cooling (Section 1.7). Where possible, estimates of section removed by uplift and erosion are obtained from the paleotemperature constraints, allowing reconstruction of the burial history. Burial history reconstruction depends on a number of assumptions, with respect to the thermal structure of the eroded section, which are not directly known (Section 1.8). Therefore, the results should be regarded as indicative of the general magnitude, and corroboration of the removed section estimates by other techniques (e.g., sonic velocity compaction studies, seismic reconstruction on structures, etc.) is always desirable. Comparison of data from all wells with the geological setting then allows a regional framework to be

established, within which the implications of the regional variation of thermal history concerning patterns of hydrocarbon generation can be understood.

## 1.2 Report structure

The main conclusions of this report on the **Platypus-1 and Duntroon-1** wells are summarised in the Executive Summary. The thermal history interpretations of AFTA and VR data for the two wells are summarised in Tables i and ii, in terms of quantitative constraints on the magnitude and timing of maximum paleotemperatures. Figures i and ii illustrate the constrained thermal history derived from AFTA and VR data in each of the two wells.

In Section 1, introductory aspects of the report are discussed, including comments on data quality. The approach to thermal history reconstruction employed in this report is also described in Section 1. Sections 2 and 3 summarise the thermal history interpretation of the AFTA and VR data for the **Platypus-1 and Duntroon-1** wells, respectively, under various headings, including implications of the thermal history for source rock maturation and hydrocarbon exploration. Section 4 gives concluding remarks on the geological history of the **Duntroon Basin**. Section 5 discusses possibilities for further work, which might allow further insight into the thermal and hydrocarbon generation history on the wells analysed.

Supporting information is provided in four Appendices. Details of all AFTA samples, including depths, stratigraphic details and present temperatures in each well, are presented in Appendix A, together with the yields of detrital apatite obtained after mineral separation, apatite grain morphologies and apatite compositions (Cl contents). Sample preparation and analytical details are described in Appendix B, followed by the presentation of all AFTA data, including raw track counts and fission track ages for individual grains. Details of the presentation of data in the form of Tables and Figures throughout the report are also discussed in detail in Appendix B. Appendix C outlines the principles employed in interpreting the AFTA data in terms of thermal history. In Appendix D, the results of all new VR analyses obtained for this report, including sample details and analytical methods, are presented, along with a listing of open-file VR data used in this report. Appendix D also discusses the principles involved in integrating AFTA and VR data to provide coherent thermal history interpretations.

## 1.3 Data quality

*AFTA data*

The AFTA data generated for this report are generally of very high quality. The yields of detrital apatite obtained after mineral separation from all samples processed are summarised in Table A.1. Yields of apatite varied from none to excellent, with the majority excellent. The quality of the etched surfaces of the apatites obtained for analysis was high in all samples. The overall high quality of the AFTA data in key samples results in reliable thermal history interpretations for both the Platypus-1 and Duntroon-1 wells.

*VR data*

New vitrinite reflectance data from Keiraville Konsultants, were collected on 17 samples from the Platypus-1 well and 15 samples from the Duntroon-1 well, to provide good coverage of the paleotemperature profile in each well. The majority of the vitrinite reflectance data used in this study are considered to be of high quality, with most samples yielding 20 or more measurements (Tables D.2 and D.3). A mean value based on 10 or more measurements from Keiraville Konsultants is considered reliable because of the way in which the VR data are gathered, with primary in-situ vitrinite identified on petrographic grounds within polished blocks (see Appendix D).

In general, the supplied VR data are difficult to assess quantitatively as details of the number of fields measured and the measurement methodology are not recorded. For Platypus-1, simple comparison on mean maximum reflectance data from the new Keiraville data and supplied data sets from different laboratories shows that VR levels for similar depths in each data set are generally consistent (Tables D.2 and D.3), suggesting we can have some confidence in the maturity levels. For Duntroon-1 this analysis is less straight-forward, with comparison of data in part of the section suggesting inconsistencies in the existing VR data set. In this case, we consider that the new data gives a better indication of the true maturity levels in the well.

## 1.4 Apatite compositions

The annealing kinetics of fission tracks in apatite are affected by chemical composition, specifically the Cl content, as explained in more detail in Appendix C. Thus, an assessment of the chlorine content in apatite is essential in interpreting AFTA data, often providing greater accuracy in establishing the time and magnitude of thermal events.

For this study, chlorine compositions were determined for all individual apatite grains in which fission track ages were determined and lengths measured for the seven samples which provided apatite from the two wells studied.

The measured range of chlorine contents of dated grains and grains in which length were measured is shown in histogram format in Figure A.2. A plot of single grain age versus weight % chlorine is shown in Figure B.5. Chlorine contents, which are presented in numerical format for age grains, appear in the fission track age summary sheets in Appendix B.

## 1.5 Thermal history reconstruction and use of thermal gradients vs heat flow

Most approaches to thermal history reconstruction in sedimentary basins are based on consideration of the variation of heat flow through time, using models often based solely on theoretical grounds. However, this approach is beset by problems, particularly in sections which have been hotter in the past. Use of a heat flow-based approach depends critically on knowledge of thermal conductivities through the section. When considerable section has been removed, no information is available on lithologies (and hence thermal conductivities) in the removed section. In addition, large variation in thermal conductivities within similar lithological units (e.g., Corrigan, 1991) introduces considerable uncertainty into the relationship between heat flow and thermal gradient, even in relatively simple cases. For further illustration of these problems, see Waples et al. (1992). The influence of factors such as porosity, compaction and diagenesis is difficult to assess quantitatively, and the effects of greater depth of burial are unpredictable in a sequence affected by uplift and erosion, particularly when the magnitude of burial is unknown before the analysis. A heat flow-based approach to determining amounts of removed section is subject to considerable uncertainty because of problems such as these. This point has been discussed in greater detail by Duddy et al. (1991).

It is also important to realise the validity of theoretical heat-flow models is largely untested. High heat flow associated with rifting and early subsidence leaves no measurable effect if subsidence later in the basin's history has caused higher temperatures than those attained during the assumed high heat-flow episode. In many sedimentary basins, deep burial late in the subsidence history has caused maximum temperatures, and no record of earlier heat-flow variation is preserved either in the level of measured source rock maturity or in the AFTA parameters, as these data are dominated by the effects of maximum paleotemperature. Elevated heat-flow episodes associated with rifting are known to leave a measurable signature only where cooling

has occurred shortly after the initial rifting phase and where temperatures have subsequently remained low through to the present day (Duddy et al., 1991).

We have adopted an alternative approach, based on measurement of thermal gradients (present and past), using an integrated AFTA and VR methodology, because of these problems with a heat flow-based approach to thermal history reconstruction. This approach yields direct measurement of the time at which cooling from maximum paleotemperatures began (from AFTA), and the paleogeothermal gradient at that time (from AFTA and VR). The style of cooling from maximum paleotemperatures to present temperatures can also be constrained (from AFTA). This approach allows definition of all the major facets of the thermal history of a sedimentary section through time, and is *based on directly measurable parameters*, rather than on *assumed* values of highly unpredictable factors. The information provided can still ultimately be interpreted in terms of paleo-heat flow, if desired.

It should also be appreciated that the thermal history prior to the time at which cooling from maximum paleotemperatures begins cannot be constrained from any of the available in-situ paleotemperature indicators based on thermally activated reactions. This arises because of the dominance of temperature over time in the kinetics of the systems employed in this way (i.e., fission track annealing, vitrinite reflectance, etc.). For this reason, these data can only constrain the thermal history from the onset of cooling from maximum paleotemperatures to the present day. Information on the earlier history can only be obtained indirectly, e.g., from geological information, perhaps by reconstructing patterns of burial based on section preserved in neighbouring regions, from theoretical heat-flow models (given the above caveats), or possibly by more subtle means, such as the presence of residual hydrocarbon products generated during earlier heating to lower peak paleotemperatures.

## 1.6 Outline of our approach to interpretation of AFTA and VR data

Interpretation of AFTA and VR data in this report begins by assessing whether the AFTA and/or VR data in each sample could have been produced if the sample has never been hotter than its present temperature at any time since deposition. The burial history derived from the stratigraphy of the preserved sedimentary section and the present geothermal gradient are used to predict a "Default Thermal History" for each sample, which forms the basis of interpretation.

If the data show a greater degree of fission track annealing and/or a higher VR value than expected on the basis of this history, the sample must have been hotter at some time in the past. In this case, the AFTA data are analysed to provide estimates of the

magnitude of the maximum paleotemperature in that sample, and the timing of cooling from the thermal maximum. VR data provide an independent estimate of maximum paleotemperature. Paleotemperature estimates from both AFTA and VR are then used to reconstruct a paleogeothermal gradient, and, where appropriate, to estimate the amount of section removed by uplift and erosion.

The heating rate assumed in calculating paleotemperatures affects the magnitude of paleotemperature required to produce a given set of data. As AFTA and VR data do not independently constrain the heating rate, paleotemperatures are estimated by assuming simple linear heating between a point on the Default Thermal History and the maximum paleotemperature. This will not give the actual paleotemperature, in general, but this procedure at least allows AFTA and VR data to be analysed within a common thermal history framework in the absence of any other constraint on heating rate. If any evidence of the real time-scale of heating is available, this can easily be incorporated into the analysis. Note AFTA data provide some constraint on cooling rates, as explained in more detail in Appendix C.

Estimates of maximum paleotemperature from AFTA are often quoted in terms of a range of paleotemperatures, as the data can often be explained by a variety of scenarios. Paleotemperature estimates from VR are usually quoted to the nearest degree Celsius, as the value which predicts the measured reflectance. This is not meant to imply VR data can be used to estimate paleotemperatures to this degree of precision. VR data from individual samples typically show a scatter equivalent to a range of between ±5 and ±10°C. Estimates from a series of samples are normally used to define a paleotemperature profile in samples from a well, or a regional trend in paleotemperatures from outcrop samples.

If the data show a lower degree of fission track annealing and/or a lower VR value than expected on the basis of the Default Thermal History, this suggests either present temperatures may be overestimated or temperatures have increased very recently. In such cases, the data may allow an estimate of the true thermal gradient, or some estimate of the time over which temperatures have increased.

Further discussion of the methodology employed in interpreting AFTA and VR data are given in Appendices C and D.

AFTA data are interpreted using a new multi-compositional kinetic model for fission track annealing in apatite developed by Geotrack, details of which are provided in Appendix C. Vitrinite reflectance data are interpreted using the distributed activation energy model describing the evolution of VR, with temperature and time developed by

Burnham and Sweeney (1989) (see also Sweeney and Burnham, 1990), as implemented in the BasinMod™ software package of Platte River Associates (using version 3.15).

## 1.7 Paleogeothermal gradients

### *Basic principles*

A series of paleotemperature estimates from AFTA and/or VR over a range of depths can be used to reconstruct a paleotemperature profile through the preserved section. The slope of this profile defines the paleogeothermal gradient. As explained by Bray et al. (1992), the shape of the paleotemperature profile and the magnitude of the paleogeothermal gradient provides unique insights into the origin and nature of the heating and cooling episodes expressed in the observed paleotemperatures.

Linear paleotemperature profiles with paleogeothermal gradients close to the present-day geothermal gradient provide strong evidence that heating was caused by greater depth of burial with no significant increase in basal heat-flow, implying in turn that cooling was due to uplift and erosion. Paleogeothermal gradients significantly higher than the present-day geothermal gradient suggest that heating was due, at least in part, to increased basal heat flow, while a component of deeper burial may also be important as discussed in the next section. Paleogeothermal gradients significantly lower than the present-day geothermal gradient suggest that a simple conductive model is inappropriate, and more complex mechanisms must be sought for the observed heating. One common cause of low paleogeothermal gradients is transport of hot fluids shallow in the section. However, the presence of large thicknesses of sediment with uniform lithology dominated by high thermal conductivities can produce similar paleotemperature profiles, and each case has to be considered individually.

A paleotemperature profile can only be characterised by a single value of paleogeothermal gradient when the profile is linear. Departures from linearity may occur where strong contrasts in thermal conductivities occur within the section, or where hot fluid movement or intrusive bodies have produced localised heating effects. In such cases, a single value of paleogeothermal gradient cannot be calculated. However, it is important to recognise that the validity of the paleotemperatures determined from AFTA and/or VR are independent of these considerations, and can still be used to control possible thermal history models.

### *Estimation of paleogeothermal gradients in this report*

Note that in this report, the reconstructed thermal history is such that paleogeothermal gradients cannot be determined.

In other cases, paleogeothermal gradients are estimated using methods outlined in Appendix C, for each well analysed in which paleotemperature estimates are available over a range of depths. These methods provide a best estimate of the gradient ("maximum likelihood value") and upper and lower 95% confidence limits on this estimate (analogous to ±2s limits). The "goodness of fit" is displayed in the form of a log-likelihood profile, which is expected to show good quadratic behaviour for a data set which agrees with a linear profile. This analysis depends on the assumption that the paleogeothermal gradient through the preserved section is linear. Visual inspection is usually sufficient to confirm or deny this assumption.

## 1.8 Eroded section

### *Basic principles*

Subject to a number of important assumptions, extrapolation of a linear paleotemperature profile to a paleo-surface temperature allows estimation of the amount of eroded section represented by an unconformity, as explained in more detail in Section C.9 (Appendix C).

Specifically, this analysis assumes:

- The paleotemperature profile through the preserved section is linear;
- The paleogeothermal gradient through the preserved section can be extrapolated linearly through the missing section;
- The paleo-surface temperature is known; and,
- The heating rate used to estimate the paleotemperatures defining the paleogeothermal gradient is correct.

It is important to realise that any method of determining the amount of eroded section based on thermal methods is subject to these and/or additional assumptions. For example, methods based on heat-flow modelling must assume values of thermal conductivities in the eroded section, which can never be known with confidence. Such models also require some initial assumption of the amount of eroded section to

allow for the effect of compaction on thermal conductivity. Methods based on geothermal gradients, as used in this study, are unaffected by this consideration, and can therefore provide independent estimates of the amount of eroded section. However, these estimates are always subject to the assumptions set out above and should be considered with this in mind.

***Estimation of eroded section in this report***

As noted above, in this report the reconstructed thermal history is such that paleogeothermal gradients cannot be determined, and therefore determination of uplift and erosion for the paleotemperatures data is not relevant.

Normally, the analysis used to estimate paleogeothermal gradients is easily extended to provide maximum likelihood values of eroded section for an assumed paleo-surface temperature, together with ±95% confidence limits. These parameters are quoted for each well in which the paleotemperature profile suggests that heating may have been due, at least in part, to deeper burial.

# 2. Thermal history reconstruction in the Platypus-1 well

## 2.1 Geological background

The preserved stratigraphy for Platypus-1 as provided by BHPP is listed in Table A.3 and depicted schematically in Figure 2.1. In general terms, the well intersected a ~1700 m thick Tertiary section overlying ~1500 m of Late Cretaceous and 500 m of Early Cretaceous section with TD in Aptian age Early Cretaceous at 3893 m (total vertical depth below RT). The present-day geothermal gradient is calculated from corrected BHT data at 30.9°C/km using a sea-bed temperature of 10°C (Appendix A).

## 2.2 Evidence for elevated paleotemperatures from the AFTA data

Fission track parameters in each of the six samples analysed are summarised in Table 2.1, together with values of fission track age and mean track length calculated from the Default Thermal History for each sample (Section 1.6) and using the appropriate measured Cl-composition determined in each sample (Section 1.4). The ranges of measured apatite chlorine compositions used in calculating the Default History values for each AFTA sample are listed in Appendix B. The calculation of these default values includes only those tracks formed after deposition of the sample, and therefore does not account for tracks inherited from sediment source areas. The use of these parameters in interpreting AFTA data is outlined in Section 1.6 and Appendix C.

The measured AFTA parameters are also plotted as a function of depth and present temperature in Figure 2.1. The variation in stratigraphic age with depth in the well in also shown in Figure 2.1 allowing direct comparison between the fission track age and the corresponding depositional age in each sample.

Interpretation of the AFTA data from the six Platypus-1 samples in terms of evidence of higher temperatures in the past is described in Table 2.2. To summarise, results of detailed kinetic modelling of the AFTA data from the six samples analysed reveal no evidence of these samples having experienced paleotemperatures higher than present temperatures at any time after deposition. In the deepest sample (GC589-12; Ceduna Formation), the relatively high present temperature of ~110°C could partially mask any evidence of higher paleotemperatures, but when considered in conjunction with the associated VR levels, any period of higher paleotemperatures is considered to be unlikely.

## 2.3 Magnitude of maximum paleotemperatures from the AFTA data

Estimates of the magnitude of maximum paleotemperature allowed by the AFTA data in each sample have been obtained by iteratively predicting AFTA parameters for a range of thermal history scenarios and comparing these predicted parameters with the measured data.

For each sample, the maximum paleotemperature allowed by the AFTA data are either equal to the present temperature of the sample, or up to ~15°C higher in the case of the deepest sample (GC589-12), as listed in Table i. The data do not provide any constraints on the time of cooling from such temperatures, with any time after deposition possible. On balance, the AFTA data from all samples can be reconciled if the entire drilled section is at maximum temperatures at the present day.

Paleotemperature estimates from each AFTA sample are listed in Table i (Executive Summary) and plotted against depth in Figure 2.4 .

## 2.4 Evidence for elevated paleotemperatures from the VR data

The Default Thermal History for Platypus-1, i.e., the thermal history of the well if the section has never been hotter than present temperatures (as described in Section 1.6), and based on the preserved stratigraphy, a present-day geothermal gradient of 30.9°C/km and a sea-bed temperature of 10°C is used to predict a VR profile for the well. The predicted profile is then compared with the measured VR data as illustrated in Figure 2.2 (Profile 1). The burial history used in calculating this profile is shown in Figure 2.3.

Vitrinite reflectance data are available from 17 new samples analysed by Keiraville Konsultants (Table D.2) and existing data on 33 samples supplied by BHPP (Table D.3). Data from both data sets are reasonably consistent and are therefore discussed together. $R_o$max values range from ~0.28% in the Nullarbor limestone to ~0.75% in the Upper Borda Formation (Figure 2.2). The measured VR data plot close to, or marginally below, the profile calculated from the Default History. At face value, the tendency for the bulk of the data through the Cretaceous section to plot below the Default History profile suggests that these measured data underestimate the present temperatures, and certainly show no evidence for higher temperatures in the past. This could result from the present temperatures being overcorrected, a real but recent transient increase in present temperatures or geochemical suppression of the measured

VR levels. On balance, such a situation is less likely to be due to a transient recent increase in geothermal gradient than either a slight overestimation of the present day geothermal gradient (due to slight overcorrection of the measured BHT data) or systematic suppression of the VR levels through the Late Cretaceous marine section. For example, reducing the present day gradient from the calculated value of 30.9°C/km to 28°C/km results in a satisfactory fit to the measured data as shown by Profile 2 in Figure 2.2, and this is preferred over any significant VR suppression explanation.

To summarise, comparison of the measured VR data with the predicted VR profile reveal no evidence of the sampled units having experienced paleotemperatures higher than present temperatures at any time after deposition. Any slight uncertainty in present day geothermal gradient does not materially affect the conclusion from the VR data that the entire drilled section is currently at its maximum temperatures at any time since deposition.

## 2.5 Magnitude of maximum paleotemperatures from the VR data

Maximum paleotemperature can be estimated from each measured VR value by using the algorithm of Burnham and Sweeney (1989) as described in more detail in Section 1.6 and Appendix D.

Paleotemperatures, based on a heating rate of 1°C/Ma, estimated from each VR value are listed in Table i (Executive Summary) and plotted against depth in Figure 2.4 (note that, in the case of the supplied VR data listed in Table D.3, paleotemperatures have only been estimated for those data in which the number of measurements have been recorded). Most VR-derived paleotemperature estimates are within a few degrees of the present temperatures, emphasising the conclusions made above from inspection of the VR-depth plot (Figure 2.2), that the drilled section in Platypus-1 is currently at maximum temperatures since deposition. Note that any slight differences can easily be accounted for by the typical errors in BHT measurement or correction, poor control on some individual VR values, or small errors in the Burnham and Sweeney (1989) kinetic VR description.

## 2.6 Estimation of paleogeothermal gradient

The AFTA and VR thermal history constraints indicate maximum paleotemperatures throughout the drilled section occur at the present-day, so that there is no basis for calculation of a paleogeothermal gradient for any post-depositional time period.

## 2.7 Estimates of removed section and burial history reconstruction

As no heating and cooling event have been identified, no estimation of removed section is required. Note that palynological information supplied by BHPP shows the presence of the P. pannosus spore pollen zone ~200 m thick at the top of the Early Cretaceous section indicating little if any erosion is possible at the mid-Cretaceous "unconformity". Therefore, the burial history derived from the preserved stratigraphy and illustrated in Figure 2.3 is considered to be a close reflection of the *actual* burial history at the Platypus-1 well site.

## 2.8 Integration of regional information - Thermal history synthesis

A schematic illustration of the main features of the thermal history in the Platypus-1 well is presented in Figure i (Executive Summary).

The data discussed in the previous sections, while providing excellent control on the Tertiary-Recent thermal history at Platypus-1, do not allow us to constrain the pre-Late Cretaceous thermal history to any meaningful degree, due principally to a combination of the relatively thick Late Cretaceous to Recent section, and the relatively thin Early Cretaceous section, penetrated by the drill.

Thus, to more fully reconstruct the thermal history at the Platypus-1 well site it is essential to incorporate regional thermal history information. A key feature of the regional history is the occurrence of a period of high heat flow in the Early Cretaceous which terminated in the mid-Cretaceous, at around 95 Ma (Geotrack Report #569). Paleogeothermal gradients during the Early Cretaceous have been constrained to 60°C/km by AFTA and VR data in the Vivonne-1 well (Geotrack Report #569), and a very similar paleogeothermal gradient can be inferred from open file VR data available for Echidna-1 (internal assessment, Geotrack International).

On this basis, Figure 2.5 illustrates the preferred reconstructed thermal history for the Platypus-1 well site derived by using the measured regional geothermal gradient of 60°C/km for the period prior to the Mid-Cretaceous, decreasing to a gradient of 30.9°C/km (i.e., the present-day value for Platypus-1) for the period from 80 Ma to the present.

Inspection of the plot in Figure 2.5 shows that even though the Early Cretaceous and deeper section experienced high paleotemperatures prior to the regional mid-Cretaceous cooling event, the entire *drilled* section was subsequently heated to even higher temperatures during the Late Cretaceous to Recent burial phase, with maximum temperatures experienced at the present-day.

## 2.9 Implications for source rock maturation at the Platypus-1 well site

The preferred thermal history shown in Figure 2.5 allows construction of a maturity profile in the preserved section at the Platypus-1 well, as shown in Figure 2.6. The predicted VR-profile shows a good fit to the measured VR data, and is also coincident with the profile derived from the Default Thermal History previously shown in Figure 2.2, since maximum temperatures occur at the present day in both histories. However, even though the Reconstructed Thermal History results in the same VR maturity profile as the Default Thermal History, recognition of the regional significance of high Early Cretaceous heat flow has significant implications for the timing of hydrocarbon generation in the basin.

Figure 2.7 shows the variation of maturity (vitrinite reflectance) with time at the Platypus-1 well site predicted from the Regional Thermal History illustrated in Figure 2.5 (using Burnham and Sweeney, 1989). The plot graphically illustrates that the drilled section has matured essentially continuously to the present-day with the deepest parts (U. Borda Formation) becoming early mature (0.5% $R_o$max) for hydrocarbon generation at around 50 Ma and reaching mid maturity (0.75% $R_o$max) at the present-day. On the other hand, the plot shows cessation of maturation in three notional units (i.e., U. Borda, L. Borda and Jurassic units each assumed to be 1000 m thick) below TD in the well coincident with cooling at 95 Ma (shown in Figure 2.5), and with additional maturation of these units beginning at progressively more recent times with increasing depth. For example, the base of the notional L. Borda unit (~6000 m present depth), reached a maturity of ~1.4% $R_o$max at 95 Ma, and did not begin to gain additional maturity until ~25 Ma, at which time the amount of post-Early Cretaceous section deposited was sufficient to cause the section at this depth to reach paleotemperatures higher than those reached at 95 Ma. Significantly, even when the effects of high Early Cretaceous are considered, a large thickness of Early

Cretaceous (and possibly older) section with source potential became mature for oil and gas throughout the Tertiary.

In summary, we can infer from these results that a more than 4000 m of Cretaceous and possibly Jurassic section at the Platypus-1 location, from ~2800 m present depth (near base Wigunda Fm) up to ~7000 m depth was actively generation hydrocarbons at maturities between 0.5 and ~3% $R_o$max during the period from ~50 Ma to the present-day (Figure 2.7).

**Table 2.1: Summary of AFTA data in samples from the Platypus-1 well, Duntroon Basin, offshore South Australia (Geotrack Report #589)**

| Sample number | Average Depth*1 | Present temperature*2 | Stratigraphic Age | Mean track length | Default mean track length *3 | Apatite fission track age | Default fission track age*3 | Measured Ro (max)*4 | Default Ro (max)*5 |
|---|---|---|---|---|---|---|---|---|---|
| GC | (m) | (°C) | (Ma) | (μm) | (μm) | (Ma) | (Ma) | (%) | (%) |
| 589-3 | 1950 | 64 | 73-65 | 14.08±0.49 | 13.2 | 127.1±11.5 | 57 | 0.43 | 0.39 |
| 589-5 | 2250 | 74 | 85-73 | 13.43±0.26 | 12.6 | 127.9±20.1 | 64 | 0.42 | 0.43 |
| 589-8 | 2600 | 85 | 85-73 | 13.38±0.14 | 12.4 | 124.6±16.5 | 65 | 0.45 | 0.50 |
| 589-9 | 2910 | 94 | 85-73 | 12.93±0.33 | 11.7 | 104.9±22.6 | 66 | 0.51 | 0.55 |
| 589-10 | 3040 | 98 | 96-85 | 12.37±0.28 | 11.3 | 93.5±12.2 | 57 | 0.52 | 0.58 |
| 589-12 | 3440 | 110 | 100-96 | No lengths | 10.2 | 41.4±18.3 | 44 | 0.62 | 0.65 |

*1 All depths quoted are total vertical depth (TVD) with respect to KB.

*2 See Appendix A for a discussion of present temperature estimation.

*3 AFTA values predicted from the "Default Thermal History" (Section 1.6); i.e., assuming that each sample is now at its maximum temperature since deposition. The values refer only to tracks formed after deposition. Samples may also contain tracks inherited from sediment provenance areas. Calculations for the ranges given refer to actual measured compositions of apatites analysed within a particular sample, which is discussed in Appendix A.

*4 Vitrinite reflectance values at the level of the AFTA sample either measured, or interpolated from adjacent VR determinations.

*5 Vitrinite reflectance values predicted from the "Default Thermal History" (see point *3), using the Burnham and Sweeney (1989) algorithm - see Appendices C and D for discussion.

**Table 2.2: Summary of thermal history interpretation of AFTA and VR data in samples from the Platypus-1 well, Duntroon Basin, offshore South Australia (Geotrack Report #589)**

| Sample number | Do AFTA data require revision of present temperature ? | Evidence of higher temperatures in the past from length data? | Evidence of higher temperatures in the past from fission track age data? | Evidence of higher temperatures in the past from vitrinite reflectance data? | Conclusion |
|---|---|---|---|---|---|
| 589-3<br>1950 m | No<br>64°C | No<br>[Mean track length greater than that calculated from Default History. Modelling of the length parameters indicates paleotemperatures slightly higher than present temperatures are possible, but are not required.] | No<br>[Pooled fission track age is older than the age range calculated from the Default History.] | No<br>[Measured vitrinite reflectance is similar to that calculated from the Default History.] | Sample has never been hotter than its present temperature at any time since deposition |
| 589-5<br>2250 m | No<br>74°C | No<br>[Mean track length greater than that calculated from Default History. Modelling of the length parameters indicates that present temperatures are the highest at any time since deposition.] | No<br>[Central fission track age and all individual grain ages are either older than, or not significantly younger than, the age range calculated from the Default History.] | No<br>[Measured vitrinite reflectance is similar to that calculated from the Default History.] | Sample has never been hotter than its present temperature at any time since deposition |
| 589-8<br>2600 m | No<br>85°C | No<br>[Mean track length greater than that calculated from Default History. Modelling of the length parameters indicates that present temperatures are the highest at any time since deposition.] | No<br>[Central fission track age and all individual grain ages are either older than, or not significantly younger than, the age range calculated from the Default History.] | No<br>[Measured vitrinite reflectance is similar to that calculated from the Default History.] | Sample has never been hotter than its present temperature at any time since deposition |

Note: Interpretation of AFTA data is based on comparison of measured AFTA parameters with values predicted from the "Default Thermal History" (Section 1.6); i.e., assuming that each sample is now at its maximum temperature since deposition. The predicted values for each sample are summarised in Table 2.1, and refer only to tracks formed after deposition. Samples may also contain tracks inherited from sediment provenance areas, which has been allowed for in interpreting the data.

**Table 2.2: Continued**

| Sample number | Do AFTA data require revision of present temperature ? | Evidence of higher temperatures in the past from length data? | Evidence of higher temperatures in the past from fission track age data? | Evidence of higher temperatures in the past from vitrinite reflectance data? | Conclusion |
|---|---|---|---|---|---|
| 589-9<br>2910 m | No<br>94°C | No<br>[Mean track length greater than that calculated from Default History. Modelling of the length parameters indicates that present temperatures are the highest at any time since deposition.] | No<br>[Central fission track age and all individual grain ages are either older than, or not significantly younger than, the age range calculated from the Default History.] | No<br>[Measured vitrinite reflectance is similar to that calculated from the Default History.] | Sample has never been hotter than its present temperature at any time since deposition |
| 589-10<br>3040 m | No<br>98°C | No<br>[Mean track length greater than that calculated from Default History. Modelling of the length parameters indicates that present temperatures are the highest at any time since deposition.] | No<br>[Central fission track age and all individual grain ages are either older than, or similar to, the age range calculated from the Default History.] | No<br>[Measured vitrinite reflectance is similar to that calculated from the Default History.] | Sample has never been hotter than its present temperature at any time since deposition |
| 589-12<br>3440 m | No<br>110°C | No track lengths | No<br>[Central fission track age and all individual grain ages are similar to the age range calculated from the Default History.] | No<br>[Measured vitrinite reflectance is similar to that calculated from the Default History.] | Sample has never been hotter than its present temperature at any time since deposition |

Note: Interpretation of AFTA data is based on comparison of measured AFTA parameters with values predicted from the "Default Thermal History" (Section 1.6); i.e., assuming that each sample is now at its maximum temperature since deposition. The predicted values for each sample are summarised in Table 2.1, and refer only to tracks formed after deposition. Samples may also contain tracks inherited from sediment provenance areas, which has been allowed for in interpreting the data.

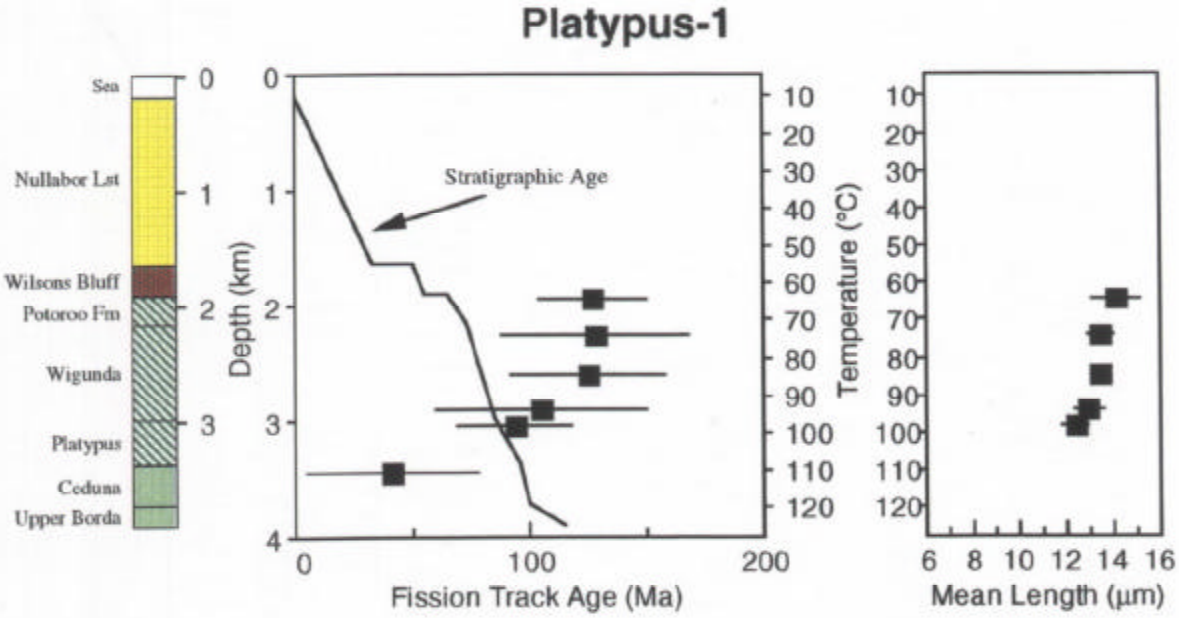


**Figure 2.1:** AFTA parameters plotted against sample depth and present temperature for samples from **Platypus-1, Duntroon Basin.** The variation of stratigraphic age with depth is also shown, as the solid line in the central panel.

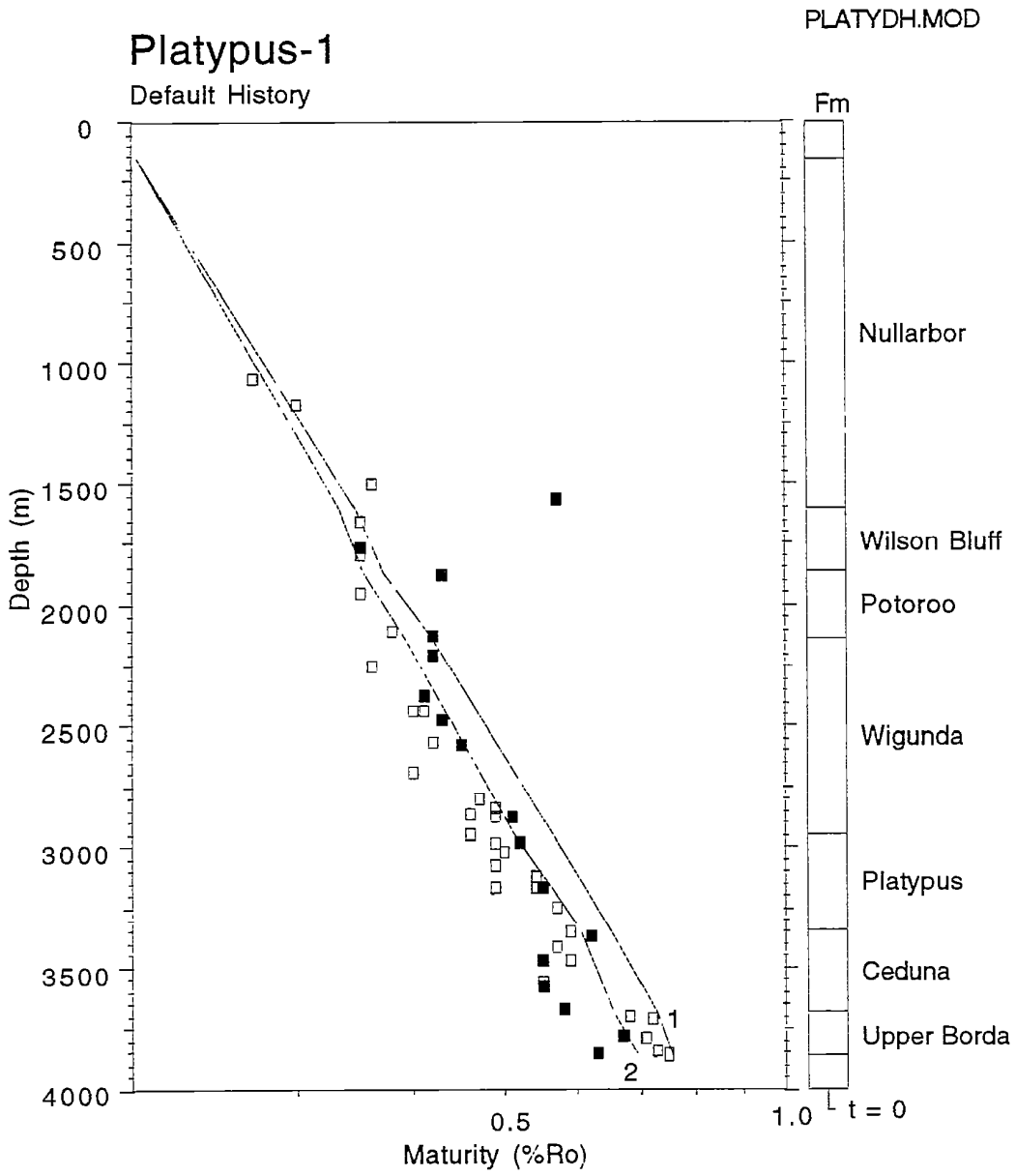


**Figure 2.2:** Vitrinite reflectance profile based on the "Default History" for the **Platypus-1 well, Duntroon Basin**, (Section 1.6), i.e., the profile expected if samples throughout the section are currently at their maximum temperature since deposition. The majority of measured VR data (new Keiraville data as solid symbols; BHP supplied data open symbols) fall below the Default History profile (1) and are more consistent with profile (2), based on lower present-day gradient of 28°C/km. The results suggest that the section is currently at maximum temperatures when possible overestimation of present temperatures or VR suppression are considered. See text for details.

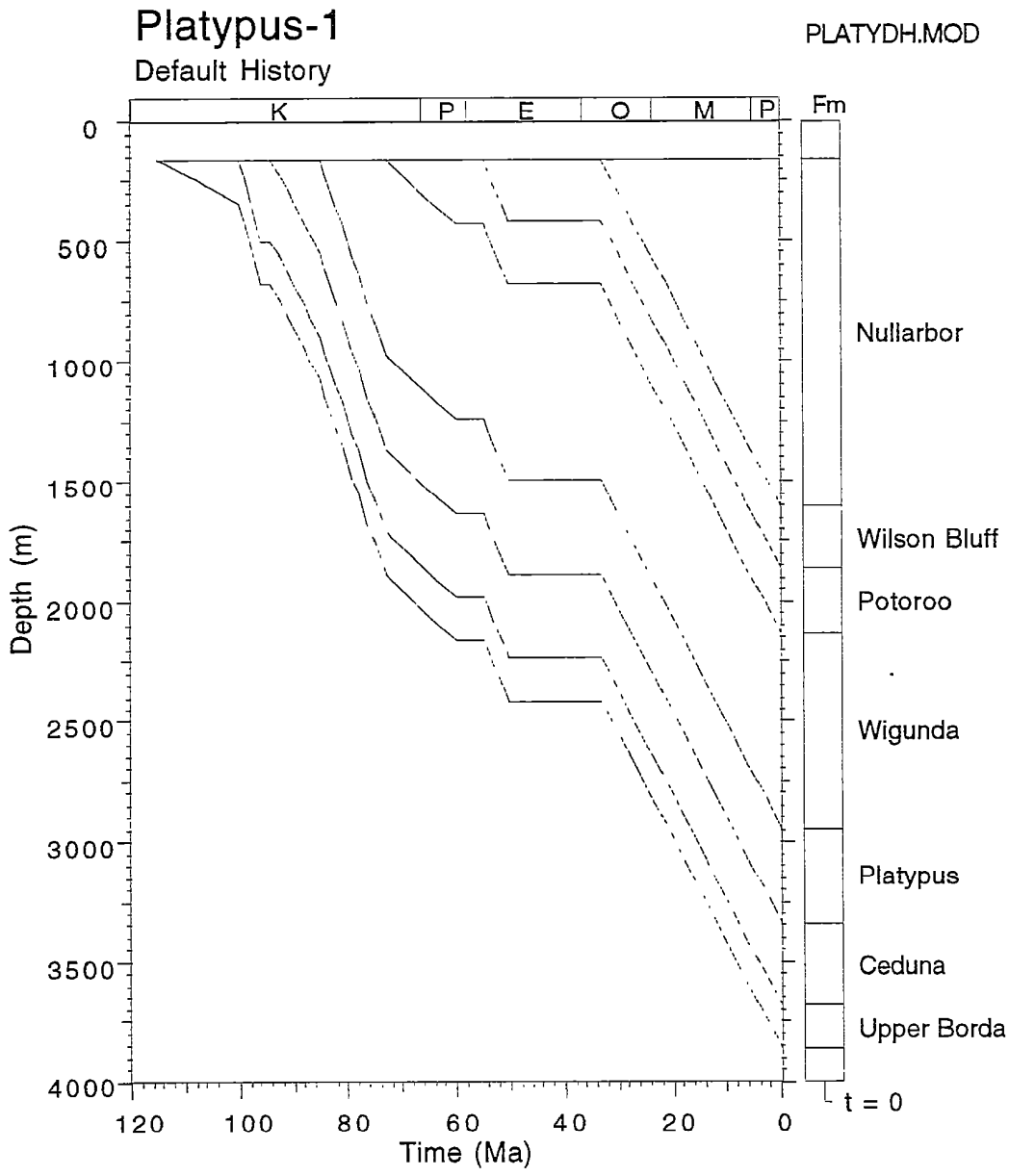


**Figure 2.3:** Default Burial History for the **Platypus-1 well, Duntroon Basin,** derived from the preserved section, which, combined with a present-day linear geothermal gradient of 30.9°C/km (Appendix A), is used in predicting the VR profile shown in Figure 2.2.

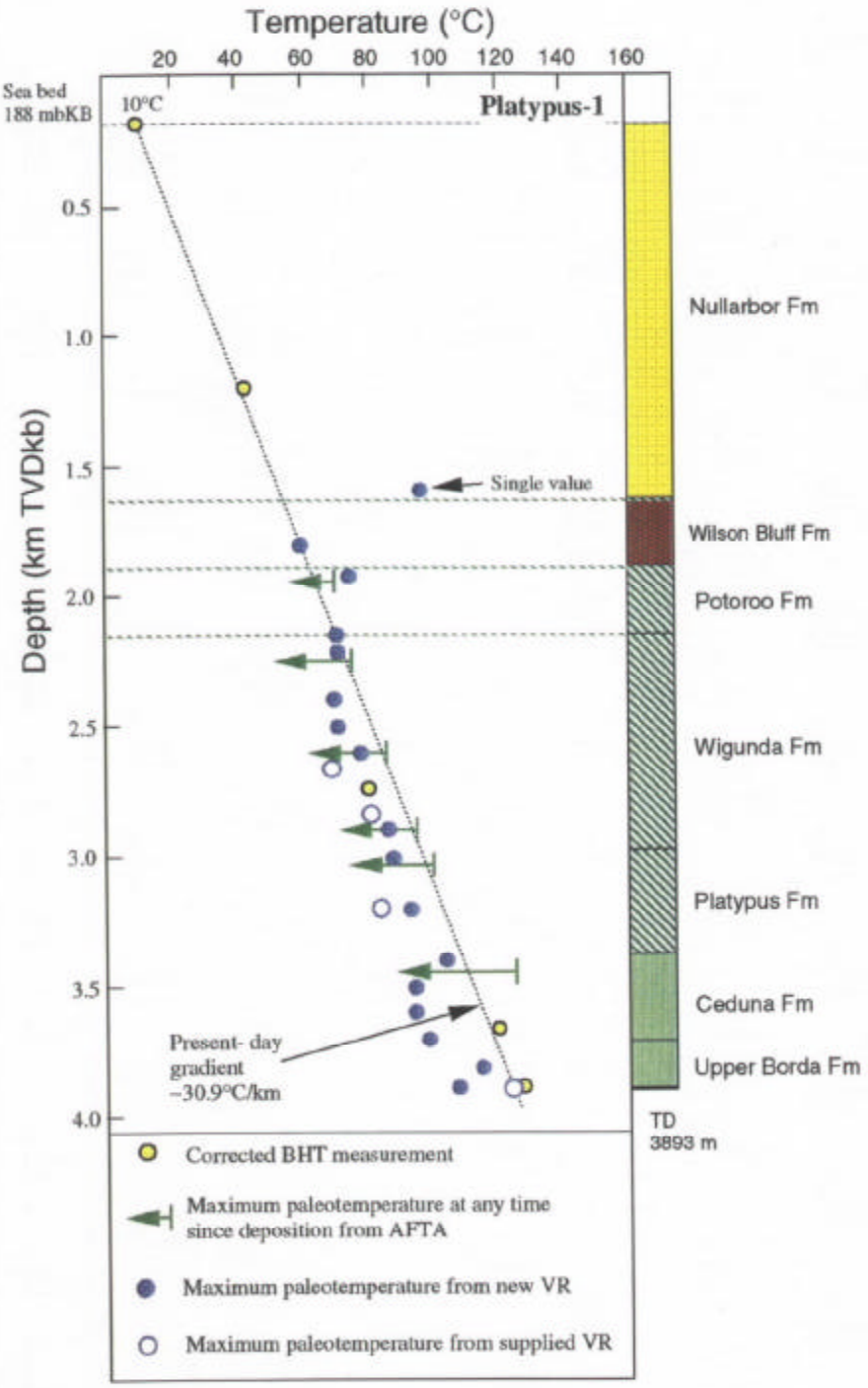


**Figure 2.4:** Plot of paleotemperatures derived from AFTA and VR data in the **Platypus-1 well, Duntroon Basin**, against sample depth and the estimated present temperature profile for this well (see Appendix A). The AFTA- and VR-derived (only selected values for supplied VR) paleotemperature values indicate that the sampled section is currently at maximum temperatures since deposition, although slight overestimation of the present temperatures and possible vitrinite suppression is noted - see text.

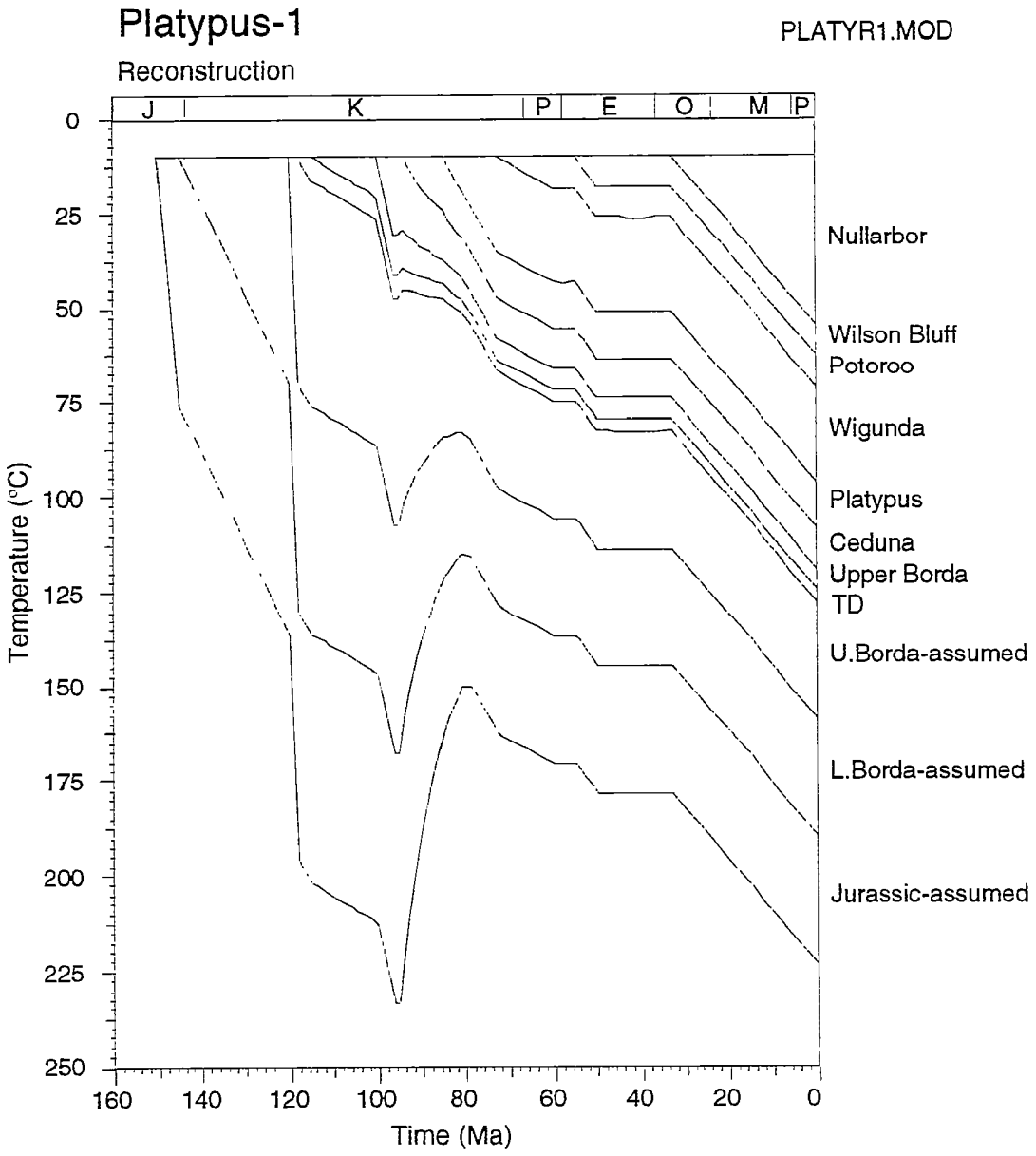


**Figure 2.5:** Reconstructed thermal history in the **Platypus-1 well** derived from the AFTA and VR paleotemperature data, assuming a regional paleogeothermal gradient of 60°C/km through the Early Cretaceous until ~95 Ma, declining to the present-day level of 30.9°C/km by ~80 Ma - see text.

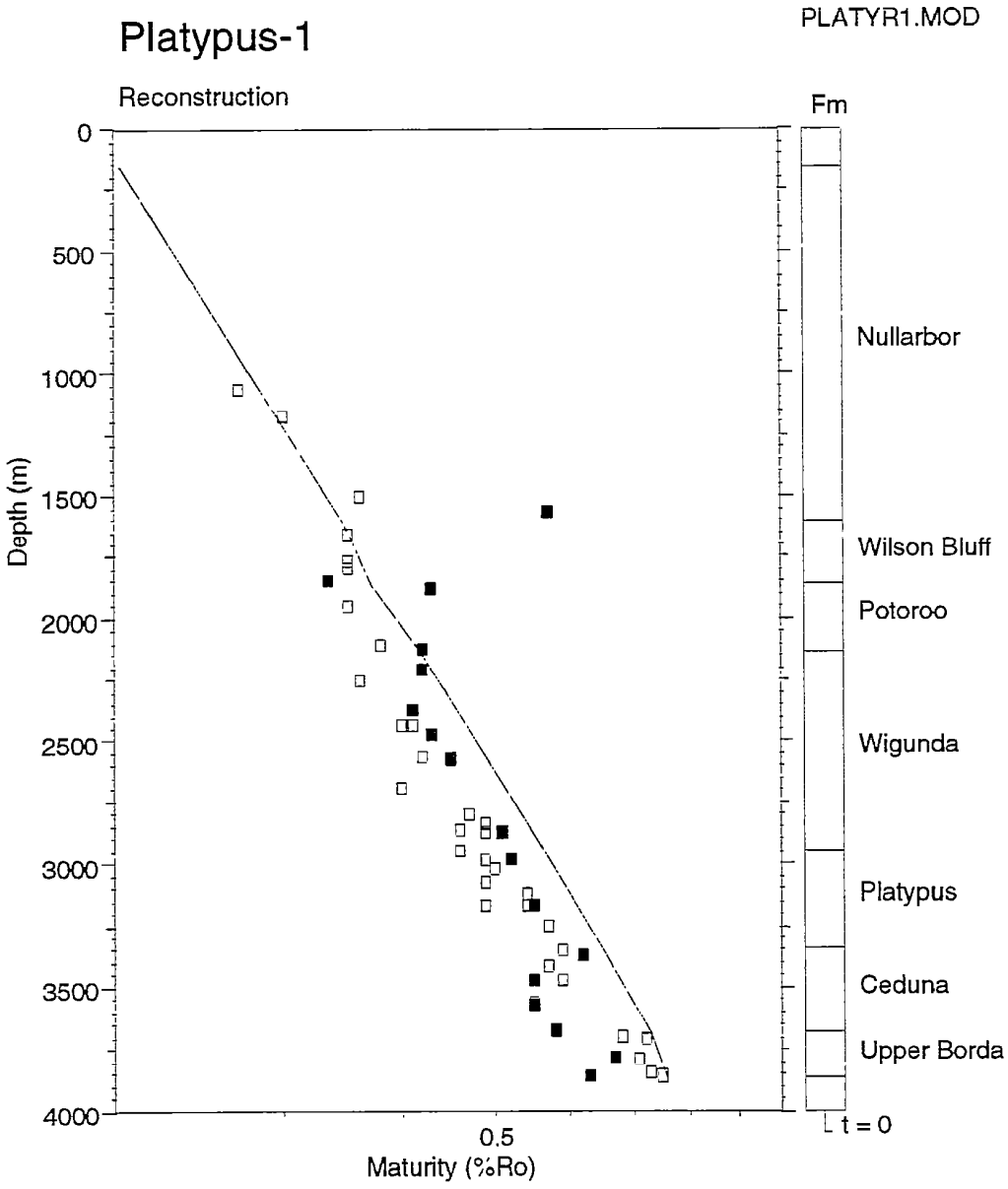


**Figure 2.6:** Measured vitrinite reflectance data (new Keiraville VR data as solid symbols) in samples from the **Platypus-1 well**, and the VR profile predicted by the reconstructed thermal history characterised by high heat flow in the Early Cretaceous as shown in Figure 2.5. The VR profile for this history is coincident with that from the Default History (Profile 1 in Figure 2.2), showing that the drilled section is currently at maximum temperatures at the present-day, and is not affected by past higher heat flow - see text.

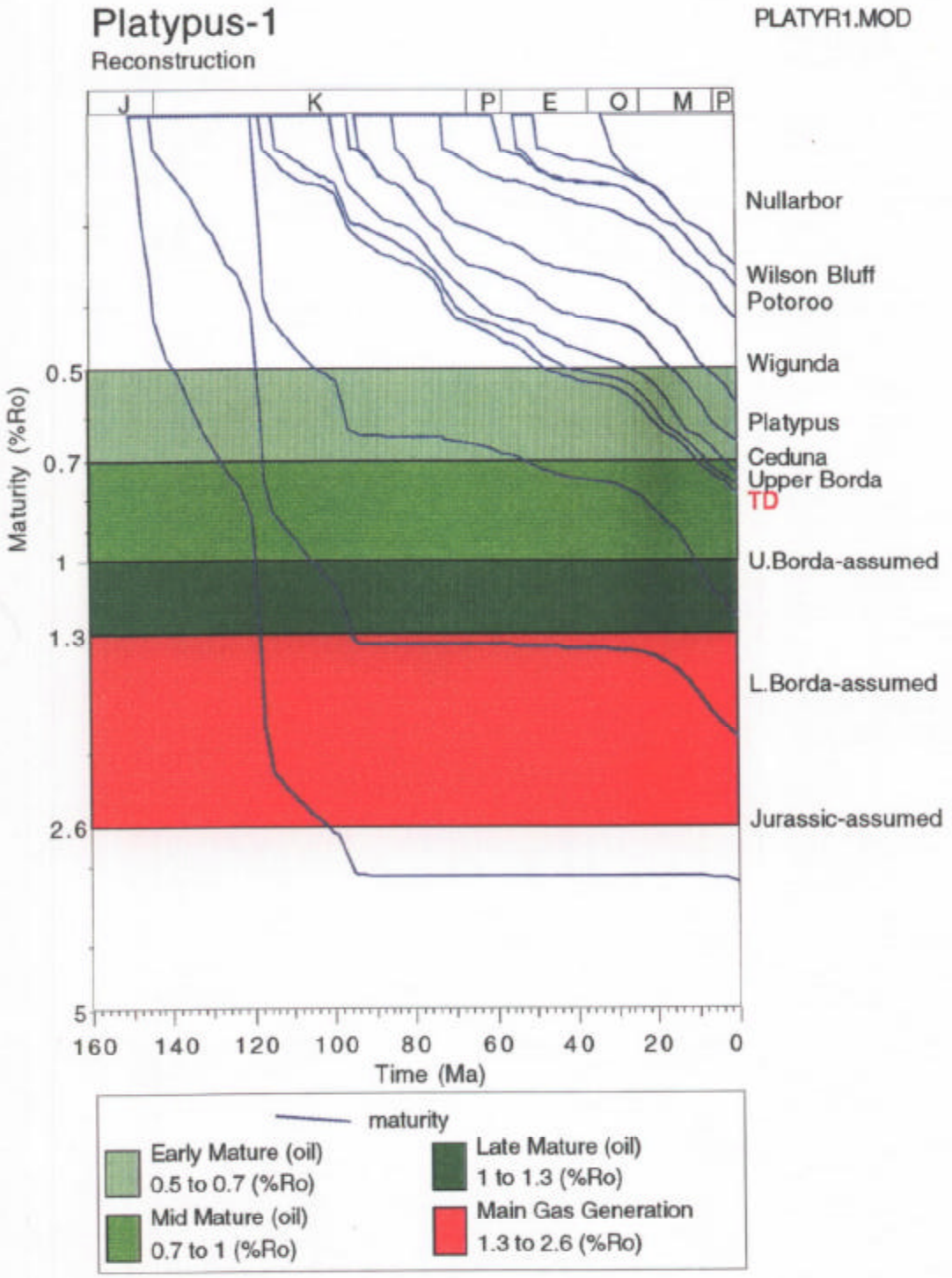


**Figure 2.7:** Predicted development of maturity with time in the **Platypus-1 well, Duntroon Basin,** controlled by the AFTA and VR results. Around 4000 m of section containing potential Early Cretaceous and Jurassic source rocks was actively generating hydrocarbons at maturities from 0.5% up to ~3% $R_o$max during the period from ~50 Ma to the present-day. The relatively thick Tertiary section (Figure 2.3) ensured this outcome in spite of an early phase of hydrocarbon generation from the deeper of these potential source rocks prior to regional **Mid-Cretaceous** cooling ~95 Ma. - See text for details.

# 3. Thermal history reconstruction in the Duntroon-1 well

## 3.1 Geological Background

The preserved stratigraphy for Duntroon-1 as provided by BHPP is listed in Table A.3 and depicted schematically in Figure 3.1. In general terms, the well intersected a ~1700 m thick Tertiary section overlying ~750 m of Late Cretaceous and ~950 m of Early Cretaceous section with TD in Aptian age Early Cretaceous at 3515 m (total vertical depth below RT). The present-day geothermal gradient is calculated from corrected BHT data at 32.6°C/km for a sea-bed temperature of 10°C (Appendix A).

## 3.2 Evidence for elevated paleotemperatures from the AFTA data

Fission track parameters in each of the six samples analysed are summarised in Table 3.1 (full details in Tables B.2 and B.3), together with values of fission track age and mean track length predicted on the basis of the Default Thermal History for each sample (Section 1.6) and using the appropriate measured Cl-composition determined in each sample (Section 1.4). The ranges of measured apatite chlorine compositions used in calculating predicted values for each AFTA sample are listed in Appendix B. The calculation of these default values includes only those tracks formed after deposition of the sample, and therefore does not account for tracks inherited from sediment source areas. The use of these parameters in interpreting AFTA data is outlined in Section 1.6 and Appendix C.

The measured AFTA parameters are also plotted as a function of depth and present temperature in Figure 3.1. The variation in stratigraphic age with depth in the well in also shown in Figure 3.1 allowing direct comparison between the fission track age and the corresponding depositional age in each sample.

Interpretation of the AFTA data from the seven Duntroon-1 samples with sufficient apatite for analysis in terms of evidence of higher temperatures in the past is described in Table 3.2. To summarise, results of detailed kinetic modelling of the AFTA data from all seven samples analysed reveal no evidence of these samples having experienced paleotemperatures higher than present temperatures at any time after deposition. For example, sample 8622-46 (Ceduna Formation), is a key sample in which the occurrence of F-rich grains with fission track ages older than the stratigraphic age (Figure B.5b), restricts the maximum paleotemperatures to no higher than the present temperature of 92°C.

In the two deeper samples (8622-47 & 49; Upper Borda Formation), the relatively high present temperatures of ~102 and 119°C could partially mask any evidence of higher paleotemperatures, but when considered in conjunction with the associated VR levels (see below), any period of higher paleotemperatures allowed by AFTA in these samples is considered to be unlikely.

## 3.3 Magnitude of maximum paleotemperatures from the AFTA data

Estimates of the magnitude of maximum paleotemperature allowed by the AFTA data in each sample have been obtained by iteratively predicting AFTA parameters for a range of thermal history scenarios and comparing these predicted parameters with the measured data.

For each sample, the maximum paleotemperature allowed by the AFTA data are either equal to the present temperature of the sample, or in the case of several of the shallower samples with relatively poorer data, paleotemperatures up to ~10 to 30°C higher than present temperatures are allowed, but not required, as listed in Table i. The data do not provide any constraints on the time of cooling from such temperatures, with any time after deposition possible. On balance, the AFTA data from all samples can be reconciled if the entire drilled section is at maximum temperatures at the present day, although the supplied VR data may provide tentative evidence for a transient Miocene-Recent heating episode in the shallow section as discussed below. Note, however, that even if such a heating episode is present it does not affect the main conclusion that the present temperatures through the Early Cretaceous section are the maximum experienced since deposition.

Paleotemperature estimates from each AFTA sample are listed in Table i (Executive Summary) and plotted against depth in Figure 3.4 .

## 3.4 Evidence for elevated paleotemperatures from the VR data

Vitrinite reflectance data are available from 15 new samples analysed by Keiraville Konsultants (Table D.2) and existing data on 34 samples supplied by BHPP (Table D.3).

The Default Thermal History for Duntroon-1, i.e., the thermal history of the well if the section has never been hotter than present temperatures (as described in section 1.6), and based on the preserved stratigraphy, a present-day geothermal gradient of 32.6°C/km and a sea-bed temperature of 10°C is used to predict a VR profile for the

well. The predicted profile is then compared with the measured VR data as illustrated in Figure 3.2. The burial history used in calculating this profile is shown in Figure 3.3.

The majority of new VR data (solid symbols) fall near, or marginally below, the Default History profile whereas the BHPP supplied data (open symbols) tend to be more scattered, with a particularly noticeable group of results above the Wigunda Fm plotting well above the predicted profile. However, consideration of the deeper VR data from both data sets suggests that the Cretaceous section below the Potoroo Fm is currently at maximum temperatures, with the new data again conforming more closely with the Default History Profile.

No new samples were processed from the Nullarbor Limestone section in which the BHPP supplied data shows the largest departure from the Default History predicted profile, so there is limited basis for direct comparison. Nevertheless, comparison of the two data sets is possible in the section through the Potoroo, Pidinga and Wilson Bluff Formations, and this suggests that the new data reported here is consistently lower than the supplied data (3 out of the 4 new determinations, with the highest new data point based on only two measurement - Table D.2), and more consistent with the Default History. On balance, we consider the new data more accurately reflects the thermal history in this part of the well section, but tentative evidence remains for higher paleotemperatures in this section and in the Nullarbor Limestone above. Note, however, that if such a heating event did occur, the shape of the VR profile shows it *must* have been a transient lateral heating event at some time in the Miocene to Recent. If the heating was sustained for a million years or more, the vitrinite reflectance levels throughout the entire section should show a steady increase with increasing depth, rather than the arcuate profile which is apparent in Figure 3.2.

## 3.5 Magnitude of maximum paleotemperatures from the VR data

Maximum paleotemperature have been estimated from each measured VR value by using the algorithm of Burnham and Sweeney (1989) as described in more detail in Section 1.6 and Appendix D.

Paleotemperatures, based on a heating rate of 1°C/Ma, estimated from each Duntroon-1 VR value in Tables D.2 and D.3 are listed in Table ii (Executive Summary) and plotted against depth in Figure 3.4. The majority of the paleotemperature estimates derived from the new VR data are within a few degrees of the present temperatures, emphasising the conclusions made above from inspection of the VR-depth plot

(Figure 3.2), that at least the Cretaceous section drilled in Duntroon-1 is currently at maximum temperatures since deposition.

## 3.6 Estimation of paleogeothermal gradient

The AFTA and VR thermal history constraints indicate maximum paleotemperatures throughout the drilled section are at the present-day, so that there is no basis for calculation of a paleogeothermal gradient for any post-depositional time period.

## 3.7 Estimates of removed section and burial history reconstruction

As no heating and cooling event have been identified, no estimation of removed section is relevant.

Note that palynological information supplied by BHPP shows the presence of the P. pannosus spore pollen zone ~250 m thick at the top of the Early Cretaceous section indicating little if any erosion is possible at the mid-Cretaceous "unconformity". Therefore, the burial history derived from the preserved stratigraphy and illustrated in Figure 3.3 is considered to be a close reflection of the *actual* burial history at the Duntroon-1 well site.

## 3.8 Thermal history synthesis - Integration of regional information

A schematic illustration of the main features of the thermal history in the Duntroon-1 well is presented in Figure ii (Executive Summary).

The data discussed in the previous sections provide excellent control on the Tertiary-Recent thermal history at Duntroon-1 showing that the Cretaceous section is currently at maximum temperatures, but the combination of the relatively thick Late Cretaceous to Recent section, and the relatively thin Early Cretaceous section drilled, results in a lack of control on the important Mid-Cretaceous thermal event identified elsewhere in the region (see Geotrack Report #569 for details of this event) .

Therefore, in order to fully reconstruct the thermal history in Duntroon-1 regional thermal history information must be incorporated. A key feature of the regional history is the occurrence of a period of high heat flow in the Early Cretaceous which

terminated in the Mid-Cretaceous, at around 95 Ma. Paleogeothermal gradients in the Mid-Cretaceous have been constrained to 60°C/km by AFTA and VR data in the Vivonne-1 well (Geotrack Report #569), and a very similar paleogeothermal gradient can be inferred from open file VR data available for Echidna-1 (internal assessment, Geotrack International).

On this basis, Figure 3.5 illustrates the preferred reconstructed thermal history for the Duntroon-1 well site derived by using the measured regional geothermal gradient of 60°C/km for the period prior to the Mid-Cretaceous, decreasing to a gradient of 32.6°C/km (i.e., the present-day value for Duntroon-1) for the period from 80 Ma to the present.

Inspection of the plot shows that even though the Early Cretaceous and deeper section experienced high paleotemperatures prior to the regional Mid-Cretaceous cooling event, the entire drilled section was subsequently heated to even higher temperatures during the Late Cretaceous to Recent burial phase, with maximum temperatures experienced at the present-day.

Note that a hypothetical deeper section is also shown in Figure 3.5, and down to ~5000 m this hypothetical section is also at higher temperature at the present-day than reached in the Mid-Cretaceous. Deeper than 5000 m, however, the reconstructed history shows that maximum temperatures were experienced in the Mid-Cretaceous.

## 3.9 Implications for source rock maturation at the Duntroon-1 well site

The preferred thermal history shown in Figure 3.5 allows construction of a maturity profile in the preserved section at the Duntroon-1 well, as shown in Figure 3.6. The predicted VR-profile shows a good fit to the measured VR data, and is also coincident with the profile derived from the Default Thermal History previously shown in Figure 3.2, since maximum temperatures in the *drilled section* occur at the present day in both histories.

However, even though the Reconstructed Thermal History results in the same VR maturity profile as the Default Thermal History, recognition of the regional significance of high Early Cretaceous heat flow has significant implications for the timing of hydrocarbon generation in the basin.

Figure 3.7 shows the variation of maturity (vitrinite reflectance) with time at the Duntroon-1 well site predicted from the Regional Thermal History illustrated in

Figure 3.5. The plot graphically illustrates that the drilled section has matured essentially continuously to the present-day, with the section at TD becoming early mature (0.5% $R_o$max) for hydrocarbon generation at around 25 Ma and reaching mid maturity (0.75% $R_o$max) at the present-day. On the other hand, the plot shows a number of notional units below TD in the well where cessation of maturation is coincident with cooling at 95 Ma (shown in Figure 3.5), and with additional maturation from these units beginning at progressively more recent times with increasing depth. For example, the base of the notional E. Cretaceous B unit (~5000 m present depth), reached a maturity of ~1.2 % $R_o$max at 95 Ma, and did not begin to gain additional maturity until ~10 Ma, reaching ~1.5 % $R_o$max at the present-day. In contrast, the section deeper than ~5000 m present depth reached maximum maturity at 95 Ma, and no significant maturation has occurred since that time (see Figures 3.6 and 3.7).

Nevertheless, even when the effect of high Early Cretaceous heat flow is considered, some 3000 m of sedimentary section with source potential at the Duntroon-1 well site, between ~2500 m present depth (near base Wigunda Fm) up to ~5500 m depth was actively generating hydrocarbons at maturities between 0.5 and ~1.5% $R_o$max during the period from ~25 Ma to the present-day (Figure 3.7).

**Table 3.1: Summary of AFTA data in samples from the Duntroon-1 well, Duntroon Basin, offshore South Australia (Geotrack Report #589)**

| Sample number | Average Depth*1 (m) | Present temperature*2 (°C) | Stratigraphic Age (Ma) | Mean track length (µm) | Default mean track length *3 (µm) | Apatite fission track age (Ma) | Default fission track age*3 (Ma) | Measured Ro (max)*4 (%) | Default Ro (max)*5 (%) |
|---|---|---|---|---|---|---|---|---|---|
| 8622-40 | 1500 | 53 | 55-50 | No apatite | - | No apatite | - | - | - |
| 8622-41 | 1630 | 58 | 65-60 | 11.37±0.17 | 13.5 | 258.0±13.2 | 50 | 0.33 | 0.35 |
| 8622-42 | 1800 | 63 | 65-60 | No lengths | 13.2 | 27.0±16.6 | 57 | 0.35 | 0.36 |
| 8622-43 | 2100 | 73 | 85-73 | 11.27±0.28 | 12.8 | 131.5±23.6 | 64 | 0.39-0.45 | 0.42 |
| 8622-45 | 2507 | 86 | 85-73 | 10.89±0.50 | 12.3 | 96.4±19.4 | 67 | 0.52 | 0.50 |
| 8622-46 | 2700 | 92 | 100-96 | 11.94±0.28 | 12.1 | 120.4±9.9 | 78 | 0.55 | 0.53 |
| 8622-47 | 3000 | 102 | 119-100 | 11.03±0.22 | 11.2 | 51.6±7.3 | 71 | 0.53 | 0.60 |
| 8622-49 | 3510 | 119 | 119-100 | 11.38±0.39 | 10.1 | 33.8±8.3 | 38 | 0.71 | 0.70 |

*1 All depths quoted are total vertical depth (TVD) with respect to KB.

*2 See Appendix A for a discussion of present temperature estimation.

*3 AFTA values predicted from the "Default Thermal History" (Section 1.6); i.e., assuming that each sample is now at its maximum temperature since deposition. The values refer only to tracks formed after deposition. Samples may also contain tracks inherited from sediment provenance areas. Calculations for the ranges given refer to actual measured compositions of apatites analysed within a particular sample, which is discussed in Appendix A.

*4 Vitrinite reflectance values at the level of the AFTA sample either measured, or interpolated from adjacent VR determinations.

*5 Vitrinite reflectance values predicted from the "Default Thermal History" (see point *3), using the Burnham and Sweeney (1989) algorithm - see Appendices C and D for discussion.

**Table 3.2: Summary of thermal history interpretation of AFTA and VR data in samples from the Duntroon-1 well, Duntroon Basin, offshore South Australia (Geotrack Report #589)**

| Sample number | Do AFTA data require revision of present temperature ? | Evidence of higher temperatures in the past from length data? | Evidence of higher temperatures in the past from fission track age data? | Evidence of higher temperatures in the past from vitrinite reflectance data? | Conclusion |
|---|---|---|---|---|---|
| 8622-40<br>1500 m | No data<br>53°C | No Apatite | No Apatite | Insufficient vitrinite data | No information |
| 8622-41<br>1630 m | No<br>58°C | No, equivocal<br>[Mean track length less than calculated from Default History. Modelling the fission track age and length data indicate the observed shortening can be explained either by inheritance of all short tracks from sediment provenance terrains, or by paleotemperatures higher than present temperatures after deposition.] | No<br>[Pooled fission track age is older than the age range calculated from the Default History.] | No<br>[Measured vitrinite reflectance is similar to that calculated from the Default History.] | Sample has never been hotter than its present temperature at any time since deposition |
| 8622-42<br>1800 m | No<br>63°C | No track lengths | No, equivocal<br>[Only one grain with fission track age broadly compatible with the age range calculated from the Default History.] | No<br>[Measured vitrinite reflectance is similar to that calculated from the Default History.] | Sample has never been hotter than its present temperature at any time since deposition |

Note: Interpretation of AFTA data is based on comparison of measured AFTA parameters with values predicted from the "Default Thermal History" (Section 1.6); i.e., assuming that each sample is now at its maximum temperature since deposition. The predicted values for each sample are summarised in Table 2.1, and refer only to tracks formed after deposition. Samples may also contain tracks inherited from sediment provenance areas, which has been allowed for in interpreting the data.

**Table 3.2: Continued**

| Sample number | Do AFTA data require revision of present temperature ? | Evidence of higher temperatures in the past from length data? | Evidence of higher temperatures in the past from fission track age data? | Evidence of higher temperatures in the past from vitrinite reflectance data? | Conclusion |
|---|---|---|---|---|---|
| 8622-43<br>2100 m | No<br>73°C | No, equivocal<br>[Mean track length less than calculated from Default History. Modelling the fission track age and length data indicate the observed shortening can be explained either by inheritance of all short tracks from sediment provenance terrains, or by paleotemperatures higher than present temperatures after deposition.] | No<br>[Central fission track age and all individual grain ages are either older than, or not significantly younger than, the age range calculated from the Default History.] | No<br>[Measured vitrinite reflectance is similar to that calculated from the Default History.] | Sample has never been hotter than its present temperature at any time since deposition |
| 8622-45<br>2507 m | No<br>86°C | No, equivocal<br>[Mean track length less than calculated from Default History. Modelling the fission track age and length data indicate the observed shortening can be explained either by inheritance of all short tracks from sediment provenance terrains, or by paleotemperatures higher than present temperatures after deposition.] | No<br>[Central fission track age and all individual grain ages are either older than, or similar to, the age range calculated from the Default History.] | No<br>[Measured vitrinite reflectance is similar to that calculated from the Default History.] | Sample has never been hotter than its present temperature at any time since deposition |

Note: Interpretation of AFTA data is based on comparison of measured AFTA parameters with values predicted from the "Default Thermal History" (Section 1.6); i.e., assuming that each sample is now at its maximum temperature since deposition. The predicted values for each sample are summarised in Table 2.1, and refer only to tracks formed after deposition. Samples may also contain tracks inherited from sediment provenance areas, which has been allowed for in interpreting the data.

**Table 3.2: Continued**

| Sample number | Do AFTA data require revision of present temperature ? | Evidence of higher temperatures in the past from length data? | Evidence of higher temperatures in the past from fission track age data? | Evidence of higher temperatures in the past from vitrinite reflectance data? | Conclusion |
|---|---|---|---|---|---|
| 8622-46<br>2700 m | No<br>92°C | No<br>[Mean track length is compatible within error of that calculated from Default History.] | No<br>[Central fission track age and all individual grain ages are either older than, or not significantly younger than, the age range calculated from the Default History.] | No<br>[Measured vitrinite reflectance is similar to that calculated from the Default History.] | Sample has never been hotter than its present temperature at any time since deposition |
| 8622-47<br>3000 m | No<br>102°C | No<br>[Mean track length is compatible within error of that calculated from Default History.] | No<br>[Central fission track age and all individual grain ages are either older than, or similar to, the age range calculated from the Default History.] | No<br>[Measured vitrinite reflectance is similar to that calculated from the Default History.] | Sample is currently at maximum temperatures at any time since deposition |
| 589-12<br>3510 m | No<br>119°C | No,<br>[Mean track length is greater than that calculated from Default History.] | No<br>[Central fission track age and all individual grain ages are similar to the age range calculated from the Default History.] | No<br>[Measured vitrinite reflectance is similar to that calculated from the Default History.] | Sample has never been hotter than its present temperature at any time since deposition |

Note: Interpretation of AFTA data is based on comparison of measured AFTA parameters with values predicted from the "Default Thermal History" (Section 1.6); i.e., assuming that each sample is now at its maximum temperature since deposition. The predicted values for each sample are summarised in Table 2.1, and refer only to tracks formed after deposition. Samples may also contain tracks inherited from sediment provenance areas, which has been allowed for in interpreting the data.

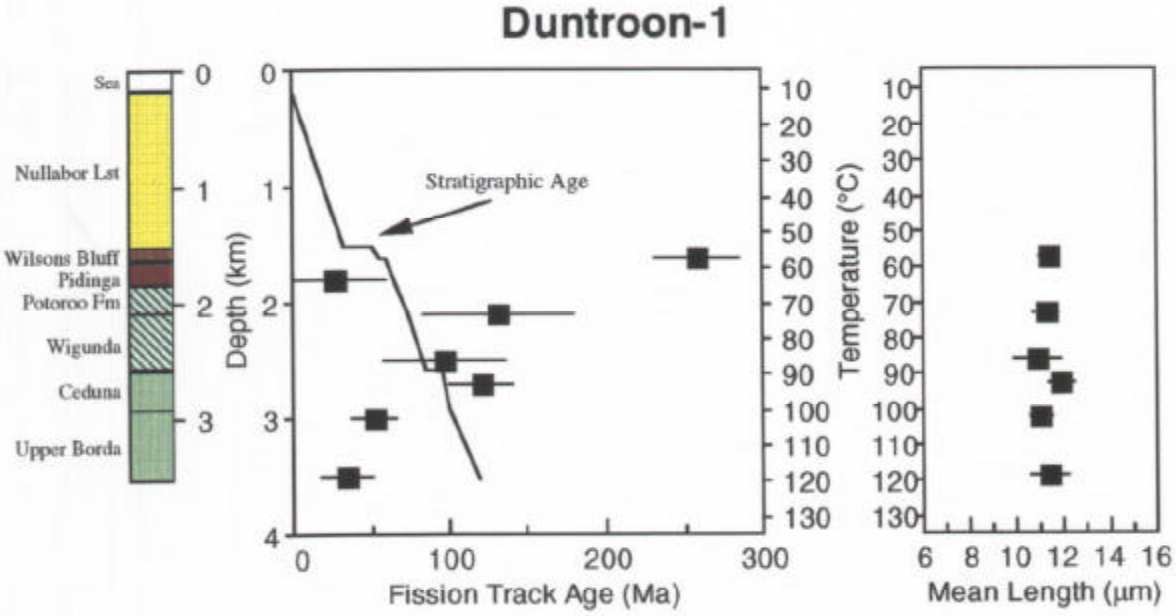


**Figure 3.1:** AFTA parameters plotted against sample depth and present temperature for samples from **Duntroon-1, Duntroon Basin.** The variation of stratigraphic age with depth is also shown, as the solid line in the central panel.

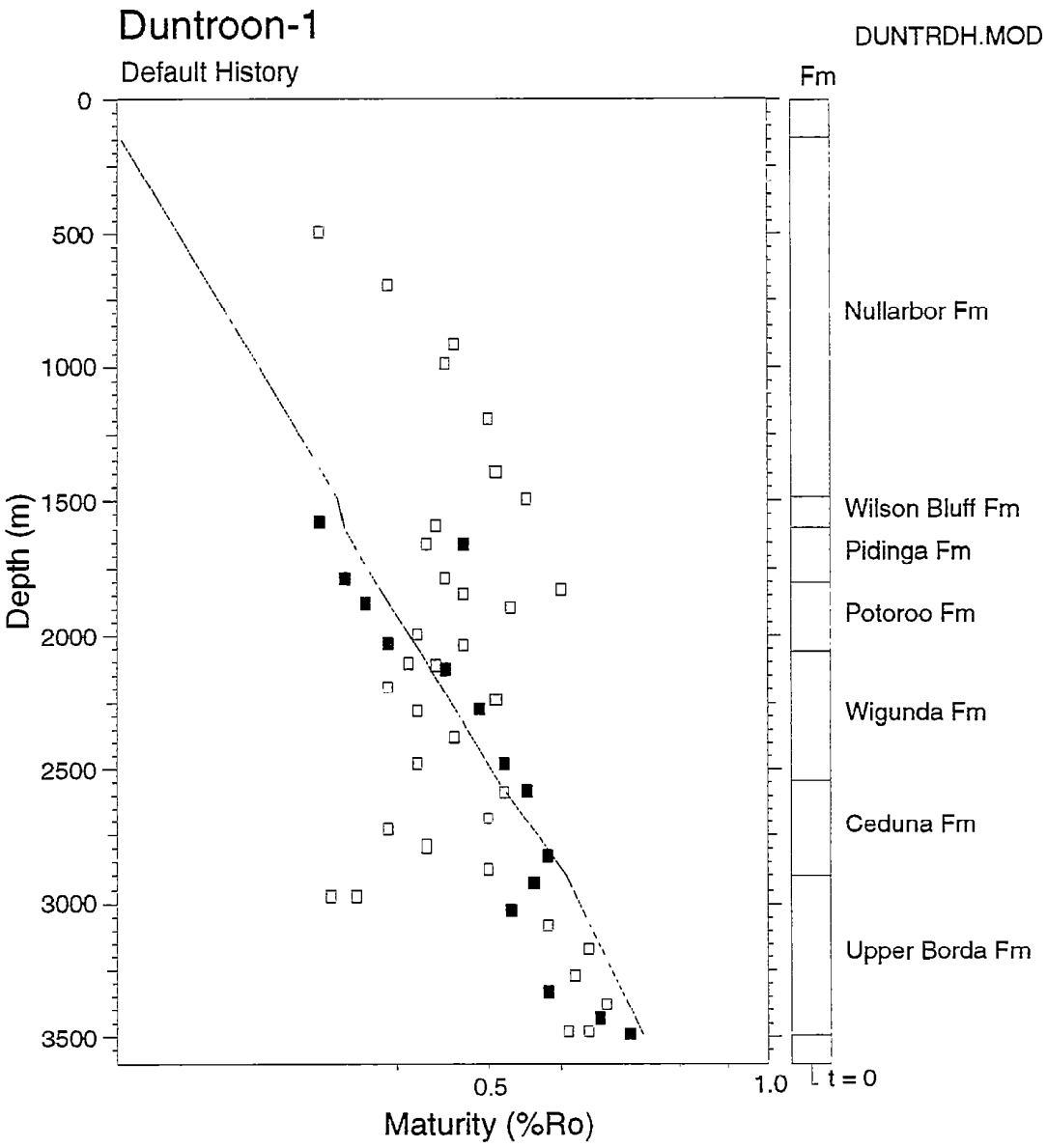


**Figure 3.2:** Vitrinite reflectance profile calculated from the "Default History" for the **Duntroon-1 well, Duntroon Basin.** The majority of new VR data (solid symbols) fall near, or marginally below, the Default History profile whereas the BHPP supplied data (open symbols) tend to be more scattered, with a particularly noticeable group of results above the Wigunda Fm plotting well above the predicted profile. Consideration of all data suggests that the Cretaceous section below the Potoroo Fm is currently at maximum temperatures, while the shallower section show tentative evidence of having been subjected to a transient lateral heating event in the Miocene to Recent. See text for details.

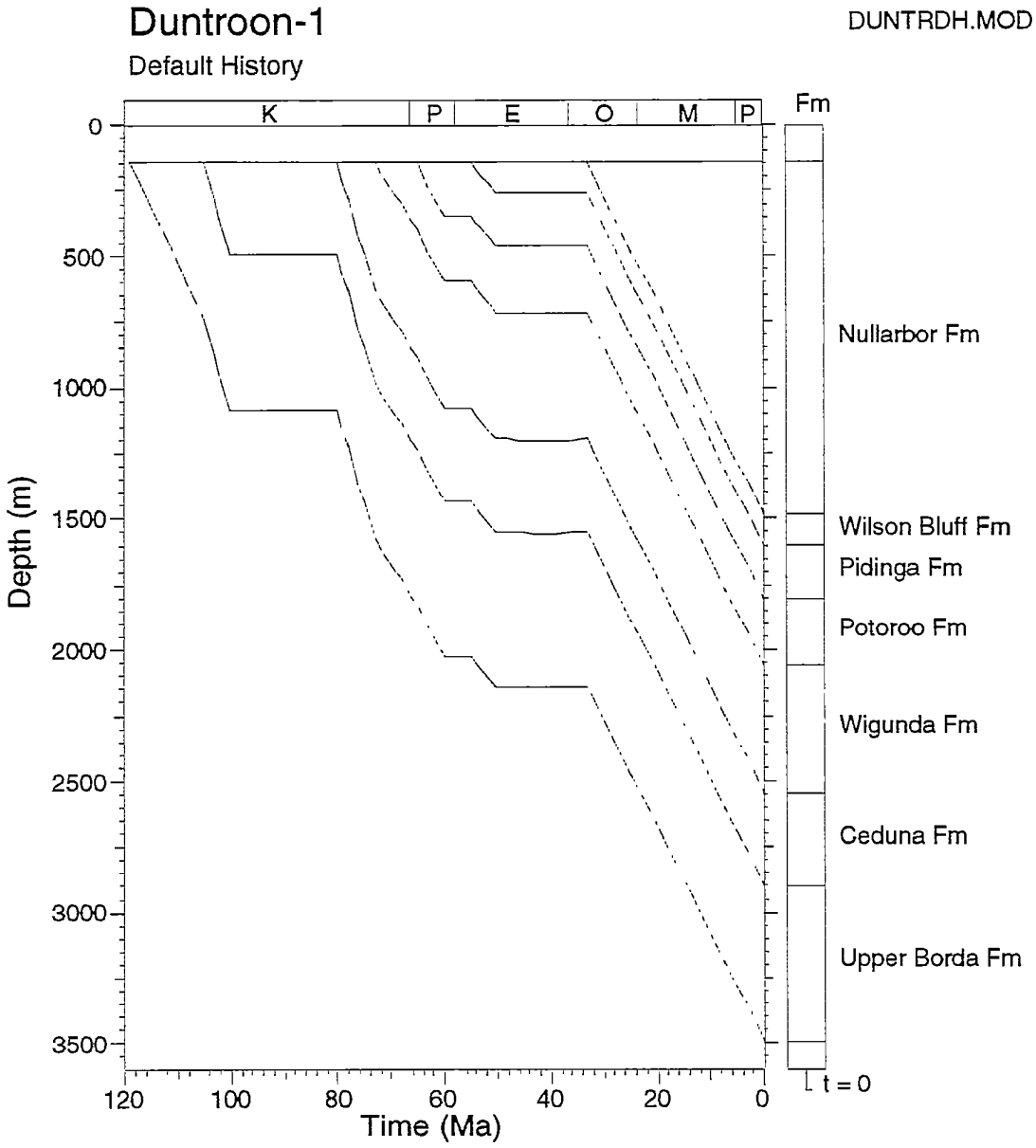


**Figure 3.3:** Default Burial History for the **Duntroon-1 well, Duntroon Basin,** derived from the preserved section, which, combined with a present-day linear geothermal gradient of 32.6°C/km (Appendix A), is used in predicting the VR profile shown in Figure 3.2.

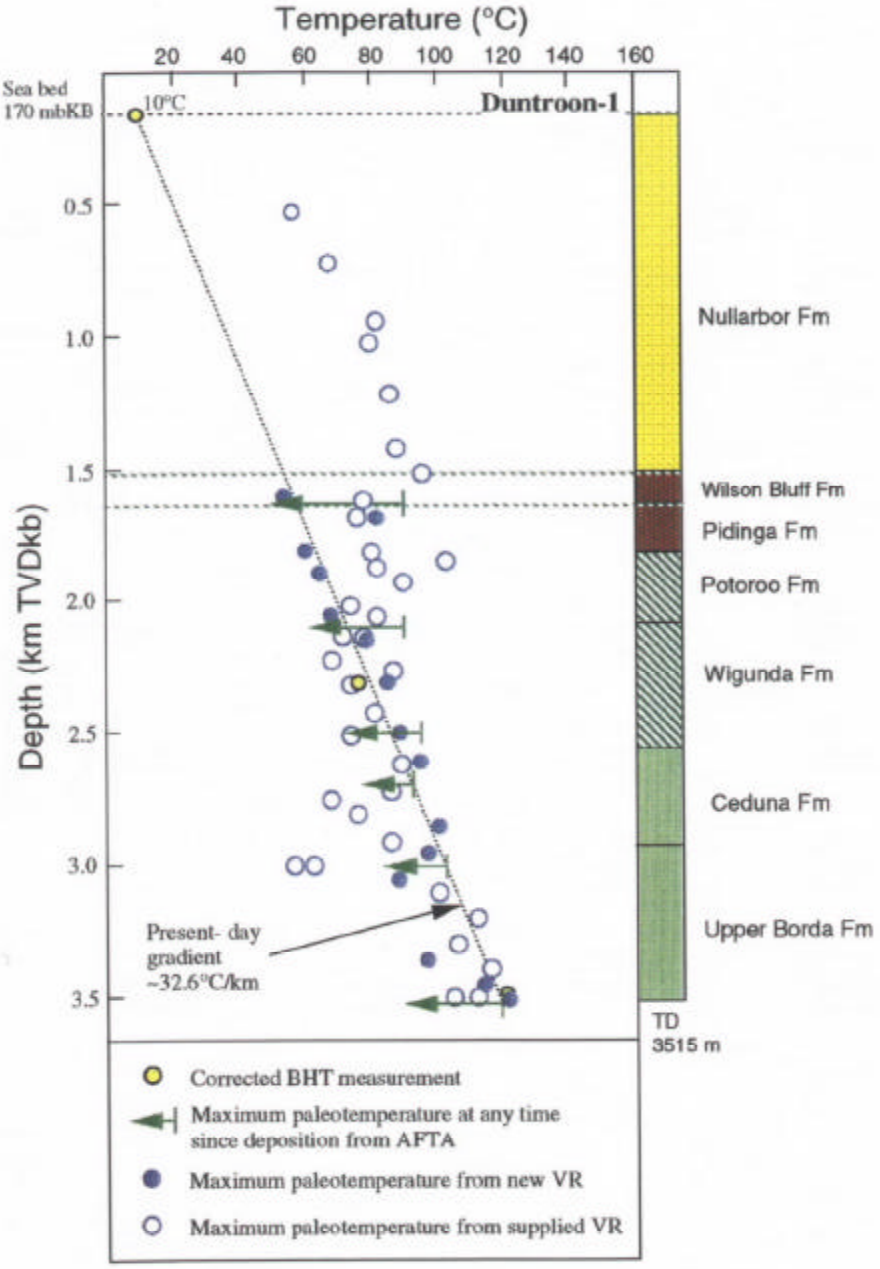


**Figure 3.4:** Plot of paleotemperatures for a range of heating rates derived from AFTA and VR data in the **Duntroon-1 well, Duntroon Basin**, against sample depth and the estimated present temperature profile for this well, including corrected BHT values (see Appendix A). The paleotemperature estimates provide tentative evidence of the shallower part of the sampled section having cooled from elevated paleotemperatures after deposition - see text for details.

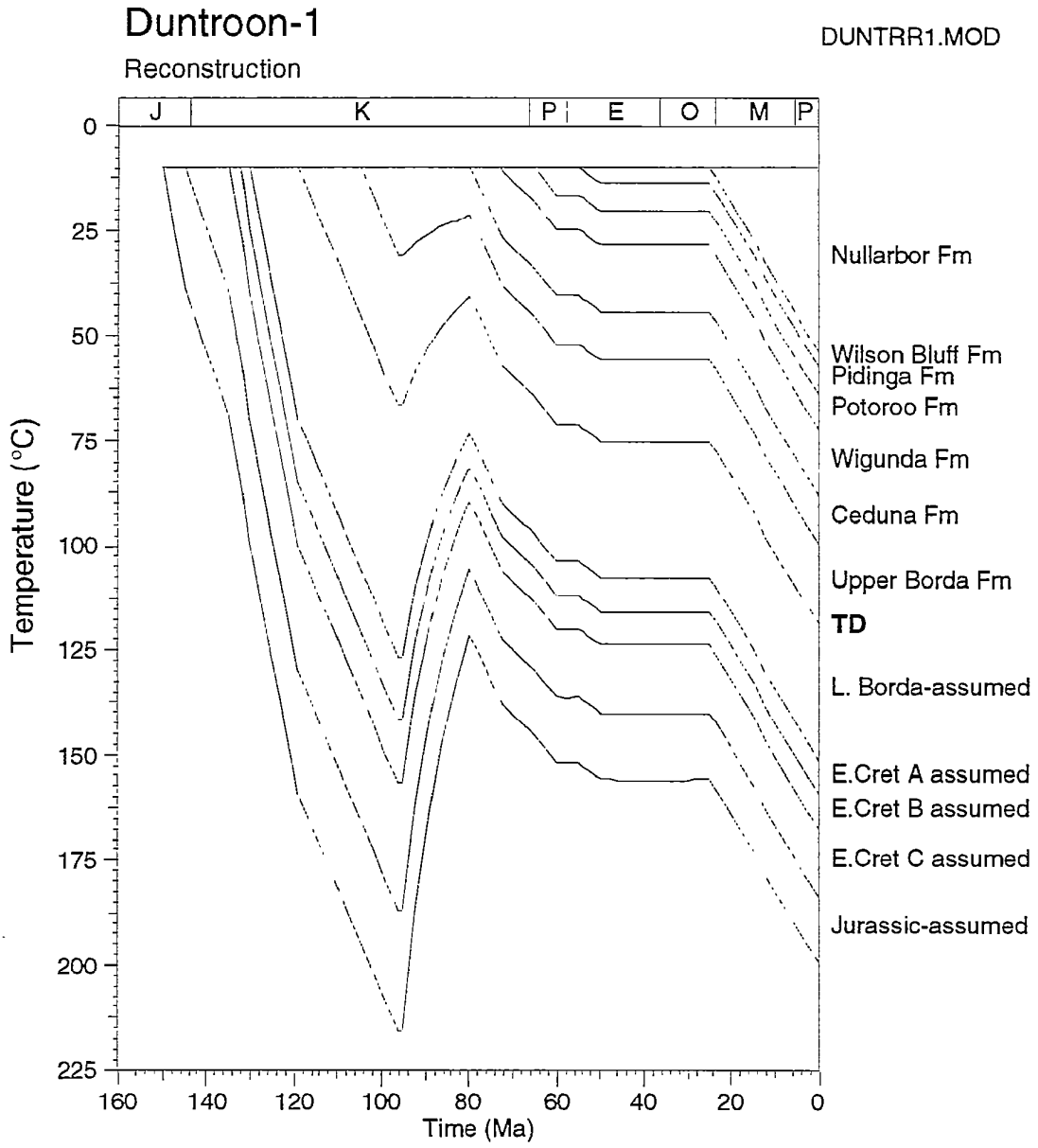


**Figure 3.5:** Reconstructed thermal history in the **Duntroon-1 well** derived from the AFTA and VR paleotemperature data, assuming a regional paleogeothermal gradient of 60°C/km through the Early Cretaceous until ~95 Ma, declining to the present-day level of 32.6°C/km by ~80 Ma - see text.

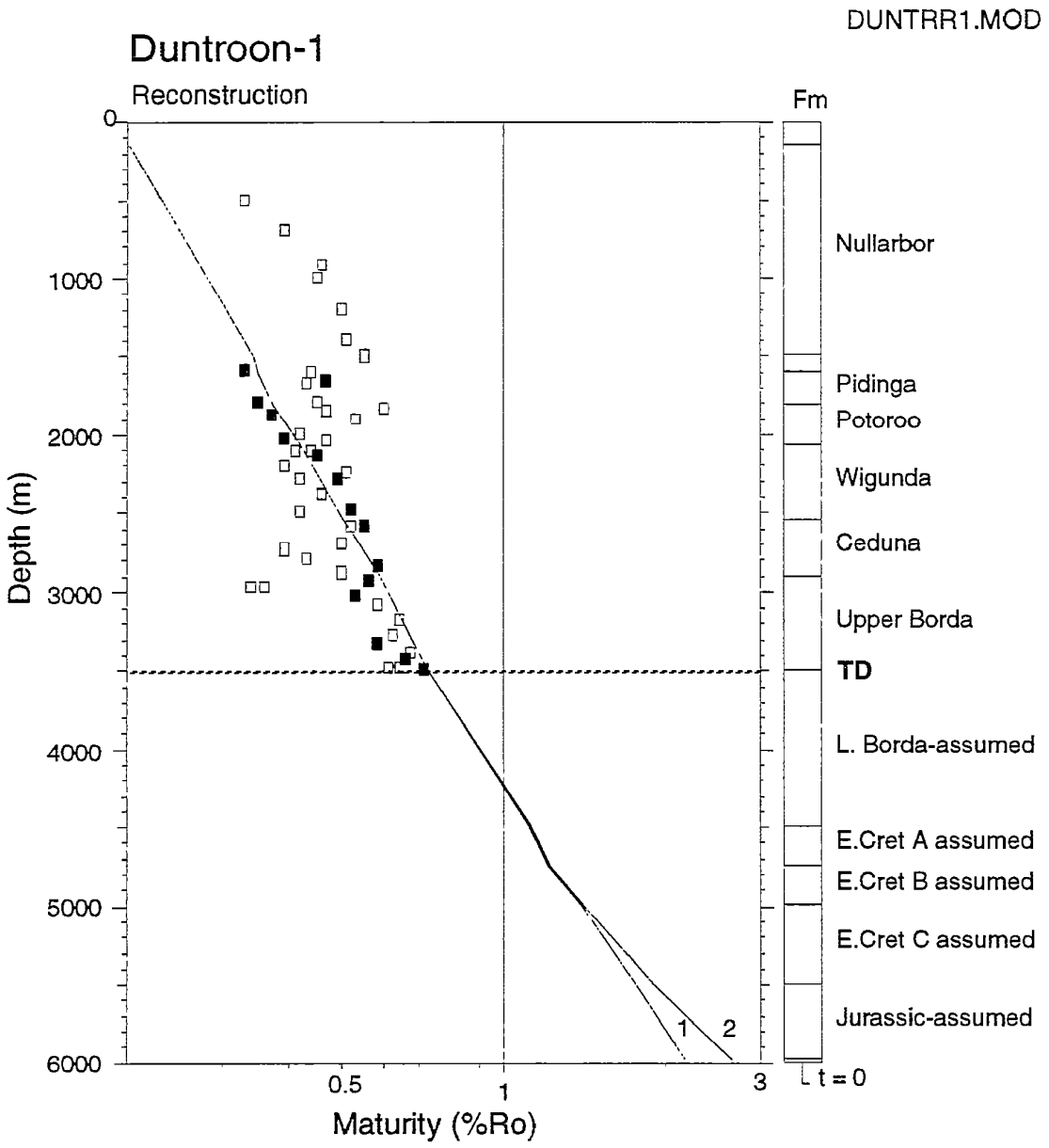


**Figure 3.6:** Measured vitrinite reflectance data (new Keiraville VR data as solid symbols) in samples from the **Duntroon-1 well**, and the VR profile predicted by the reconstructed thermal history characterised by high heat flow in the Early Cretaceous as shown in Figure 3.5. The VR profile for this history (Profile 2) is coincident with that from the Default History (Profile 1, see also Figure 2.2), through the drilled section and down to ~5000 m depth. This confirms that the drilled section is currently at maximum temperatures at the present-day, and is not affected by past higher heat flow. In contrast, the section below 5000 m is predicted to still record the effects of the high heat flow event, and as a consequence this section will not have regenerated hydrocarbons during the Tertiary - see also Figure 3.7 and the text for details.

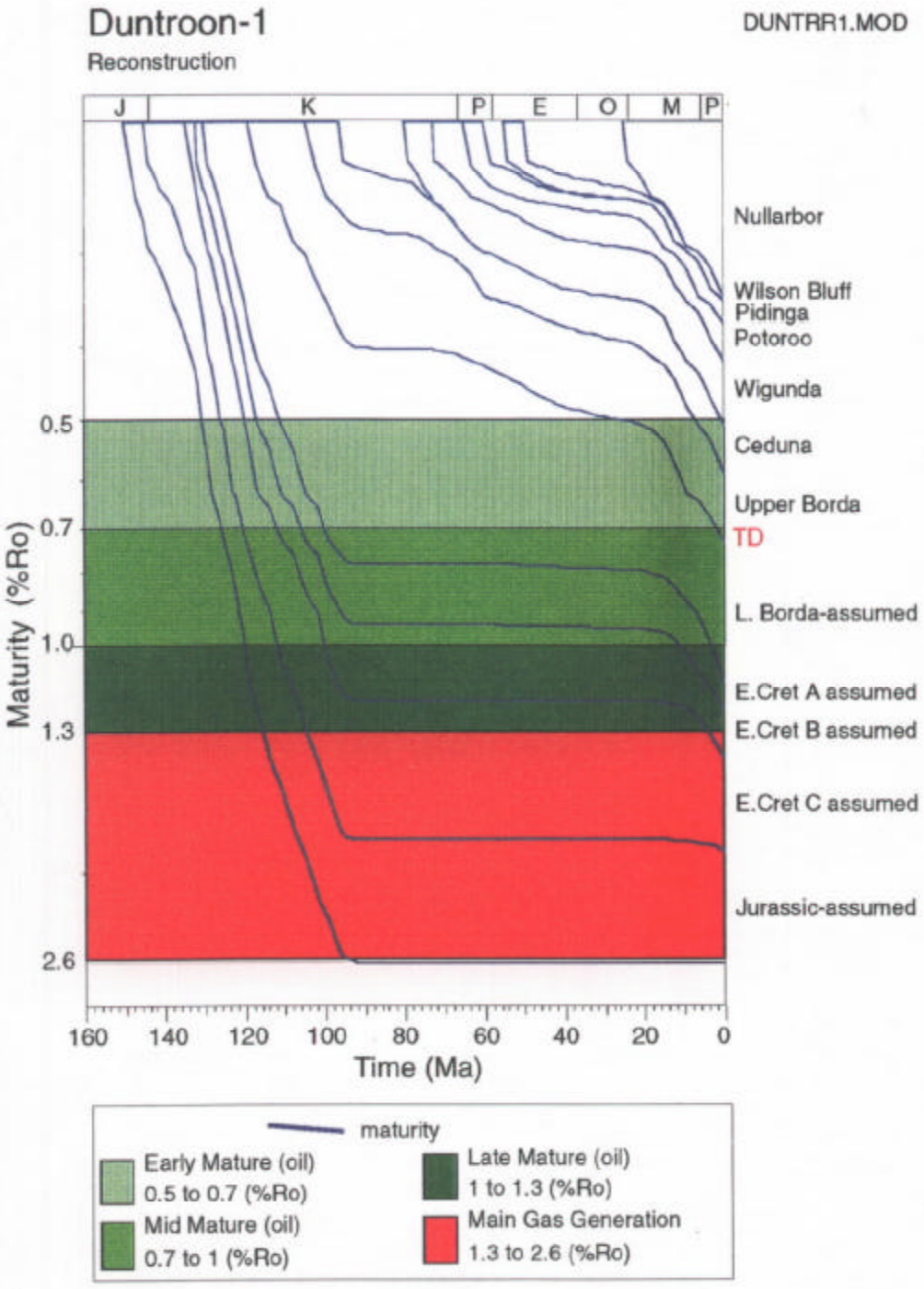


**Figure 3.7:** Predicted development of maturity with time in the **Duntroon-1 well, Duntroon Basin,** controlled by the AFTA and VR data. Around 3000 m of section containing potential Early Cretaceous and Jurassic source rocks was actively generating hydrocarbons at maturities from 0.5% up to ~2.0% $R_o$max during the period from ~25 Ma to the present-day. The relatively thick Tertiary section (Figure 3.3) ensured this outcome in spite of an early phase of hydrocarbon generation from the deeper of these potential source rocks prior to regional **Mid-Cretaceous** cooling ~95 Ma. - See text for details.

# 4. Concluding remarks on the geological history of the Duntroon Basin

## 4.1 Elevated Mid-Cretaceous heat flow - "inverted" maturation in Australia's Southern margin basins

The regional significance of elevated Mid-Cretaceous paleogeothermal gradients in the Australia's Southern margin basins, including the Duntroon Basin has been discussed previously in Geotrack Report #569 (concerning the Vivonne-1 and Borda-1 wells in the Duntroon Basin). Measured paleogeothermal gradients in the Mid-Cretaceous (~95 Ma) are consistently around 60°C/km, declining rapidly by the early Late Cretaceous (~80 Ma) to values similar to present-day values which are typically near ~30°C/km.

Thus, even at locations such as Platypus-1 and Duntroon-1 analysed here, where subsequent burial by thick Late Cretaceous and Tertiary sections has masked any direct evidence for elevated Mid-Cretaceous heat flow, this event must be incorporated in prospect assessment as it exerts a key control of hydrocarbon generation from potential Early Cretaceous and older source rocks.

The major effect of this elevated heat flow is that a large part of the potential Jurassic to Early Cretaceous source rock-bearing sequence will have generated hydrocarbons prior to the Mid-Cretaceous. At some basin locations this will have significantly decreased the source rock volume available for generation in the structurally more favourable Tertiary to Recent time period.

However, in areas where these potential Jurassic to Early Cretaceous source rocks have been subsequently buried sufficiently by Late Cretaceous and, in particular, Tertiary section (e.g., Platypus-1 and Duntroon-1), a second phase of hydrocarbon generation can occur from these source rocks. Such a maturation scenario is characterised by a distinct pattern, referred to here as "inverted maturation", as it is the source rocks shallower in the pre-Mid Cretaceous section that recommence maturation prior to those deeper in the section.

This is graphically illustrated in Figures 2.7 and 3.7 for Platypus-1 and Duntroon-1, respectively.

In general, recognition of the regional effects of elevated Early Cretaceous heat flow allows the post-mid Cretaceous burial history to be used in order to identify areas with optimum Late Tertiary hydrocarbon generation. For example, in areas with a large thickness of Late Cretaceous deposition and little Tertiary deposition, hydrocarbon generation from Early Cretaceous source rocks will recommence early,

resulting in a less favourable scenario for hydrocarbon accumulation and preservation than at Platypus-1 and Duntroon-1, for instance. This is illustrated in Figures 4.1 and 4.2, showing hypothetical burial and maturation histories at a site (Prospect A) with 4000 m of Late Cretaceous section and 200 m of Tertiary section overlying the Early Cretaceous source sequence, using the regional thermal history discussed above (i.e., 60°C/km declining to 30°C/km by ~80 Ma and maintained to the present-day).

The maturation-time plot shows that most of the Early Cretaceous section reached a maturity >1.3% Ro(max) prior to 60 Ma, and would have therefore generated most of its oil by this time. Only around 500 m at the top of the Early Cretaceous could have generated oil during the Tertiary, and at a relatively slow rate.

Conversely, in areas with a relatively thin Late Cretaceous section, temperatures reached during the important Tertiary-Recent period may not be high enough to cause maturation to recommence in Early Cretaceous source rocks at levels that will generate hydrocarbons, even when Tertiary burial is relatively large. This is illustrated in Figures 4.3 and 4.4, which show hypothetical burial and maturation histories at a site (Prospect B) with 350 m Late Cretaceous section and 1000 m of Tertiary section overlying the Early Cretaceous source sequence (using the same regional thermal history discussed above with 60°C/km up to 95 Ma declining to 30°C/km by ~80 Ma and maintained to the present-day). In this case, the maturation-time plot shows that most of the Early Cretaceous section reached maximum maturities between ~0.5 and 2.8% prior to 95 Ma, and would have therefore generated most of its oil by this time. Only around 500 m at the top of the Mid early Cretaceous unit could have generated minor oil at low maturities during the Tertiary.

Thus, recognition of the fundamental control that the thermal history places on source rock maturation allows the distribution of the main sediment packages to be used as a simple tool for focussing exploration in the most prospective areas.

## 4.2 Provenance of the Cretaceous sediments - Cl content of detrital apatite

A link between the provenance of apatites in the Early Cretaceous Otway Group and chlorine content of contained apatite has been established for more than a decade. Sediments derived from contemporaneous volcanogenic sources show a wide range of Cl abundance in the derived apatites due to derivation from a range of igneous rock types, while sediment derived from a granitic basement-type provenance have a very narrow range of Cl-contents. Typical "volcanogenic-type" distributions based on a large number of samples from the volcanogenic Otway Group are shown in Figure C.4.c.

Distributions of Cl in apatite from the thirteen AFTA samples from Platypus-1 and Duntroon-1 analysed in this study are given in Figures A.3 a and b (Appendix A).

The broad apatite chlorine distributions in samples from the Early Cretaceous section in both wells provide clear evidence of derivation of most of the Early Cretaceous detritus from contemporaneous explosive volcanic activity as seen previously in the Duntroon Basin (Geotrack Report #569).

In the case of Platypus-1 and Duntroon-1, however, both the Cl data and the fission track ages (Figures B.5 and b) suggest significant reworking of the Early Cretaceous detritus into the Late Cretaceous sequence (e.g., samples GC589-3, 5, 8 and 9 in Platypus-1 and 8622-43 and 45 in Duntroon-1), presumably as a consequence of nearby mid-Cretaceous uplift and erosion. This reworking will potentially have an effect on the quality of Late Cretaceous reservoir sands. The increase in labile materials including feldspar and volcanic rock fragments expected to accompany the apatites and diluting the quartzose detritus of the normal basement provenance, will tend to result in both lower porosity and permeability in these Late Cretaceous sandstones.

## 4.3 Comments on Tertiary heating - hot fluid flow

There is only tenuous evidence from the supplied VR data for a Miocene to Recent heating episode in the Duntroon-1 well. The VR pattern is not well supported by the few new VR determinations in the shallow part of the sequence, but at face value the data suggest a local transient thermal effects that could be due to flow of heated fluids through suitable porous sections in the Tertiary section including the Nullarbor Limestone.

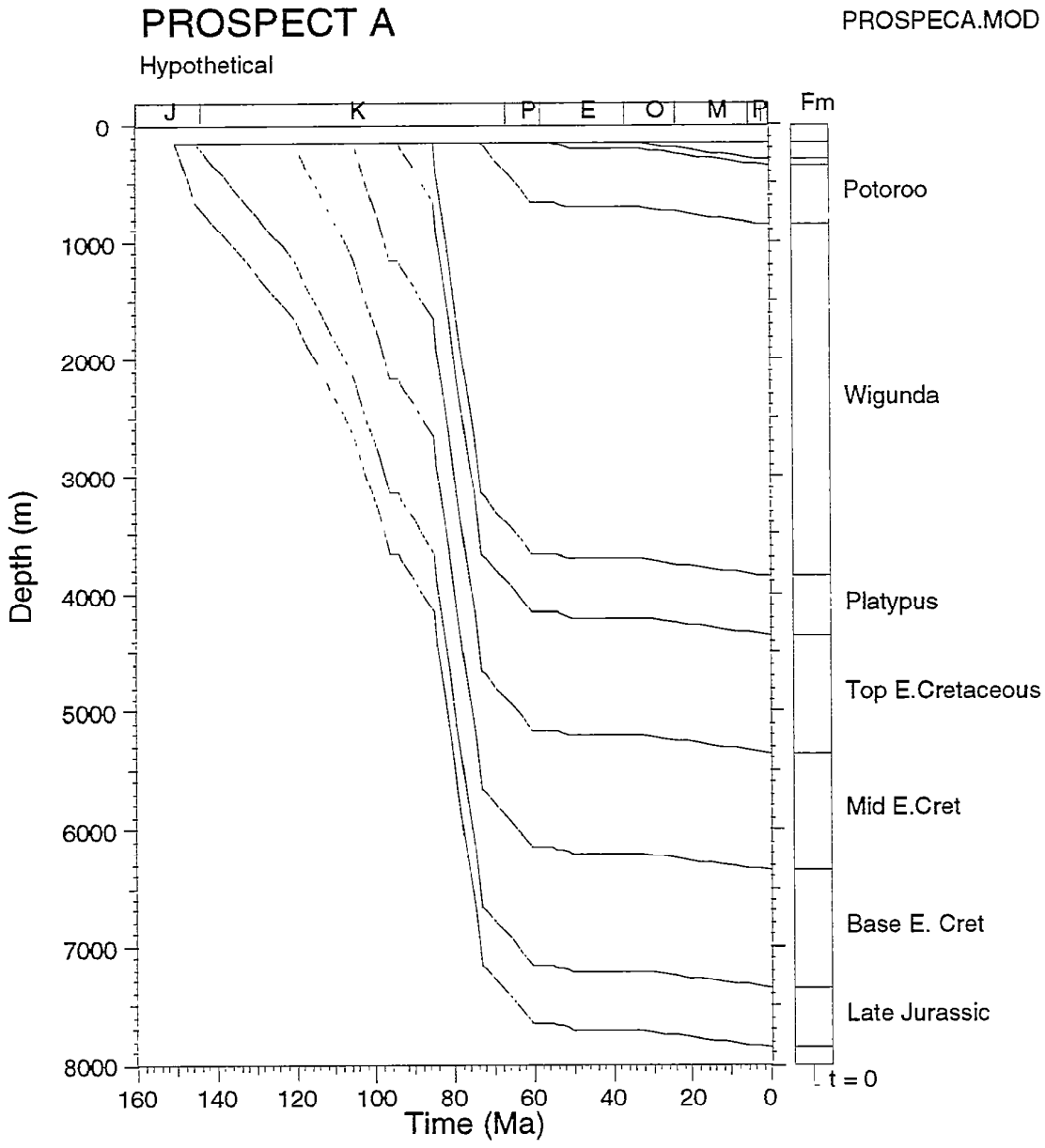


**Figure 4.1:** Burial History for an hypothetical **Duntroon Basin Prospect (A)** with 200 m of Tertiary section, and 4000 m of Late Cretaceous section overlying the Early Cretaceous-Jurassic source-rock bearing sequence. See Figure 4.2 for predicted maturation with time.

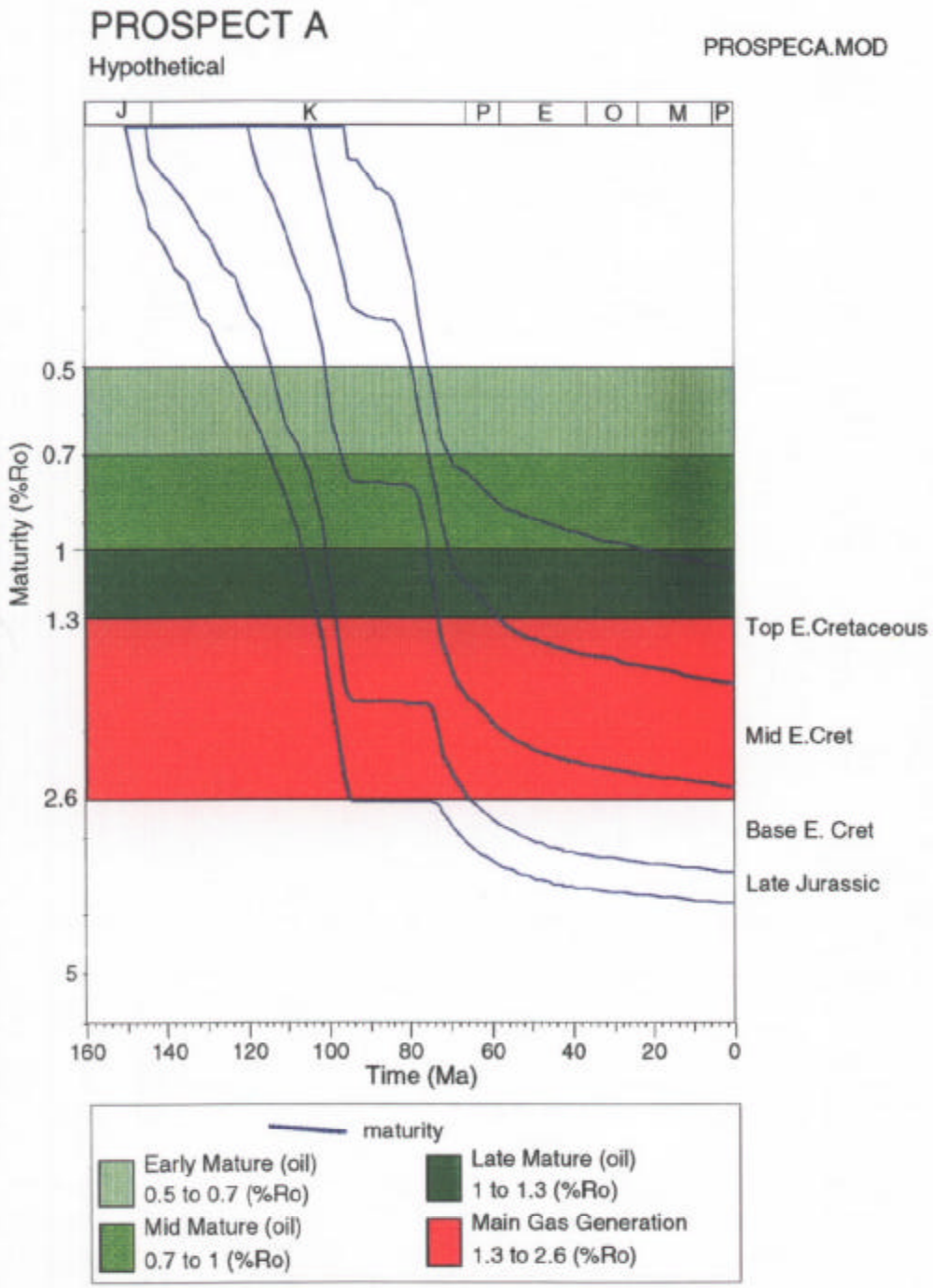


**Figure 4.2:** Predicted development of maturity with time for hypothetical **Duntroon Basin Prospect (A)** based on the burial history shown in Figure 4.1 and the regional thermal history with 60°C/km up to 95 Ma declining to 30°C/km by ~80 Ma and maintained to the present-day. Most of the Early Cretaceous section reached a maturity >1.3% Ro(max) prior to 60 Ma, and would have therefore generated most of its oil by this time. Only around 500 m at the top of the Early Cretaceous could have generated oil during the Tertiary.

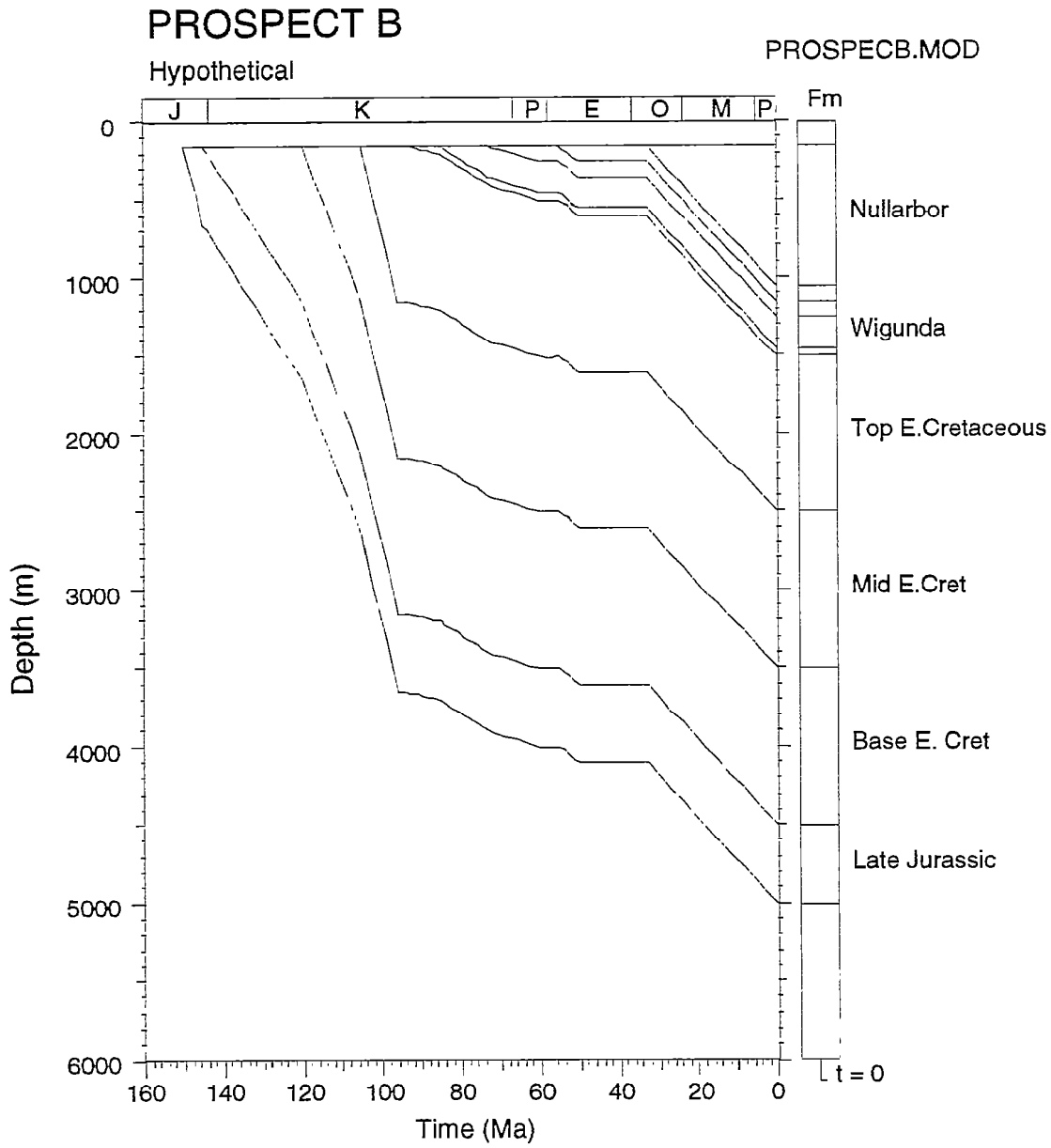


**Figure 4.3:** Burial History for an hypothetical **Duntroon Basin Prospect (B)** with 1000 m of Tertiary section, and 350 m of Late Cretaceous section overlying the Early Cretaceous-Jurassic source-rock bearing sequence. See Figure 4.4 for predicted maturation with time.

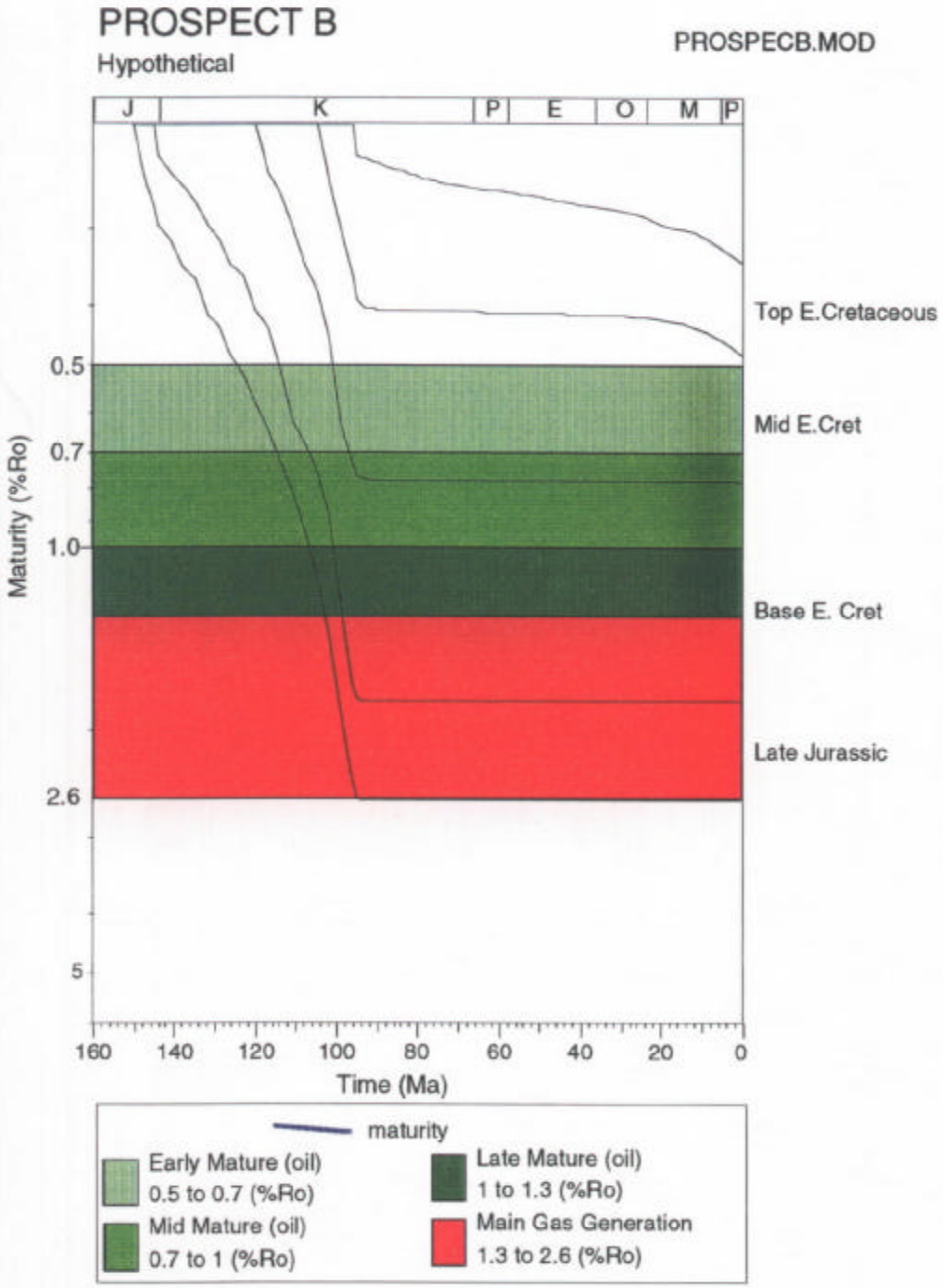


**Figure 4.4:** Predicted development of maturity with time for hypothetical **Duntroon Basin Prospect (B)** based on the burial history shown in Figure 4.3 and the regional thermal history with 60°C/km up to 95 Ma declining to 30°C/km by ~80 Ma and maintained to the present-day. In this case, most of the Early Cretaceous section reached maximum maturities between ~0.5 and 2.8% prior to 95 Ma, and would have therefore generated most of its oil by this time. Only around 500 m at the top of the Mid early Cretaceous unit could have generated minor oil at low maturities during the Tertiary.

# 5. Further work which would significantly improve knowledge of the geological history of the region

## 5.1 Early Cretaceous high heat flow

Previous work (Geotrack Report #569) has shown conclusively the occurrence of highly elevated Early Cretaceous heat flow in the Duntroon Basin. It is recommended that AFTA and selected VR data be collected on the Echidna-1 well, in which open file VR data suggest a similar high paleogeothermal gradient, in order to more fully document the elevated heat-flow event and its effect on regional source rock maturation patterns.

## 5.2 Late Tertiary to Recent hot fluids:

Existing VR data from the Nullarbor Limestone section in Duntroon-1 suggest a transient lateral heating episode has affected the section. This event has not been specifically investigated with new samples in this study, but the problem could be addressed using a combined AFTA, VR and fluid inclusion approach.

## References

Burnham, A. K. and Sweeney, J. J. (1989). A chemical kinetic model of vitrinite reflectance maturation. *Geochimica et Cosmochimica Acta.*, 53, 2649-2657.

Corrigan, J. D. (1991). Thermal anomalies in the Central Indian Ocean: Evidence for de-watering of the Bengal Fan. *Journal of Geophysical Research*, 96, 14263 - 14275.

Duddy, I. R. (1983). The geology, petrology and geochemistry of the Otway Formation volcanogenic sediments. Ph.D thesis, University of Melbourne (unpubl.), 426pp.

Duddy, I. R. (1994). The Otway Basin: Thermal, structural, tectonic and hydrocarbon generation histories. *In*: Finlayson, D. M. (*compiler*), NGMA/PESA Otway Basin Symposium, Melbourne, April 20, 1994. Australian Geological Survey Organisation, Record 1994/14.

Green, P. F., Duddy, I. R., Gleadow, A. J. W., Tingate, P. R. and Laslett, G. M. (1985). Fission track annealing in apatite: Track length measurements and the form of the Arrhenius Plot. *Nuclear Tracks*, 10, 323-328.

Duddy, I. R., Green, P. F., Hegarty, K. A. and Bray, R. J. (1991). Reconstruction of thermal history in basin modelling using Apatite Fission Track Analysis: what is really possible. Proceedings of the First Offshore Australia Conference (Melbourne). III-49 - III-61.

Green, P. F., Duddy, I. R. and Bray, R. J. (1995). Variation in thermal history styles around the Irish Sea and adjacent areas: implications for hydrocarbon occurrence and tectonic evolution. *In:* Petroleum Geology of the Irish Sea and adjacent areas. The Geological Society, Special Publication. Submitted 1995.

Sweeney, J. J. and Burnham, A. K. (1990). Evaluation of a simple model of vitrinite reflectance based on chemical kinetics. *The American Association of Petroleum Geologists' Bulletin*, 74, 1559 - 1570.

Waples, D. W., Kamata, H. and Suizu, M. (1992). The art of maturity modelling. Part 1: Finding a satisfactory geologic model. *The American Association of Petroleum Geologists' Bulletin*, 76, 31 - 46.

# APPENDIX A

## Sample Details, Apatite Compositions and Geological Data

### A.1 Sample details

Six AFTA and 17 VR samples from the **Platypus-1** well and eight AFTA and 15 VR samples from the **Duntroon-1 well, Duntroon Basin, South Australia** were analysed using Apatite Fission Track Analysis (AFTA®), on behalf of **BHP Petroleum (Australia/Asia Region).** The report was completed in February 1996.

AFTA samples from Platypus-1 and VR samples from Platypus-1 and Duntroon-1 were obtained from AGSO and the Petroleum Division Mines and Energy South Australia (MESA). Eight open file AFTA samples from Duntroon-1 (Geotrack Report #44 for BP Australia, 1986) were recounted and reprocessed for this report.

In addition, existing VR data on 33 samples from Platypus-1 and 34 samples from Duntroon-1 (Table D.3, Appendix D) were supplied by BHPP, and have been compared with the new data set in order to provide a quality assessment of the existing data.

Details of all samples, including depths and stratigraphic ages and present temperatures, supplied by BHPP, are listed for each sample in Table A.1.

### A.2 Stratigraphic details

The details of each stratigraphic interval in the preserved sections of Platypus-1 and Duntroon-1 were supplied by BHPP. Also supplied were the depths (mKB) of each AFTA and VR sample. Based on the chronostratigraphic age, a numerical age (Ma) was assigned for each sample using Harland et al. (1989). The stratigraphic ages, or age ranges, of each AFTA sample are summarised in Table A.1.

### A.3 Present temperatures

In application of any technique involving estimation of paleotemperatures, it is critical to control the present temperature profile, since estimation of maximum paleotemperatures proceeds from assessing how much of the observed effect can be explained by the magnitude of present temperatures.

Extrapolated formation temperatures were supplied by BHPP for a number of log runs in both Duntroon-1 and Platypus-1 and no further correction were applied to these values. In addition, a single measured BHT value in Platypus-1 was corrected using a simplified correction procedure adapted from the literature (Oxburgh and Andrews-Speed, 1981; Andrews-Speed et al., 1984). This procedure corrects measured BHT data by increasing the difference between the sea-bed temperature (assumed to be 10°C) and the uncorrected BHT value by 20% for uncorrected temperatures below 150°F (66°C), and by 25% above 150°F. Uncorrected and corrected BHT data from each well are summarised in Table A.2.

The corrected temperature values in **Platypus-1** define a broadly linear trend (Figure A.1) with an average linear gradient of 30.9°C/km, constrained using all BHT data and a sea-bed temperature of 10°C, as summarised in Table A.2. For **Duntroon-1**, the corrected temperature values (Table A.2) define a present-day geothermal gradient of 32.6°C/km when combined with an assumed sea-bed temperature of 10°C (Figure A.1).

In general, the simple linear geothermal gradient in each well is considered to provide an adequate representation of the present-day geothermal regime in both wells, providing reasonable estimates of the present temperature for each AFTA and VR sample. This interpretation is also supported by the AFTA data in most samples, which are consistent with the present temperatures estimated in this way. Likely departures from this trend should not have any significant effect on the thermal history interpretations presented in this report.

## A.4 Apatite yields

Yields of detrital apatite obtained after mineral separation from all samples processed are summarised in Table A.1. Yields varied from none to excellent, with samples providing between zero and more than 20 grains suitable for fission track age determination. Most samples (eight of fourteen) provided 20 grains (Table A.1). Generally, in the Mesozoic to Tertiary sequences of southern Australia, the better apatite yields are obtained from the volcanogenic Early Cretaceous section, with poor to fair yields characterising the more quartzose Late Cretaceous and Tertiary sandstones. This is also generally true for the apatite recovery in Duntroon-1, although an excellent yield was also obtained from one of the two Pidinga (Paleocene) sandstones processed (Table A.1). In the case of Platypus-1, however, excellent yields of apatite were provided by sandstones from the Late Cretaceous Platypus and Wigunda units (Table A.1), but analysis of the AFTA age and Cl-compositional data suggests that the majority of these apatite were probably reworked from Early Cretaceous volcanic sources (see text for further provenance discussion).

Two of the six Platypus-1 samples with apatite provided more than 30 confined track length measurements and are considered of very high quality, with three of the remaining samples giving between seven and 19 measurements, which are adequate for general conclusions. In Duntroon-1, more than 40 length were obtained from four samples, 14 and 16 from two samples, with no length measurements from the remaining two samples.

The quality of the etched surfaces of the apatites obtained for analysis was high in all samples, and the overall high quality of the AFTA data in key samples results in reliable thermal history interpretations for the two wells studied.

## A.5 Apatite quality and grain morphologies

The majority of apatite grain morphologies from the Late Cretaceous and Early Cretaceous section are euhedral to sub-rounded euhedral forms, consistent with either a direct provenance from Early Cretaceous contemporaneous volcanic activity ( Duddy, 1983), or reworked from such sources during the Late Cretaceous, as discussed above and in the text.

The Paleocene sample 8622-41 (Pidinga Fm) from Duntroon-1 provided a similar mixture of euhedral to sub-rounded euhedral forms but the AFTA age data suggest derivation from a pre-existing Paleozoic or older basement source terrain (see text).

## A.6 Apatite compositions

The annealing kinetics of fission tracks in apatite are affected by chemical composition, specifically the Cl content, as explained in more detail in Appendix C. Compilation of data from a wide variety of geological environments from around the world suggests that apatites from common sedimentary rocks (such as quartzo-feldspathic sandstones) are characterised by a distribution of chlorine contents similar to the distribution shown in Figure C.4b. The majority of grains from quartzo-feldspathic sandstones have chlorine contents between 0 and 0.1 wt%, while a smaller number of grains give values up to ~0.5 wt%, close to the value found in the Durango apatite, on which Geotrack's original kinetic model of fission track behaviour was based (Appendix C). Occasional grains may give Cl contents up to ~1 wt%, but higher amounts are unusual. On the other hand, apatite grains from volcanogenic sandstones have chlorine contents between 0 and ~3 wt%, as shown in Figure C.4c, indicative of derivation from a wide range of original volcanic rock types.

For this study, chlorine compositions were determined for all individual apatite grains in which fission track ages were determined and/or lengths were measured. Chlorine contents were measured using a semi-automated Jeol JXA-5A electron microprobe equipped with three wavelength dispersive crystal spectrometers, with an accelerating voltage of 15 KV and beam current of 25 nA. The beam was defocussed to 20μm to avoid the problems associated with apatite decomposition, which occur under a fully focussed 1μm - 2μm beam. The X-Y co-ordinates of apatite grains within the grain mount were transferred from the Autoscan Fission Track Stage to a file suitable for direct input into the electron microprobe. Pure rock salt (NaCl) was used to peak the spectrometer for chlorine, which was the only element determined in each apatite grain. Cl count rates were converted to wt% Cl by reference to measured count rates for a Durango Apatite standard (Melbourne University Standard APT151), analysed at regular intervals during an analysis session. A value of 0.43 wt% Cl was used for Durango APT151, based on repeated measurements of the same fragment using pure rock salt (NaCl) as the ultimate standard for chlorine. This approach giving essentially identical results to Cl determined from full compositional measurements of apatite, but has the advantage of reducing measurement time by a factor of 10 or more.

Using this approach, lower limits of detection for chlorine content have been calculated for typical analytical conditions (beam current, counting time, etc.) and are listed in Table A.4. Errors in wt% composition are given as a percentage and quoted at 1σ for chlorine determinations. A generalised summary of error values for various values of wt% chlorine is presented in Table A.5.

The measured range of chlorine contents of apatites (both age and length grains) within each sample is shown in histogram format in Figure A.3. Plots of single grain age versus weight % chlorine are shown in Figure B.5. Chlorine contents, which are presented in numerical format for dated grains only, appear in the fission track age summary sheets in Appendix B. The chlorine data are employed in interpreting the AFTA data for each sample, using methods outlined in Appendix C.

## References

Andrews-Speed, C. P., Oxburgh, E. R. and Cooper, B. A. (1984). Temperatures and depth-dependent heat flow in the South-western North Sea. *In:* L. V. and Hobson, G. D. (*eds.*), The petroleum geology of the continental shelf of NW Europe, 3, 141-151.

Duddy, I. R. (1983). The geology, petrology and geochemistry of the Otway formation volcanogenic sediments. Ph.D thesis, University of Melbourne (unpubl.), 426pp.

Harland, W. B., Armstrong, R. L., Cox, A. V., Craig, L. E., Smith, A. G. and Smith, D. G. (1989). A geologic time scale 1989, Cambridge University Press.

Oxburgh, E. R. and Andrews-Speed, C. P. (1981). Temperatures and depth-dependent heat flow in the Western North Sea. *AAPG Bulletin*, 68, 1764-1781.

# Table A.1: Details of AFTA samples and apatite yields - well samples from the Duntroon Basin (Geotrack Report #589)

| Sample number | Depth (m) | Sample type | Stratigraphic subdivision | Stratigraphic age (Ma) | Present temperature *1 (°C) | Raw weight (g) | Washed weight (g) | Apatite yield *2 |
|---|---|---|---|---|---|---|---|---|
| **Platypus-1** | | | | | | | | |
| GC589-3 | 1900-2000 *(6234-6562')* | cuttings | Potoroo | 73-65 | 64 | 510 | 84 | Fair |
| GC589-5 | 2200-2300 *(7218-7547')* | cuttings | Wigunda | 85-73 | 74 | 650 | 93 | Excellent |
| GC589-8 | 2550-2650 *(8367-8694')* | cuttings | Wigunda | 85-73 | 85 | 730 | 512 | Excellent |
| GC589-9 | 2870-2950 *(9416-9678')* | cuttings | Wigunda | 85-73 | 94 | 650 | 482 | Excellent |
| GC589-10 | 2990-3090 *(9810-10138')* | cuttings | Platypus | 96-85 | 98 | 410 | 130 | Excellent |
| GC589-12 | 3390-3490 *(11123-11451')* | cuttings | Ceduna | 100-96 | 110 | 380 | 216 | Poor |
| **Duntroon-1** | | | | | | | | |
| 8622-40 | 1500 *(4922')* | cuttings | Wilsons Bluff | 55-50 | 53 | - | - | None |
| 8622-41 | 1630 *(5348')* | cuttings | Pidinga | 65-60 | 58 | - | - | Excellent |
| 8622-42 | 1800 *(5906')* | cuttings | Pidinga | 65-60 | 63 | - | - | Very Poor |
| 8622-43 | 2100 *(6890')* | cuttings | Wigunda | 85-73 | 73 | - | - | Fair |
| 8622-45 | 2507 *(8225')* | cuttings | Wigunda | 85-73 | 86 | - | - | Fair |
| 8622-46 | 2700 *(8859')* | cuttings | Ceduna | 100-96 | 92 | - | - | Excellent |
| 8622-47 | 3000 *(9843')* | cuttings | Upper Borda | 119-100 | 102 | - | - | Excellent |
| 8622-49 | 3510 *(11516')* | cuttings | Upper Borda | 119-100 | 119 | - | - | Excellent |

*1 See Appendix A for discussion of present temperature data.

*2 Yield based on quantity of mineral suitable for age determination. Excellent: >20 grains; Very Good: ~20 grains; Good: 15-20 grains; Fair: 10-15 grains; Poor: 5-10 grains; Very Poor: <5 grains.

Note: All depths quoted are TVD with respect to KB.

## Table A.2: Summary of present temperature measurements - wells from the Duntroon Basin (Geotrack Report #589)

| Sea bed (ft) | Sea bed (m) | Depth (log) (ft) | Uncorrected temperature (°F) | Uncorrected temperature (°C) | Time since circulation (hrs) | Depth (m) | Corrected temperature (°C) | Geothermal gradient (°C/km) |
|---|---|---|---|---|---|---|---|---|
| **Platypus-1** | | | | | | | | |
| 617 | 188 | 3944 | - | 39 | - | 1202 | 43.8 | 30.9 |
| | | 9003 | - | - | - | 2744 | 81* | |
| | | 12014 | - | - | - | 3662 | 119* | |
| | | 12730 | - | - | - | 3880 | 127* | |
| **Duntroon-1** | | | | | | | | |
| 558 | 170 | 7595 | - | - | - | 2315 | 76* | 32.6 |
| | | 11483 | - | - | - | 3500 | 121* | |

Quoted BHT values have been corrected by increasing the difference between sea bed temperature and measured BHT by 20% for measured temperatures <150°F (<66°C) and by 25% for temperatures >150°F (>66°C). A sea bed temperature of 10°C has been assumed.
All depths quoted are with respect to KB, except where otherwise stated.
*Data are extrapolated formation temperatures supplied by client.

Table A.3: Summary of stratigraphy - wells from the Duntroon Basin (Geotrack Report #589)

| | KB elevation (mAMSL) | Water Depth (m) | Stratigraphic Interval | Age of Top (Ma) | Depth of Top TVD rKB (m) |
|---|---|---|---|---|---|
| **Platypus-1** | | | | | |
| | 30 | 158 | Nullabor Lst | 0 | 188 |
| | | | *Unconformity* | 33 | 1636 |
| | | | Wilsons Bluff | 50 | 1636 |
| | | | *Unconformity* | 55 | 1893 |
| | | | Potoroo Fm | 65 | 1893 |
| | | | Wigunda | 73 | 2162 |
| | | | Platypus | 85 | 2974 |
| | | | Ceduna | 96 | 3368 |
| | | | Upper Borda | 100 | 3713 |
| | | | Total Depth | 115 | 3893 |
| **Duntroon-1** | | | | | |
| | 26 | 144 | Nullabor Lst | 0 | 170 |
| | | | *Unconformity* | 33 | 1513 |
| | | | Wilsons Bluff | 50 | 1513 |
| | | | *Unconformity* | 55 | 1630 |
| | | | Pidinga | 60 | 1630 |
| | | | Potoroo Fm | 65 | 1833 |
| | | | Wigunda | 73 | 2085 |
| | | | *Unconformity* | 85 | 2570 |
| | | | Ceduna | 96 | 2570 |
| | | | Upper Borda | 100 | 2924 |
| | | | Total Depth | 119 | 3515 |

All depths quoted are with respect to KB, except where otherwise stated.

**Table A.4: Lower Limits of Detection for Apatite Analyses (Geotrack Report #589)**

| Element | LLD (95% c.l.) | | LLD (99% c.l.) | |
|---|---|---|---|---|
| | (wt%) | (ppm) | (wt%) | (ppm) |
| Cl | 0.01 | 126 | 0.02 | 182 |

**Table A.5: Per cent errors in chlorine content (Geotrack Report #589)**

| Chlorine content (wt%) | Error (%) |
|---|---|
| 0.01 | 9.3 |
| 0.02 | 8.7 |
| 0.05 | 7.3 |
| 0.10 | 6.1 |
| 0.20 | 4.7 |
| 0.50 | 3.2 |
| 1.00 | 2.3 |
| 1.50 | 1.9 |
| 2.00 | 1.7 |
| 2.50 | 1.5 |
| 3.00 | 1.4 |

Errors quoted are at 1σ. See Appendix A for more details.

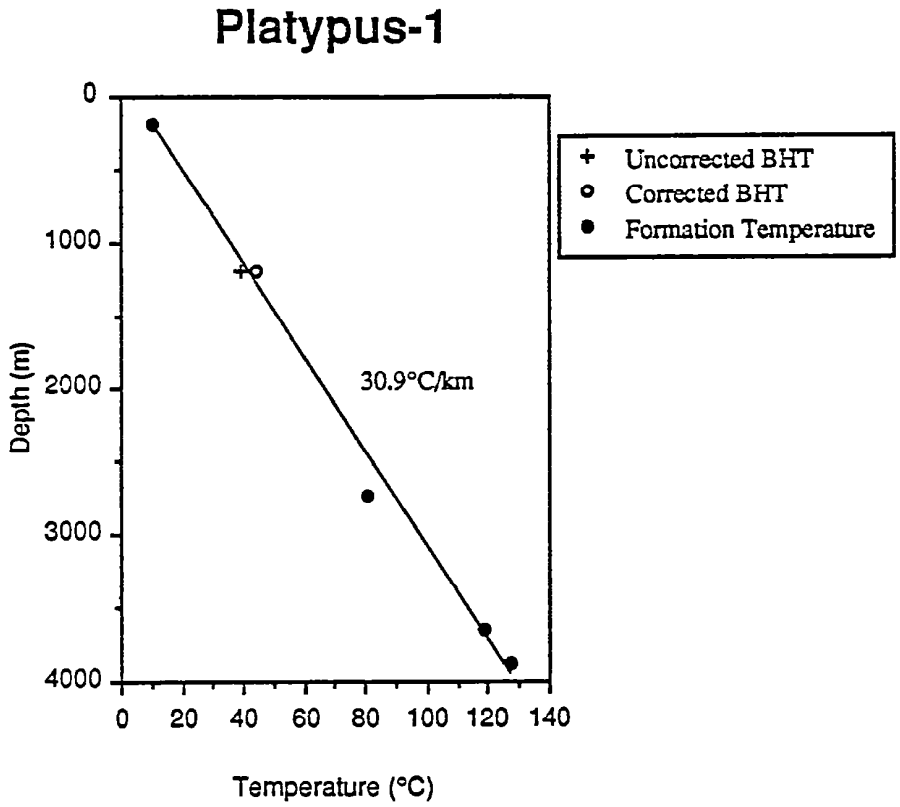


**Figure A.1:** Present temperature profile calculated for well **Platypus-1, Duntroon Basin.** See Table A.2 and Appendix A for more detail.

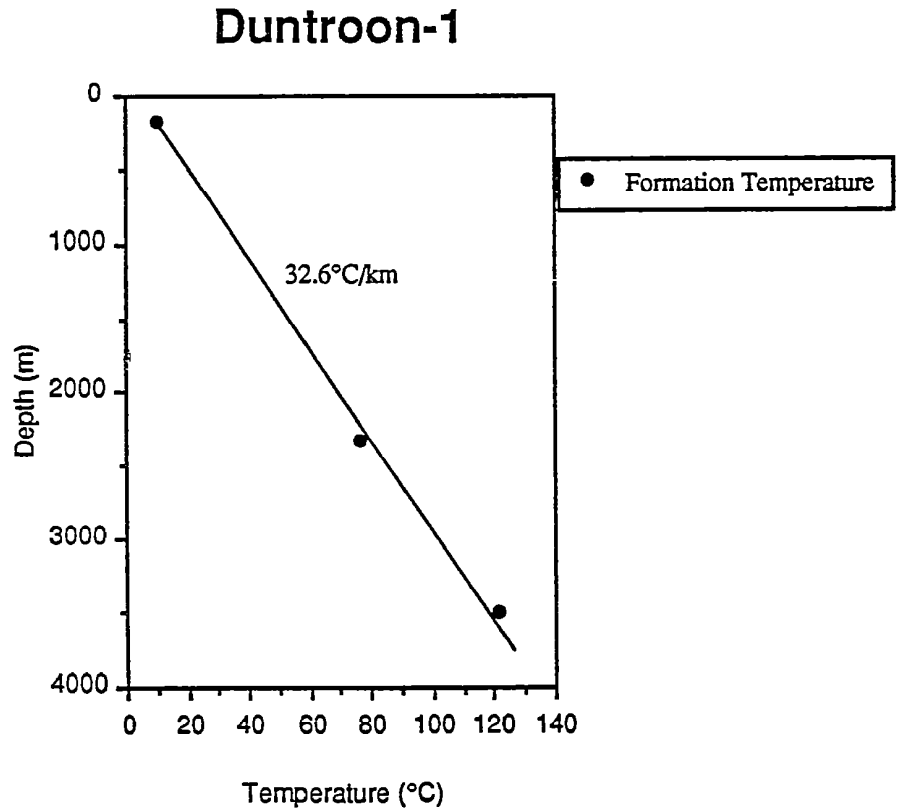


**Figure A.2:** Present temperature profile calculated for well **Duntroon-1, Duntroon Basin.** See Table A.2 and Appendix A for more detail.

GC589-3

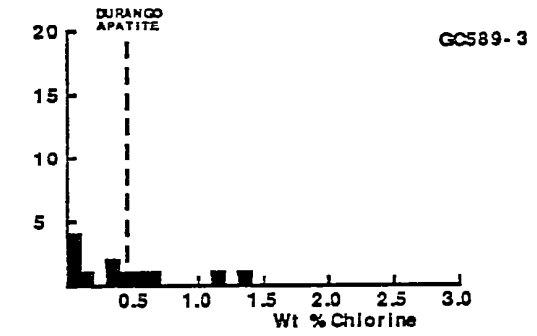


GC589-10

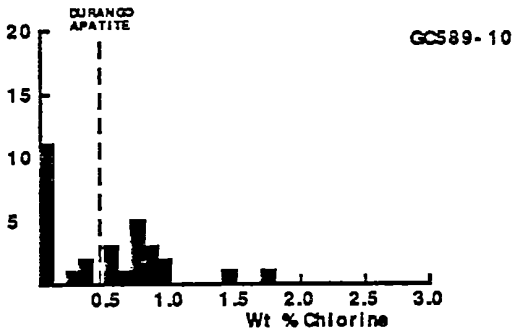


GC589-5

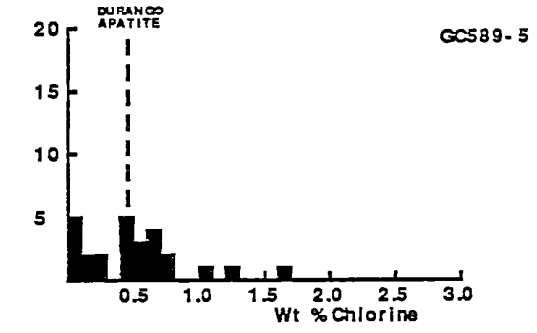


GC589-12

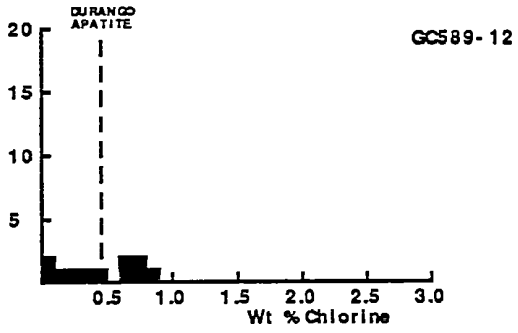


GC589-8

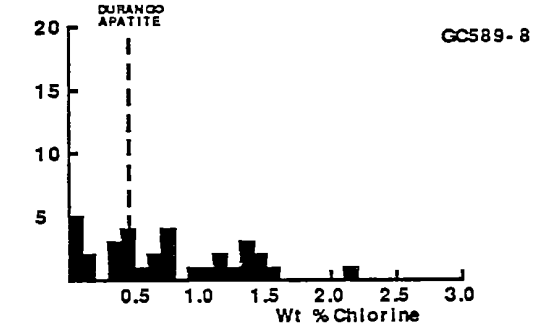


GC589-9

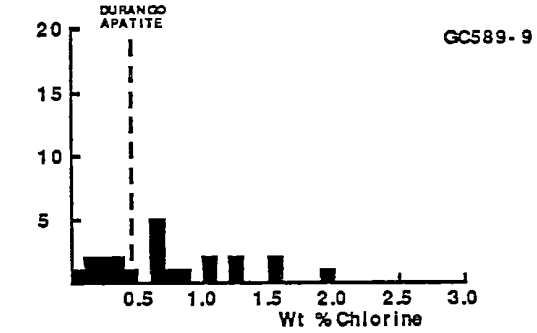


**Figure A.3a:** Distributions of chlorine content in samples from well **Platypus-1, Duntroon Basin.**

8622-40

No Apatite

8622-45

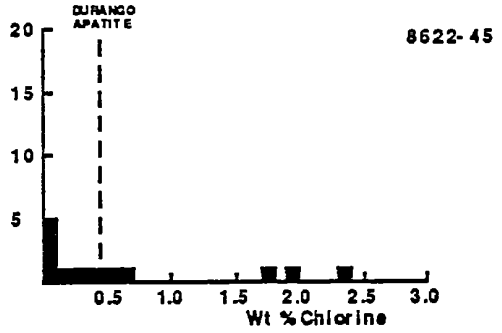


8622-41

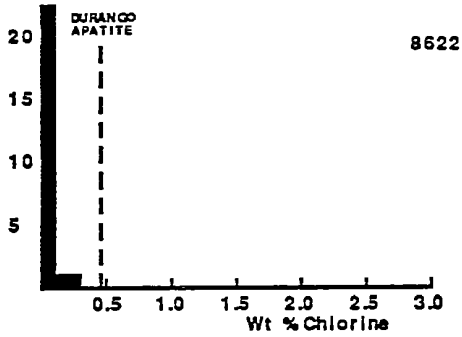


8622-46

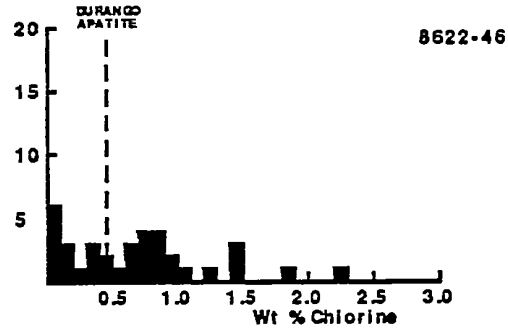


8622-42

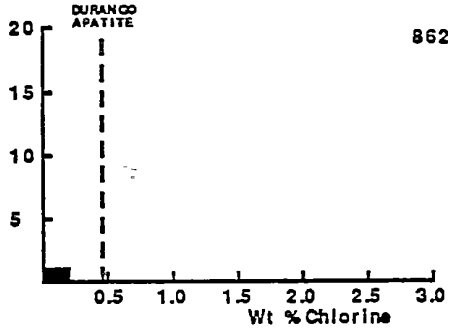


8622-47

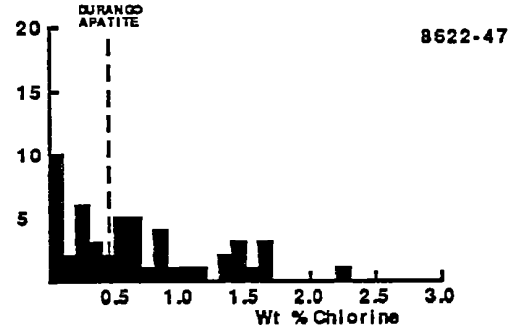


8622-43

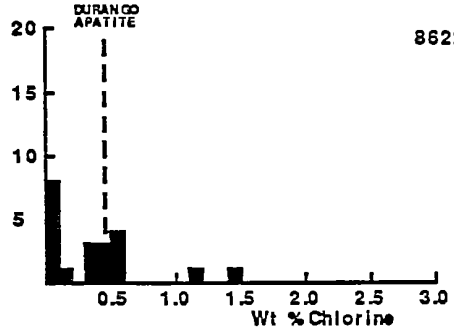


8622-49

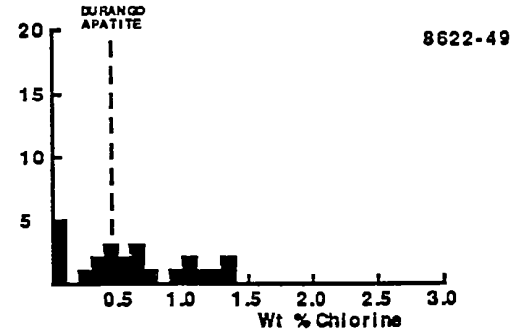


**Figure A.3b:** Distributions of chlorine content in samples from well **Duntroon-1**, **Duntroon Basin.**

# APPENDIX B

## Sample Preparation, Analytical Details and Data Presentation

### B.1 Sample Preparation

Core and outcrop samples are crushed in a jaw crusher and then ground to sand grade in a rotary disc mill. Cuttings samples are washed and dried before grinding to sand grade. The ground material is then washed to remove dust, dried and processed by conventional heavy liquid and magnetic separation techniques to recover heavy minerals. Apatite grains are mounted in epoxy resin on glass slides, polished and etched for 20 sec in 5M $HNO_3$ at 20°C to reveal the fossil fission tracks.

After etching, all mounts are cut down to 1.5 X 1 cm, and cleaned in detergent, alcohol and distilled water. The mounts are then sealed in intimate contact with low-uranium muscovite detectors within heat-shrink plastic film. Each batch of mounts is stacked between two pieces of uranium standard glass, which has been prepared in similar fashion. The stack is then inserted into an aluminium can for irradiation.

After irradiation, the mica detectors are removed from the grain mounts and standard glasses and etched in hydrofluoric acid to reveal the fission tracks produced by induced fission of $^{235}U$ in the apatite and standard glass.

### B.2 Analytical Details

***Fission track ages***

Fission track ages are calculated using the standard fission track age equation using the zeta calibration method (equation five of Hurford and Green, 1983), viz:

$$\text{F.T. AGE} = \frac{1}{\lambda_D} \ln \left[ 1 + \left( \frac{\zeta \lambda_D \rho_s g \rho_D}{\rho_i} \right) \right] \qquad \text{B.1}$$

where:
- $\lambda_D$ = Total decay constant of $^{238}U$ ( = 1.55125 x $10^{-10}$)
- $\zeta$ = Zeta calibration factor
- $\rho_s$ = Spontaneous track density
- $\rho_i$ = Induced track density
- $\rho_D$ = Track density from uranium standard glass
- g = A geometry factor (= 0.5)

Fission track ages are determined by the external detector method or EDM (Gleadow, 1981). The EDM has the advantage of allowing fission track ages to be determined on single grains. In apatite, tracks are counted in 20 grains from each mount wherever possible. In those samples where the desired number is not present, all available grains are counted, the actual number depending on the availability of suitably etched and oriented grains. Only grains oriented with surfaces parallel to the crystallographic c-axis are analysed. Such grains can be identified on the basis of the etching characteristics, as well as from morphological evidence in euhedral grains. The grain mount is scanned sequentially, and the first 20 suitably oriented grains identified are analysed.

Tracks are counted within an eyepiece graticule divided into 100 grid squares. In each grain, the number of spontaneous tracks ($N_s$) within a certain number of grid squares ($N_a$) is recorded. The number of induced tracks ($N_i$) in the corresponding location within the mica external detector is then counted. Spontaneous and induced track densities ($\rho_s$ and $\rho_i$, respectively) are calculated by dividing the track counts by the total area counted, given by the product of Na and the area or each grid square (determined by calibration against a ruled stage graticule or diffraction grating). Fission track ages may be calculated by substituting track counts ($N_s$ and $N_i$) for track densities ($\rho_s$ and $\rho_i$) in equation B.1, since the areas cancel in the ratio.

Translation between apatite grains in the grain mount and external detector locations corresponding to each grain is carried out using Autoscan™ microcomputer-controlled automatic stages (Smith and Leigh Jones, 1985). This system allows repeated movement between grain and detector, and all grain locations are stored for later reference if required.

Neutron irradiations are carried out in a well-thermalised flux (X-7 facility; Cd ratio for Au ~98) in the Australian Atomic Energy Commission's HIFAR research reactor. Total neutron fluence is monitored by counting tracks in mica external detectors attached to two pieces of Corning Glass Works standard glass CN5 (containing ~11 ppm Uranium) included in the irradiation canister at each end of the sample stack. In determining track densities in external detectors irradiated adjacent to uranium standard glasses, 25 fields are normally counted in each detector. The total track count ($N_D$) is divided by the total area counted to obtain the track density ($\rho_D$). The positions of the counted fields are arranged in a 5 X 5 grid covering the whole area of the detector. For typical track densities of between ~$5 \times 10^5$ and $5 \times 10^6$, this is a convenient arrangement to sample across the detector while gathering sufficient counts to achieve a precision of ~±2% in a reasonable time.

A small flux gradient is often present in the irradiation facility over the length of the sample package. If a detectable gradient is present, the track count in the external detector adjacent to each standard glass is converted to a track density ($\rho_D$) and a value for each mount in the stack is calculated by linear interpolation. When no detectable gradient is present, the track counts in the two external detectors are pooled to give a single value of $\rho_D$, which is used to calculate fission track ages for each sample.

A Zeta calibration factor ($\zeta$) has been determined empirically for each observer by analysing a set of carefully chosen age standards with independently known K-Ar ages, following the methods outlined by Hurford and Green (1983) and Green (1985).

All track counting is carried out using Zeiss(R) Axioplan microscopes, with an overall linear magnification of 1068 x using dry objectives.

For further details and background information on practical aspects of fission track age determination, see e.g., Fleischer, Price and Walker (1975), Naeser (1979) and Hurford (1986).

***Track length measurements***

For track length studies in apatite, the full lengths of "confined" fission tracks are measured. Confined tracks are those which do not intersect the polished surface but have been etched from other tracks or fractures, so that the whole length of the track is etched. Confined track lengths are measured using a digitising tablet connected to a microcomputer, superimposed on the microscope field of view via a projection tube. With this system, calibrated against a stage graticule ruled in 2 μm divisions, individual tracks can be measured to a precision of ± 0.2 μm. Tracks are measured only in prismatic grains, characterised by sharp polishing scratches with well-etched tracks of narrow cone angle in all orientations, because of the anisotropy of annealing of fission tracks in apatite (as discussed by Green et al., 1986). Tracks are also measured following the recommendations of Laslett et al. (1982), the most important of which is that only horizontal tracks should be measured. One hundred tracks are measured whenever possible. In apatite samples with low track density, or in those samples in which only a small number of apatite grains are obtained, fewer confined tracks may be available. In such cases, the whole mount is scanned to measure as many confined tracks as possible.

***Integrated fission track age and length measurement***

Fission track age determination and length measurement are now made in a single pass of the grain mount, in an integrated approach. The location of each grain in which tracks are

either counted or measured is recorded for future reference. Thus, track length measurements can be tied to age determination in individual grains. As a routine procedure we do not measure the age of every grain in which lengths are determined, as this would be much too time-consuming. Likewise we do not only measure ages in grain in which lengths are measured, as this would bias the age data against low track density grains. Nevertheless, the ability to determine the fission track age of certain grains from which length data originate can be a particularly useful aid to interpretation in some cases. Grain location data are not provided in this report, but are available on request.

## B.3 Data Presentation

### *Fission track age data*

Data sheets summarising the apatite fission track age data, including full details of fission track age data for individual apatite grains in each sample, together with the primary counting results and statistical data, are given in the following pages. Individual grain fission track ages are calculated from the ratio of spontaneous to induced fission track counts for each grain using equation B.1, and errors in the single grain ages are calculated using Poissonian statistics, as explained in more detail by Galbraith (1981) and Green (1981). All errors are quoted as $\pm 1\sigma$ throughout this report, unless otherwise stated.

The variability of fission track ages between individual apatite grains within each sample can be assessed using a chi-squared ($\chi^2$) statistic (Galbraith, 1981), the results of which are summarised for each sample in the data sheets. If all the grains counted belong to a single age population, the probability of obtaining the observed $\chi^2$ value, for $\nu$ degrees of freedom (where $\nu$ = number of crystals -1), is listed in the data sheets as $P(\chi^2)$ or P(chi squared).

A $P(\chi^2)$ value greater than 5% can be taken as evidence that all grains are consistent with a single population of fission track age. In this case, the best estimate of the fission track age of the sample is given by the "pooled age", calculated from the ratio of the total spontaneous and induced track counts in all grains analysed. Errors for the pooled age are calculated using the "conventional" technique outlined by Green (1981), based on the total number of tracks counted for each track density measurement (see also Galbraith, 1981).

A $P(\chi^2)$ value of less than 5% denotes a significant spread of single grain ages, suggesting real differences exist between the fission track ages of individual apatite grains. A significant spread in grain ages can result either from inheritance of detrital

grains from mixed source areas (in sedimentary rocks), or from differential annealing in apatite grains of different composition, within a narrow range of temperature.

Calculation of the pooled age inherently assumes that only a single population of ages is present, and is thus not appropriate to samples containing a significant spread of fission track ages. In such cases Galbraith, has recently devised a means of estimating the modal age of a distribution of single grain fission track ages which is referred to as the "central age". Calculation of the central age assumes that all single grain ages belong to a Normal distribution of ages, with a standard deviation ($\sigma$) known as the "age dispersion". An iterative algorithm (as yet unpublished) is used to provide estimates of the central age with its associated error, and the age dispersion, which are all quoted in the data sheets. Note that this treatment replaces use of the "mean age", which has used been in the past for those samples in which $P(\chi^2)<5\%$. For samples in which $P(\chi^2)>5\%$, the central age and the pooled age should be equal, and the age dispersion should be less than ~10%.

Table B.1 summarises the fission track age data in apatite from each sample analysed.

***Construction of radial plots of single grain age data***

Single grain age data are best represented in the form of radial plot diagrams (Galbraith, 1988, 1990). As illustrated in Figure B.1, these plots display the variation of individual grain ages in a plot of y against x, where:

$$y = (z_j - z_o)/\sigma_i \qquad x = 1/\sigma_j \qquad \text{B.2}$$

and; $z_j$ = Fission track age of grain j
$z_o$ = A reference age
$\sigma_j$ = Error in age for grain j

In this plot, all points on a straight line from the origin define a single value of fission track age, and, at any point, the value of x is a measure of the precision of each individual grain age. Therefore, precise individual grain ages fall to the right of the plot (small error, high x), which is useful, for example, in enabling precise, young grains to be identified. The age scale is shown radially around the perimeter of the plot (in Ma). If all grains belong to a single age population, all data should scatter between y = +2 and y = -2, equivalent to scatter within $\pm 2\sigma$. Scatter outside these boundaries shows a significant spread of individual grain ages, as also reflected in the values of $P(\chi^2)$ and age dispersion.

In detail, rather than using the fission track age for each grain as in equation B.2, we use:

$$z_j = \frac{N_{sj}}{N_{ij}} \qquad \sigma_j = \{1/N_{sj} + 1/N_{ij}\} \qquad \text{B.3}$$

as we are interested in displaying the scatter within the data from each sample in comparison with that allowed by the Poissonian uncertainty in track counts, without the additional terms which are involved in determination of the fission track age ($\rho_D$, $\zeta$, etc).

Zero ages cannot be displayed in such a plot. This can be achieved using a modified plot, (Galbraith, 1990) with:

$$z_j = \arcsin\sqrt{\left\{\frac{N_{sj}+3/8}{N_{sj}+N_{ij}+3/4}\right\}} \qquad \sigma_j = \frac{1}{2}\sqrt{\left\{\frac{1}{N_{sj}+N_{ij}}\right\}} \qquad \text{B.4}$$

Note that the numerical terms in the equation for $z_j$ are standard terms, introduced for statistical reasons. Using this arc-sin transformation, zero ages plot on a diagonal line which slopes from upper left to lower right. Note that this line does not go through the origin. Figure B.2 illustrates this difference between conventional and arc-sin radial plots, and also provides a simple guide to the structure of radial plots.

Use of arc-sin radial plots is particularly useful in assessing the relative importance of zero ages. For instance, grains with $N_s = 0$, $N_i = 1$ are compatible with ages up to ~900 Ma (at the 95% confidence level), whereas grains with $N_s = 0$, $N_i = 50$ are only compatible with ages up to ~14 Ma. The two data would readily be distinguishable on the radial plot as the 0,50 datum would plot well to the right (high x) compared to the 0,1 datum.

In this report the value of z corresponding to the stratigraphic age of each sample (or the midpoint of the range where appropriate) is adopted as the reference value, $z_o$. This allows rapid assessment of the fission track age of individual grains in relation to the stratigraphic age, which is a key component in the interpretation of AFTA data, as explained in more detail in Appendix C.

Note that the x axis of the radial plot is normally not labelled, as this would obscure the age scale around the plot. In general labelling is not considered necessary, as we are concerned only with relative variation within the data, rather than absolute values of precision.

Radial plots of the single grain age data in apatite from each sample analysed in this report are shown in Figure B.3. Use of radial plots to provide thermal history information is explained in Appendix C and Figure C.7.

*Smoothed probability distributions*

The single grain ages within each sample are also shown in Figure B.3 in histogram form and also as smoothed probability distributions (Hurford et al., 1984). In constructing these distributions, each grain is represented by a normal probability curve, with mean equal to the single grain age, standard deviation given by the error on the single grain age and the contributions from all grains analysed in each sample summed to produce the plotted curve. These distributions are generally not as informative as the radial plot presentation of single grain age data as they convey little assessment of the relative precision of the fission track ages of different grains. However, they can be useful for portraying the general form of the distribution of ages within a sample.

*Track length data*

Distributions of confined track lengths in apatite from each sample are shown as simple histograms in Figure B.4. For every track length measurement, the length is recorded to the nearest 0.1 μm, but the measurements have been grouped into 1 μm intervals in the histograms in Figure B.4. Each distribution has been normalised to 100 tracks for each sample to facilitate comparison. A summary of the length distribution in each sample is presented in Table B.2, which also shows the mean track length in each sample and its associated error, the standard deviation of each distribution and the number of tracks (N) measured in each sample. The angle which each confined track makes with the crystallographic c-axis is also routinely recorded, as is the width of each fracture within which tracks are revealed. These data are not provided in this report, but can be supplied on request.

*Breakdown of data into compositional groups*

In Table B.3, AFTA data are grouped into compositional intervals of 0.1 wt% Cl width. Parameters for each interval represent the data from all grains with Cl contents within each interval. Also shown are the parameters for each compositional interval predicted from the Default Thermal History. These data form the basis of interpretation of the AFTA data, which takes full account of the influence of Cl content on annealing kinetics, as described in Appendix C.

*Plots of fission track age against Cl content for individual apatite grains*

In Figure B.5, fission track ages of single apatite grains within individual samples are plotted against the Cl content of each grain. These plots are useful in assessing the degree of annealing, as expressed by the fission track age data. For example, if grains with a range of Cl contents from zero to some upper limit all give similar fission track ages which are significantly less than the stratigraphic age, then grains with these compositions must have been totally annealed. Alternatively, if fission track age falls rapidly with decreasing Cl content, the sample displays a high degree of partial annealing.

## B.4 A note on terminology

Note that throughout this report, the term "fission track age" is understood to denote the parameter calculated from the fission track age equation, using the observed spontaneous and induced track counts (either pooled for all grains or for individual grains). The resulting number (with units of Ma) should not be taken as possessing any significance in terms of events taking place at the time indicated by the measured fission track age, but should rather be regarded as a measure of the integrated thermal history of the sample, and should be interpreted in that light using the principles outlined in Appendix C. Use of the term "apparent age" is not considered to be useful in this regard, as almost every fission track age should be regarded as an apparent age, in the classic sense, and repeated use becomes cumbersome.

## References

Fleischer, R. L., Price, P. B., and Walker, R. M. (1975). Nuclear tracks in solids, University of California Press, Berkeley.

Galbraith, R. F. (1981). On statistical models for fission-track counts. *Mathematical Geology*, 13, 471-488.

Galbraith, R. F. (1988). Graphical display of estimates having differing standard errors. *Technometrics*, 30, 271-281.

Galbraith, R. F. (1990). The radial plot: graphical assessment of spread in ages. *Nuclear Tracks*, 17, 207-214.

Gleadow, A. J. W. (1981). Fission track dating methods; what are the real alternatives? *Nuclear Tracks*, 5, 3-14.

Green, P. F. (1981). A new look at statistics in fission track dating. *Nuclear Tracks 5*, 77-86.

Green, P. F. (1985). A comparison of zeta calibration baselines in zircon, sphene and apatite. *Chem. Geol. (Isot. Geol. Sect.)*, 58, 1-22.

Green, P. F., Duddy, I. R., Gleadow, A. J. W., Tingate, P. R. and Laslett, G. M. (1986). Thermal annealing of fission tracks in apatite 1. A qualitative description. *Chem. Geol. (Isot. Geosci. Sect.)*, 59, 237-253.

Hurford, A. J. (1986). Application of the fission track dating method to young sediments: Principles, methodology and Examples. *In:* Hurford, A. J., Jäger, E. and Ten Cate, J. A. M. (*eds*), Dating young sediments, CCOP Technical Publication 16, CCOP Technical Secretariat, Bangkok, Thailand.

Hurford, A. J., Fitch, F. J. and Clarke, A. (1984). Resolution of the age structure of the detrital zircon populations of two Lower Cretaceous sandstones from the Weald of England by fission track dating. *Geological Magazine*, 121, 269-396.

Hurford, A. J. and Green, P. F. (1982). A user's guide to fission track dating calibration. *Earth. Planet. Sci Lett.* 59, 343-354.

Hurford, A. J. and Green, P. F. (1983). The zeta age calibration of fission track dating. *Isotope Geoscience* 1, 285-317.

Laslett, G. M., Kendall, W. S., Gleadow, A. J. W. and Duddy, I. R. (1982). Bias in measurement of fission track length distributions. *Nuclear Tracks*, 6, 79-85.

Naeser, C. W. (1979). Fission track dating and geologic annealing of fission tracks. *In:* Jäger, E. and Hunziker, J. C. (*eds*), Lectures in Isotope Geology, Springer Verlag, Berlin.

Smith, M. J. and Leigh-Jones, P. (1985). An automated microscope scanning stage for fission-track dating. *Nuclear Tracks*, 10, 395-400.

## Table B.1: Apatite fission track analytical results - samples from the Duntroon Basin (Geotrack Report #589)

| Sample number | Number of grains | Rho D x10$^6$ (ND) | Rho S x10$^6$ (Ns) | Rho I x10$^6$ (Ni) | Uranium content (ppm) | P(chi squared) (%) | Age dispersion (%) | Fission track age (Ma) |
|---|---|---|---|---|---|---|---|---|
| **Platypus-1** | | | | | | | | |
| GC589-3 | 11 | 1.292 (2123) | 0.994 (204) | 1.935 (397) | 17 | 9 | 22 | 127.1 ± 11.5 |
| GC589-5 | 20 | 1.325 (2123) | 0.843 (271) | 1.409 (453) | 12 | <1 | 50 | 151.5 ± 12.4<br>*127.9 ± 20.1** |
| GC589-8 | 20 | 1.341 (2123) | 0.805 (269) | 1.568 (524) | 13 | <1 | 41 | 131.8 ± 10.6<br>*124.6 ± 16.5** |
| GC589-9 | 20 | 1.358 (2123) | 0.325 (137) | 0.878 (370) | 7 | <1 | 78 | 96.5 ± 10.0<br>*104.9 ± 22.6** |
| GC589-10 | 20 | 1.374 (2123) | 0.486 (206) | 1.270 (538) | 11 | 4 | 34 | 101.0 ± 8.7<br>*93.5 ± 12.2** |
| GC589-12 | 10 | 1.391 (2123) | 0.188 (48) | 0.957 (244) | 8 | <1 | 118 | 52.7 ± 8.5<br>*41.4 ± 18.3** |
| **Duntroon-1** | | | | | | | | |
| 8622-40 | | | No apatite | | | | | |
| 8622-41 | 20 | 1.150 (5050) | 1.932 (1103) | 1.521 (868) | 17 | 82 | <1 | 258.0 ± 13.2 |
| 8622-42 | 1 | 1.150 (5050) | 0.079 (3) | 0.609 (23) | 7 | - | - | 27.0 ± 16.6 |
| 8622-43 | 15 | 1.150 (5050) | 1.200 (438) | 1.874 (684) | 20 | <1 | 57 | 131.3 ± 8.6<br>*131.5 ± 23.6** |
| 8622-45 | 11 | 1.150 (5050) | 0.710 (126) | 1.533 (272) | 17 | <1 | 51 | 95.3 ± 10.5<br>*96.4 ± 19.4** |
| 8622-46 | 20 | 1.150 (5050) | 0.609 (677) | 0.964 (1071) | 10 | <1 | 22 | 129.6 ± 7.1<br>*120.4 ± 9.9** |
| 8622-47 | 20 | 1.150 (5050) | 0.542 (255) | 1.923 (904) | 21 | <1 | 46 | 58.2 ± 4.3<br>*51.6 ± 7.3** |
| 8622-49 | 20 | 1.150 (5050) | 0.119 (55) | 0.876 (405) | 10 | <1 | 85 | 28.1 ± 4.1<br>*33.8 ± 8.3** |

Rho S = spontaneous track density; Rho I = induced track density; Rho D = track density in glass standard external detector.
All track densities quoted in units of 1000000 tracks per square cm. Brackets show number of tracks counted.
Rho D and Rho I measured in mica external detectors; Rho S measured in internal surfaces.
* Central age, used where sample contains a significant spread of single grain ages—P(chi squared)<5%. Errors quoted at ±1 sigma.
Ages calculated using dosimeter glass CN5, with a zeta of 386.9 ± 6.9 (H.Gibson) for samples 3-12
SRM612, with a zeta of 360.3±6.8 (M.Moore) for samples 40-49

## Table B.2: Length distribution summary data - samples from the Duntroon Basin (Geotrack Report #589)

| Sample number | Mean track length (µm) | Standard deviation (µm) | Number of tracks (N) | Number of Tracks in Length Intervals (µm) 1 | 2 | 3 | 4 | 5 | 6 | 7 | 8 | 9 | 10 | 11 | 12 | 13 | 14 | 15 | 16 | 17 | 18 | 19 | 20 |
|---|---|---|---|---|---|---|---|---|---|---|---|---|---|---|---|---|---|---|---|---|---|---|---|
| **Platypus-1** | | | | | | | | | | | | | | | | | | | | | | | |
| GC589-3 | 14.08 ± 0.49 | 1.30 | 7 | - | - | - | - | - | - | - | - | - | - | - | - | 1 | 3 | 1 | 2 | - | - | - | - |
| GC589-5 | 13.43 ± 0.26 | 1.15 | 19 | - | - | - | - | - | - | - | - | - | - | - | 2 | 4 | 6 | 6 | 1 | - | - | - | - |
| GC589-8 | 13.38 ± 0.14 | 0.76 | 32 | - | - | - | - | - | - | - | - | - | - | - | 1 | 10 | 14 | 7 | - | - | - | - | - |
| GC589-9 | 12.93 ± 0.33 | 1.15 | 12 | - | - | - | - | - | - | - | - | - | - | 1 | 1 | 3 | 5 | 2 | - | - | - | - | - |
| GC589-10 | 12.37 ± 0.28 | 1.52 | 30 | - | - | - | - | - | - | - | 1 | - | 1 | 1 | 5 | 12 | 9 | - | 1 | - | - | - | - |
| GC589-12 | No confined | tracks | - | - | - | - | - | - | - | - | - | - | - | - | - | - | - | - | - | - | - | - | - |
| **Duntroon-1** | | | | | | | | | | | | | | | | | | | | | | | |
| 8622-40 | No apatite | - | - | - | - | - | - | - | - | - | - | - | - | - | - | - | - | - | - | - | - | - | - |
| 8622-41 | 11.37 ± 0.17 | 1.70 | 102 | - | - | - | - | - | 1 | - | 1 | 7 | 12 | 21 | 22 | 20 | 13 | 4 | 1 | - | - | - | - |
| 8622-42 | No confined | tracks | - | - | - | - | - | - | - | - | - | - | - | - | - | - | - | - | - | - | - | - | - |
| 8622-43 | 11.27 ± 0.28 | 1.81 | 43 | - | - | - | - | 1 | - | - | 1 | 2 | 4 | 6 | 15 | 10 | 2 | 2 | - | - | - | - | - |
| 8622-45 | 10.89 ± 0.50 | 1.98 | 16 | - | - | - | - | - | - | - | 1 | - | 6 | 2 | 3 | - | 2 | 2 | - | - | - | - | - |
| 8622-46 | 11.94 ± 0.28 | 2.02 | 52 | - | - | - | - | - | 2 | - | 1 | - | 1 | 5 | 17 | 16 | 6 | 2 | - | 2 | - | - | - |
| 8622-47 | 11.03 ± 0.22 | 2.18 | 103 | - | - | 1 | - | 1 | - | 2 | 3 | 11 | 12 | 13 | 23 | 21 | 7 | 8 | 1 | - | - | - | - |
| 8622-49 | 11.38 ± 0.39 | 1.47 | 14 | - | - | - | - | - | - | - | 1 | - | 1 | 2 | 6 | 2 | 2 | - | - | - | - | - | - |

Track length measurements by H.Gibson for samples 3-12
M.Moore for samples 40-49

**Table B.3: AFTA Data in Compositional Groups - (Geotrack Report #589)**

| Cl Wt % | Default fission track age* (Ma) | Measured fission track age (Ma) | Error in age (Ma) | P (χ 2) | Number of grains | Default fission track length* (µm) | Mean track length (µm) | Error in length (µm) | Std deviation (µm) | Number of lengths | Number of grains | Number of tracks in length interval (µm) 1 | 2 | 3 | 4 | 5 | 6 | 7 | 8 | 9 | 10 | 11 | 12 | 13 | 14 | 15 | 16 | 17 | 18 | 19 | 20 |
|---|---|---|---|---|---|---|---|---|---|---|---|---|---|---|---|---|---|---|---|---|---|---|---|---|---|---|---|---|---|---|---|
| **Platypus-1** | | | | | | | | | | | | | | | | | | | | | | | | | | | | | | | |
| †589-3 | 56.6 | 127.1 | 11.5 | 9.0 | 11 | 13.2 | 14.1 | 0.5 | 1.3 | 7 | 5 | 0 | 0 | 0 | 0 | 0 | 0 | 0 | 0 | 0 | 0 | 0 | 0 | 1 | 3 | 1 | 2 | 0 | 0 | 0 | 0 |
| 0.0-0.1 | 55.1 | 162.4 | 20.6 | 98.0 | 3 | 12.9 | 13.6 | 0.5 | 1.1 | 5 | 3 | 0 | 0 | 0 | 0 | 0 | 0 | 0 | 0 | 0 | 0 | 0 | 0 | 1 | 3 | 0 | 1 | 0 | 0 | 0 | 0 |
| 0.1-0.2 | 55.6 | 160.2 | 34.0 | 100.0 | 1 | 13.0 | 0.0 | 0.0 | 0.0 | 0 | 0 | 0 | 0 | 0 | 0 | 0 | 0 | 0 | 0 | 0 | 0 | 0 | 0 | 0 | 0 | 0 | 0 | 0 | 0 | 0 | 0 |
| 0.2-0.3 | - | - | - | - | - | - | - | - | - | - | - | - | - | - | - | - | - | - | - | - | - | - | - | - | - | - | - | - | - | - | - |
| 0.3-0.4 | 56.6 | 78.1 | 27.0 | 59.0 | 2 | 13.2 | 0.0 | 0.0 | 0.0 | 0 | 0 | 0 | 0 | 0 | 0 | 0 | 0 | 0 | 0 | 0 | 0 | 0 | 0 | 0 | 0 | 0 | 0 | 0 | 0 | 0 | 0 |
| 0.4-0.5 | 57.0 | 49.8 | 38.6 | 100.0 | 1 | 13.3 | 0.0 | 0.0 | 0.0 | 0 | 0 | 0 | 0 | 0 | 0 | 0 | 0 | 0 | 0 | 0 | 0 | 0 | 0 | 0 | 0 | 0 | 0 | 0 | 0 | 0 | 0 |
| 0.5-0.6 | 57.3 | 76.2 | 16.9 | 100.0 | 1 | 13.4 | 0.0 | 0.0 | 0.0 | 0 | 0 | 0 | 0 | 0 | 0 | 0 | 0 | 0 | 0 | 0 | 0 | 0 | 0 | 0 | 0 | 0 | 0 | 0 | 0 | 0 | 0 |
| 0.6-0.7 | 57.7 | 131.4 | 39.5 | 100.0 | 1 | 13.5 | 0.0 | 0.0 | 0.0 | 0 | 0 | 0 | 0 | 0 | 0 | 0 | 0 | 0 | 0 | 0 | 0 | 0 | 0 | 0 | 0 | 0 | 0 | 0 | 0 | 0 | 0 |
| 0.7-0.8 | - | - | - | - | - | - | - | - | - | - | - | - | - | - | - | - | - | - | - | - | - | - | - | - | - | - | - | - | - | - | - |
| 0.8-0.9 | - | - | - | - | - | - | - | - | - | - | - | - | - | - | - | - | - | - | - | - | - | - | - | - | - | - | - | - | - | - | - |
| 0.9-1.0 | - | - | - | - | - | - | - | - | - | - | - | - | - | - | - | - | - | - | - | - | - | - | - | - | - | - | - | - | - | - | - |
| 1.0-1.1 | - | - | - | - | - | - | - | - | - | - | - | - | - | - | - | - | - | - | - | - | - | - | - | - | - | - | - | - | - | - | - |
| 1.1-1.2 | 58.6 | 49.8 | 38.6 | 100.0 | 1 | 13.7 | 14.9 | 0.0 | 0.0 | 1 | 1 | 0 | 0 | 0 | 0 | 0 | 0 | 0 | 0 | 0 | 0 | 0 | 0 | 0 | 0 | 1 | 0 | 0 | 0 | 0 | 0 |
| 1.2-1.3 | - | - | - | - | - | - | - | - | - | - | - | - | - | - | - | - | - | - | - | - | - | - | - | - | - | - | - | - | - | - | - |
| 1.3-1.4 | 58.7 | 123.7 | 107.2 | 100.0 | 1 | 13.7 | 15.8 | 0.0 | 0.0 | 1 | 1 | 0 | 0 | 0 | 0 | 0 | 0 | 0 | 0 | 0 | 0 | 0 | 0 | 0 | 0 | 0 | 1 | 0 | 0 | 0 | 0 |
| †589-5 | 64.4 | 127.9 | 20.1 | 0.0 | 20 | 12.6 | 13.4 | 0.3 | 1.1 | 19 | 11 | 0 | 0 | 0 | 0 | 0 | 0 | 0 | 0 | 0 | 0 | 0 | 2 | 4 | 6 | 6 | 1 | 0 | 0 | 0 | 0 |
| 0.0-0.1 | 61.3 | 249.5 | 63.8 | 1.0 | 3 | 12.2 | 12.6 | 0.2 | 0.6 | 8 | 3 | 0 | 0 | 0 | 0 | 0 | 0 | 0 | 0 | 0 | 0 | 0 | 1 | 4 | 3 | 0 | 0 | 0 | 0 | 0 | 0 |
| 0.1-0.2 | 62.1 | 144.8 | 40.7 | 100.0 | 1 | 12.4 | 12.9 | 1.3 | 1.9 | 2 | 2 | 0 | 0 | 0 | 0 | 0 | 0 | 0 | 0 | 0 | 0 | 0 | 1 | 0 | 0 | 1 | 0 | 0 | 0 | 0 | 0 |
| 0.2-0.3 | 62.9 | 60.7 | 21.4 | 17.0 | 2 | 12.5 | 14.1 | 0.0 | 0.0 | 1 | 1 | 0 | 0 | 0 | 0 | 0 | 0 | 0 | 0 | 0 | 0 | 0 | 0 | 0 | 0 | 1 | 0 | 0 | 0 | 0 | 0 |
| 0.3-0.4 | - | - | - | - | - | - | - | - | - | - | - | - | - | - | - | - | - | - | - | - | - | - | - | - | - | - | - | - | - | - | - |
| 0.4-0.5 | 64.5 | 189.4 | 45.9 | 37.0 | 2 | 12.9 | 13.8 | 0.5 | 0.8 | 3 | 3 | 0 | 0 | 0 | 0 | 0 | 0 | 0 | 0 | 0 | 0 | 0 | 0 | 0 | 0 | 2 | 1 | 0 | 0 | 0 | 0 |
| 0.5-0.6 | 65.0 | 109.9 | 17.0 | 18.0 | 3 | 13.0 | 0.0 | 0.0 | 0.0 | 0 | 0 | 0 | 0 | 0 | 0 | 0 | 0 | 0 | 0 | 0 | 0 | 0 | 0 | 0 | 0 | 0 | 0 | 0 | 0 | 0 | 0 |
| 0.6-0.7 | 65.5 | 117.2 | 57.9 | 49.0 | 4 | 13.1 | 14.1 | 0.0 | 0.0 | 1 | 1 | 0 | 0 | 0 | 0 | 0 | 0 | 0 | 0 | 0 | 0 | 0 | 0 | 0 | 0 | 0 | 1 | 0 | 0 | 0 | 0 |
| 0.7-0.8 | 66.0 | 155.8 | 70.1 | 85.0 | 2 | 13.2 | 0.0 | 0.0 | 0.0 | 0 | 0 | 0 | 0 | 0 | 0 | 0 | 0 | 0 | 0 | 0 | 0 | 0 | 0 | 0 | 0 | 0 | 0 | 0 | 0 | 0 | 0 |
| 0.8-0.9 | - | - | - | - | - | - | - | - | - | - | - | - | - | - | - | - | - | - | - | - | - | - | - | - | - | - | - | - | - | - | - |
| 0.9-1.0 | - | - | - | - | - | - | - | - | - | - | - | - | - | - | - | - | - | - | - | - | - | - | - | - | - | - | - | - | - | - | - |
| 1.0-1.1 | 66.7 | 81.0 | 35.2 | 100.0 | 1 | 13.3 | 0.0 | 0.0 | 0.0 | 0 | 0 | 0 | 0 | 0 | 0 | 0 | 0 | 0 | 0 | 0 | 0 | 0 | 0 | 0 | 0 | 0 | 0 | 0 | 0 | 0 | 0 |
| 1.1-1.2 | - | - | - | - | - | - | - | - | - | - | - | - | - | - | - | - | - | - | - | - | - | - | - | - | - | - | - | - | - | - | - |
| 1.2-1.3 | 66.9 | 0.0 | 0.0 | 0.0 | 0 | 13.3 | 14.5 | 1.4 | 2.0 | 2 | 1 | 0 | 0 | 0 | 0 | 0 | 0 | 0 | 0 | 0 | 0 | 0 | 0 | 0 | 0 | 1 | 0 | 1 | 0 | 0 | 0 |
| 1.3-1.4 | - | - | - | - | - | - | - | - | - | - | - | - | - | - | - | - | - | - | - | - | - | - | - | - | - | - | - | - | - | - | - |
| 1.4-1.5 | - | - | - | - | - | - | - | - | - | - | - | - | - | - | - | - | - | - | - | - | - | - | - | - | - | - | - | - | - | - | - |
| 1.5-1.6 | - | - | - | - | - | - | - | - | - | - | - | - | - | - | - | - | - | - | - | - | - | - | - | - | - | - | - | - | - | - | - |
| 1.6-1.7 | 67.2 | 36.5 | 39.0 | 100.0 | 1 | 13.4 | 0.0 | 0.0 | 0.0 | 0 | 0 | 0 | 0 | 0 | 0 | 0 | 0 | 0 | 0 | 0 | 0 | 0 | 0 | 0 | 0 | 0 | 0 | 0 | 0 | 0 | 0 |

*Fission Track Age and Mean Track Length predicted from the Default Thermal History (i.e. if the sample has not been hotter in the past)
†Combined data for all compositional groups

**Table B.3: Continued - (Geotrack Report #589)**

| Cl Wt % | Default fission track age* (Ma) | Measured fission track age (Ma) | Error in age (Ma) | P (χ 2) | Number of grains | Default fission track length* (µm) | Mean track length (µm) | Error in length (µm) | Std deviation (µm) | Number of lengths | Number of grains | Number of tracks in length interval (µm) 1 | 2 | 3 | 4 | 5 | 6 | 7 | 8 | 9 | 10 | 11 | 12 | 13 | 14 | 15 | 16 | 17 | 18 | 19 | 20 |
|---|---|---|---|---|---|---|---|---|---|---|---|---|---|---|---|---|---|---|---|---|---|---|---|---|---|---|---|---|---|---|---|
| †589-8 | 65.3 | 124.6 | 16.5 | 0.0 | 20 | 12.4 | 13.4 | 0.1 | 0.8 | 32 | 22 | 0 | 0 | 0 | 0 | 0 | 0 | 0 | 0 | 0 | 0 | 0 | 1 | 10 | 14 | 7 | 0 | 0 | 0 | 0 | 0 |
| 0.0-0.1 | 60.3 | 207.2 | 37.6 | 29.0 | 3 | 11.3 | 13.0 | 0.2 | 0.5 | 4 | 2 | 0 | 0 | 0 | 0 | 0 | 0 | 0 | 0 | 0 | 0 | 0 | 0 | 2 | 2 | 0 | 0 | 0 | 0 | 0 | 0 |
| 0.1-0.2 | 61.6 | 111.3 | 48.3 | 2.0 | 2 | 11.5 | 13.1 | 0.1 | 0.2 | 3 | 2 | 0 | 0 | 0 | 0 | 0 | 0 | 0 | 0 | 0 | 0 | 0 | 0 | 1 | 2 | 0 | 0 | 0 | 0 | 0 | 0 |
| 0.2-0.3 | - | - | - | - | - | - | - | - | - | - | - | - | - | - | - | - | - | - | - | - | - | - | - | - | - | - | - | - | - | - | - |
| 0.3-0.4 | 64.2 | 80.2 | 17.5 | 42.0 | 3 | 12.0 | 13.2 | 0.8 | 1.1 | 2 | 2 | 0 | 0 | 0 | 0 | 0 | 0 | 0 | 0 | 0 | 0 | 0 | 0 | 1 | 1 | 0 | 0 | 0 | 0 | 0 | 0 |
| 0.4-0.5 | 65.3 | 96.3 | 76.3 | 0.0 | 2 | 12.2 | 12.7 | 0.2 | 0.3 | 3 | 2 | 0 | 0 | 0 | 0 | 0 | 0 | 0 | 0 | 0 | 0 | 0 | 0 | 3 | 0 | 0 | 0 | 0 | 0 | 0 | 0 |
| 0.5-0.6 | 66.0 | 166.5 | 59.4 | 100.0 | 1 | 12.3 | 0.0 | 0.0 | 0.0 | 0 | 0 | 0 | 0 | 0 | 0 | 0 | 0 | 0 | 0 | 0 | 0 | 0 | 0 | 0 | 0 | 0 | 0 | 0 | 0 | 0 | 0 |
| 0.6-0.7 | 66.7 | 191.7 | 84.6 | 13.0 | 2 | 12.5 | 14.8 | 0.0 | 0.0 | 1 | 1 | 0 | 0 | 0 | 0 | 0 | 0 | 0 | 0 | 0 | 0 | 0 | 0 | 0 | 0 | 1 | 0 | 0 | 0 | 0 | 0 |
| 0.7-0.8 | 67.4 | 153.8 | 112.4 | 100.0 | 1 | 12.6 | 13.1 | 0.8 | 1.3 | 3 | 3 | 0 | 0 | 0 | 0 | 0 | 0 | 0 | 0 | 0 | 0 | 0 | 0 | 2 | 0 | 1 | 0 | 0 | 0 | 0 | 0 |
| 0.8-0.9 | - | - | - | - | - | - | - | - | - | - | - | - | - | - | - | - | - | - | - | - | - | - | - | - | - | - | - | - | - | - | - |
| 0.9-1.0 | 68.4 | 0.0 | 0.0 | 0.0 | 0 | 12.8 | 13.7 | 0.0 | 0.0 | 2 | 1 | 0 | 0 | 0 | 0 | 0 | 0 | 0 | 0 | 0 | 0 | 0 | 0 | 0 | 2 | 0 | 0 | 0 | 0 | 0 | 0 |
| 1.0-1.1 | 68.5 | 98.7 | 24.3 | 100.0 | 1 | 12.8 | 13.9 | 0.1 | 0.1 | 3 | 1 | 0 | 0 | 0 | 0 | 0 | 0 | 0 | 0 | 0 | 0 | 0 | 0 | 0 | 3 | 0 | 0 | 0 | 0 | 0 | 0 |
| 1.1-1.2 | 68.6 | 195.4 | 36.3 | 7.0 | 2 | 12.8 | 14.0 | 0.0 | 0.0 | 1 | 1 | 0 | 0 | 0 | 0 | 0 | 0 | 0 | 0 | 0 | 0 | 0 | 0 | 0 | 0 | 1 | 0 | 0 | 0 | 0 | 0 |
| 1.2-1.3 | 68.7 | 131.9 | 37.3 | 100.0 | 1 | 12.8 | 13.9 | 0.5 | 0.8 | 2 | 1 | 0 | 0 | 0 | 0 | 0 | 0 | 0 | 0 | 0 | 0 | 0 | 0 | 0 | 1 | 1 | 0 | 0 | 0 | 0 | 0 |
| 1.3-1.4 | 68.8 | 0.0 | 0.0 | 0.0 | 0 | 12.8 | 12.8 | 0.7 | 1.2 | 3 | 3 | 0 | 0 | 0 | 0 | 0 | 0 | 0 | 0 | 0 | 0 | 0 | 1 | 1 | 0 | 1 | 0 | 0 | 0 | 0 | 0 |
| 1.4-1.5 | 68.9 | 0.0 | 0.0 | 0.0 | 0 | 12.9 | 13.9 | 0.3 | 0.5 | 3 | 2 | 0 | 0 | 0 | 0 | 0 | 0 | 0 | 0 | 0 | 0 | 0 | 0 | 0 | 1 | 2 | 0 | 0 | 0 | 0 | 0 |
| 1.5-1.6 | 69.0 | 128.4 | 157.3 | 100.0 | 1 | 12.9 | 0.0 | 0.0 | 0.0 | 0 | 0 | 0 | 0 | 0 | 0 | 0 | 0 | 0 | 0 | 0 | 0 | 0 | 0 | 0 | 0 | 0 | 0 | 0 | 0 | 0 | 0 |
| 1.6-1.7 | - | - | - | - | - | - | - | - | - | - | - | - | - | - | - | - | - | - | - | - | - | - | - | - | - | - | - | - | - | - | - |
| 1.7-1.8 | - | - | - | - | - | - | - | - | - | - | - | - | - | - | - | - | - | - | - | - | - | - | - | - | - | - | - | - | - | - | - |
| 1.8-1.9 | - | - | - | - | - | - | - | - | - | - | - | - | - | - | - | - | - | - | - | - | - | - | - | - | - | - | - | - | - | - | - |
| 1.9-2.0 | - | - | - | - | - | - | - | - | - | - | - | - | - | - | - | - | - | - | - | - | - | - | - | - | - | - | - | - | - | - | - |
| 2.0-2.1 | - | - | - | - | - | - | - | - | - | - | - | - | - | - | - | - | - | - | - | - | - | - | - | - | - | - | - | - | - | - | - |
| 2.1-2.2 | 69.6 | 90.2 | 19.9 | 100.0 | 1 | 13.0 | 13.7 | 0.0 | 0.0 | 2 | 1 | 0 | 0 | 0 | 0 | 0 | 0 | 0 | 0 | 0 | 0 | 0 | 0 | 0 | 2 | 0 | 0 | 0 | 0 | 0 | 0 |

* Fission Track Age and Mean Track Length predicted from the Default Thermal History (i.e. if the sample has not been hotter in the past)

† Combined data for all compositional groups

**Table B.3: Continued - (Geotrack Report #589)**

| Cl Wt % | Default fission track age* (Ma) | Measured fission track age (Ma) | Error in age (Ma) | P (χ 2) | Number of grains | Default fission track length* (µm) | Mean track length (µm) | Error in length (µm) | Std deviation (µm) | Number of lengths | Number of grains | Number of tracks in length interval (µm) 1 | 2 | 3 | 4 | 5 | 6 | 7 | 8 | 9 | 10 | 11 | 12 | 13 | 14 | 15 | 16 | 17 | 18 | 19 | 20 |
|---|---|---|---|---|---|---|---|---|---|---|---|---|---|---|---|---|---|---|---|---|---|---|---|---|---|---|---|---|---|---|---|
| †589-9 | 66.4 | 104.9 | 22.6 | 0.0 | 20 | 11.7 | 12.9 | 0.3 | 1.1 | 12 | 7 | 0 | 0 | 0 | 0 | 0 | 0 | 0 | 0 | 0 | 0 | 1 | 1 | 3 | 5 | 2 | 0 | 0 | 0 | 0 | 0 |
| 0.0-0.1 | - | - | - | - | - | - | - | - | - | - | - | - | - | - | - | - | - | - | - | - | - | - | - | - | - | - | - | - | - | - | - |
| 0.1-0.2 | 59.4 | 197.6 | 106.2 | 0.0 | 2 | 10.5 | 11.8 | 0.6 | 0.8 | 2 | 1 | 0 | 0 | 0 | 0 | 0 | 0 | 0 | 0 | 0 | 0 | 0 | 1 | 1 | 0 | 0 | 0 | 0 | 0 | 0 | 0 |
| 0.2-0.3 | 61.5 | 46.2 | 20.5 | 32.0 | 2 | 10.8 | 13.4 | 0.9 | 1.3 | 2 | 2 | 0 | 0 | 0 | 0 | 0 | 0 | 0 | 0 | 0 | 0 | 0 | 0 | 1 | 0 | 1 | 0 | 0 | 0 | 0 | 0 |
| 0.3-0.4 | 63.5 | 23.8 | 17.6 | 19.0 | 2 | 11.2 | 0.0 | 0.0 | 0.0 | 0 | 0 | 0 | 0 | 0 | 0 | 0 | 0 | 0 | 0 | 0 | 0 | 0 | 0 | 0 | 0 | 0 | 0 | 0 | 0 | 0 | 0 |
| 0.4-0.5 | 65.2 | 37.4 | 40.0 | 100.0 | 1 | 11.4 | 0.0 | 0.0 | 0.0 | 0 | 0 | 0 | 0 | 0 | 0 | 0 | 0 | 0 | 0 | 0 | 0 | 0 | 0 | 0 | 0 | 0 | 0 | 0 | 0 | 0 | 0 |
| 0.5-0.6 | - | - | - | - | - | - | - | - | - | - | - | - | - | - | - | - | - | - | - | - | - | - | - | - | - | - | - | - | - | - | - |
| 0.6-0.7 | 67.2 | 108.5 | 33.4 | 7.0 | 5 | 11.8 | 0.0 | 0.0 | 0.0 | 0 | 0 | 0 | 0 | 0 | 0 | 0 | 0 | 0 | 0 | 0 | 0 | 0 | 0 | 0 | 0 | 0 | 0 | 0 | 0 | 0 | 0 |
| 0.7-0.8 | 68.2 | 93.1 | 48.6 | 100.0 | 1 | 12.0 | 13.3 | 0.0 | 0.1 | 2 | 1 | 0 | 0 | 0 | 0 | 0 | 0 | 0 | 0 | 0 | 0 | 0 | 0 | 0 | 2 | 0 | 0 | 0 | 0 | 0 | 0 |
| 0.8-0.9 | 69.3 | 87.0 | 100.4 | 100.0 | 1 | 12.2 | 0.0 | 0.0 | 0.0 | 0 | 0 | 0 | 0 | 0 | 0 | 0 | 0 | 0 | 0 | 0 | 0 | 0 | 0 | 0 | 0 | 0 | 0 | 0 | 0 | 0 | 0 |
| 0.9-1.0 | - | - | - | - | - | - | - | - | - | - | - | - | - | - | - | - | - | - | - | - | - | - | - | - | - | - | - | - | - | - | - |
| 1.0-1.1 | 69.6 | 146.1 | 61.2 | 1.0 | 2 | 12.2 | 13.4 | 0.4 | 0.6 | 3 | 1 | 0 | 0 | 0 | 0 | 0 | 0 | 0 | 0 | 0 | 0 | 0 | 0 | 1 | 1 | 1 | 0 | 0 | 0 | 0 | 0 |
| 1.1-1.2 | - | - | - | - | - | - | - | - | - | - | - | - | - | - | - | - | - | - | - | - | - | - | - | - | - | - | - | - | - | - | - |
| 1.2-1.3 | 69.9 | 161.8 | 120.3 | 0.0 | 2 | 12.3 | 13.8 | 0.1 | 0.2 | 2 | 1 | 0 | 0 | 0 | 0 | 0 | 0 | 0 | 0 | 0 | 0 | 0 | 0 | 0 | 2 | 0 | 0 | 0 | 0 | 0 | 0 |
| 1.3-1.4 | - | - | - | - | - | - | - | - | - | - | - | - | - | - | - | - | - | - | - | - | - | - | - | - | - | - | - | - | - | - | - |
| 1.4-1.5 | - | - | - | - | - | - | - | - | - | - | - | - | - | - | - | - | - | - | - | - | - | - | - | - | - | - | - | - | - | - | - |
| 1.5-1.6 | 70.4 | 65.3 | 32.7 | 84.0 | 2 | 12.4 | 0.0 | 0.0 | 0.0 | 0 | 0 | 0 | 0 | 0 | 0 | 0 | 0 | 0 | 0 | 0 | 0 | 0 | 0 | 0 | 0 | 0 | 0 | 0 | 0 | 0 | 0 |
| 1.6-1.7 | - | - | - | - | - | - | - | - | - | - | - | - | - | - | - | - | - | - | - | - | - | - | - | - | - | - | - | - | - | - | - |
| 1.7-1.8 | - | - | - | - | - | - | - | - | - | - | - | - | - | - | - | - | - | - | - | - | - | - | - | - | - | - | - | - | - | - | - |
| 1.8-1.9 | - | - | - | - | - | - | - | - | - | - | - | - | - | - | - | - | - | - | - | - | - | - | - | - | - | - | - | - | - | - | - |
| 1.9-2.0 | 70.9 | 0.0 | 0.0 | 0.0 | 0 | 12.5 | 10.5 | 0.0 | 0.0 | 1 | 1 | 0 | 0 | 0 | 0 | 0 | 0 | 0 | 0 | 0 | 0 | 1 | 0 | 0 | 0 | 0 | 0 | 0 | 0 | 0 | 0 |

*Fission Track Age and Mean Track Length predicted from the Default Thermal History (i.e. if the sample has not been hotter in the past)
†Combined data for all compositional groups

**Table B.3: Continued - (Geotrack Report #589)**

| Cl Wt % | Default fission track age* (Ma) | Measured fission track age (Ma) | Error in age (Ma) | P (χ 2) | Number of grains | Default fission track length* (µm) | Mean track length (µm) | Error in length (µm) | Std deviation (µm) | Number of lengths | Number of grains | Number of tracks in length interval (µm) 1 | 2 | 3 | 4 | 5 | 6 | 7 | 8 | 9 | 10 | 11 | 12 | 13 | 14 | 15 | 16 | 17 | 18 | 19 | 20 |
|---|---|---|---|---|---|---|---|---|---|---|---|---|---|---|---|---|---|---|---|---|---|---|---|---|---|---|---|---|---|---|---|
| †589-10 | 56.5 | 93.5 | 12.2 | 4.0 | 20 | 11.3 | 12.4 | 0.3 | 1.5 | 30 | 17 | 0 | 0 | 0 | 0 | 0 | 0 | 0 | 1 | 0 | 1 | 1 | 5 | 12 | 9 | 0 | 1 | 0 | 0 | 0 | 0 |
| 0.0-0.1 | 41.5 | 97.0 | 21.1 | 1.0 | 9 | 9.4 | 10.8 | 0.7 | 1.4 | 4 | 4 | 0 | 0 | 0 | 0 | 0 | 0 | 0 | 0 | 0 | 1 | 1 | 1 | 1 | 0 | 0 | 0 | 0 | 0 | 0 | 0 |
| 0.1-0.2 | - | - | - | - | - | - | - | - | - | - | - | - | - | - | - | - | - | - | - | - | - | - | - | - | - | - | - | - | - | - | - |
| 0.2-0.3 | 58.9 | 0.0 | 0.0 | 0.0 | 0 | 10.3 | 13.2 | 0.0 | 0.0 | 1 | 1 | 0 | 0 | 0 | 0 | 0 | 0 | 0 | 0 | 0 | 0 | 0 | 0 | 0 | 1 | 0 | 0 | 0 | 0 | 0 | 0 |
| 0.3-0.4 | 63.1 | 44.2 | 47.7 | 100.0 | 1 | 10.7 | 13.8 | 0.0 | 0.0 | 1 | 1 | 0 | 0 | 0 | 0 | 0 | 0 | 0 | 0 | 0 | 0 | 0 | 0 | 0 | 1 | 0 | 0 | 0 | 0 | 0 | 0 |
| 0.4-0.5 | - | - | - | - | - | - | - | - | - | - | - | - | - | - | - | - | - | - | - | - | - | - | - | - | - | - | - | - | - | - | - |
| 0.5-0.6 | 66.4 | 39.8 | 24.6 | 100.0 | 1 | 11.3 | 12.0 | 0.6 | 1.8 | 10 | 2 | 0 | 0 | 0 | 0 | 0 | 0 | 0 | 1 | 0 | 0 | 0 | 2 | 5 | 2 | 0 | 0 | 0 | 0 | 0 | 0 |
| 0.6-0.7 | 67.6 | 0.0 | 0.0 | 0.0 | 0 | 11.5 | 13.5 | 0.0 | 0.0 | 1 | 1 | 0 | 0 | 0 | 0 | 0 | 0 | 0 | 0 | 0 | 0 | 0 | 0 | 0 | 1 | 0 | 0 | 0 | 0 | 0 | 0 |
| 0.7-0.8 | 68.8 | 80.3 | 18.8 | 37.0 | 4 | 11.7 | 13.1 | 0.9 | 1.6 | 3 | 2 | 0 | 0 | 0 | 0 | 0 | 0 | 0 | 0 | 0 | 0 | 0 | 0 | 2 | 0 | 0 | 1 | 0 | 0 | 0 | 0 |
| 0.8-0.9 | 70.1 | 121.5 | 27.0 | 50.0 | 2 | 11.9 | 12.2 | 0.5 | 0.8 | 3 | 3 | 0 | 0 | 0 | 0 | 0 | 0 | 0 | 0 | 0 | 0 | 0 | 1 | 2 | 0 | 0 | 0 | 0 | 0 | 0 | 0 |
| 0.9-1.0 | 70.3 | 72.9 | 29.2 | 74.0 | 2 | 11.9 | 13.6 | 0.3 | 0.5 | 2 | 2 | 0 | 0 | 0 | 0 | 0 | 0 | 0 | 0 | 0 | 0 | 0 | 0 | 0 | 2 | 0 | 0 | 0 | 0 | 0 | 0 |
| 1.0-1.1 | - | - | - | - | - | - | - | - | - | - | - | - | - | - | - | - | - | - | - | - | - | - | - | - | - | - | - | - | - | - | - |
| 1.1-1.2 | - | - | - | - | - | - | - | - | - | - | - | - | - | - | - | - | - | - | - | - | - | - | - | - | - | - | - | - | - | - | - |
| 1.2-1.3 | - | - | - | - | - | - | - | - | - | - | - | - | - | - | - | - | - | - | - | - | - | - | - | - | - | - | - | - | - | - | - |
| 1.3-1.4 | - | - | - | - | - | - | - | - | - | - | - | - | - | - | - | - | - | - | - | - | - | - | - | - | - | - | - | - | - | - | - |
| 1.4-1.5 | 71.2 | 0.0 | 0.0 | 0.0 | 0 | 12.1 | 12.9 | 0.4 | 1.0 | 5 | 1 | 0 | 0 | 0 | 0 | 0 | 0 | 0 | 0 | 0 | 0 | 0 | 1 | 2 | 2 | 0 | 0 | 0 | 0 | 0 | 0 |
| 1.5-1.6 | - | - | - | - | - | - | - | - | - | - | - | - | - | - | - | - | - | - | - | - | - | - | - | - | - | - | - | - | - | - | - |
| 1.6-1.7 | - | - | - | - | - | - | - | - | - | - | - | - | - | - | - | - | - | - | - | - | - | - | - | - | - | - | - | - | - | - | - |
| 1.7-1.8 | 71.6 | 117.1 | 70.4 | 100.0 | 1 | 12.1 | 0.0 | 0.0 | 0.0 | 0 | 0 | 0 | 0 | 0 | 0 | 0 | 0 | 0 | 0 | 0 | 0 | 0 | 0 | 0 | 0 | 0 | 0 | 0 | 0 | 0 | 0 |
| †589-12 | 44.2 | 41.4 | 18.3 | 0.0 | 10 | 10.2 | 11.0 | 1.0 | 1.5 | 2 | 1 | 0 | 0 | 0 | 0 | 0 | 0 | 0 | 0 | 0 | 0 | 1 | 0 | 1 | 0 | 0 | 0 | 0 | 0 | 0 | 0 |
| 0.0-0.1 | 0.6 | 0.0 | 0.0 | 110.0 | 1 | 8.6 | 0.0 | 0.0 | 0.0 | 0 | 0 | 0 | 0 | 0 | 0 | 0 | 0 | 0 | 0 | 0 | 0 | 0 | 0 | 0 | 0 | 0 | 0 | 0 | 0 | 0 | 0 |
| 0.1-0.2 | 1.5 | 0.0 | 0.0 | 110.0 | 1 | 8.8 | 0.0 | 0.0 | 0.0 | 0 | 0 | 0 | 0 | 0 | 0 | 0 | 0 | 0 | 0 | 0 | 0 | 0 | 0 | 0 | 0 | 0 | 0 | 0 | 0 | 0 | 0 |
| 0.2-0.3 | 17.8 | 0.0 | 0.0 | 110.0 | 1 | 8.3 | 0.0 | 0.0 | 0.0 | 0 | 0 | 0 | 0 | 0 | 0 | 0 | 0 | 0 | 0 | 0 | 0 | 0 | 0 | 0 | 0 | 0 | 0 | 0 | 0 | 0 | 0 |
| 0.3-0.4 | 35.8 | 24.4 | 25.5 | 100.0 | 1 | 8.9 | 0.0 | 0.0 | 0.0 | 0 | 0 | 0 | 0 | 0 | 0 | 0 | 0 | 0 | 0 | 0 | 0 | 0 | 0 | 0 | 0 | 0 | 0 | 0 | 0 | 0 | 0 |
| 0.4-0.5 | 49.5 | 5.5 | 4.0 | 100.0 | 1 | 9.5 | 0.0 | 0.0 | 0.0 | 0 | 0 | 0 | 0 | 0 | 0 | 0 | 0 | 0 | 0 | 0 | 0 | 0 | 0 | 0 | 0 | 0 | 0 | 0 | 0 | 0 | 0 |
| 0.5-0.6 | - | - | - | - | - | - | - | - | - | - | - | - | - | - | - | - | - | - | - | - | - | - | - | - | - | - | - | - | - | - | - |
| 0.6-0.7 | 63.8 | 85.2 | 35.4 | 3.0 | 2 | 10.2 | 11.0 | 1.0 | 1.5 | 2 | 1 | 0 | 0 | 0 | 0 | 0 | 0 | 0 | 0 | 0 | 0 | 1 | 0 | 1 | 0 | 0 | 0 | 0 | 0 | 0 | 0 |
| 0.7-0.8 | 69.1 | 42.3 | 26.3 | 20.0 | 2 | 10.5 | 0.0 | 0.0 | 0.0 | 0 | 0 | 0 | 0 | 0 | 0 | 0 | 0 | 0 | 0 | 0 | 0 | 0 | 0 | 0 | 0 | 0 | 0 | 0 | 0 | 0 | 0 |
| 0.8-0.9 | 71.4 | 231.2 | 119.8 | 100.0 | 1 | 10.9 | 0.0 | 0.0 | 0.0 | 0 | 0 | 0 | 0 | 0 | 0 | 0 | 0 | 0 | 0 | 0 | 0 | 0 | 0 | 0 | 0 | 0 | 0 | 0 | 0 | 0 | 0 |

* Fission Track Age and Mean Track Length predicted from the Default Thermal History (i.e. if the sample has not been hotter in the past)
† Combined data for all compositional groups

**Table B.3: Continued - (Geotrack Report #589)**

| Cl Wt % | Default fission track age* (Ma) | Measured fission track age (Ma) | Error in age (Ma) | P (χ 2) | Number of grains | Default fission track length* (µm) | Mean track length (µm) | Error in length (µm) | Std deviation (µm) | Number of lengths | Number of grains | Number of tracks in length interval (µm) 1 | 2 | 3 | 4 | 5 | 6 | 7 | 8 | 9 | 10 | 11 | 12 | 13 | 14 | 15 | 16 | 17 | 18 | 19 | 20 |
|---|---|---|---|---|---|---|---|---|---|---|---|---|---|---|---|---|---|---|---|---|---|---|---|---|---|---|---|---|---|---|---|
| Duntroon-1 | | | | | | | | | | | | | | | | | | | | | | | | | | | | | | | |
| †8622-41 | 50.2 | 258.0 | 13.2 | 82.0 | 20 | 13.5 | 11.4 | 0.2 | 1.7 | 102 | 28 | 0 | 0 | 0 | 0 | 0 | 1 | 0 | 1 | 7 | 12 | 21 | 22 | 20 | 13 | 4 | 1 | 0 | 0 | 0 | 0 |
| 0.0-0.1 | 50.2 | 258.0 | 13.1 | 82.0 | 20 | 13.5 | 11.4 | 0.2 | 1.7 | 94 | 26 | 0 | 0 | 0 | 0 | 0 | 1 | 0 | 1 | 7 | 11 | 18 | 19 | 20 | 12 | 4 | 1 | 0 | 0 | 0 | 0 |
| 0.1-0.2 | 50.5 | 0.0 | 0.0 | 0.0 | 0 | 13.5 | 11.2 | 0.3 | 0.6 | 4 | 1 | 0 | 0 | 0 | 0 | 0 | 0 | 0 | 0 | 0 | 0 | 2 | 2 | 0 | 0 | 0 | 0 | 0 | 0 | 0 | 0 |
| 0.2-0.3 | 50.8 | 0.0 | 0.0 | 0.0 | 0 | 13.6 | 11.2 | 0.8 | 1.6 | 4 | 1 | 0 | 0 | 0 | 0 | 0 | 0 | 0 | 0 | 0 | 1 | 1 | 1 | 0 | 1 | 0 | 0 | 0 | 0 | 0 | 0 |
| †8622-42 | 57.6 | 27.0 | 16.6 | 100.0 | 1 | 0.0 | 11.0 | 0.3 | 0.5 | 3 | 1 | 0 | 0 | 0 | 0 | 0 | 0 | 0 | 0 | 0 | 0 | 1 | 2 | 0 | 0 | 0 | 0 | 0 | 0 | 0 | 0 |
| 0.0-0.1 | 0.0 | 0.0 | 0.0 | 0.0 | 0 | 0.0 | 11.0 | 0.3 | 0.5 | 3 | 1 | 0 | 0 | 0 | 0 | 0 | 0 | 0 | 0 | 0 | 0 | 1 | 2 | 0 | 0 | 0 | 0 | 0 | 0 | 0 | 0 |
| 0.1-0.2 | 57.6 | 27.0 | 16.6 | 100.0 | 1 | 13.3 | 0.0 | 0.0 | 0.0 | 0 | 0 | 0 | 0 | 0 | 0 | 0 | 0 | 0 | 0 | 0 | 0 | 0 | 0 | 0 | 0 | 0 | 0 | 0 | 0 | 0 | 0 |
| †8622-43 | 63.8 | 131.5 | 23.6 | 0.0 | 15 | 12.8 | 11.3 | 0.3 | 1.8 | 43 | 15 | 0 | 0 | 0 | 0 | 1 | 0 | 0 | 1 | 2 | 4 | 6 | 15 | 10 | 2 | 2 | 0 | 0 | 0 | 0 | 0 |
| 0.0-0.1 | 61.9 | 123.8 | 36.8 | 0.0 | 5 | 12.5 | 10.2 | 0.4 | 1.8 | 21 | 7 | 0 | 0 | 0 | 0 | 1 | 0 | 0 | 1 | 2 | 2 | 5 | 9 | 1 | 0 | 0 | 0 | 0 | 0 | 0 | 0 |
| 0.1-0.2 | 62.6 | 270.5 | 206.7 | 100.0 | 1 | 12.7 | 12.4 | 0.0 | 0.0 | 1 | 1 | 0 | 0 | 0 | 0 | 0 | 0 | 0 | 0 | 0 | 0 | 0 | 0 | 1 | 0 | 0 | 0 | 0 | 0 | 0 | 0 |
| 0.2-0.3 | - | - | - | - | - | - | - | - | - | - | - | - | - | - | - | - | - | - | - | - | - | - | - | - | - | - | - | - | - | - | - |
| 0.3-0.4 | 64.0 | 79.2 | 29.5 | 28.0 | 2 | 12.9 | 11.9 | 0.3 | 0.4 | 2 | 1 | 0 | 0 | 0 | 0 | 0 | 0 | 0 | 0 | 0 | 0 | 0 | 1 | 1 | 0 | 0 | 0 | 0 | 0 | 0 | 0 |
| 0.4-0.5 | 64.7 | 151.5 | 72.7 | 1.0 | 2 | 13.1 | 12.2 | 0.9 | 1.8 | 4 | 3 | 0 | 0 | 0 | 0 | 0 | 0 | 0 | 0 | 0 | 1 | 0 | 0 | 2 | 0 | 1 | 0 | 0 | 0 | 0 | 0 |
| 0.5-0.6 | 65.1 | 137.9 | 41.8 | 3.0 | 4 | 13.2 | 12.3 | 0.3 | 1.3 | 14 | 2 | 0 | 0 | 0 | 0 | 0 | 0 | 0 | 0 | 0 | 1 | 1 | 5 | 4 | 2 | 1 | 0 | 0 | 0 | 0 | 0 |
| 0.6-0.7 | - | - | - | - | - | - | - | - | - | - | - | - | - | - | - | - | - | - | - | - | - | - | - | - | - | - | - | - | - | - | - |
| 0.7-0.8 | - | - | - | - | - | - | - | - | - | - | - | - | - | - | - | - | - | - | - | - | - | - | - | - | - | - | - | - | - | - | - |
| 0.8-0.9 | - | - | - | - | - | - | - | - | - | - | - | - | - | - | - | - | - | - | - | - | - | - | - | - | - | - | - | - | - | - | - |
| 0.9-1.0 | - | - | - | - | - | - | - | - | - | - | - | - | - | - | - | - | - | - | - | - | - | - | - | - | - | - | - | - | - | - | - |
| 1.0-1.1 | - | - | - | - | - | - | - | - | - | - | - | - | - | - | - | - | - | - | - | - | - | - | - | - | - | - | - | - | - | - | - |
| 1.1-1.2 | 66.7 | 0.0 | 0.0 | 0.0 | 0 | 13.5 | 12.7 | 0.0 | 0.0 | 1 | 1 | 0 | 0 | 0 | 0 | 0 | 0 | 0 | 0 | 0 | 0 | 0 | 0 | 1 | 0 | 0 | 0 | 0 | 0 | 0 | 0 |
| 1.2-1.3 | - | - | - | - | - | - | - | - | - | - | - | - | - | - | - | - | - | - | - | - | - | - | - | - | - | - | - | - | - | - | - |
| 1.3-1.4 | - | - | - | - | - | - | - | - | - | - | - | - | - | - | - | - | - | - | - | - | - | - | - | - | - | - | - | - | - | - | - |
| 1.4-1.5 | 66.9 | 352.7 | 221.2 | 100.0 | 1 | 13.5 | 0.0 | 0.0 | 0.0 | 0 | 0 | 0 | 0 | 0 | 0 | 0 | 0 | 0 | 0 | 0 | 0 | 0 | 0 | 0 | 0 | 0 | 0 | 0 | 0 | 0 | 0 |

*Fission Track Age and Mean Track Length predicted from the Default Thermal History (i.e. if the sample has not been hotter in the past)
†Combined data for all compositional groups

**Table B.3: Continued - (Geotrack Report #589)**

| Cl Wt % | Default fission track age* (Ma) | Measured fission track age (Ma) | Error in age (Ma) | P (χ 2) | Number of grains | Default fission track length* (µm) | Mean track length (µm) | Error in length (µm) | Std deviation (µm) | Number of lengths | Number of grains | Number of tracks in length interval (µm) 1 | 2 | 3 | 4 | 5 | 6 | 7 | 8 | 9 | 10 | 11 | 12 | 13 | 14 | 15 | 16 | 17 | 18 | 19 | 20 |
|---|---|---|---|---|---|---|---|---|---|---|---|---|---|---|---|---|---|---|---|---|---|---|---|---|---|---|---|---|---|---|---|
| †8622-45 | 67.3 | 96.4 | 19.4 | 0.0 | 11 | 12.2 | 10.9 | 0.5 | 2.0 | 16 | 7 | 0 | 0 | 0 | 0 | 0 | 0 | 0 | 1 | 0 | 6 | 2 | 3 | 0 | 2 | 2 | 0 | 0 | 0 | 0 | 0 |
| 0.0-0.1 | 63.8 | 146.3 | 26.0 | 20.0 | 4 | 11.3 | 9.7 | 0.5 | 1.4 | 7 | 2 | 0 | 0 | 0 | 0 | 0 | 0 | 0 | 1 | 0 | 4 | 0 | 2 | 0 | 0 | 0 | 0 | 0 | 0 | 0 | 0 |
| 0.1-0.2 | 65.1 | 241.4 | 82.1 | 100.0 | 1 | 11.6 | 9.7 | 0.3 | 0.6 | 3 | 1 | 0 | 0 | 0 | 0 | 0 | 0 | 0 | 0 | 0 | 2 | 1 | 0 | 0 | 0 | 0 | 0 | 0 | 0 | 0 | 0 |
| 0.2-0.3 | 66.5 | 41.3 | 45.3 | 100.0 | 1 | 11.8 | 0.0 | 0.0 | 0.0 | 0 | 0 | 0 | 0 | 0 | 0 | 0 | 0 | 0 | 0 | 0 | 0 | 0 | 0 | 0 | 0 | 0 | 0 | 0 | 0 | 0 | 0 |
| 0.3-0.4 | 67.7 | 71.9 | 17.9 | 100.0 | 1 | 12.0 | 0.0 | 0.0 | 0.0 | 0 | 0 | 0 | 0 | 0 | 0 | 0 | 0 | 0 | 0 | 0 | 0 | 0 | 0 | 0 | 0 | 0 | 0 | 0 | 0 | 0 | 0 |
| 0.4-0.5 | 68.9 | 35.6 | 17.3 | 100.0 | 1 | 12.2 | 0.0 | 0.0 | 0.0 | 0 | 0 | 0 | 0 | 0 | 0 | 0 | 0 | 0 | 0 | 0 | 0 | 0 | 0 | 0 | 0 | 0 | 0 | 0 | 0 | 0 | 0 |
| 0.5-0.6 | 69.6 | 0.0 | 0.0 | 0.0 | 0 | 12.4 | 12.0 | 1.2 | 1.7 | 2 | 1 | 0 | 0 | 0 | 0 | 0 | 0 | 0 | 0 | 0 | 0 | 1 | 0 | 0 | 1 | 0 | 0 | 0 | 0 | 0 | 0 |
| 0.6-0.7 | 70.4 | 80.1 | 35.7 | 100.0 | 1 | 12.5 | 11.4 | 0.0 | 0.0 | 1 | 1 | 0 | 0 | 0 | 0 | 0 | 0 | 0 | 0 | 0 | 0 | 0 | 1 | 0 | 0 | 0 | 0 | 0 | 0 | 0 | 0 |
| 0.7-0.8 | - | - | - | - | - | - | - | - | - | - | - | - | - | - | - | - | - | - | - | - | - | - | - | - | - | - | - | - | - | - | - |
| 0.8-0.9 | - | - | - | - | - | - | - | - | - | - | - | - | - | - | - | - | - | - | - | - | - | - | - | - | - | - | - | - | - | - | - |
| 0.9-1.0 | - | - | - | - | - | - | - | - | - | - | - | - | - | - | - | - | - | - | - | - | - | - | - | - | - | - | - | - | - | - | - |
| 1.0-1.1 | - | - | - | - | - | - | - | - | - | - | - | - | - | - | - | - | - | - | - | - | - | - | - | - | - | - | - | - | - | - | - |
| 1.1-1.2 | - | - | - | - | - | - | - | - | - | - | - | - | - | - | - | - | - | - | - | - | - | - | - | - | - | - | - | - | - | - | - |
| 1.2-1.3 | - | - | - | - | - | - | - | - | - | - | - | - | - | - | - | - | - | - | - | - | - | - | - | - | - | - | - | - | - | - | - |
| 1.3-1.4 | - | - | - | - | - | - | - | - | - | - | - | - | - | - | - | - | - | - | - | - | - | - | - | - | - | - | - | - | - | - | - |
| 1.4-1.5 | - | - | - | - | - | - | - | - | - | - | - | - | - | - | - | - | - | - | - | - | - | - | - | - | - | - | - | - | - | - | - |
| 1.5-1.6 | - | - | - | - | - | - | - | - | - | - | - | - | - | - | - | - | - | - | - | - | - | - | - | - | - | - | - | - | - | - | - |
| 1.6-1.7 | - | - | - | - | - | - | - | - | - | - | - | - | - | - | - | - | - | - | - | - | - | - | - | - | - | - | - | - | - | - | - |
| 1.7-1.8 | 72.9 | 51.6 | 33.3 | 100.0 | 1 | 13.0 | 0.0 | 0.0 | 0.0 | 0 | 0 | 0 | 0 | 0 | 0 | 0 | 0 | 0 | 0 | 0 | 0 | 0 | 0 | 0 | 0 | 0 | 0 | 0 | 0 | 0 | 0 |
| 1.8-1.9 | - | - | - | - | - | - | - | - | - | - | - | - | - | - | - | - | - | - | - | - | - | - | - | - | - | - | - | - | - | - | - |
| 1.9-2.0 | 73.2 | 55.5 | 16.8 | 100.0 | 1 | 13.0 | 14.2 | 0.0 | 0.0 | 2 | 1 | 0 | 0 | 0 | 0 | 0 | 0 | 0 | 0 | 0 | 0 | 0 | 0 | 0 | 0 | 2 | 0 | 0 | 0 | 0 | 0 |
| 2.0-2.1 | - | - | - | - | - | - | - | - | - | - | - | - | - | - | - | - | - | - | - | - | - | - | - | - | - | - | - | - | - | - | - |
| 2.1-2.2 | - | - | - | - | - | - | - | - | - | - | - | - | - | - | - | - | - | - | - | - | - | - | - | - | - | - | - | - | - | - | - |
| 2.2-2.3 | - | - | - | - | - | - | - | - | - | - | - | - | - | - | - | - | - | - | - | - | - | - | - | - | - | - | - | - | - | - | - |
| 2.3-2.4 | 73.6 | 0.0 | 0.0 | 0.0 | 0 | 13.1 | 13.3 | 0.0 | 0.0 | 1 | 1 | 0 | 0 | 0 | 0 | 0 | 0 | 0 | 0 | 0 | 0 | 0 | 0 | 0 | 0 | 1 | 0 | 0 | 0 | 0 | 0 |

*Fission Track Age and Mean Track Length predicted from the Default Thermal History (i.e. if the sample has not been hotter in the past)

†Combined data for all compositional groups

**Table B.3: Continued - (Geotrack Report #589)**

| Cl<br>Wt % | Default fission track age* (Ma) | Measured fission track age (Ma) | Error in age (Ma) | P (χ 2) | Number of grains | Default fission track length* (μm) | Mean track length (μm) | Error in length (μm) | Std deviation (μm) | Number of lengths | Number of grains | Number of tracks in length interval (μm) 1 | 2 | 3 | 4 | 5 | 6 | 7 | 8 | 9 | 10 | 11 | 12 | 13 | 14 | 15 | 16 | 17 | 18 | 19 | 20 |
|---|---|---|---|---|---|---|---|---|---|---|---|---|---|---|---|---|---|---|---|---|---|---|---|---|---|---|---|---|---|---|---|
| †8622-46 | 78.2 | 120.4 | 9.9 | 1.0 | 20 | 12.1 | 11.9 | 0.3 | 2.0 | 52 | 25 | 0 | 0 | 0 | 0 | 0 | 2 | 0 | 1 | 0 | 1 | 5 | 17 | 16 | 6 | 2 | 0 | 2 | 0 | 0 | 0 |
| 0.0-0.1 | 71.1 | 148.5 | 21.8 | 4.0 | 5 | 10.6 | 11.0 | 0.4 | 0.8 | 4 | 1 | 0 | 0 | 0 | 0 | 0 | 0 | 0 | 0 | 0 | 0 | 2 | 2 | 0 | 0 | 0 | 0 | 0 | 0 | 0 | 0 |
| 0.1-0.2 | 73.2 | 147.2 | 16.8 | 8.0 | 3 | 10.9 | 11.4 | 1.1 | 3.2 | 8 | 2 | 0 | 0 | 0 | 0 | 0 | 1 | 0 | 0 | 0 | 0 | 1 | 4 | 1 | 0 | 0 | 0 | 1 | 0 | 0 | 0 |
| 0.2-0.3 | 75.3 | 0.0 | 0.0 | 0.0 | 0 | 11.2 | 11.5 | 0.0 | 0.0 | 1 | 1 | 0 | 0 | 0 | 0 | 0 | 0 | 0 | 0 | 0 | 0 | 0 | 1 | 0 | 0 | 0 | 0 | 0 | 0 | 0 | 0 |
| 0.3-0.4 | 77.2 | 133.3 | 33.7 | 100.0 | 1 | 11.5 | 11.2 | 0.4 | 0.7 | 3 | 2 | 0 | 0 | 0 | 0 | 0 | 0 | 0 | 0 | 0 | 0 | 1 | 2 | 0 | 0 | 0 | 0 | 0 | 0 | 0 | 0 |
| 0.4-0.5 | 79.0 | 0.0 | 0.0 | 0.0 | 0 | 11.8 | 12.0 | 0.3 | 0.6 | 5 | 2 | 0 | 0 | 0 | 0 | 0 | 0 | 0 | 0 | 0 | 0 | 0 | 2 | 3 | 0 | 0 | 0 | 0 | 0 | 0 | 0 |
| 0.5-0.6 | 80.0 | 76.7 | 20.7 | 100.0 | 1 | 11.9 | 0.0 | 0.0 | 0.0 | 0 | 0 | 0 | 0 | 0 | 0 | 0 | 0 | 0 | 0 | 0 | 0 | 0 | 0 | 0 | 0 | 0 | 0 | 0 | 0 | 0 | 0 |
| 0.6-0.7 | 81.1 | 123.6 | 22.3 | 43.0 | 2 | 12.1 | 12.6 | 0.7 | 1.2 | 3 | 3 | 0 | 0 | 0 | 0 | 0 | 0 | 0 | 0 | 0 | 0 | 0 | 1 | 1 | 1 | 0 | 0 | 0 | 0 | 0 | 0 |
| 0.7-0.8 | 82.1 | 88.2 | 27.3 | 100.0 | 1 | 12.2 | 11.6 | 0.7 | 1.8 | 7 | 3 | 0 | 0 | 0 | 0 | 0 | 0 | 0 | 1 | 0 | 0 | 1 | 1 | 4 | 0 | 0 | 0 | 0 | 0 | 0 | 0 |
| 0.8-0.9 | 83.3 | 137.7 | 27.3 | 22.0 | 2 | 12.4 | 12.0 | 0.5 | 1.3 | 8 | 3 | 0 | 0 | 0 | 0 | 0 | 0 | 0 | 0 | 0 | 1 | 0 | 2 | 4 | 0 | 1 | 0 | 0 | 0 | 0 | 0 |
| 0.9-1.0 | 83.5 | 170.4 | 46.3 | 100.0 | 1 | 12.4 | 12.2 | 0.4 | 0.7 | 3 | 2 | 0 | 0 | 0 | 0 | 0 | 0 | 0 | 0 | 0 | 0 | 0 | 1 | 2 | 0 | 0 | 0 | 0 | 0 | 0 | 0 |
| 1.0-1.1 | 83.6 | 111.3 | 19.3 | 100.0 | 1 | 12.5 | 14.0 | 0.0 | 0.0 | 1 | 1 | 0 | 0 | 0 | 0 | 0 | 0 | 0 | 0 | 0 | 0 | 0 | 0 | 0 | 1 | 0 | 0 | 0 | 0 | 0 | 0 |
| 1.1-1.2 | - | - | - | - | - | - | - | - | - | - | - | - | - | - | - | - | - | - | - | - | - | - | - | - | - | - | - | - | - | - | - |
| 1.2-1.3 | 84.0 | 0.0 | 0.0 | 0.0 | 0 | 12.5 | 13.3 | 0.0 | 0.0 | 1 | 1 | 0 | 0 | 0 | 0 | 0 | 0 | 0 | 0 | 0 | 0 | 0 | 0 | 0 | 1 | 0 | 0 | 0 | 0 | 0 | 0 |
| 1.3-1.4 | - | - | - | - | - | - | - | - | - | - | - | - | - | - | - | - | - | - | - | - | - | - | - | - | - | - | - | - | - | - | - |
| 1.4-1.5 | 84.3 | 94.8 | 15.1 | 10.0 | 2 | 12.6 | 12.5 | 1.3 | 3.6 | 7 | 3 | 0 | 0 | 0 | 0 | 0 | 1 | 0 | 0 | 0 | 0 | 0 | 1 | 1 | 2 | 1 | 0 | 1 | 0 | 0 | 0 |
| 1.5-1.6 | - | - | - | - | - | - | - | - | - | - | - | - | - | - | - | - | - | - | - | - | - | - | - | - | - | - | - | - | - | - | - |
| 1.6-1.7 | - | - | - | - | - | - | - | - | - | - | - | - | - | - | - | - | - | - | - | - | - | - | - | - | - | - | - | - | - | - | - |
| 1.7-1.8 | - | - | - | - | - | - | - | - | - | - | - | - | - | - | - | - | - | - | - | - | - | - | - | - | - | - | - | - | - | - | - |
| 1.8-1.9 | 84.9 | 0.0 | 0.0 | 0.0 | 0 | 12.6 | 13.6 | 0.0 | 0.0 | 1 | 1 | 0 | 0 | 0 | 0 | 0 | 0 | 0 | 0 | 0 | 0 | 0 | 0 | 0 | 1 | 0 | 0 | 0 | 0 | 0 | 0 |
| 1.9-2.0 | - | - | - | - | - | - | - | - | - | - | - | - | - | - | - | - | - | - | - | - | - | - | - | - | - | - | - | - | - | - | - |
| 2.0-2.1 | - | - | - | - | - | - | - | - | - | - | - | - | - | - | - | - | - | - | - | - | - | - | - | - | - | - | - | - | - | - | - |
| 2.1-2.2 | - | - | - | - | - | - | - | - | - | - | - | - | - | - | - | - | - | - | - | - | - | - | - | - | - | - | - | - | - | - | - |
| 2.2-2.3 | 85.5 | 85.7 | 32.3 | 100.0 | 1 | 12.7 | 0.0 | 0.0 | 0.0 | 0 | 0 | 0 | 0 | 0 | 0 | 0 | 0 | 0 | 0 | 0 | 0 | 0 | 0 | 0 | 0 | 0 | 0 | 0 | 0 | 0 | 0 |

*Fission Track Age and Mean Track Length predicted from the Default Thermal History (i.e. if the sample has not been hotter in the past)
†Combined data for all compositional groups

**Table B.3: Continued - (Geotrack Report #589)**

| Cl Wt % | Default fission track age* (Ma) | Measured fission track age (Ma) | Error in age (Ma) | P (χ 2) | Number of grains | Default fission track length* (µm) | Mean track length (µm) | Error in length (µm) | Std deviation (µm) | Number of lengths | Number of grains | Number of tracks in length interval (µm) 1 | 2 | 3 | 4 | 5 | 6 | 7 | 8 | 9 | 10 | 11 | 12 | 13 | 14 | 15 | 16 | 17 | 18 | 19 | 20 |
|---|---|---|---|---|---|---|---|---|---|---|---|---|---|---|---|---|---|---|---|---|---|---|---|---|---|---|---|---|---|---|---|
| †8622-47 | 71.2 | 51.6 | 7.3 | 0.0 | 20 | 11.2 | 11.0 | 0.2 | 2.2 | 103 | 42 | 0 | 0 | 1 | 0 | 1 | 0 | 2 | 3 | 11 | 12 | 13 | 23 | 21 | 7 | 8 | 1 | 0 | 0 | 0 | 0 |
| 0.0-0.1 | 40.5 | 0.0 | 0.0 | 110.0 | 2 | 8.9 | 9.1 | 0.5 | 2.2 | 22 | 7 | 0 | 0 | 1 | 0 | 1 | 0 | 0 | 2 | 6 | 4 | 5 | 1 | 2 | 0 | 0 | 0 | 0 | 0 | 0 | 0 |
| 0.1-0.2 | 53.5 | 8.0 | 5.7 | 35.0 | 2 | 9.5 | 10.4 | 1.5 | 2.1 | 2 | 1 | 0 | 0 | 0 | 0 | 0 | 0 | 0 | 0 | 1 | 0 | 0 | 1 | 0 | 0 | 0 | 0 | 0 | 0 | 0 | 0 |
| 0.2-0.3 | 65.2 | 50.8 | 10.8 | 2.0 | 5 | 10.0 | 10.5 | 0.8 | 2.5 | 9 | 4 | 0 | 0 | 0 | 0 | 0 | 0 | 1 | 1 | 0 | 2 | 2 | 0 | 1 | 1 | 1 | 0 | 0 | 0 | 0 | 0 |
| 0.3-0.4 | 75.6 | 77.2 | 26.2 | 100.0 | 1 | 10.4 | 10.9 | 0.3 | 1.1 | 11 | 3 | 0 | 0 | 0 | 0 | 0 | 0 | 0 | 0 | 1 | 2 | 2 | 4 | 2 | 0 | 0 | 0 | 0 | 0 | 0 | 0 |
| 0.4-0.5 | 78.5 | 47.6 | 30.5 | 100.0 | 1 | 10.8 | 11.0 | 0.3 | 0.4 | 2 | 1 | 0 | 0 | 0 | 0 | 0 | 0 | 0 | 0 | 0 | 0 | 1 | 1 | 0 | 0 | 0 | 0 | 0 | 0 | 0 | 0 |
| 0.5-0.6 | 80.1 | 47.2 | 7.6 | 76.0 | 2 | 11.0 | 11.0 | 0.6 | 1.6 | 8 | 4 | 0 | 0 | 0 | 0 | 0 | 0 | 0 | 0 | 1 | 1 | 0 | 4 | 1 | 1 | 0 | 0 | 0 | 0 | 0 | 0 |
| 0.6-0.7 | 81.7 | 61.9 | 23.5 | 100.0 | 1 | 11.3 | 11.8 | 0.5 | 1.2 | 6 | 5 | 0 | 0 | 0 | 0 | 0 | 0 | 0 | 0 | 0 | 0 | 2 | 1 | 2 | 1 | 0 | 0 | 0 | 0 | 0 | 0 |
| 0.7-0.8 | 83.3 | 0.0 | 0.0 | 0.0 | 0 | 11.5 | 11.6 | 0.3 | 0.6 | 4 | 1 | 0 | 0 | 0 | 0 | 0 | 0 | 0 | 0 | 0 | 0 | 0 | 3 | 1 | 0 | 0 | 0 | 0 | 0 | 0 | 0 |
| 0.8-0.9 | 85.0 | 62.1 | 13.5 | 76.0 | 3 | 11.7 | 11.6 | 1.2 | 2.4 | 4 | 3 | 0 | 0 | 0 | 0 | 0 | 0 | 0 | 0 | 0 | 1 | 1 | 1 | 0 | 0 | 1 | 0 | 0 | 0 | 0 | 0 |
| 0.9-1.0 | 85.3 | 270.5 | 206.7 | 100.0 | 1 | 11.8 | 8.3 | 0.0 | 0.0 | 1 | 1 | 0 | 0 | 0 | 0 | 0 | 0 | 0 | 0 | 1 | 0 | 0 | 0 | 0 | 0 | 0 | 0 | 0 | 0 | 0 | 0 |
| 1.0-1.1 | 85.5 | 0.0 | 0.0 | 0.0 | 0 | 11.8 | 9.6 | 0.0 | 0.0 | 1 | 1 | 0 | 0 | 0 | 0 | 0 | 0 | 0 | 0 | 0 | 1 | 0 | 0 | 0 | 0 | 0 | 0 | 0 | 0 | 0 | 0 |
| 1.1-1.2 | 85.7 | 0.0 | 0.0 | 0.0 | 0 | 11.8 | 12.7 | 0.6 | 1.2 | 5 | 1 | 0 | 0 | 0 | 0 | 0 | 0 | 0 | 0 | 0 | 0 | 0 | 2 | 2 | 0 | 1 | 0 | 0 | 0 | 0 | 0 |
| 1.2-1.3 | - | - | - | - | - | - | - | - | - | - | - | - | - | - | - | - | - | - | - | - | - | - | - | - | - | - | - | - | - | - | - |
| 1.3-1.4 | 86.1 | 29.5 | 22.3 | 100.0 | 1 | 11.9 | 13.3 | 0.5 | 1.2 | 7 | 2 | 0 | 0 | 0 | 0 | 0 | 0 | 0 | 0 | 0 | 0 | 0 | 0 | 4 | 1 | 1 | 1 | 0 | 0 | 0 | 0 |
| 1.4-1.5 | 86.4 | 0.0 | 0.0 | 0.0 | 0 | 11.9 | 11.1 | 1.8 | 3.5 | 4 | 3 | 0 | 0 | 0 | 0 | 0 | 0 | 1 | 0 | 0 | 0 | 0 | 1 | 1 | 0 | 1 | 0 | 0 | 0 | 0 | 0 |
| 1.5-1.6 | 86.6 | 0.0 | 0.0 | 0.0 | 0 | 11.9 | 13.9 | 0.5 | 0.9 | 3 | 1 | 0 | 0 | 0 | 0 | 0 | 0 | 0 | 0 | 0 | 0 | 0 | 0 | 1 | 0 | 2 | 0 | 0 | 0 | 0 | 0 |
| 1.6-1.7 | 86.8 | 114.1 | 18.5 | 100.0 | 1 | 12.0 | 12.0 | 0.4 | 1.4 | 10 | 3 | 0 | 0 | 0 | 0 | 0 | 0 | 0 | 0 | 1 | 0 | 0 | 3 | 3 | 3 | 0 | 0 | 0 | 0 | 0 | 0 |
| 1.7-1.8 | - | - | - | - | - | - | - | - | - | - | - | - | - | - | - | - | - | - | - | - | - | - | - | - | - | - | - | - | - | - | - |
| 1.8-1.9 | - | - | - | - | - | - | - | - | - | - | - | - | - | - | - | - | - | - | - | - | - | - | - | - | - | - | - | - | - | - | - |
| 1.9-2.0 | - | - | - | - | - | - | - | - | - | - | - | - | - | - | - | - | - | - | - | - | - | - | - | - | - | - | - | - | - | - | - |
| 2.0-2.1 | - | - | - | - | - | - | - | - | - | - | - | - | - | - | - | - | - | - | - | - | - | - | - | - | - | - | - | - | - | - | - |
| 2.1-2.2 | - | - | - | - | - | - | - | - | - | - | - | - | - | - | - | - | - | - | - | - | - | - | - | - | - | - | - | - | - | - | - |
| 2.2-2.3 | 88.1 | 0.0 | 0.0 | 0.0 | 0 | 12.1 | 11.7 | 1.0 | 2.1 | 4 | 1 | 0 | 0 | 0 | 0 | 0 | 0 | 0 | 0 | 0 | 1 | 0 | 1 | 1 | 0 | 1 | 0 | 0 | 0 | 0 | 0 |

* Fission Track Age and Mean Track Length predicted from the Default Thermal History (i.e. if the sample has not been hotter in the past)
† Combined data for all compositional groups

**Table B.3: Continued - (Geotrack Report #589)**

| Cl Wt % | Default fission track age* (Ma) | Measured fission track age (Ma) | Error in age (Ma) | P (χ 2) | Number of grains | Default fission track length* (μm) | Mean track length (μm) | Error in length (μm) | Std deviation (μm) | Number of lengths | Number of grains | Number of tracks in length interval 1 (μm) | 2 | 3 | 4 | 5 | 6 | 7 | 8 | 9 | 10 | 11 | 12 | 13 | 14 | 15 | 16 | 17 | 18 | 19 | 20 |
|---|---|---|---|---|---|---|---|---|---|---|---|---|---|---|---|---|---|---|---|---|---|---|---|---|---|---|---|---|---|---|
| †8622-49 | 38.1 | 33.8 | 8.3 | 0.0 | 20 | 10.1 | 11.4 | 0.4 | 1.5 | 14 | 7 | 0 | 0 | 0 | 0 | 0 | 0 | 0 | 1 | 0 | 1 | 2 | 6 | 2 | 2 | 0 | 0 | 0 | 0 | 0 | 0 |
| 0.0-0.1 | 0.0 | 1.1 | 1.1 | 50.0 | 4 | 0.0 | 0.0 | 0.0 | 0.0 | 0 | 0 | 0 | 0 | 0 | 0 | 0 | 0 | 0 | 0 | 0 | 0 | 0 | 0 | 0 | 0 | 0 | 0 | 0 | 0 | 0 | 0 |
| 0.1-0.2 | - | - | - | - | - | - | - | - | - | - | - | - | - | - | - | - | - | - | - | - | - | - | - | - | - | - | - | - | - | - | - |
| 0.2-0.3 | 0.2 | 0.0 | 0.0 | 0.0 | 0 | 8.1 | 10.3 | 0.0 | 0.0 | 1 | 1 | 0 | 0 | 0 | 0 | 0 | 0 | 0 | 0 | 0 | 0 | 1 | 0 | 0 | 0 | 0 | 0 | 0 | 0 | 0 | 0 |
| 0.3-0.4 | 1.0 | 96.8 | 41.5 | 24.0 | 2 | 8.4 | 0.0 | 0.0 | 0.0 | 0 | 0 | 0 | 0 | 0 | 0 | 0 | 0 | 0 | 0 | 0 | 0 | 0 | 0 | 0 | 0 | 0 | 0 | 0 | 0 | 0 | 0 |
| 0.4-0.5 | 24.9 | 22.2 | 13.5 | 65.0 | 3 | 8.2 | 0.0 | 0.0 | 0.0 | 0 | 0 | 0 | 0 | 0 | 0 | 0 | 0 | 0 | 0 | 0 | 0 | 0 | 0 | 0 | 0 | 0 | 0 | 0 | 0 | 0 | 0 |
| 0.5-0.6 | 38.9 | 28.7 | 13.7 | 17.0 | 2 | 8.7 | 0.0 | 0.0 | 0.0 | 0 | 0 | 0 | 0 | 0 | 0 | 0 | 0 | 0 | 0 | 0 | 0 | 0 | 0 | 0 | 0 | 0 | 0 | 0 | 0 | 0 | 0 |
| 0.6-0.7 | 51.4 | 39.3 | 21.5 | 12.0 | 3 | 9.2 | 10.9 | 0.5 | 0.8 | 3 | 1 | 0 | 0 | 0 | 0 | 0 | 0 | 0 | 0 | 0 | 1 | 0 | 2 | 0 | 0 | 0 | 0 | 0 | 0 | 0 | 0 |
| 0.7-0.8 | 62.5 | 46.9 | 16.5 | 100.0 | 1 | 9.6 | 12.7 | 0.8 | 1.2 | 2 | 1 | 0 | 0 | 0 | 0 | 0 | 0 | 0 | 0 | 0 | 0 | 0 | 1 | 0 | 1 | 0 | 0 | 0 | 0 | 0 | 0 |
| 0.8-0.9 | - | - | - | - | - | - | - | - | - | - | - | - | - | - | - | - | - | - | - | - | - | - | - | - | - | - | - | - | - | - | - |
| 0.9-1.0 | 76.0 | 65.1 | 30.5 | 100.0 | 1 | 10.1 | 0.0 | 0.0 | 0.0 | 0 | 0 | 0 | 0 | 0 | 0 | 0 | 0 | 0 | 0 | 0 | 0 | 0 | 0 | 0 | 0 | 0 | 0 | 0 | 0 | 0 | 0 |
| 1.0-1.1 | 77.4 | 89.2 | 29.7 | 64.0 | 2 | 10.2 | 0.0 | 0.0 | 0.0 | 0 | 0 | 0 | 0 | 0 | 0 | 0 | 0 | 0 | 0 | 0 | 0 | 0 | 0 | 0 | 0 | 0 | 0 | 0 | 0 | 0 | 0 |
| 1.1-1.2 | 78.8 | 74.9 | 43.8 | 100.0 | 1 | 10.2 | 12.3 | 0.8 | 1.4 | 3 | 1 | 0 | 0 | 0 | 0 | 0 | 0 | 0 | 0 | 0 | 0 | 1 | 0 | 1 | 1 | 0 | 0 | 0 | 0 | 0 | 0 |
| 1.2-1.3 | 80.2 | 0.0 | 0.0 | 0.0 | 0 | 10.3 | 11.5 | 0.2 | 0.4 | 3 | 1 | 0 | 0 | 0 | 0 | 0 | 0 | 0 | 0 | 0 | 0 | 0 | 2 | 1 | 0 | 0 | 0 | 0 | 0 | 0 | 0 |
| 1.3-1.4 | 81.6 | 12.2 | 12.5 | 100.0 | 1 | 10.3 | 9.8 | 2.0 | 2.8 | 2 | 2 | 0 | 0 | 0 | 0 | 0 | 0 | 0 | 1 | 0 | 0 | 0 | 1 | 0 | 0 | 0 | 0 | 0 | 0 | 0 | 0 |

*Fission Track Age and Mean Track Length predicted from the Default Thermal History (i.e. if the sample has not been hotter in the past)
†Combined data for all compositional groups

| | |
|---|---|
| Estimates | $z_i$ |
| Standard errors | $\sigma_i$ |
| Reference value | $z_o$ |
| Standardised estimates | $y_i = ( z_i - z_o) / \sigma_i$ |
| Precision | $x_i = 1 / \sigma_i$ |

**PLOT $y_i$ against $x_i$**

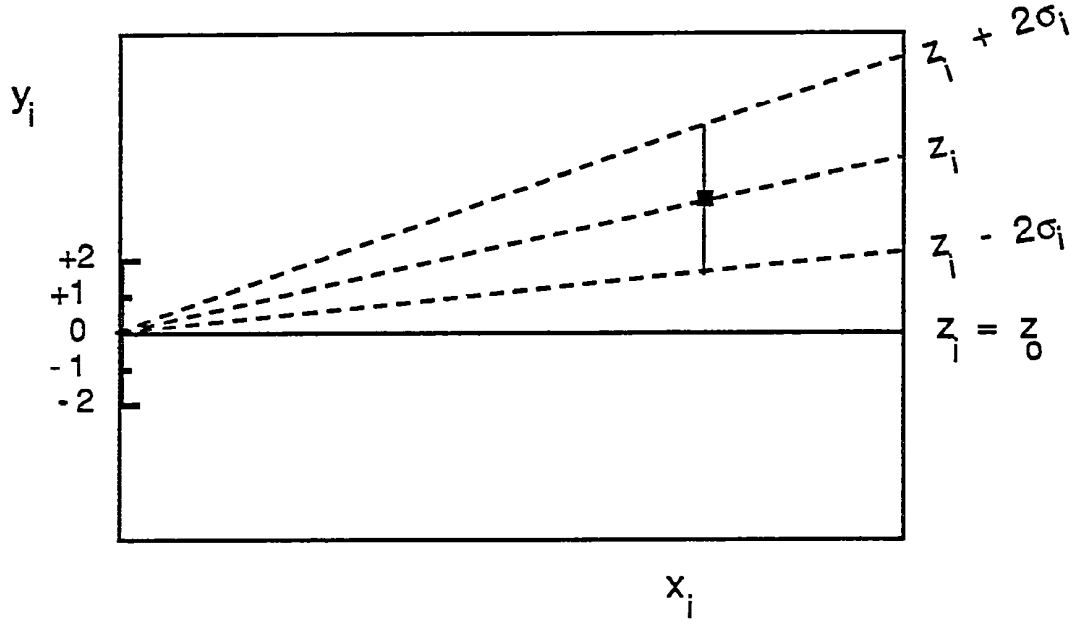


Slope of line from origin through data point $= y_i / x_i$

$= \{(z_i - z_o)/\sigma_i\} / \{1/\sigma_i\}$

$= z_i - z_o$

## Key Points:

Radial lines emanating from the origin correspond to fixed values of z

Data points with higher values of $x_i$ have greater precision.

Error bars on all points are the same size in this plot.

**Figure B.1** Basic construction of a radial plot. In AFTA, the estimates $z_i$ correspond to the fission track age values for individual apatite grains. Any convenient value of age can be chosen as the reference value corresponding to the horizontal in the radial plot. Radial lines emanating from the origin with positive slopes correspond to fission track ages greater than the reference value. Lines with negative slopes correspond to fission track ages less than the reference value.

*Normal radial plot (equations B.2 and B.3)*

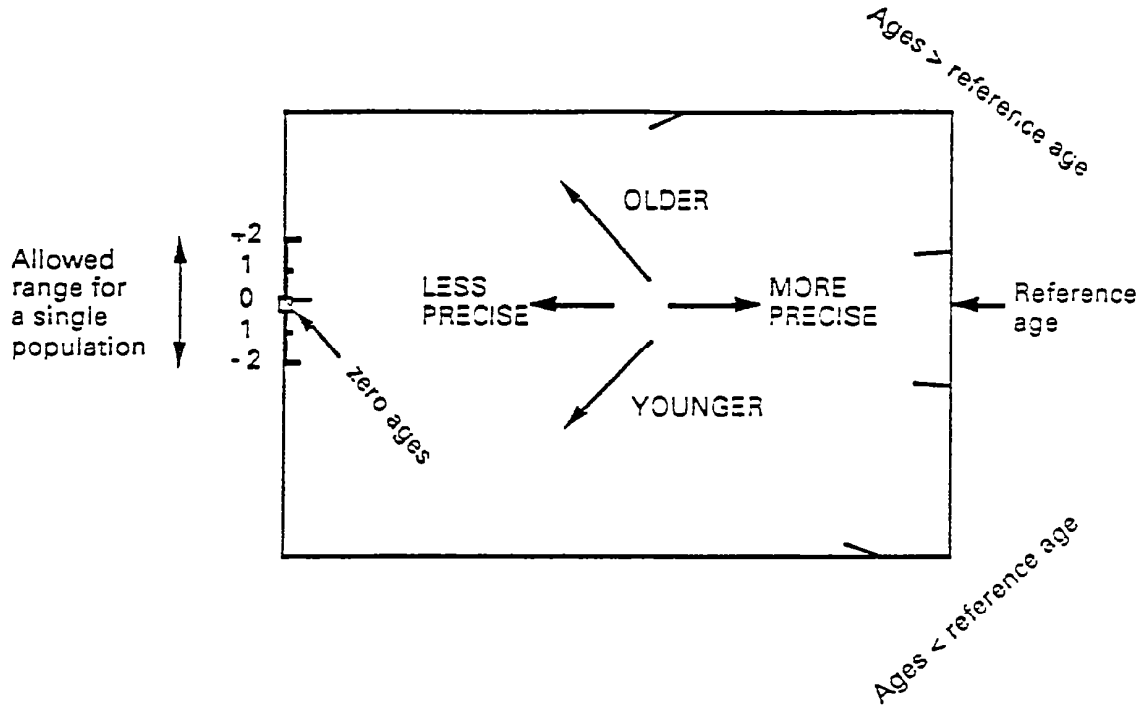


Arc-sin radial plot (equations B.2 and B.4)

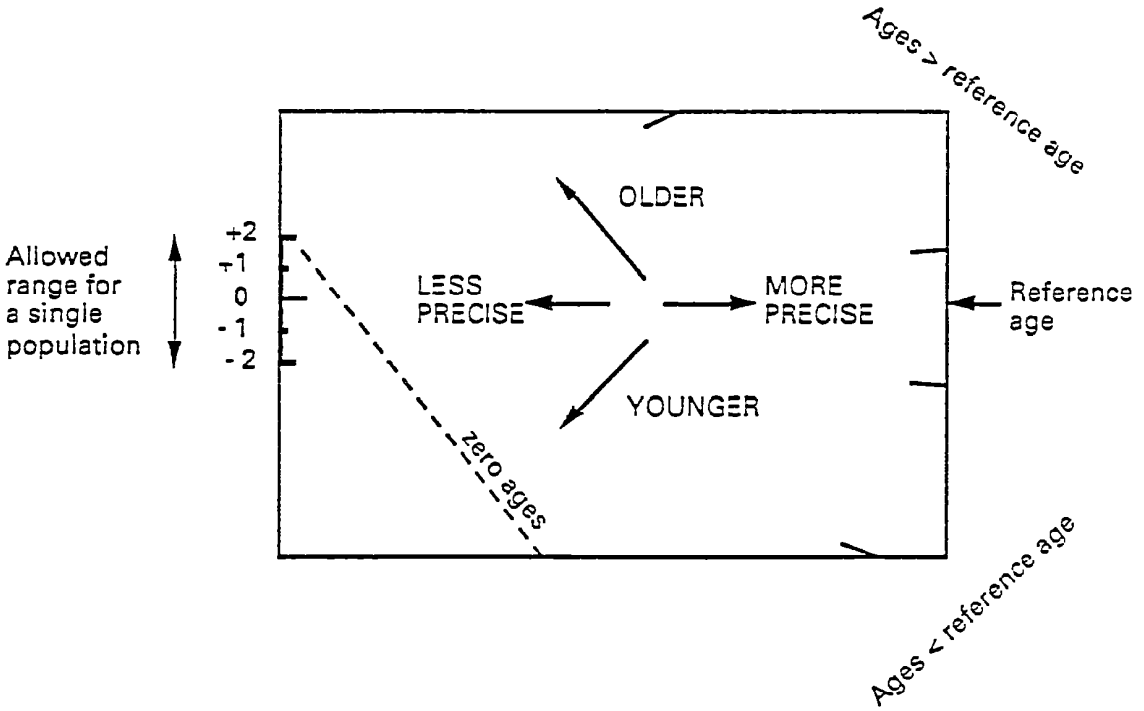


**Figure B.2** Simplified structure of Normal and Arc-sin radial plots.

GC589-3

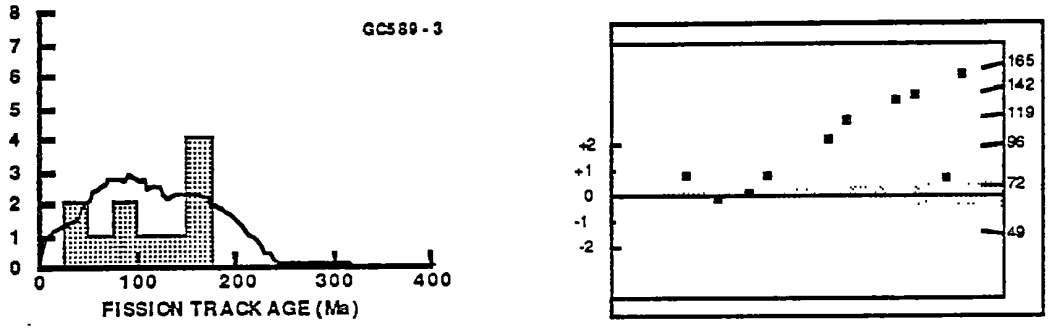


GC589-5

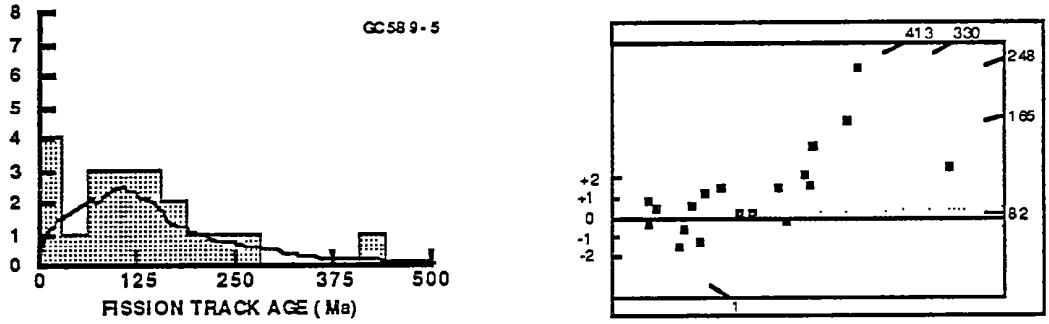


GC589-8

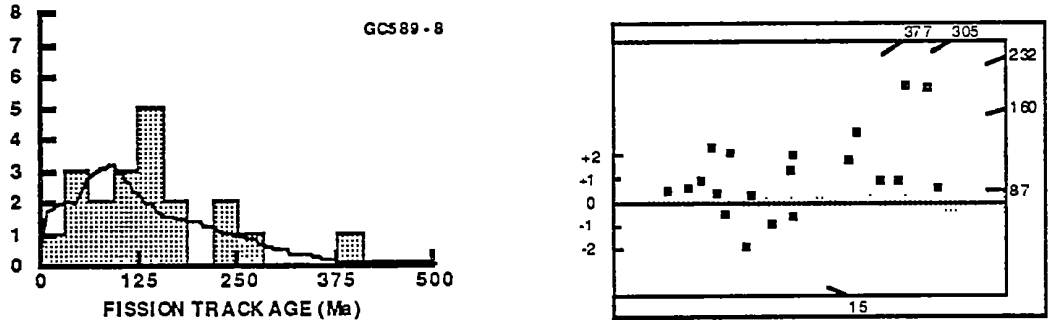


GC589-9

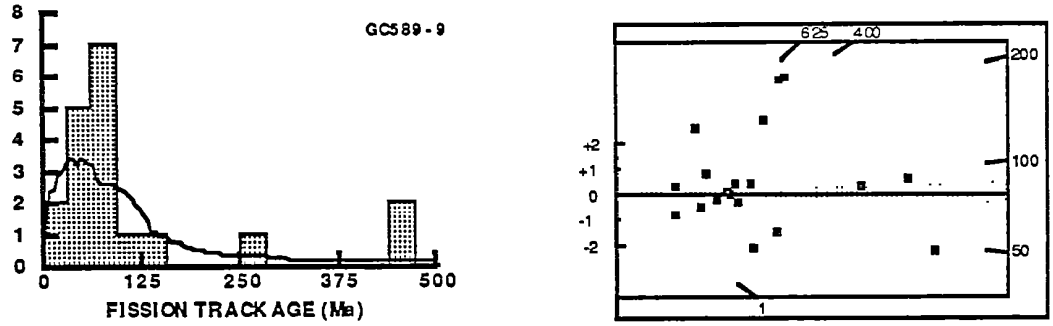


**Figure B.3a:** Single grain age figures for samples from **well Platypus-1, Duntroon Basin.** The horizontal line or shaded area in the radial plot diagrams shows the stratigraphic age. See Appendix B for further details.

GC589-10

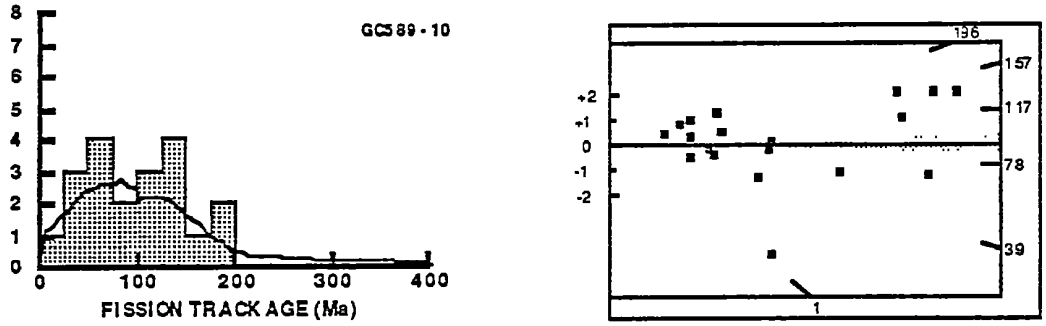


GC589-12

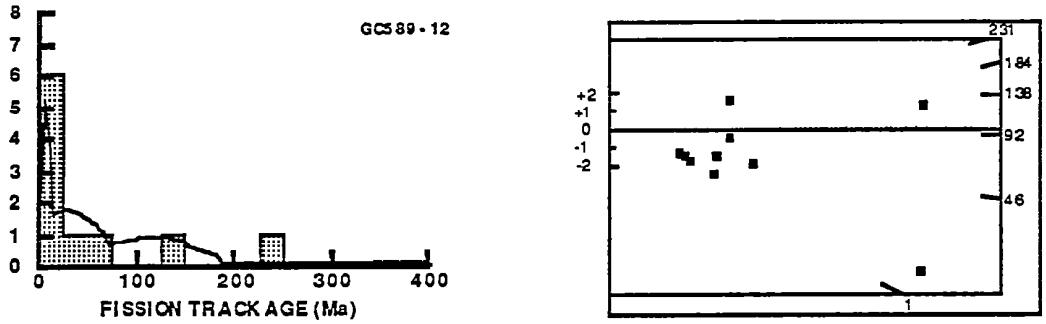


Figure B.3a: Continued.

8622-40

No Apatite

8622-41

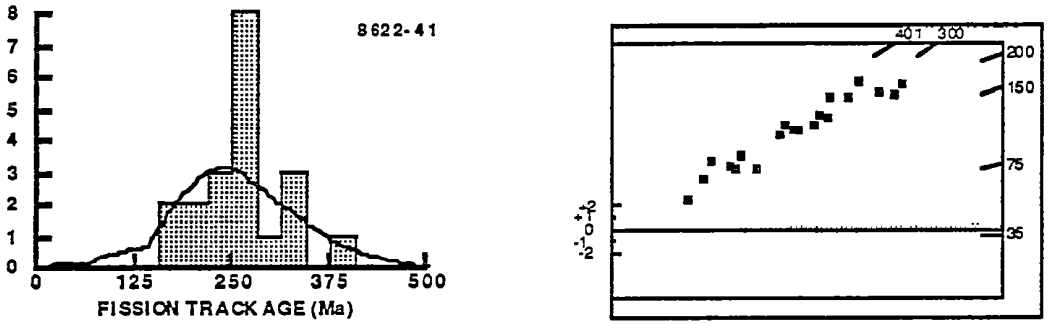


8622-42

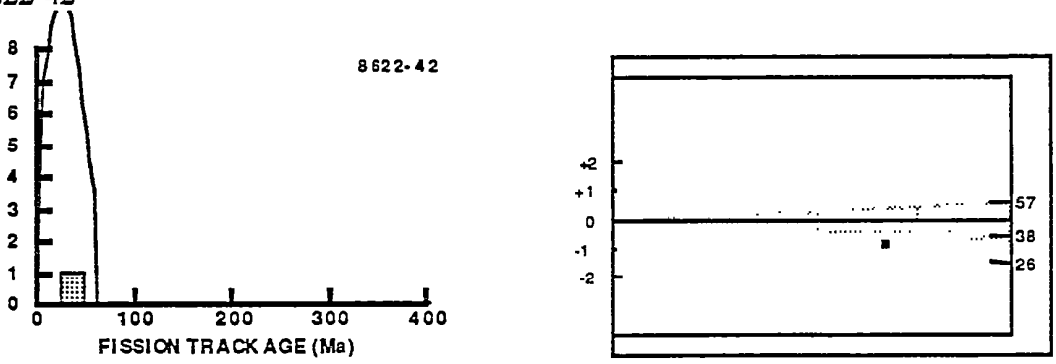


8622-43

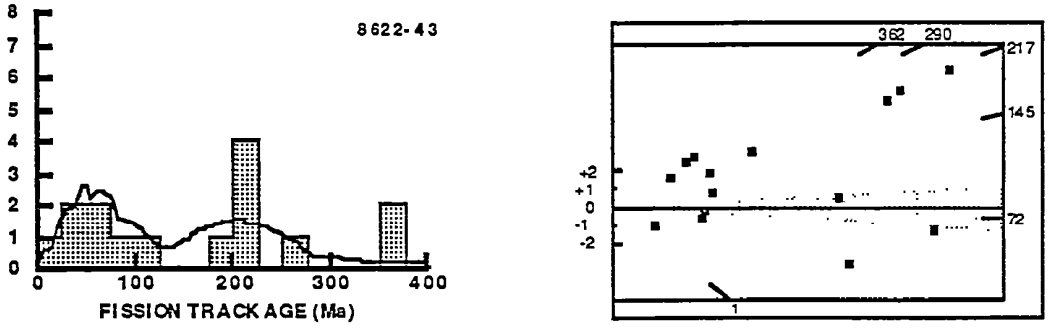


**Figure B.3b:** Single grain age figures for samples from **well Duntroon-1, Duntroon Basin.** The horizontal line or shaded area in the radial plot diagrams shows the stratigraphic age. See Appendix B for further details.

8622-45

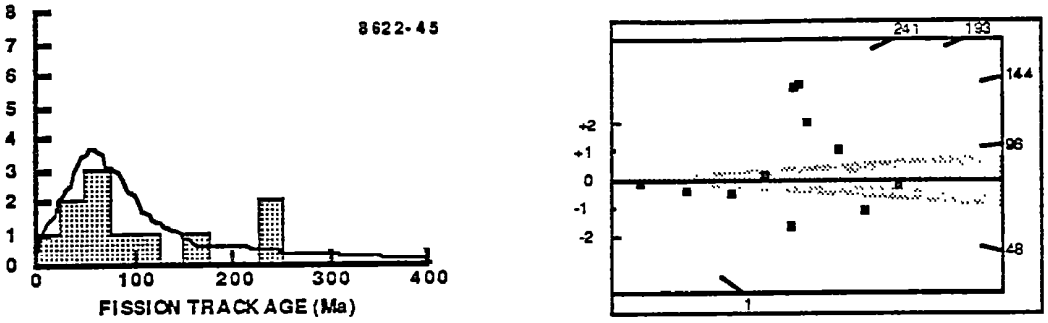


8622-46

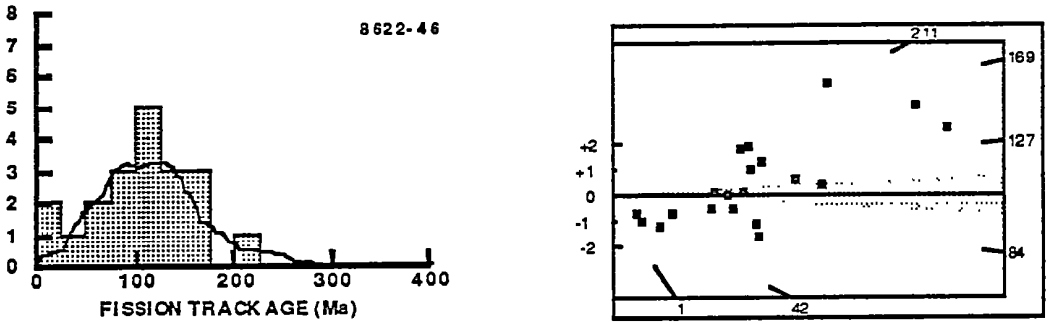


8622-47

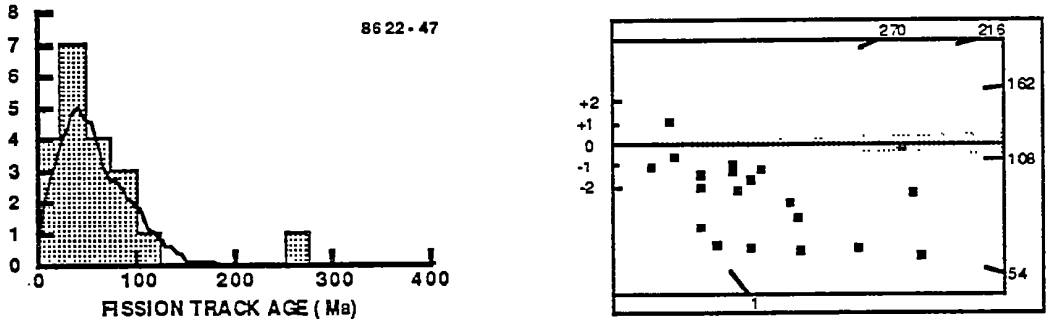


8622-49

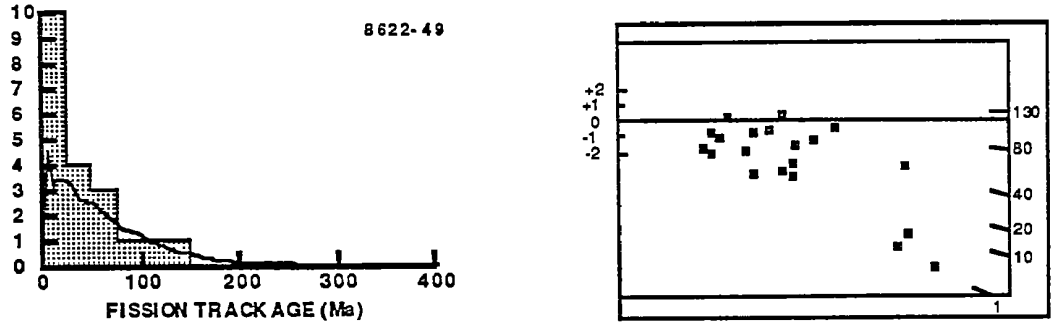


**Figure B.3b:** Continued.

GC589-3

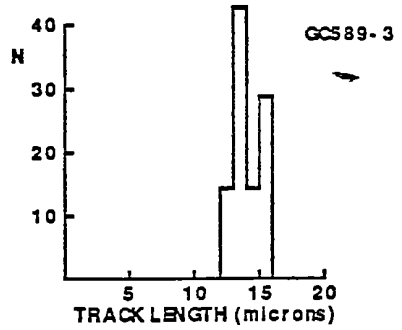


GC589-5

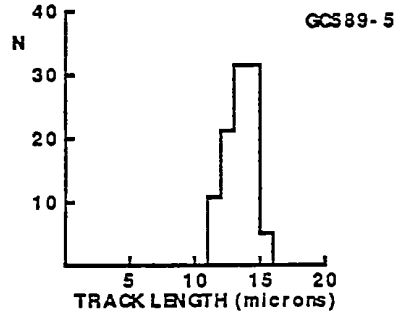


GC589-8

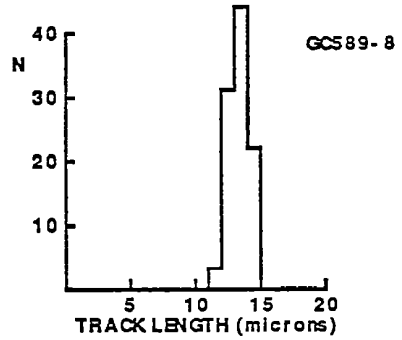


GC589-9

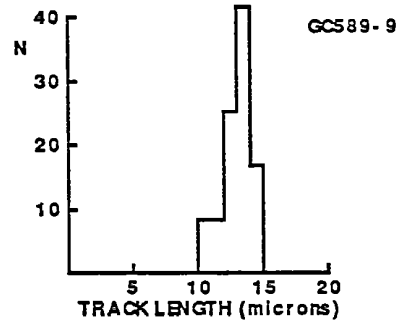


GC589-10

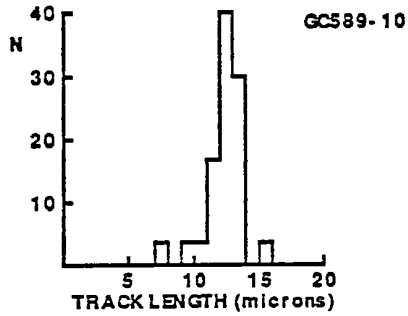


GC589-12

No Confined Tracks

**Figure B.4a:** Distributions of confined track lengths in samples from well Platypus-1, Duntroon Basin.

8622-40

No Apatite

8622-41

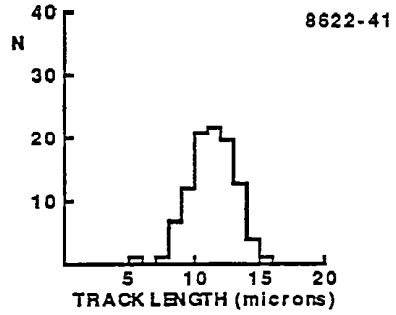


8622-42

No Confined Tracks

8622-43

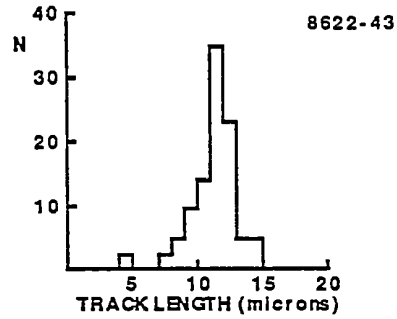


8622-45

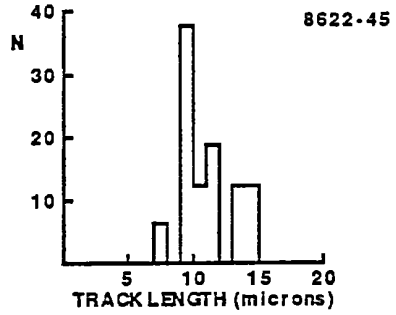


8622-46

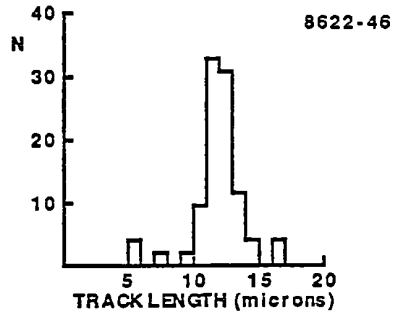


8622-47

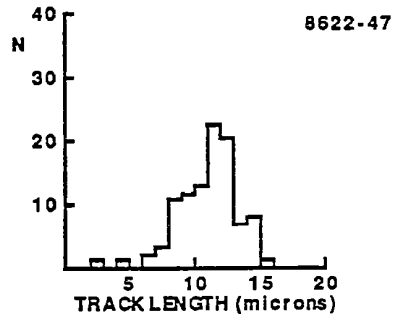


8622-49

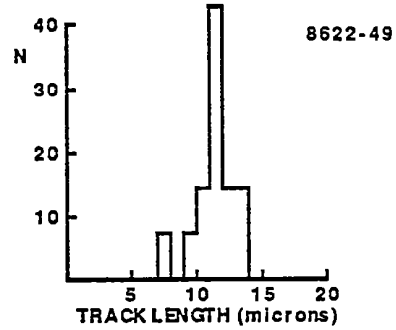


**Figure B.4b:** Distributions of confined track lengths in samples from well **Duntroon-1, Duntroon Basin.**

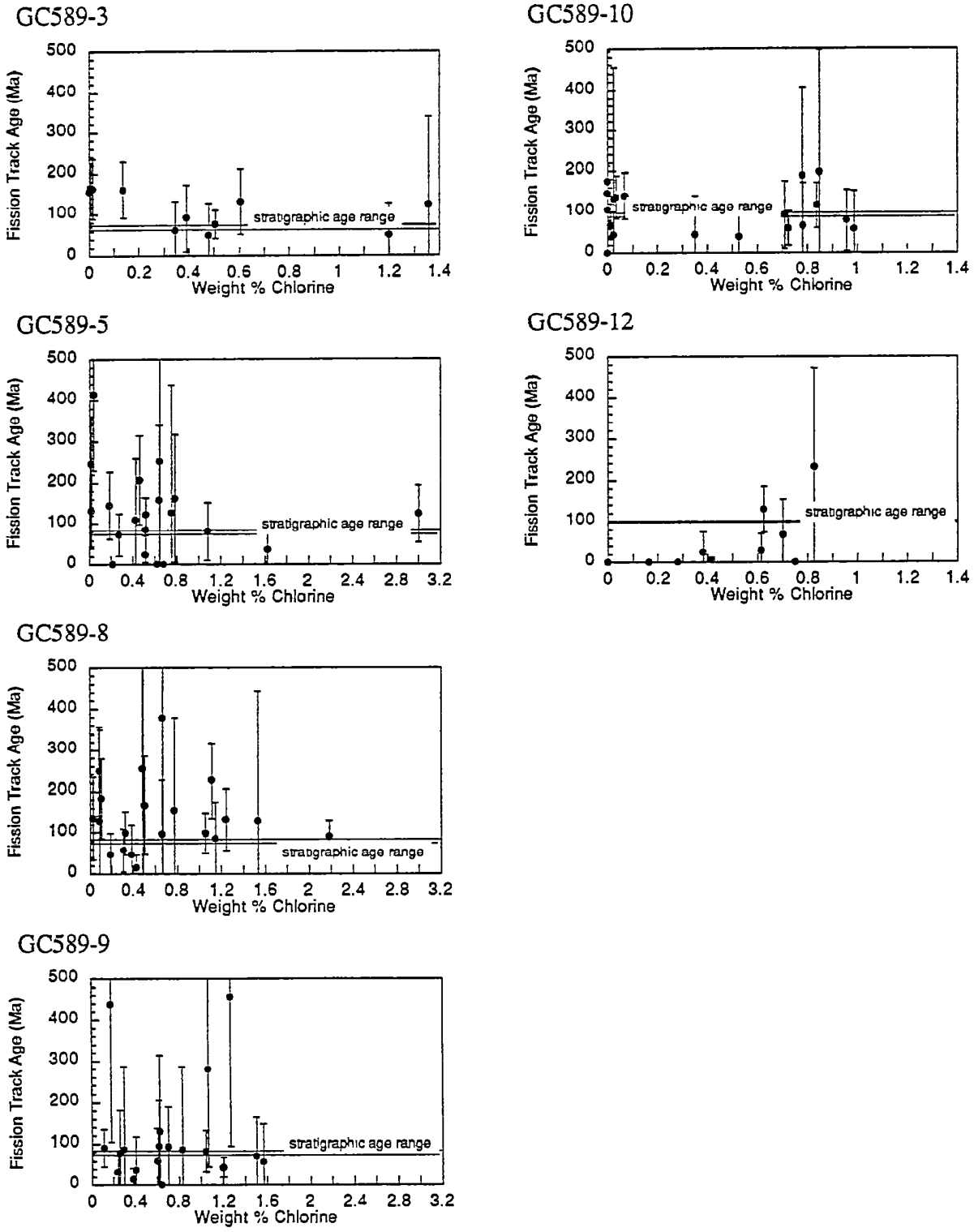


**Figure B.5a:** Plots of single grain age against weight percent chlorine for samples from well **Platypus-1, Duntroon Basin.**

8622-40

No Apatite

8622-45

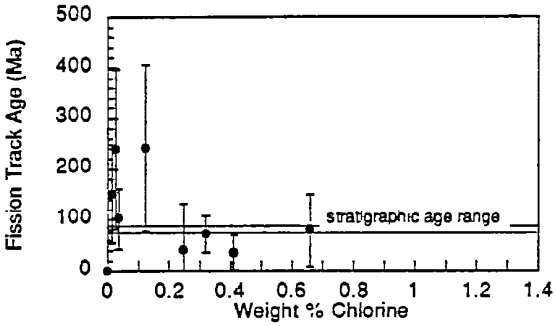


8622-41

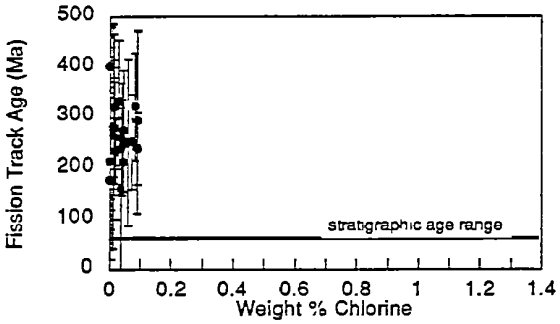


8622-46

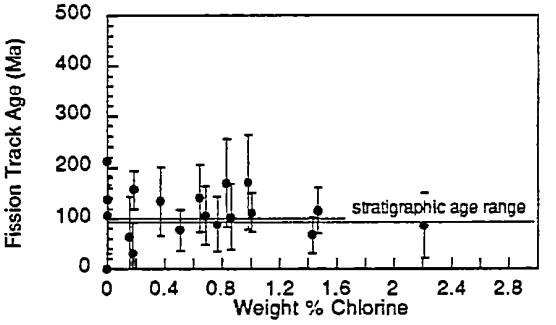


8622-42

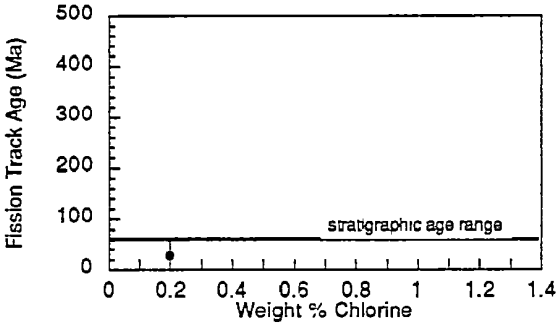


8622-47

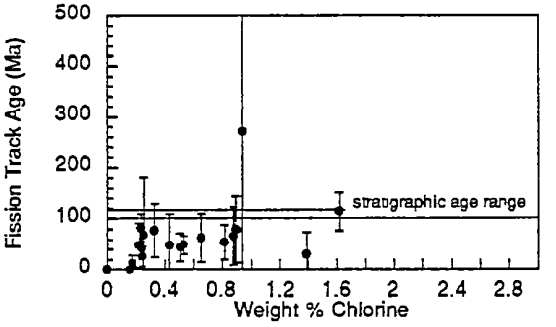


8622-43

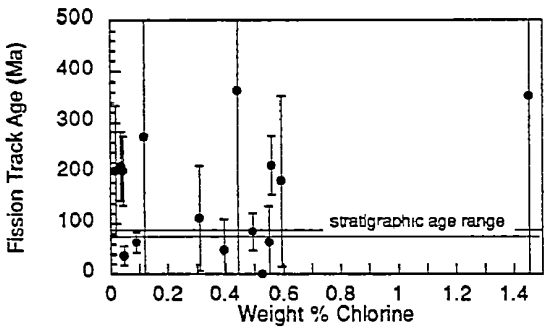


8622-49

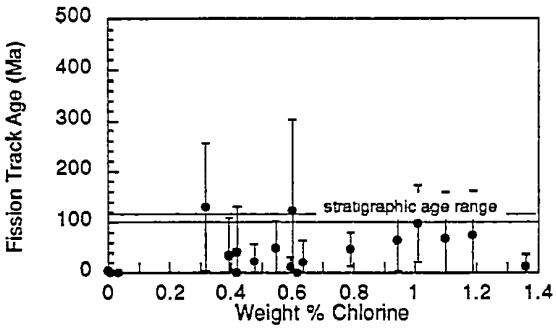


**Figure B.5b:** Plots of single grain age against weight percent chlorine for samples from well **Duntroon-1, Duntroon Basin.**

# Fission Track Age Data Sheets - Glossary

| | | |
|---|---|---|
| Ns | = | Number of spontaneous tracks in Na grid squares |
| Ni | = | Number of induced tracks in Na grid squares |
| Na | = | Number of grid squares counted in each grain |
| RATIO | = | Ns/Ni |
| U (ppm) | = | Uranium content of each grain (= U content of standard glass * $\rho i/\rho_D$) |
| Cl (wt%) | = | Weight percent chlorine content of each grain |
| RHOs | = | Spontaneous track density ($\rho s$) = Ns/ (Na*area of basic unit) |
| RHOi | = | Induced track density ($\rho i$) = Ni/ (Na*area of basic unit) |
| F.T.AGE | = | Fission track age, calculated using equation B.1 |
| Area of basic unit | = | Area of one grid square |
| Chi squared | = | $\chi^2$ parameter, used to assess variation of single grain ages within the sample |
| P(chi squared) | = | Probability of obtaining observed $\chi^2$ value for the relevant number of degrees of freedom, if all grains belong to a single population |
| Correlation coefficient | = | Correlation coefficient between Ns and Ni |
| Variance of SQR(Ns) | = | Variance of square root of Ns values - should be ~ 0.25 for Poisson distribution; greater if additional variation present |
| Variance of SQR(Ni) | = | Variance of square root of Ni values - should be ~ 0.25 for Poisson distribution; greater if additional variation present |
| Age Dispersion | = | % variation in single grain ages - see discussion in text re "Central age" |
| Ns/Ni | = | Pooled ratio, total spontaneous tracks divided by total induced tracks for all grains |
| Mean ratio | = | Mean of (Ns/Ni) for individual grains |
| Zeta | = | Calibration constant, determined empirically for each observer |
| RhoD | = | Track density ($\rho_D$) from uranium standard glass (interpolated from values at each end of stack) |
| ND | = | Total number of tracks counted for determining $\rho_D$ |
| POOLED AGE | = | Fission track age calculated from pooled ratio Ns/Ni. Valid only when $\chi^2 > 5\%$ |
| CENTRAL AGE | = | Alternative to pooled age when $\chi^2 < 5\%$ |

GC589-3 APATITE

IRRADIATION G597
SLIDE NUMBER 1 and 2
COUNTED BY: HJG

| Current grain no. | Ns | Ni | Na | RHOs | RHOi | RATIO | U (ppm) | Cl (wt%) | F.T. AGE (Ma) |
|---|---|---|---|---|---|---|---|---|---|
| 4 | 7 | 19 | 50 | 2.225E+05 | 6.038E+05 | 0.368 | 5.3 | 0.39 | 91.4 ± 40.5 |
| 5 | 2 | 10 | 15 | 2.119E+05 | 1.059E+06 | 0.200 | 9.4 | 1.20 | 49.8 ± 38.6 |
| 6 | 37 | 57 | 18 | 3.266E+06 | 5.032E+06 | 0.649 | 44.4 | 0.14 | 160.2 ± 34.1 |
| 7 | 17 | 32 | 15 | 1.801E+06 | 3.390E+06 | 0.531 | 29.9 | 0.60 | 131.4 ± 39.6 |
| 53 | 51 | 76 | 42 | 1.930E+06 | 2.875E+06 | 0.671 | 25.4 | 0.00 | 165.5 ± 30.3 |
| 54 | 22 | 35 | 30 | 1.165E+06 | 1.854E+06 | 0.629 | 16.4 | 0.00 | 155.2 ± 42.4 |
| 55 | 4 | 16 | 16 | 3.973E+05 | 1.589E+06 | 0.250 | 14.0 | 0.34 | 62.2 ± 34.8 |
| 56 | 27 | 88 | 50 | 8.581E+05 | 2.797E+06 | 0.307 | 24.7 | 0.50 | 76.2 ± 16.9 |
| 57 | 33 | 50 | 36 | 1.457E+06 | 2.207E+06 | 0.660 | 19.5 | 0.02 | 162.8 ± 36.8 |
| 58 | 2 | 10 | 30 | 1.059E+05 | 5.297E+05 | 0.200 | 4.7 | 0.48 | 49.8 ± 38.6 |
| 59 | 2 | 4 | 24 | 1.324E+05 | 2.648E+05 | 0.500 | 2.3 | 1.36 | 123.7 ± 107.2 |
| | 204 | 397 | | 9.944E+05 | 1.935E+06 | | 17.1 | | |

Area of basic unit = 6.293E-07 cm-2

Chi Squared = 16.351 with 10 degrees of freedom
P(chi squared) = 9.0 %
Correlation Coefficient = 0.879
Variance of SQR(Ns) = 4.47
Variance of SQR(Ni) = 5.90
Age Dispersion = 22.020 %

Ns/Ni = 0.514 ± 0.044
Mean Ratio = 0.451 ± 0.058

Ages calculated using a zeta of 386.9 ± 6.9 for CN5 glass
Rho D = 1.292E+06cm-2; ND = 2123
Rho D interpolated between top of can; Rho D = 1.292E+06cm-2, ND = 1016
bottom of can; Rho D = 1.407E+06cm-2, ND = 1107

**POOLED AGE = 127.1 ± 11.5 Ma**
CENTRAL AGE = 122.8 ± 14.8 Ma

GC589-5 APATITE

IRRADIATION G597
SLIDE NUMBER 3
COUNTED BY: HJG

| Current grain no. | Ns | Ni | Na | RHOs | RHOi | RATIO | U (ppm) | Cl (wt%) | F.T. AGE (Ma) |
|---|---|---|---|---|---|---|---|---|---|
| 5 | 5 | 8 | 40 | 1.986E+05 | 3.178E+05 | 0.625 | 2.7 | 0.64 | 158.2 ± 90.3 |
| 7 | 40 | 41 | 16 | 3.973E+06 | 4.072E+06 | 0.976 | 35.0 | 0.02 | 245.3 ± 54.9 |
| 10 | 20 | 35 | 40 | 7.945E+05 | 1.390E+06 | 0.571 | 12.0 | 0.19 | 144.8 ± 40.8 |
| 11 | 0 | 2 | 24 | 0.000E+00 | 1.324E+05 | 0.000 | 1.1 | 0.68 | 0.0 ± 0.0 |
| 12 | 55 | 33 | 30 | 2.913E+06 | 1.748E+06 | 1.667 | 15.0 | 0.04 | 413.5 ± 91.8 |
| 13 | 27 | 33 | 10 | 4.290E+06 | 5.244E+06 | 0.818 | 45.1 | 0.46 | 206.3 ± 53.9 |
| 14 | 1 | 11 | 36 | 4.414E+04 | 4.855E+05 | 0.091 | 4.2 | 0.52 | 23.3 ± 24.3 |
| 15 | 0 | 2 | 24 | 0.000E+00 | 1.324E+05 | 0.000 | 1.1 | 0.62 | 0.0 ± 0.0 |
| 17 | 7 | 11 | 30 | 3.708E+05 | 5.827E+05 | 0.636 | 5.0 | 0.78 | 161.0 ± 78.0 |
| 20 | 1 | 1 | 30 | 5.297E+04 | 5.297E+04 | 1.000 | 0.5 | 0.64 | 251.3 ± 355.5 |
| 21 | 0 | 7 | 24 | 0.000E+00 | 4.635E+05 | 0.000 | 4.0 | 0.22 | 0.0 ± 0.0 |
| 23 | 19 | 39 | 16 | 1.887E+06 | 3.873E+06 | 0.487 | 33.3 | 3.00 | 123.6 ± 34.8 |
| 25 | 14 | 27 | 30 | 7.416E+05 | 1.430E+06 | 0.519 | 12.3 | 0.02 | 131.5 ± 43.5 |
| 26 | 7 | 22 | 16 | 6.952E+05 | 2.185E+06 | 0.318 | 18.8 | 1.08 | 81.0 ± 35.2 |
| 27 | 54 | 112 | 25 | 3.432E+06 | 7.119E+06 | 0.482 | 61.3 | 0.52 | 122.4 ± 20.6 |
| 28 | 10 | 35 | 12 | 1.324E+06 | 4.635E+06 | 0.286 | 39.9 | 0.28 | 72.8 ± 26.2 |
| 29 | 1 | 7 | 40 | 3.973E+04 | 2.781E+05 | 0.143 | 2.4 | 1.63 | 36.5 ± 39.0 |
| 30 | 6 | 18 | 16 | 5.959E+05 | 1.788E+06 | 0.333 | 15.4 | 0.52 | 84.9 ± 40.1 |
| 31 | 1 | 2 | 12 | 1.324E+05 | 2.648E+05 | 0.500 | 2.3 | 0.75 | 126.9 ± 155.4 |
| 33 | 3 | 7 | 40 | 1.192E+05 | 2.781E+05 | 0.429 | 2.4 | 0.43 | 108.9 ± 75.2 |
| | 271 | 453 | | 8.427E+05 | 1.409E+06 | | 12.1 | | |

Area of basic unit = 6.293E-07 cm-2

Chi Squared = 54.153 with 19 degrees of freedom
P(chi squared) = 0.0 %
Correlation Coefficient = 0.815
Variance of SQR(Ns) = 5.49
Variance of SQR(Ni) = 5.57
Age Dispersion = 49.555 %

Ns/Ni = 0.598 ± 0.046
Mean Ratio = 0.494 ± 0.091

Ages calculated using a zeta of 386.9 ± 6.9 for CN5 glass
Rho D = 1.325E+06cm-2; ND = 2123
Rho D interpolated between top of can; Rho D = 1.292E+06cm-2, ND = 1016
bottom of can; Rho D = 1.407E+06cm-2, ND = 1107

POOLED AGE = 151.5 ± 12.4 Ma
**CENTRAL AGE = 127.9 ± 20.1 Ma**

GC589-8 APATITE

IRRADIATION G597
SLIDE NUMBER 4
COUNTED BY: HJG

| Current grain no. | Ns | Ni | Na | RHOs | RHOi | RATIO | U (ppm) | Cl (wt%) | F.T. AGE (Ma) |
|---|---|---|---|---|---|---|---|---|---|
| 4 | 4 | 22 | 50 | 1.271E+05 | 6.992E+05 | 0.182 | 5.9 | 0.19 | 47.0 ± 25.6 |
| 5 | 19 | 37 | 30 | 1.006E+06 | 1.960E+06 | 0.514 | 16.7 | 1.24 | 131.9 ± 37.4 |
| 6 | 28 | 80 | 16 | 2.781E+06 | 7.945E+06 | 0.350 | 67.5 | 2.18 | 90.2 ± 20.0 |
| 7 | 6 | 4 | 30 | 3.178E+05 | 2.119E+05 | 1.500 | 1.8 | 0.67 | 377.9 ± 244.2 |
| 9 | 2 | 4 | 12 | 2.648E+05 | 5.297E+05 | 0.500 | 4.5 | 0.09 | 128.4 ± 111.3 |
| 11 | 25 | 35 | 24 | 1.655E+06 | 2.317E+06 | 0.714 | 19.7 | 0.11 | 182.7 ± 48.1 |
| 12 | 5 | 15 | 24 | 3.311E+05 | 9.932E+05 | 0.333 | 8.4 | 1.15 | 85.9 ± 44.4 |
| 13 | 23 | 60 | 50 | 7.310E+05 | 1.907E+06 | 0.383 | 16.2 | 1.06 | 98.7 ± 24.4 |
| 14 | 2 | 11 | 24 | 1.324E+05 | 7.283E+05 | 0.182 | 6.2 | 0.39 | 47.0 ± 36.2 |
| 15 | 1 | 2 | 15 | 1.059E+05 | 2.119E+05 | 0.500 | 1.8 | 1.53 | 128.4 ± 157.3 |
| 16 | 6 | 27 | 16 | 5.959E+05 | 2.682E+06 | 0.222 | 22.8 | 0.31 | 57.4 ± 26.0 |
| 22 | 47 | 53 | 20 | 3.734E+06 | 4.211E+06 | 0.887 | 35.8 | 1.12 | 226.1 ± 45.7 |
| 23 | 13 | 20 | 30 | 6.886E+05 | 1.059E+06 | 0.650 | 9.0 | 0.50 | 166.5 ± 59.5 |
| 24 | 20 | 52 | 18 | 1.766E+06 | 4.591E+06 | 0.385 | 39.0 | 0.33 | 99.0 ± 26.2 |
| 25 | 43 | 44 | 30 | 2.278E+06 | 2.331E+06 | 0.977 | 19.8 | 0.09 | 248.7 ± 53.8 |
| 26 | 7 | 7 | 40 | 2.781E+05 | 2.781E+05 | 1.000 | 2.4 | 0.49 | 254.4 ± 136.2 |
| 27 | 3 | 5 | 16 | 2.980E+05 | 4.966E+05 | 0.600 | 4.2 | 0.78 | 153.8 ± 112.4 |
| 29 | 11 | 21 | 16 | 1.092E+06 | 2.086E+06 | 0.524 | 17.7 | 0.03 | 134.5 ± 50.2 |
| 31 | 3 | 8 | 20 | 2.384E+05 | 6.356E+05 | 0.375 | 5.4 | 0.66 | 96.6 ± 65.4 |
| 32 | 1 | 17 | 50 | 3.178E+04 | 5.403E+05 | 0.059 | 4.6 | 0.43 | 15.2 ± 15.7 |
| | 269 | 524 | | 8.050E+05 | 1.568E+06 | | 13.3 | | |

Area of basic unit = 6.293E-07 cm-2

Chi Squared = 46.441 with 19 degrees of freedom
P(chi squared) = 0.0 %
Correlation Coefficient = 0.790
Variance of SQR(Ns) = 3.27
Variance of SQR(Ni) = 4.72
Age Dispersion = 40.864 %

Ns/Ni = 0.513 ± 0.038
Mean Ratio = 0.542 ± 0.077

Ages calculated using a zeta of 386.9 ± 6.9 for CN5 glass
Rho D = 1.341E+06cm-2; ND = 2123
Rho D interpolated between top of can; Rho D = 1.292E+06cm-2, ND = 1016
bottom of can; Rho D = 1.407E+06cm-2, ND = 1107

POOLED AGE = 131.8 ± 10.6 Ma
**CENTRAL AGE = 124.6 ± 16.5 Ma**

GC589-9 APATITE

IRRADIATION G597
SLIDE NUMBER 5
COUNTED BY: HJG

| Current grain no. | Ns | Ni | Na | RHOs | RHOi | RATIO | U (ppm) | Cl (wt%) | F.T. AGE (Ma) |
|---|---|---|---|---|---|---|---|---|---|
| 4 | 18 | 10 | 25 | 1.144E+06 | 6.356E+05 | 1.800 | 5.3 | 1.27 | 456.2 ± 180.4 |
| 5 | 1 | 3 | 15 | 1.059E+05 | 3.178E+05 | 0.333 | 2.7 | 0.30 | 87.0 ± 100.4 |
| 8 | 5 | 14 | 60 | 1.324E+05 | 3.708E+05 | 0.357 | 3.1 | 0.71 | 93.1 ± 48.6 |
| 9 | 3 | 6 | 40 | 1.192E+05 | 2.384E+05 | 0.500 | 2.0 | 0.63 | 130.0 ± 92.0 |
| 10 | 0 | 4 | 30 | 0.000E+00 | 2.119E+05 | 0.000 | 1.8 | 0.64 | 0.0 ± 0.0 |
| 11 | 19 | 11 | 24 | 1.258E+06 | 7.283E+05 | 1.727 | 6.1 | 0.18 | 438.4 ± 166.6 |
| 12 | 15 | 47 | 50 | 4.767E+05 | 1.494E+06 | 0.319 | 12.5 | 1.05 | 83.3 ± 24.8 |
| 13 | 15 | 89 | 80 | 2.980E+05 | 1.768E+06 | 0.169 | 14.8 | 1.20 | 44.1 ± 12.4 |
| 14 | 12 | 11 | 25 | 7.628E+05 | 6.992E+05 | 1.091 | 5.9 | 1.07 | 280.3 ± 117.3 |
| 15 | 1 | 3 | 25 | 6.356E+04 | 1.907E+05 | 0.333 | 1.6 | 0.83 | 87.0 ± 100.4 |
| 16 | 3 | 11 | 32 | 1.490E+05 | 5.462E+05 | 0.273 | 4.6 | 1.50 | 71.2 ± 46.4 |
| 17 | 3 | 10 | 25 | 1.907E+05 | 6.356E+05 | 0.300 | 5.3 | 0.26 | 78.3 ± 51.6 |
| 18 | 23 | 66 | 16 | 2.284E+06 | 6.555E+06 | 0.348 | 55.0 | 0.12 | 90.9 ± 22.2 |
| 19 | 1 | 19 | 60 | 2.648E+04 | 5.032E+05 | 0.053 | 4.2 | 0.39 | 13.8 ± 14.2 |
| 20 | 3 | 13 | 30 | 1.589E+05 | 6.886E+05 | 0.231 | 5.8 | 0.61 | 60.3 ± 38.7 |
| 21 | 5 | 2 | 20 | 3.973E+05 | 1.589E+05 | 2.500 | 1.3 | 0.64 | 625.3 ± 523.4 |
| 22 | 2 | 9 | 24 | 1.324E+05 | 5.959E+05 | 0.222 | 5.0 | 1.57 | 58.1 ± 45.4 |
| 23 | 3 | 24 | 24 | 1.986E+05 | 1.589E+06 | 0.125 | 13.3 | 0.24 | 32.7 ± 20.1 |
| 24 | 1 | 7 | 30 | 5.297E+04 | 3.708E+05 | 0.143 | 3.1 | 0.41 | 37.4 ± 40.0 |
| 25 | 4 | 11 | 35 | 1.816E+05 | 4.994E+05 | 0.364 | 4.2 | 0.62 | 94.8 ± 55.4 |
| | 137 | 370 | | 3.249E+05 | 8.775E+05 | | 7.4 | | |

Area of basic unit = 6.293E-07 cm-2

Chi Squared = 75.080 with 19 degrees of freedom
P(chi squared) = 0.0 %
Correlation Coefficient = 0.613
Variance of SQR(Ns) = 1.84
Variance of SQR(Ni) = 4.44
Age Dispersion = 77.875 %

Ns/Ni = 0.370 ± 0.037
Mean Ratio = 0.559 ± 0.151

Ages calculated using a zeta of 386.9 ± 6.9 for CN5 glass
Rho D = 1.358E+06cm-2; ND = 2123
Rho D interpolated between top of can; Rho D = 1.292E+06cm-2, ND = 1016
bottom of can; Rho D = 1.407E+06cm-2, ND = 1107

POOLED AGE = 96.5 ± 10.0 Ma
**CENTRAL AGE = 104.9 ± 22.6 Ma**

GC589-10 APATITE

IRRADIATION G597
SLIDE NUMBER 6
COUNTED BY: HJG

| Current grain no. | Ns | Ni | Na | RHOs | RHOi | RATIO | U (ppm) | Cl (wt%) | F.T. AGE (Ma) |
|---|---|---|---|---|---|---|---|---|---|
| 3 | 5 | 7 | 30 | 2.648E+05 | 3.708E+05 | 0.714 | 3.1 | 0.78 | 187.1 ± 109.7 |
| 4 | 2 | 5 | 24 | 1.324E+05 | 3.311E+05 | 0.400 | 2.7 | 0.00 | 105.5 ± 88.3 |
| 5 | 7 | 20 | 40 | 2.781E+05 | 7.945E+05 | 0.350 | 6.6 | 0.71 | 92.4 ± 40.7 |
| 6 | 21 | 82 | 30 | 1.112E+06 | 4.343E+06 | 0.256 | 36.0 | 0.01 | 67.7 ± 16.7 |
| 7 | 3 | 20 | 25 | 1.907E+05 | 1.271E+06 | 0.150 | 10.5 | 0.53 | 39.8 ± 24.6 |
| 8 | 1 | 6 | 9 | 1.766E+05 | 1.059E+06 | 0.167 | 8.8 | 0.35 | 44.2 ± 47.7 |
| 9 | 2 | 3 | 60 | 5.297E+04 | 7.945E+04 | 0.667 | 0.7 | 0.00 | 174.8 ± 159.7 |
| 10 | 42 | 81 | 30 | 2.225E+06 | 4.290E+06 | 0.519 | 35.6 | 0.04 | 136.4 ± 26.2 |
| 11 | 37 | 70 | 40 | 1.470E+06 | 2.781E+06 | 0.529 | 23.1 | 0.07 | 139.0 ± 28.5 |
| 12 | 3 | 4 | 25 | 1.907E+05 | 2.542E+05 | 0.750 | 2.1 | 0.85 | 196.4 ± 150.1 |
| 13 | 27 | 61 | 40 | 1.073E+06 | 2.423E+06 | 0.443 | 20.1 | 0.84 | 116.6 ± 27.2 |
| 14 | 6 | 20 | 30 | 3.178E+05 | 1.059E+06 | 0.300 | 8.8 | 0.96 | 79.3 ± 37.0 |
| 15 | 1 | 6 | 15 | 1.059E+05 | 6.356E+05 | 0.167 | 5.3 | 0.02 | 44.2 ± 47.7 |
| 16 | 2 | 9 | 25 | 1.271E+05 | 5.721E+05 | 0.222 | 4.7 | 0.99 | 58.8 ± 46.0 |
| 17 | 0 | 27 | 60 | 0.000E+00 | 7.151E+05 | 0.000 | 5.9 | 0.00 | 0.0 ± 0.0 |
| 18 | 10 | 44 | 40 | 3.973E+05 | 1.748E+06 | 0.227 | 14.5 | 0.72 | 60.1 ± 21.1 |
| 19 | 2 | 8 | 40 | 7.945E+04 | 3.178E+05 | 0.250 | 2.6 | 0.78 | 66.1 ± 52.3 |
| 20 | 1 | 2 | 30 | 5.297E+04 | 1.059E+05 | 0.500 | 0.9 | 0.03 | 131.6 ± 161.2 |
| 21 | 4 | 9 | 40 | 1.589E+05 | 3.575E+05 | 0.444 | 3.0 | 1.78 | 117.1 ± 70.4 |
| 22 | 30 | 54 | 40 | 1.192E+06 | 2.145E+06 | 0.556 | 17.8 | 0.00 | 146.0 ± 33.5 |
| | 206 | 538 | | 4.864E+05 | 1.270E+06 | | 10.5 | | |

Area of basic unit = 6.293E-07 cm-2

Chi Squared = 30.840 with 19 degrees of freedom
P(chi squared) = 4.2 %
Correlation Coefficient = 0.908
Variance of SQR(Ns) = 3.61
Variance of SQR(Ni) = 6.72
Age Dispersion = 33.916 %

Ns/Ni = 0.383 ± 0.031
Mean Ratio = 0.380 ± 0.046

Ages calculated using a zeta of 386.9 ± 6.9 for CN5 glass
Rho D = 1.374E+06cm-2; ND = 2123
Rho D interpolated between top of can; Rho D = 1.292E+06cm-2, ND = 1016
bottom of can; Rho D = 1.407E+06cm-2, ND = 1107

POOLED AGE = 101.0 ± 8.7 Ma
**CENTRAL AGE = 93.5 ± 12.2 Ma**

GC589-12 APATITE

IRRADIATION G597
SLIDE NUMBER 7
COUNTED BY: HJG

| Current grain no. | Ns | Ni | Na | RHOs | RHOi | RATIO | U (ppm) | Cl (wt%) | F.T. AGE (Ma) |
|---|---|---|---|---|---|---|---|---|---|
| 3 | 0 | 7 | 36 | 0.000E+00 | 3.090E+05 | 0.000 | 2.5 | 0.75 | 0.0 ± 0.0 |
| 4 | 7 | 8 | 25 | 4.449E+05 | 5.085E+05 | 0.875 | 4.2 | 0.83 | 231.2 ± 119.8 |
| 5 | 0 | 11 | 30 | 0.000E+00 | 5.827E+05 | 0.000 | 4.8 | 0.00 | 0.0 ± 0.0 |
| 6 | 33 | 68 | 60 | 8.740E+05 | 1.801E+06 | 0.485 | 14.8 | 0.63 | 129.3 ± 27.7 |
| 7 | 0 | 6 | 20 | 0.000E+00 | 4.767E+05 | 0.000 | 3.9 | 0.16 | 0.0 ± 0.0 |
| 9 | 1 | 11 | 50 | 3.178E+04 | 3.496E+05 | 0.091 | 2.9 | 0.38 | 24.4 ± 25.5 |
| 10 | 2 | 97 | 30 | 1.059E+05 | 5.138E+06 | 0.021 | 42.1 | 0.42 | 5.5 ± 4.0 |
| 11 | 0 | 5 | 70 | 0.000E+00 | 1.135E+05 | 0.000 | 0.9 | 0.28 | 0.0 ± 0.0 |
| 12 | 3 | 12 | 24 | 1.986E+05 | 7.945E+05 | 0.250 | 6.5 | 0.70 | 66.9 ± 43.2 |
| 13 | 2 | 19 | 60 | 5.297E+04 | 5.032E+05 | 0.105 | 4.1 | 0.62 | 28.3 ± 21.0 |
| | 48 | 244 | | 1.883E+05 | 9.574E+05 | | 7.8 | | |

Area of basic unit = 6.293E-07 cm-2

Chi Squared = 51.489 with 9 degrees of freedom
P(chi squared) = -0.0 %
Correlation Coefficient = 0.488
Variance of SQR(Ns) = 3.17
Variance of SQR(Ni) = 6.84
Age Dispersion = 118.330 %

Ns/Ni = 0.197 ± 0.031
Mean Ratio = 0.183 ± 0.091

Ages calculated using a zeta of 386.9 ± 6.9 for CN5 glass
Rho D = 1.391E+06cm-2; ND = 2123
Rho D interpolated between top of can; Rho D = 1.292E+06cm-2, ND = 1016
bottom of can; Rho D = 1.407E+06cm-2, ND = 1107

POOLED AGE = 52.7 ± 8.5 Ma
**CENTRAL AGE = 41.4 ± 18.3 Ma**

8622-41 APATITE

IRRADIATION PT766
SLIDE NUMBER 2
COUNTED BY: MEM

| Current grain no. | Ns | Ni | Na | RHOs | RHOi | RATIO | U (ppm) | Cl (wt%) | F.T. AGE (Ma) |
|---|---|---|---|---|---|---|---|---|---|
| 3 | 77 | 47 | 100 | 1.224E+06 | 7.469E+05 | 1.638 | 8.1 | 0.03 | 330.8 ± 61.7 |
| 4 | 18 | 9 | 42 | 6.810E+05 | 3.405E+05 | 2.000 | 3.7 | 0.00 | 401.6 ± 164.2 |
| 5 | 67 | 54 | 28 | 3.802E+06 | 3.065E+06 | 1.241 | 33.3 | 0.07 | 252.1 ± 46.5 |
| 6 | 26 | 30 | 14 | 2.951E+06 | 3.405E+06 | 0.867 | 37.0 | 0.00 | 177.1 ± 47.6 |
| 7 | 58 | 49 | 18 | 5.120E+06 | 4.326E+06 | 1.184 | 47.0 | 0.04 | 240.7 ± 47.0 |
| 10 | 13 | 10 | 20 | 1.033E+06 | 7.945E+05 | 1.300 | 8.6 | 0.01 | 263.8 ± 111.2 |
| 11 | 21 | 20 | 42 | 7.945E+05 | 7.567E+05 | 1.050 | 8.2 | 0.00 | 213.9 ± 67.0 |
| 12 | 50 | 37 | 40 | 1.986E+06 | 1.470E+06 | 1.351 | 16.0 | 0.05 | 274.1 ± 59.8 |
| 13 | 97 | 61 | 48 | 3.211E+06 | 2.019E+06 | 1.590 | 22.0 | 0.08 | 321.3 ± 53.0 |
| 14 | 119 | 104 | 100 | 1.891E+06 | 1.653E+06 | 1.144 | 18.0 | 0.02 | 232.8 ± 31.7 |
| 15 | 21 | 17 | 32 | 1.043E+06 | 8.442E+05 | 1.235 | 9.2 | 0.06 | 251.0 ± 82.1 |
| 16 | 43 | 31 | 24 | 2.847E+06 | 2.053E+06 | 1.387 | 22.3 | 0.01 | 281.1 ± 66.6 |
| 17 | 102 | 87 | 80 | 2.026E+06 | 1.728E+06 | 1.172 | 18.8 | 0.09 | 238.4 ± 35.2 |
| 18 | 108 | 104 | 70 | 2.452E+06 | 2.361E+06 | 1.038 | 25.7 | 0.04 | 211.6 ± 29.5 |
| 19 | 51 | 40 | 100 | 8.104E+05 | 6.356E+05 | 1.275 | 6.9 | 0.04 | 258.9 ± 55.0 |
| 20 | 49 | 31 | 40 | 1.947E+06 | 1.232E+06 | 1.581 | 13.4 | 0.02 | 319.4 ± 73.7 |
| 23 | 85 | 62 | 27 | 5.003E+06 | 3.649E+06 | 1.371 | 39.7 | 0.02 | 277.9 ± 46.9 |
| 25 | 26 | 18 | 20 | 2.066E+06 | 1.430E+06 | 1.444 | 15.5 | 0.09 | 292.5 ± 90.0 |
| 26 | 7 | 9 | 30 | 3.708E+05 | 4.767E+05 | 0.778 | 5.2 | 0.04 | 159.2 ± 80.3 |
| 30 | 65 | 48 | 32 | 3.228E+06 | 2.384E+06 | 1.354 | 25.9 | 0.01 | 274.6 ± 52.7 |
| | 1103 | 868 | | 1.932E+06 | 1.521E+06 | | 16.5 | | |

Area of basic unit = 6.293E-07 cm-2

Chi Squared = 13.311 with 19 degrees of freedom
P(chi squared) = 82.2 %
Correlation Coefficient = 0.962
Variance of SQR(Ns) = 5.93
Variance of SQR(Ni) = 4.85
Age Dispersion = 0.614 % (did not converge)

Ns/Ni = 1.271 ± 0.058
Mean Ratio = 1.300 ± 0.062

Ages calculated using a zeta of 360.3 ± 6.8 for SRM612 glass
Rho D = 1.150E+06cm-2; ND = 5050

**POOLED AGE = 258.0 ± 13.2 Ma**
CENTRAL AGE = 258.0 ± 13.2 Ma

8622-42 APATITE

IRRADIATION PT766
SLIDE NUMBER 3
COUNTED BY: MEM

| Current grain no. | Ns | Ni | Na | RHOs | RHOi | RATIO | U (ppm) | Cl (wt%) | F.T. AGE (Ma) |
|---|---|---|---|---|---|---|---|---|---|
| 3 | 3 | 23 | 60 | 7.945E+04 | 6.091E+05 | 0.130 | 6.6 | 0.20 | 27.0 ± 16.6 |
| | 3 | 23 | | 7.945E+04 | 6.091E+05 | | 6.6 | | |

Area of basic unit = 6.293E-07 cm-2

Ns/Ni = 0.130 ± 0.080

Ages calculated using a zeta of 360.3 ± 6.8 for SRM612 glass
Rho D = 1.150E+06cm-2; ND = 5050

**POOLED AGE = 27.0 ± 16.6 Ma**

8622-43 APATITE

IRRADIATION PT766
SLIDE NUMBER 4
COUNTED BY: MEM

| Current grain no. | Ns | Ni | Na | RHOs | RHOi | RATIO | U (ppm) | Cl (wt%) | F.T. AGE (Ma) |
|---|---|---|---|---|---|---|---|---|---|
| 4 | 20 | 20 | 14 | 2.270E+06 | 2.270E+06 | 1.000 | 24.7 | 0.02 | 203.9 ± 64.7 |
| 6 | 76 | 76 | 32 | 3.774E+06 | 3.774E+06 | 1.000 | 41.0 | 0.05 | 203.9 ± 33.4 |
| 7 | 3 | 13 | 56 | 8.513E+04 | 3.689E+05 | 0.231 | 4.0 | 0.40 | 47.6 ± 30.5 |
| 8 | 49 | 161 | 80 | 9.733E+05 | 3.198E+06 | 0.304 | 34.8 | 0.09 | 62.7 ± 10.3 |
| 10 | 0 | 4 | 30 | 0.000E+00 | 2.119E+05 | 0.000 | 2.3 | 0.53 | 0.0 ± 0.0 |
| 11 | 9 | 10 | 30 | 4.767E+05 | 5.297E+05 | 0.900 | 5.8 | 0.60 | 183.8 ± 84.6 |
| 14 | 30 | 73 | 40 | 1.192E+06 | 2.900E+06 | 0.411 | 31.5 | 0.50 | 84.6 ± 18.4 |
| 15 | 4 | 13 | 70 | 9.080E+04 | 2.951E+05 | 0.308 | 3.2 | 0.55 | 63.4 ± 36.3 |
| 21 | 17 | 96 | 60 | 4.502E+05 | 2.542E+06 | 0.177 | 27.6 | 0.05 | 36.6 ± 9.7 |
| 22 | 4 | 3 | 16 | 3.973E+05 | 2.980E+05 | 1.333 | 3.2 | 0.12 | 270.5 ± 206.7 |
| 24 | 7 | 4 | 12 | 9.270E+05 | 5.297E+05 | 1.750 | 5.8 | 1.46 | 352.7 ± 221.2 |
| 27 | 7 | 13 | 60 | 1.854E+05 | 3.443E+05 | 0.538 | 3.7 | 0.31 | 110.6 ± 51.9 |
| 29 | 86 | 82 | 20 | 6.833E+06 | 6.515E+06 | 1.049 | 70.8 | 0.04 | 213.7 ± 33.4 |
| 30 | 9 | 5 | 20 | 7.151E+05 | 3.973E+05 | 1.800 | 4.3 | 0.44 | 362.5 ± 202.4 |
| 31 | 117 | 111 | 40 | 4.648E+06 | 4.410E+06 | 1.054 | 47.9 | 0.56 | 214.8 ± 28.9 |
| | 438 | 684 | | 1.200E+06 | 1.874E+06 | | 20.4 | | |

Area of basic unit = 6.293E-07 cm-2

Chi Squared = 103.163 with 14 degrees of freedom
P(chi squared) = 0.0 %
Correlation Coefficient = 0.721
Variance of SQR(Ns) = 9.97
Variance of SQR(Ni) = 13.84
Age Dispersion = 57.367 %

Ns/Ni = 0.640 ± 0.039
Mean Ratio = 0.790 ± 0.146

Ages calculated using a zeta of 360.3 ± 6.8 for SRM612 glass
Rho D = 1.150E+06cm-2; ND = 5050

POOLED AGE = 131.3 ± 8.6 Ma
**CENTRAL AGE = 131.5 ± 23.6 Ma**

8622-45 APATITE

IRRADIATION PT766
SLIDE NUMBER 5
COUNTED BY: MEM

| Current grain no. | Ns | Ni | Na | RHOs | RHOi | RATIO | U (ppm) | Cl (wt%) | F.T. AGE (Ma) |
|---|---|---|---|---|---|---|---|---|---|
| 4 | 22 | 63 | 20 | 1.748E+06 | 5.006E+06 | 0.349 | 54.4 | 0.32 | 71.9 ± 17.9 |
| 9 | 3 | 12 | 40 | 1.192E+05 | 4.767E+05 | 0.250 | 5.2 | 1.80 | 51.6 ± 33.3 |
| 10 | 5 | 29 | 15 | 5.297E+05 | 3.072E+06 | 0.172 | 33.4 | 0.41 | 35.6 ± 17.3 |
| 11 | 1 | 5 | 12 | 1.324E+05 | 6.621E+05 | 0.200 | 7.2 | 0.25 | 41.3 ± 45.3 |
| 12 | 18 | 36 | 14 | 2.043E+06 | 4.086E+06 | 0.500 | 44.4 | 0.04 | 102.8 ± 29.8 |
| 13 | 14 | 52 | 60 | 3.708E+05 | 1.377E+06 | 0.269 | 15.0 | 1.94 | 55.5 ± 16.8 |
| 14 | 17 | 23 | 48 | 5.628E+05 | 7.614E+05 | 0.739 | 8.3 | 0.02 | 151.3 ± 48.5 |
| 16 | 19 | 16 | 15 | 2.013E+06 | 1.695E+06 | 1.188 | 18.4 | 0.12 | 241.4 ± 82.1 |
| 24 | 7 | 18 | 20 | 5.562E+05 | 1.430E+06 | 0.389 | 15.5 | 0.66 | 80.1 ± 35.7 |
| 25 | 20 | 17 | 18 | 1.766E+06 | 1.501E+06 | 1.176 | 16.3 | 0.03 | 239.2 ± 79.1 |
| 29 | 0 | 1 | 20 | 0.000E+00 | 7.945E+04 | 0.000 | 0.9 | 0.00 | 0.0 ± 0.0 |
| | 126 | 272 | | 7.100E+05 | 1.533E+06 | | 16.7 | | |

Area of basic unit = 6.293E-07 cm-2

Chi Squared = 30.442 with 10 degrees of freedom
P(chi squared) = 0.1 %
Correlation Coefficient = 0.624
Variance of SQR(Ns) = 2.55
Variance of SQR(Ni) = 4.11
Age Dispersion = 51.267 %

Ns/Ni = 0.463 ± 0.050
Mean Ratio = 0.476 ± 0.120

Ages calculated using a zeta of 360.3 ± 6.8 for SRM612 glass
Rho D = 1.150E+06cm-2; ND = 5050

POOLED AGE = 95.3 ± 10.5 Ma
**CENTRAL AGE = 96.4 ± 19.4 Ma**

8622-46 APATITE

IRRADIATION PT766
SLIDE NUMBER 6
COUNTED BY: MEM

| Current grain no. | Ns | Ni | Na | RHOs | RHOi | RATIO | U (ppm) | Cl (wt%) | F.T. AGE (Ma) |
|---|---|---|---|---|---|---|---|---|---|
| 4 | 15 | 35 | 100 | 2.384E+05 | 5.562E+05 | 0.429 | 6.0 | 0.78 | 88.2 ± 27.3 |
| 6 | 19 | 51 | 100 | 3.019E+05 | 8.104E+05 | 0.373 | 8.8 | 0.51 | 76.7 ± 20.7 |
| 8 | 25 | 30 | 100 | 3.973E+05 | 4.767E+05 | 0.833 | 5.2 | 0.98 | 170.4 ± 46.3 |
| 9 | 3 | 10 | 50 | 9.534E+04 | 3.178E+05 | 0.300 | 3.5 | 0.16 | 61.9 ± 40.7 |
| 11 | 30 | 44 | 100 | 4.767E+05 | 6.992E+05 | 0.682 | 7.6 | 0.65 | 139.7 ± 33.2 |
| 19 | 10 | 24 | 70 | 2.270E+05 | 5.448E+05 | 0.417 | 5.9 | 2.22 | 85.7 ± 32.3 |
| 21 | 52 | 96 | 100 | 8.263E+05 | 1.526E+06 | 0.542 | 16.6 | 1.01 | 111.3 ± 19.3 |
| 27 | 28 | 34 | 100 | 4.449E+05 | 5.403E+05 | 0.824 | 5.9 | 0.83 | 168.4 ± 43.2 |
| 31 | 12 | 23 | 100 | 1.907E+05 | 3.655E+05 | 0.522 | 4.0 | 0.01 | 107.2 ± 38.3 |
| 32 | 20 | 39 | 100 | 3.178E+05 | 6.197E+05 | 0.513 | 6.7 | 0.69 | 105.4 ± 29.1 |
| 35 | 41 | 73 | 100 | 6.515E+05 | 1.160E+06 | 0.562 | 12.6 | 1.47 | 115.3 ± 22.7 |
| 36 | 0 | 2 | 100 | 0.000E+00 | 3.178E+04 | 0.000 | 0.3 | 0.00 | 0.0 ± 0.0 |
| 37 | 18 | 55 | 100 | 2.860E+05 | 8.740E+05 | 0.327 | 9.5 | 1.44 | 67.4 ± 18.4 |
| 40 | 150 | 225 | 100 | 2.384E+06 | 3.575E+06 | 0.667 | 38.9 | 0.01 | 136.7 ± 14.8 |
| 41 | 134 | 175 | 36 | 5.915E+06 | 7.725E+06 | 0.766 | 84.0 | 0.19 | 156.7 ± 18.4 |
| 45 | 1 | 7 | 50 | 3.178E+04 | 2.225E+05 | 0.143 | 2.4 | 0.18 | 29.5 ± 31.6 |
| 49 | 26 | 40 | 100 | 4.132E+05 | 6.356E+05 | 0.650 | 6.9 | 0.37 | 133.3 ± 33.7 |
| 50 | 0 | 3 | 100 | 0.000E+00 | 4.767E+04 | 0.000 | 0.5 | 0.00 | 0.0 ± 0.0 |
| 54 | 78 | 75 | 60 | 2.066E+06 | 1.986E+06 | 1.040 | 21.6 | 0.00 | 211.9 ± 34.6 |
| 56 | 15 | 30 | 100 | 2.384E+05 | 4.767E+05 | 0.500 | 5.2 | 0.86 | 102.8 ± 32.6 |
| | 677 | 1071 | | 6.092E+05 | 9.637E+05 | | 10.5 | | |

Area of basic unit = 6.293E-07 cm-2

Chi Squared = 37.295 with 19 degrees of freedom
P(chi squared) = 0.7 %
Correlation Coefficient = 0.970
Variance of SQR(Ns) = 10.71
Variance of SQR(Ni) = 11.66
Age Dispersion = 22.327 %

Ns/Ni = 0.632 ± 0.031
Mean Ratio = 0.504 ± 0.061

Ages calculated using a zeta of 360.3 ± 6.8 for SRM612 glass
Rho D = 1.150E+06cm-2; ND = 5050

POOLED AGE = 129.6 ± 7.1 Ma
**CENTRAL AGE = 120.4 ± 9.9 Ma**

8622-47 APATITE

IRRADIATION PT766
SLIDE NUMBER 7
COUNTED BY: MEM

| Current grain no. | Ns | Ni | Na | RHOs | RHOi | RATIO | U (ppm) | Cl (wt%) | F.T. AGE (Ma) |
|---|---|---|---|---|---|---|---|---|---|
| 1 | 0 | 3 | 21 | 0.000E+00 | 2.270E+05 | 0.000 | 2.5 | 0.00 | 0.0 ± 0.0 |
| 2 | 0 | 16 | 56 | 0.000E+00 | 4.540E+05 | 0.000 | 4.9 | 0.16 | 0.0 ± 0.0 |
| 3 | 0 | 22 | 60 | 0.000E+00 | 5.827E+05 | 0.000 | 6.3 | 0.00 | 0.0 ± 0.0 |
| 4 | 12 | 57 | 14 | 1.362E+06 | 6.470E+06 | 0.211 | 70.3 | 0.51 | 43.5 ± 13.8 |
| 8 | 8 | 21 | 45 | 2.825E+05 | 7.416E+05 | 0.381 | 8.1 | 0.90 | 78.4 ± 32.6 |
| 14 | 2 | 36 | 40 | 7.945E+04 | 1.430E+06 | 0.056 | 15.5 | 0.18 | 11.5 ± 8.4 |
| 16 | 60 | 108 | 20 | 4.767E+06 | 8.581E+06 | 0.556 | 93.3 | 1.62 | 114.1 ± 18.6 |
| 18 | 2 | 6 | 20 | 1.589E+05 | 4.767E+05 | 0.333 | 5.2 | 0.25 | 68.7 ± 56.1 |
| 21 | 20 | 100 | 60 | 5.297E+05 | 2.648E+06 | 0.200 | 28.8 | 0.24 | 41.3 ± 10.2 |
| 22 | 2 | 14 | 24 | 1.324E+05 | 9.270E+05 | 0.143 | 10.1 | 1.39 | 29.5 ± 22.3 |
| 23 | 3 | 13 | 30 | 1.589E+05 | 6.886E+05 | 0.231 | 7.5 | 0.43 | 47.6 ± 30.5 |
| 24 | 6 | 26 | 50 | 1.907E+05 | 8.263E+05 | 0.231 | 9.0 | 0.22 | 47.6 ± 21.6 |
| 25 | 7 | 22 | 40 | 2.781E+05 | 8.740E+05 | 0.318 | 9.5 | 0.88 | 65.6 ± 28.5 |
| 26 | 51 | 129 | 42 | 1.930E+06 | 4.881E+06 | 0.395 | 53.1 | 0.23 | 81.4 ± 13.6 |
| 27 | 36 | 153 | 50 | 1.144E+06 | 4.863E+06 | 0.235 | 52.9 | 0.53 | 48.6 ± 9.1 |
| 28 | 9 | 30 | 60 | 2.384E+05 | 7.945E+05 | 0.300 | 8.6 | 0.66 | 61.9 ± 23.6 |
| 29 | 8 | 63 | 60 | 2.119E+05 | 1.669E+06 | 0.127 | 18.1 | 0.25 | 26.3 ± 9.9 |
| 34 | 12 | 32 | 30 | 6.356E+05 | 1.695E+06 | 0.375 | 18.4 | 0.33 | 77.2 ± 26.2 |
| 35 | 4 | 3 | 10 | 6.356E+05 | 4.767E+05 | 1.333 | 5.2 | 0.94 | 270.5 ± 206.7 |
| 36 | 13 | 50 | 15 | 1.377E+06 | 5.297E+06 | 0.260 | 57.6 | 0.82 | 53.6 ± 16.7 |
| | 255 | 904 | | 5.425E+05 | 1.923E+06 | | 20.9 | | |

Area of basic unit = 6.293E-07 cm-2

Chi Squared = 56.583 with 19 degrees of freedom
P(chi squared) = 0.0 %
Correlation Coefficient = 0.864
Variance of SQR(Ns) = 4.68
Variance of SQR(Ni) = 9.60
Age Dispersion = 46.201 %

Ns/Ni = 0.282 ± 0.020
Mean Ratio = 0.284 ± 0.064

Ages calculated using a zeta of 360.3 ± 6.8 for SRM612 glass
Rho D = 1.150E+06cm-2; ND = 5050

POOLED AGE = 58.2 ± 4.3 Ma
**CENTRAL AGE = 51.6 ± 7.3 Ma**

8622-49 APATITE

IRRADIATION PT766
SLIDE NUMBER 8
COUNTED BY: MEM

| Current grain no. | Ns | Ni | Na | RHOs | RHOi | RATIO | U (ppm) | Cl (wt%) | F.T. AGE (Ma) |
|---|---|---|---|---|---|---|---|---|---|
| 3 | 10 | 21 | 60 | 2.648E+05 | 5.562E+05 | 0.476 | 6.0 | 1.01 | 97.9 ± 37.7 |
| 4 | 3 | 9 | 28 | 1.703E+05 | 5.108E+05 | 0.333 | 5.6 | 1.10 | 68.7 ± 45.8 |
| 7 | 1 | 6 | 48 | 3.311E+04 | 1.986E+05 | 0.167 | 2.2 | 0.39 | 34.4 ± 37.2 |
| 8 | 6 | 19 | 36 | 2.648E+05 | 8.387E+05 | 0.316 | 9.1 | 0.94 | 65.1 ± 30.5 |
| 9 | 1 | 5 | 32 | 4.966E+04 | 2.483E+05 | 0.200 | 2.7 | 0.42 | 41.3 ± 45.3 |
| 10 | 1 | 19 | 25 | 6.356E+04 | 1.208E+06 | 0.053 | 13.1 | 0.59 | 10.9 ± 11.2 |
| 11 | 1 | 17 | 40 | 3.973E+04 | 6.754E+05 | 0.059 | 7.3 | 1.36 | 12.2 ± 12.5 |
| 12 | 0 | 5 | 30 | 0.000E+00 | 2.648E+05 | 0.000 | 2.9 | 0.42 | 0.0 ± 0.0 |
| 13 | 0 | 65 | 24 | 0.000E+00 | 4.304E+06 | 0.000 | 46.8 | 0.01 | 0.0 ± 0.0 |
| 14 | 7 | 11 | 60 | 1.854E+05 | 2.913E+05 | 0.636 | 3.2 | 0.32 | 130.5 ± 63.2 |
| 15 | 1 | 10 | 20 | 7.945E+04 | 7.945E+05 | 0.100 | 8.6 | 0.64 | 20.7 ± 21.7 |
| 18 | 0 | 12 | 36 | 0.000E+00 | 5.297E+05 | 0.000 | 5.8 | 0.04 | 0.0 ± 0.0 |
| 19 | 3 | 5 | 28 | 1.703E+05 | 2.838E+05 | 0.600 | 3.1 | 0.60 | 123.1 ± 90.0 |
| 22 | 0 | 6 | 25 | 0.000E+00 | 3.814E+05 | 0.000 | 4.1 | 0.62 | 0.0 ± 0.0 |
| 23 | 0 | 51 | 42 | 0.000E+00 | 1.930E+06 | 0.000 | 21.0 | 0.04 | 0.0 ± 0.0 |
| 25 | 2 | 18 | 60 | 5.297E+04 | 4.767E+05 | 0.111 | 5.2 | 0.48 | 23.0 ± 17.1 |
| 26 | 4 | 11 | 40 | 1.589E+05 | 4.370E+05 | 0.364 | 4.7 | 1.19 | 74.9 ± 43.8 |
| 27 | 4 | 17 | 30 | 2.119E+05 | 9.005E+05 | 0.235 | 9.8 | 0.55 | 48.6 ± 27.0 |
| 28 | 10 | 44 | 36 | 4.414E+05 | 1.942E+06 | 0.227 | 21.1 | 0.79 | 46.9 ± 16.5 |
| 31 | 1 | 54 | 35 | 4.540E+04 | 2.452E+06 | 0.019 | 26.6 | 0.00 | 3.8 ± 3.9 |
| | 55 | 405 | | 1.189E+05 | 8.756E+05 | | 9.5 | | |

Area of basic unit = 6.293E-07 cm-2

Chi Squared = 67.366 with 19 degrees of freedom
P(chi squared) = 0.0 %
Correlation Coefficient = 0.026
Variance of SQR(Ns) = 1.07
Variance of SQR(Ni) = 3.26
Age Dispersion = 84.522 %

Ns/Ni = 0.136 ± 0.020
Mean Ratio = 0.195 ± 0.045

Ages calculated using a zeta of 360.3 ± 6.8 for SRM612 glass
Rho D = 1.150E+06cm-2; ND = 5050

POOLED AGE = 28.1 ± 4.1 Ma
**CENTRAL AGE = 33.8 ± 8.3 Ma**

# APPENDIX C

## Principles of Interpretation of AFTA Data in Sedimentary Basins

### C.1 Introduction

Detrital apatite grains are incorporated into sedimentary rocks from three dominant sources - crystalline basement rocks, older sediments and contemporaneous volcanism. Apatites derived from the first two sources will, in general, contain fission tracks when they are deposited, with AFTA parameters characteristic of the source regions. However, apatites derived from contemporaneous volcanism, or from rapidly uplifted basement, will contain no tracks when they are deposited. For now, we will restrict discussion to this situation, and generalise at a later point to cover the case of apatites which contain tracks that have been inherited from source regions.

### C.2 Basic principles of Apatite Fission Track Analysis

Fission tracks are trails of radiation damage, which are produced within apatite grains at a more or less constant rate through geological time, as a result of the spontaneous fission of $^{238}U$ impurity atoms. Therefore, the number of fission events which occur within an apatite grain during a fixed time interval depends on the magnitude of the time interval and the uranium content of the grain. Each fission event leads to the formation of a single fission track, and the proportion of tracks which can intersect a polished surface of an apatite grain depends on the length of the tracks. Therefore, the number of tracks which are etched in unit area of the surface of an apatite grain (the "spontaneous track density") depends on three factors - (i) The time over which tracks have been accumulating; (ii) The uranium content of the apatite grain; and, (iii) The distribution of track lengths in the grain. In sedimentary rocks which have not been subjected to temperatures greater than ~50°C since deposition, spontaneous fission tracks have a characteristic distribution of confined track lengths, with a mean length in the range 14-15 μm and a standard deviation of ~1 μm. In such samples, by measuring the spontaneous track density and the uranium content of a collection of apatite grains, a "fission track age" can be calculated which will be equal to the time over which tracks have been accumulating. The technique is calibrated against other isotopic systems using age standards which also have this type of length distribution (see Appendix B).

In samples which have been subjected to temperatures greater than ~50°C after deposition, fission tracks are shortened because of the gradual repair of the radiation damage which

constitutes the unetched tracks. In effect, the tracks shrink from each end, in a process which is known as fission track "annealing". The final length of each individual track is essentially determined by the maximum temperature which that track has experienced. A time difference of an order of magnitude produces a change in fission track parameters which is equivalent to a temperature change of only ~10°C, so temperature is by far the dominant factor in determining the final fission track parameters. As temperature increases, all existing tracks shorten to a length determined by the prevailing temperature, regardless of when they were formed. After the temperature has subsequently decreased, all tracks formed prior to the thermal maximum are "frozen" at the degree of length reduction they attained at that time. Thus, the length of each track can be thought of as a maximum-reading thermometer, recording the maximum temperature to which it has been subjected.

Therefore, in samples for which the present temperature is maximum, all tracks have much the same length, resulting in a narrow, symmetric distribution. The degree of shortening will depend on the temperature, with the mean track length falling progressively from ~14 μm at 50°C, to zero at around 110°-120°C - the precise temperature depending on the timescale of heating and the composition of the apatites present in the sample (see below). Values quoted here relate to times of the order of $10^7$ years (heating rates around 1 to 10°C/Ma) and average apatite composition. If the effective timescale of heating is shorter than $10^7$ years, the temperature responsible for a given degree of track shortening will be higher, depending in detail on the kinetics of the annealing process (Green et al., 1986; Laslett et al., 1987; Duddy et al., 1988; Green et al., 1989b). Shortening of tracks produces an accompanying reduction in the fission track age, because of the reduced proportion of tracks which can intersect the polished surface. Therefore, the fission track age is also highly temperature dependent, falling to zero at around 120°C due to total erasure of all tracks.

Samples which have been heated to a maximum paleotemperature less than ~120°C at some time in the past and subsequently cooled will contain two populations of tracks, and will show a more complex distribution of lengths and ages. If the maximum paleotemperature was less than ~50°C then the two components will not be resolvable, but for maximum paleotemperatures between ~50° and 120°C the presence of two components can readily be identified. Tracks formed prior to the thermal maximum will all be shortened to approximately the same degree (the precise value depending on the maximum paleotemperature), while those formed during and after cooling will be longer, due to the lower prevailing temperatures. The length distribution in such samples will be broader than in the simple case, consisting of a shorter and a longer component, and the fission track age will reflect the amount of length reduction shown by the shorter component (determined by the maximum paleotemperature).

If the maximum paleotemperature was sufficient to shorten tracks to between 9 and 11 μm, and cooling to temperatures of ~50°C or less was sufficiently rapid, tracks formed after cooling will have lengths of 14-15 μm and the resulting track length distribution will show a characteristic bimodal form. If the maximum paleotemperature was greater than ~110 to 120°C, all pre-existing tracks will be erased, and all tracks now present will have formed after the onset of cooling. The fission track age in such samples relates directly to the time of cooling.

In thermal history scenarios in which a heating episode is followed by cooling and then temperature increases again, the tracks formed during the second heating phase will undergo progressive shortening. The tracks formed prior to the initial cooling, which were shortened in the first heating episode, will not undergo further shortening until the temperature exceeds the maximum temperature reached in the earlier heating episode. (In practice, differences in timescale of heating can complicate this simple description. In detail, it is the integrated time-temperature effect of the two heating episodes which should be considered.) If the maximum and peak paleotemperatures in the two episodes are sufficiently different (>~10°C), and the later peak paleotemperature is less than the earlier maximum value, then the AFTA parameters allow determination of both episodes. As the peak paleotemperature in the later episode approaches the earlier maximum, the two generations of tracks become increasingly more difficult to resolve, and when the two paleotemperatures are the same, both components are shortened to an identical degree and all information on the earlier heating phase will be lost.

No information is preserved on the approach to maximum paleotemperature because the great majority of tracks formed up to that time have the same mean track length. Only those tracks formed in the last few per cent of the history prior to the onset of cooling are not shortened to the same degree (because temperature dominates over time in the annealing kinetics). These form a very small proportion of the total number of tracks and therefore cannot be resolved within the length distribution because of the inherent spread of several μm in the length distribution.

To summarise, AFTA allows determination of the magnitude of the maximum temperature and the time at which cooling from that maximum began. In some circumstances, determination of a subsequent peak paleotemperature and the time of cooling is also possible.

## C.3 Quantitative understanding of fission track annealing in apatite

### *Annealing kinetics and modelling the development of AFTA parameters*

Our understanding of the behaviour of fission tracks in apatite during geological thermal histories is based on study of the response of fission tracks to elevated temperatures in the laboratory (Green et al., 1986; Laslett et al., 1987; Duddy et al., 1988; Green et al., 1989b), in geological situations (Green et al., 1989a), observations of the lengths of spontaneous tracks in apatites from a wide variety of geological environments (Gleadow et al., 1986), and the relationship between track length reduction and reduction in fission track age observed in controlled laboratory experiments (Green, 1988).

These studies resulted in the capability to simulate the development of AFTA parameters resulting from geological thermal histories for an apatite of average composition (Durango apatite, ~0.43 wt% Cl). Full details of this modelling procedure have been explained in Green et al. (1989b). The following discussion presents a brief explanation of the approach.

Geological thermal histories involving temperatures varying through time are broken down into a series of isothermal steps. The progressive shortening of track length through sequential intervals is calculated using the extrapolated predictions of an empirical kinetic model fitted to laboratory annealing data. Contributions from tracks generated throughout the history (remembering that new tracks are continuously generated through time as new fissions occur) are summed to produce the final distribution of track lengths expected to result from the input history. In summing these components, care is taken to allow for various biases which affect revelation of confined tracks (Laslett et al., 1982). The final length reduction of each component of tracks is converted to a contribution of fission track age, using the relationship between track length and density reduction determined by Green (1988). These age contributions are summed to generate the final predicted fission track age.

This approach depends critically on the assumption that extrapolation of the laboratory-based kinetic model to geological timescales, over many orders of magnitude in time, is valid. This was assessed critically by Green et al. (1989b), who showed that predictions from this approach agree well with observed AFTA parameters in apatites of the appropriate composition in samples from a series of reference wells in the Otway Basin of south-east Australia (Gleadow and Duddy, 1981; Gleadow et al., 1983; Green et al., 1989a). This point is illustrated in Figure C.1. Green et al. (1989b) also quantitatively assessed the errors associated with extrapolation of the Laslett et al. (1987) model from laboratory to geological timescales (i.e., precision, as opposed to accuracy). Typical levels of precision are ~0.5 μm for mean lengths <~10 μm, and ~0.3 μm for lengths >~10 μm. These figures are equivalent to an uncertainty in estimates of maximum paleotemperature derived using this approach of

~10°C. Precision is largely independent of thermal history for any reasonable geological history. Accuracy of prediction from this model is limited principally by the effect of apatite composition on annealing kinetics, as explained in the next section.

*Compositional effects*

Natural apatites essentially have the composition $Ca_5(PO_4)_3(F,OH,Cl)$. Most common detrital and accessory apatites are predominantly Fluor-apatites, but may contain appreciable amounts of chlorine. The amount of chlorine in the apatite lattice exerts a subtle compositional control on the degree of annealing, with apatites richer in fluorine being more easily annealed than those richer in chlorine. The result of this effect is that in a single sample, individual apatite grains may show a spread in the degree of annealing (i.e., length reduction and fission track age reduction). This effect becomes most pronounced in the temperature range 90 - 120°C (assuming a heating timescale of ~10 Ma), and can be useful in identifying samples exposed to paleotemperatures in this range. At temperatures below ~80°C, the difference in annealing sensitivity is less marked, and compositional effects can largely be ignored.

Our original quantitative understanding of the kinetics of fission track annealing, as described above, relates to a single apatite (Durango apatite) with ~0.43 wt% Cl, on which most of our original experimental studies were carried out. Recently, we have extended this quantitative understanding to apatites with Cl contents up to ~3 wt%. This new, multi-compositional kinetic model is based both on new laboratory annealing studies on a range of apatites with different F-Cl compositions (Figure C.2), and on observations of geological annealing in apatites from a series of samples from exploration wells in which the section is currently at maximum temperature since deposition. A composite model for Durango apatite composition was first created by fitting a common model to the old laboratory data (from Green et al., 1986) and the new geological data for a similar composition. This was then extended to other compositions on the basis of the multi-compositional laboratory and geological data sets. Details of the multi-compositional model are contained in a Technical Note, available from Geotrack in Melbourne.

The multi-compositional model allows prediction of AFTA parameters for any Cl content between 0 and 3 wt%, using a similar approach to that used in our original single composition modelling, as outlined above. Then, for an assumed or measured distribution of Cl contents within a sample, the composite parameters for the sample can be predicted. The range of Cl contents from 0 to 3 wt% spans the range of compositions commonly encountered, as discussed in the next section.

Predictions of the new multi-compositional model are in good agreement with the geological constraints on annealing rates provided by the Otway Basin reference wells, as shown in

Figure C.3. However, note that the AFTA data from these Otway Basin wells were among those used in construction of the new model, so this should not be viewed as independent verification, but rather as a demonstration of the overall consistency of the model.

*Distributions of Cl content in common AFTA samples*

Figure C.4a shows a histogram of Cl contents, measured by electron microprobe, in apatite grains from more than 100 samples of various types. Most grains have Cl contents less than ~0.5 wt%. The majority of grains with Cl contents greater than this come from volcanic sources and basic intrusives, and contain up to ~2 wt% Cl. Figure C.4b shows the distribution of Cl contents measured in randomly selected apatite grains from 61 samples of "typical" quartzo-feldspathic sandstone. This distribution is similar to that in Figure C.4a, except for a more rapid fall-off as Cl content increases. Apatites from most common sandstones give distributions of Cl content which are very similar to that in Figure C.4b. Volcanogenic sandstones typically contain apatites with higher Cl contents, with a much flatter distribution for Cl contents up to ~1.5%, falling to zero at ~2.5 to 3 wt%, as shown in Figure C.4c. Cl contents in granitic basement samples and high-level intrusives are typically much more dominated by compositions close to end-member Fluorapatite, although many exceptions occur to this general rule.

Information about the spread of Cl contents in samples analysed in this report can be found in Appendix A.

*Alternative kinetic models*

Recently, both Carlson (1990) and Crowley et al. (1991) have published alternative kinetic models for fission track annealing in apatite. Carlson's model is based on our laboratory annealing data for Durango apatite (Green et al., 1986) and other (unpublished) data. In his abstract, Carlson claims that because his model is "based on explicit physical mechanisms, extrapolations of annealing rates to the lower temperatures and longer timescales required for the interpretation of natural fission track length distributions can be made with greater confidence than is the case for purely empirical relationships fitted to the experimental annealing data". As explained in detail by Green et al. (1993), all aspects of Carlson's model are in fact purely empirical, and his model is inherently no "better" for the interpretation of data than any other. In fact, detailed inspection shows that Carlson's model does not fit the laboratory data set at all well. Therefore, we recommend against use of this model to interpret AFTA data.

The approach taken by Crowley et al. (1991) is very similar to that taken by Laslett et al., (1987). They have fitted models to new annealing data in two apatites of different composition - one close to end-member Fluorapatite (B-5) and one having a relatively high Sr

content (113855). The model developed by Crowley et al. (1991) from their own annealing data for the B-5 apatite gives predictions in geological conditions which are consistently higher than measured values, as shown in Figure C.5. Corrigan (1992) reported a similar observation in volcanogenic apatites in samples from a series of West Texas wells. Since the B-5 apatite is close to end-member Fluor-apatite, while the Otway Group apatites contain apatites with Cl contents from zero up to ~3 wt% (and the West Texas apatites have up to 1 wt%), the fluorapatites should have mean lengths rather less than the measured values, which should represent a mean over the range of Cl contents present. Therefore, the predictions of the Crowley et al. (1991) B-5 model appear to be consistently high.

We attribute this to the rather restricted temperature-time conditions covered by the experiments of Crowley et al. (1991), with annealing times between one and 1000 hours, in contrast to times between 20 minutes and 500 days in the experiments of Green et al. (1986). In addition, few of the measured length values in Crowley et al.'s study fall below 11 μm (in only five out of 60 runs in which lengths were measured in apatite B-5) and their model is particularly poorly defined in this region.

Crowley et al. (1991) also fitted a new model to the annealing data for Durango apatite published by Green et al. (1986). Predictions of their fit to our data are not very much different to those from the Laslett et al. (1987) model (Figure C.6). We have not pursued the differences between their model and ours in detail because the advent of our multi-compositional model has rendered the single compositional approach obsolete.

## C.4 Evidence for elevated paleotemperatures from AFTA

The basic principle involved in the interpretation of AFTA data in sedimentary basins is to determine whether the degree of annealing shown by tracks in apatite from a particular sample could have been produced if the sample has never been hotter than its present temperature at any time since deposition. To do this, the burial history derived from the stratigraphy of the preserved sedimentary section is used to calculate a thermal history for each sample using the present geothermal gradient and surface temperature (i.e., assuming these have not changed through time). This is termed the "Default Thermal History". For each sample, the AFTA parameters predicted as a result of the Default Thermal History are then compared to the measured data. If the data show a greater degree of annealing than calculated on the basis of this history, the sample must have been hotter at some time in the past. In this case, the AFTA data are analysed to provide estimates of the magnitude of the maximum paleotemperature in that sample, and the time at which cooling commenced from the thermal maximum.

The degree of annealing is assessed in two ways - from fission track age and track length data. The stratigraphic age provides a basic reference point for the interpretation of fission track age, because reduction of the fission track age below the stratigraphic age unequivocally reveals that appreciable annealing has taken place after deposition of the host sediment. Large degrees of fission track age reduction, with the pooled or central fission track age very much less than the stratigraphic age, indicate severe annealing, which requires paleotemperatures of at least ~100°C for any reasonable geological time-scale of heating (>~1 Ma). Note that this applies even when apatites contain tracks inherited from source areas. More moderate degrees of annealing can be detected by inspection of the single grain age data, as the most sensitive (fluorine-rich) grains will begin to give fission track ages significantly less than the stratigraphic age before the central or pooled age has been reduced sufficiently to give a noticeable signal. Note that this aspect of the single grain age data can also be used for apatites which have tracks inherited from source areas. If signs of moderate annealing (from single grain age reduction) or severe annealing (from the reduction in pooled or central age) are seen in samples in which the Default Thermal History predicts little or no effect, the sample must have been subjected to elevated paleotemperatures at some time in the past. Figure C.7 shows how increasing degrees of annealing are observable in radial plots of the single grain fission track age data.

Similarly, the present temperature from which a sample is taken, and the way in which this has been approached (as inferred from the preserved sedimentary section), forms a basic point of reference for track length data. The observed mean track length is compared with the mean length predicted from the Default Thermal History. If the observed degree of track shortening in a sample is greater than that expected from the Default Thermal History (i.e., the mean length is significantly less than the predicted value), either the sample must have been subjected to higher paleotemperatures at some time after deposition, or the sample contains shorter tracks which were inherited from sediment source areas at the time the sediment was deposited. If shorter tracks were inherited from source areas, the sample should still contain a component of longer tracks corresponding to the tracks formed after deposition. In general, the fission track age should be greater than the stratigraphic age. This can be assessed quantitatively using the computer models for the development of AFTA parameters described in an earlier section. If the presence of shorter tracks cannot be explained by their inheritance from source areas, the sample must have been hotter in the past.

## C.5 Quantitative determination of the magnitude of maximum paleotemperature and the timing of cooling using AFTA

Values of maximum paleotemperature and timing of cooling in each sample are determined using a forward modelling approach based on the quantitative description of fission track annealing described in earlier sections. The Default Thermal History described above is used

as the basis for this forward modelling, but with the addition of episodes of elevated paleotemperatures as required to explain the data. AFTA parameters are modelled iteratively through successive thermal history scenarios in order to identify thermal histories that can account for observed parameters. The range of values of maximum paleotemperature and timing of cooling which can account for the measured AFTA parameters (fission track age and track length distribution) are defined using a maximum likelihood-based approach. In this way, best estimates ("maximum likelihood values") can be defined together with ±95% confidence limits.

In samples in which all tracks have been totally annealed at some time in the past, only a minimum estimate of maximum paleotemperature is possible. In such cases, AFTA data provide most control on the time at which the sample cooled to temperatures at which tracks could be retained. The time at which cooling began could be earlier than this time, and therefore the timing also constitutes a minimum estimate.

Comparison of the AFTA parameters predicted by the multi-compositional model with measured values in samples which are currently at their maximum temperatures since deposition shows a good degree of consistency, suggesting the uncertainty in application of the model should be less than ±10°C. This constitutes a significant improvement over earlier approaches, since the kinetic models used are constrained in both laboratory and geological conditions. It should be appreciated that relative differences in maximum paleotemperature can be identified with greater precision than absolute paleotemperatures, and it is only the estimation of absolute paleotemperature values to which the ±10°C uncertainty relates.

***Cooling history***

If the data are of high quality and provided that cooling from maximum paleotemperatures began sufficiently long ago (so that the history after this time is represented by a significant proportion of the total tracks in the sample), determination of the magnitude of a subsequent peak paleotemperature and the timing of cooling from that peak may also be possible (as explained in Section C.2). A similar approach to that outlined above provides best estimates and corresponding ±95% confidence limits for this episode. Such estimates may simply represent part of a protracted cooling history, and evidence for a later discrete cooling episode can only be accepted if this scenario provides a significantly improved fit to the data. Geological evidence and consistency of estimates between a series of samples can also be used to verify evidence for a second episode.

In practise, most typical AFTA datasets are only sufficient to resolve two discrete episodes of heating and cooling. One noteable exception to this is when a sample has been totally annealed in an early episode, and has then undergone two (or more) subsequent episodes with

progressively lower peak paleotemperatures in each. But in general, complex cooling histories involving a series of episodes of heating and cooling will allow resolution of only two episodes, and the results will depend on which episodes dominate the data. Typically this will be the earliest and latest episodes, but if multiple cooling episodes occur within a narrow time interval the result will represent an approximation to the actual history.

## C.6 Qualitative assessment of AFTA parameters

Various aspects of thermal history can often be assessed by qualitative assessment of AFTA parameters. For example, samples which have reached maximum paleotemperatures sufficient to produce total annealing, and which only contain tracks formed after the onset of cooling, can be identified from a number of lines of evidence. In a vertical sequence of samples showing increasing degrees of annealing, the transition from rapidly decreasing fission track age with increasing depth to more or less the same age over a range of depth denotes the transition from partial to total annealing of all tracks formed prior to the thermal maximum. In samples in which all tracks have been totally annealed, the single grain age data should show that none of the individual grain fission track ages are significantly older than the time of cooling, and grains in all compositional groups should give the same fission track age unless the sample has been further disturbed by a later episode. If the sample cooled rapidly to sufficiently low temperatures, little annealing will have taken place since cooling, and all grains will give ages which are compatible with a single population around the time of cooling, as shown in Figure C.7.

Inspection of the distribution of single grain ages in partially annealed samples can often yield useful information on the time of cooling, as the most easily annealed grains (those richest in fluorine) may have been totally annealed prior to cooling, while more retentive (Cl-rich) compositions were only partially annealed (as in Figure C.7, centre). The form of the track length distribution can also provide information, from the relative proportions of tracks with different lengths. All of these aspects of the data can be used to reach a preliminary thermal history interpretation.

## C.7 Allowing for tracks inherited from source areas

The effect of tracks inherited from source areas, and present at the time the apatite is deposited in the host sediment, is often posed as a potential problem for AFTA. However, this can readily be allowed for in analysing both the fission track age and length data.

In assessing fission track age data to determine the degree of annealing, the only criterion used is the comparison of fission track age with the value expected on the basis of the Default Thermal History. From this point of view, inherited tracks do not affect the conclusion: if a grain or a sample gives a fission track age which is significantly less than expected, the grain

or sample has clearly undergone a higher degree of annealing than can be accounted for by the Default Thermal History, and therefore must have been hotter in the past, whether the sample contained tracks when it was deposited or not.

The presence of inherited tracks does impose a limit on our ability to detect post-depositional annealing from age data alone, as in samples which contain a fair proportion of inherited tracks, moderate degrees of annealing may reduce the fission track age from the original value, but not to a value which is significantly less than the stratigraphic age. This is particularly noticeable in the case of Tertiary samples containing apatites derived from Paleozoic basement. In such cases, although fission track age data may show no evidence of post-depositional annealing, track length data may well show such evidence quite clearly.

The influence of track lengths inherited from source areas can be allowed for by comparison of the fission track age with the value predicted by the Default Thermal History combined with inspection of the track length distribution. If the mean length is much less than the length predicted by the Default Thermal History, either the sample has been subjected to elevated paleotemperatures, sufficient to produce the observed degree of length reduction, or else the sample contains a large proportion of shorter tracks inherited from source areas. However, in the latter case, the sample should give a pooled or central fission track age correspondingly older than the stratigraphic age, while the length distribution should contain a component of longer track lengths corresponding to the value predicted by the Default Thermal History. It is important in this regard that the length of a track depends primarily on the maximum temperature to which it has been subjected, whether in the source regions or after deposition in the sedimentary basin. Thus, any tracks retaining a provenance signature will have lengths towards the shorter end of the distribution where track lengths will not have "equilibrated" with the temperatures attained since deposition.

In general, it is only in extreme cases that inherited tracks render track length data insensitive to post-depositional annealing. For example, if practically all the tracks in a particular sample were formed prior to deposition, perhaps in a Pliocene sediment in which apatites were derived from a stable Paleozoic shield with fission track ages of ~300 Ma or more, the track length distribution will, in general, be dominated by inheritance, as only ~2% of tracks would have formed after deposition. Post-depositional heating will not be detectable as long as the maximum paleotemperature is insufficient to cause greater shortening than that which occurred in the source terrain. Even in such extreme cases, once a sample is exposed to temperatures sufficient to produce greater shortening than that inherited from source areas, the inherited tracks and those formed after deposition will all undergo the same degree of shortening, and the effects of post-depositional annealing can be recognised. In such cases, the presence of tracks inherited from source areas is actually very useful, because the number of tracks

formed after deposition is so small that little or no information would be available without the inherited tracks.

## C.8 Plots of fission track age and mean track length vs depth and temperature

AFTA data from well sequences are usually plotted as shown in Figure C.8. This figure shows AFTA data for two scenarios: one in which deposition has been essentially continuous from the Carboniferous to the present and all samples are presently at their maximum paleotemperature since deposition (Figure C.8a); and, one in which the section was exposed to elevated paleotemperatures prior to cooling in the Early Tertiary (Figure C.8b).

In both figures, fission track age and mean track length are plotted against depth and present temperature. Presentation of AFTA data in this way often provides insight into the thermal history interpretation, following principles outlined earlier in this Appendix.

In Figure C.8a, for samples at temperatures below ~70°C, the fission track age is either greater than or close to the stratigraphic age, and little fission track age reduction has affected these samples. Track lengths in these samples are all greater than ~13 μm. In progressively deeper samples, both the fission track age and mean track length are progressively reduced to zero at a present temperature of around 110°C, with the precise value depending on the spread of apatite compositions present in the sample. Track length distributions in the shallowest samples would be a mixture of tracks retaining information on the thermal history of source regions, while in deeper samples, all tracks would be shortened to a length determined by the prevailing temperature. This pattern of AFTA parameters is characteristic of a sequence which is currently at maximum temperatures.

The data in Figure C.8b show a very different pattern. The fission track age data show a rapid decrease in age, with values significantly less than the stratigraphic age at temperatures of ~40 to 50°C, at which such a degree of age reduction could not be produced in any geological timescale. Below this rapid fall, the fission track ages do not change much over ~1 km (30°C). This transition from rapid fall to consistent ages is diagnostic of the transition from partial to total annealing. Samples above the "break-in slope" contain two generations of tracks: those formed prior to the thermal maximum, which have been partially annealed (shortened) to a degree which depends on the maximum paleotemperature; and, those formed after cooling, which will be longer. Samples below the break-in slope contain only one generation of tracks, formed after cooling to lower temperatures at which tracks can be retained. At greater depths, where temperatures increase to ~90°C and above, the effect of present temperatures begins to reduce the fission track ages towards zero, as in the "maximum temperatures now" case.

The track length data also reflect the changes seen in the fission track age data. At shallow depths, the presence of the partially annealed tracks shortened prior to cooling causes the mean track length to decrease progressively as the fission track age decreases. However, at depths below the break in slope in the age profile, the track length increases again as the shorter component is totally annealed and so does not contribute to the measured distribution of track lengths. At greater depths, the mean track lengths decrease progressively to zero once more due to the effects of the present temperature regime.

Examples of such data have been presented e.g., by Green (1989) and Kamp and Green (1990).

## C.9 Determining paleogeothermal gradients and amount of section removed on unconformities

Estimates of maximum paleotemperatures in samples over a range of depths in a vertical sequence provides the capability of determining the paleogeothermal gradient immediately prior to the onset of cooling from those maximum paleotemperatures. The degree to which the paleogeothermal gradient can be constrained depends on a number of factors, particularly the depth range over which samples are analysed. If samples are only analysed over ~1 km, then the paleotemperature difference over that range may be only ~20 to 30°C. Since maximum paleotemperatures can often only be determined within a ~10°C range, this introduces considerable uncertainty into the final estimate of paleogeothermal gradient (see Figure C.9)

Another important factor is the difference between maximum paleotemperatures and present temperatures ("net cooling"). If this is only ~10°C, which is similar to the uncertainty in absolute paleotemperature determination, only broad limits can be established on the paleogeothermal gradient. In general, the control on the paleogeothermal gradient improves as the amount of net cooling increases. However, if the net cooling becomes so great that many samples were totally annealed prior to the onset of cooling - so that only minimum estimates of maximum paleotemperatures are possible - constraints on the paleogeothermal gradient from AFTA come only from that part of the section in which samples were not totally annealed. In this case, integration of AFTA data with VR measurements can be particularly useful in constraining the paleo-gradient.

Having constrained the paleogeothermal gradient at the time cooling from maximum paleotemperatures began, if we assume a value for surface temperature at that time, the amount of section subsequently removed by uplift and erosion can be calculated as shown in Figure C.10. The *net* amount of section removed is obtained by dividing the difference between the paleo-surface temperature ($T_S$) and the intercept of the paleotemperature profile at

the present ground surface ($T_i$) by the estimated paleogeothermal gradient. The *total* amount of section removed is obtained by adding the thickness of section subsequently redeposited above the unconformity to the *net* amount estimated as in Figure C.10. If the analysis is performed using depths from the appropriate unconformity, then the analysis will directly yield the *total* amount of section removed.

Geotrack have developed a method of deriving estimates of both the paleogeothermal gradient and the net amount of section removed using estimated paleotemperatures derived from AFTA and VR. Perhaps more importantly, this method also provides rigorous values for upper and lower 95% confidence limits on each parameter. The method is based on maximum likelihood estimation of the paleogeothermal gradient and the surface intercept, from a table of paleotemperature and depth values. The method is able to accept ranges for paleotemperature estimates (e.g., where the maximum paleotemperature can only be constrained to between, for example, 60 and 90°C), as well as upper and lower limits (e.g., <60°C for samples which show no detectable annealing; >110°C in samples which were totally annealed). Estimates of paleotemperature from AFTA and VR may be combined or analysed separately. Some results from this method have been reported by Bray et al. (1992). Full details of the methods employed are presented in a confidential, in-house, Geotrack research report, copies of which are available on request from the Melbourne office.

Results are presented in two forms. Likelihood profiles, plotting the log-likelihood as a function of either gradient or section removed, portray the probability of a given value of gradient or section removed. The best estimate is given by the value of gradient or section removed for which the log-likelihood is maximised. Ideally, the likelihood profiles should show a quadratic form, and values of gradient or section removed at which the log-likelihood has fallen by two from the maximum value define the upper and lower 95% confidence limits on the estimates. An alternative method of portraying this information is a crossplot of gradient against section removed, in which values which fall within 95% confidence limits (in two dimensions) are contoured. Note that the confidence limits defined by this method are rather tighter than those from the likelihood profiles, as the latter only reflect variation in one parameter, whereas the contoured crossplot takes variation of both parameters into account.

It must be emphasised that this method relies on the assumption that the paleotemperature profile was linear both throughout the section analysed and through the overlying section which has been removed. While the second part of this assumption can never be confirmed independently, visual inspection of the paleotemperature estimates as a function of depth should be sufficient to verify or deny the linearity of the paleotemperature profile through the preserved section.

Results of this procedure are shown in this report if the data allow sufficiently well-defined paleotemperature estimates to justify use of the method. Where the AFTA data suggest that the section is currently at maximum temperature since deposition, or that the paleotemperature profile was non-linear, or where data are of insufficient quality to allow rigorous paleotemperature estimation, the method is not used.

## References

Bray, R.J., Green, P.F. and Duddy, I.R. (1992). Thermal history reconstruction in sedimentary basins using apatite fission track analysis and vitrinite reflectance: a case study from the east Midlands of England and the Southern North Sea. In: Exploration Britain: Into the next decade. Geological Society Special Publication (in press).

Carlson, W.D. (1990). Mechanisms and kinetics of apatite fission-track annealing. American Mineralogist, 75, 1120 - 1139.

Corrigan, J. (1992). Annealing models under the microscope, On Track, 2, 9-11.

Crowley, K.D., Cameron, M. and Schaefer, R.L. (1991). Experimental studies of annealing of etched fission tracks in apatite. Geochimica et Cosmochimica Acta, 55, 1449-1465.

Duddy, I.R., Green, P.F. and Laslett G.M. (1988). Thermal annealing of fission tracks in apatite 3. Variable temperature behaviour. *Chem. Geol. (Isot. Geosci. Sect.)* , 73, 25-38.

Gleadow, A.J.W. and Duddy, I.R. (1981). A natural long-term track annealing experiment for apatite. *Nuclear Tracks*, 5, 169-174.

Gleadow, A.J.W., Duddy, I.R. and Lovering, J.F. (1983). Fission track analysis; a new tool for the evaluation of thermal histories and hydrocarbon potential. *APEA J*, 23, 93-102.

Gleadow, A.J.W., Duddy, I.R., Green, P.F. and Lovering, J.F. (1986). Confined fission track lengths in apatite - a diagnostic tool for thermal history analysis. *Contr. Min. Petr.*, 94, 405-415.

Green, P.F. (1988). The relationship between track shortening and fission track age reduction in apatite: Combined influences of inherent instability, annealing anisotropy, length bias and system calibration. *Earth Planet. Sci. Lett.*, 89, 335-352.

Green, P.F., Duddy, I.R., Gleadow, A.J.W., Tingate, P.R. and Laslett, G.M. (1986). Thermal annealing of fission tracks in apatite 1. A qualitative description. *Chem. Geol. (Isot. Geosci. Sect.)* , 59, 237-253.

Green, P.F., Duddy, I.R., Gleadow, A.J.W. and Lovering, J.F. (1989a). Apatite Fission Track Analysis as a paleotemperature indicator for hydrocarbon exploration. *In:* Naeser, N.D. and McCulloh, T. (eds.) *Thermal history of sedimentary basins - methods and case histories*, Springer-Verlag, New York, 181-195.

Green, P.F., Duddy, I.R., Laslett, G.M., Hegarty, K.A., Gleadow, A.J.W. and Lovering, J.F. (1989b). Thermal annealing of fission tracks in apatite 4. Quantitative modelling techniques and extension to geological timescales. *Chem. Geol. (Isot. Geosci. Sect.)*, 79, 155-182

Green, P.F., Laslett, G.M. and Duddy, I.R. (1993). Mechanisms and kinetics of apatite fission track annealing: Discussion. *American Mineralogist*, 78, 441-445.

Laslett, G.M., Kendall, W.S., Gleadow, A.J.W. and Duddy, I.R. (1982). Bias in measurement of fission track length distributions. *Nuclear Tracks*, 6, 79-85.

Laslett, G.M., Green, P.F., Duddy, I.R. and Gleadow, A.J.W. (1987). Thermal annealing of fission tracks in apatite 2. A quantitative analysis. *Chem. Geol. (Isot. Geosci. Sect.)*, 65, 1-13.

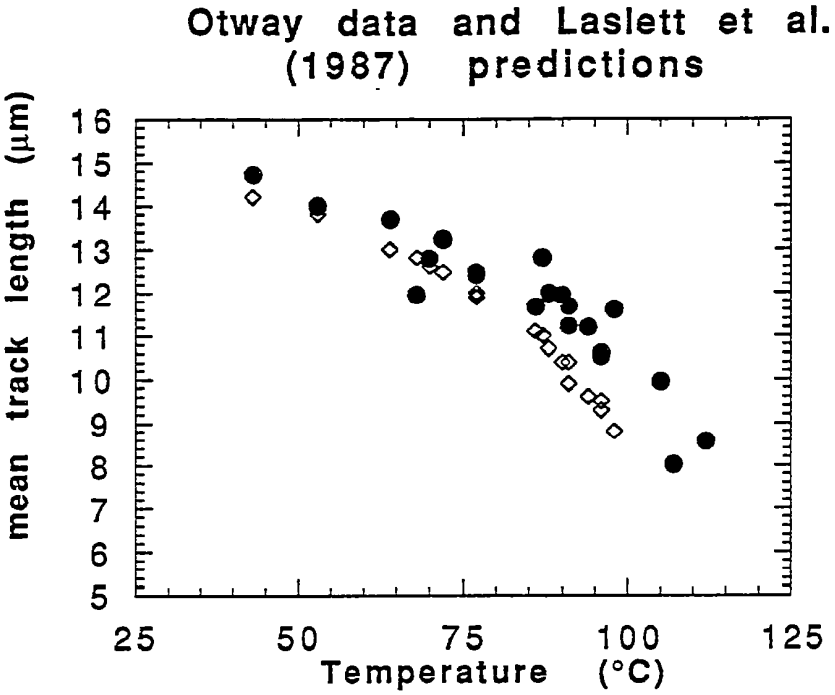


**Figure C.1a** Comparison of mean track length (solid circles) measured in samples from four Otway Basin reference wells (from Green et al, 1989a) and predicted mean track lengths (open diamonds) from the kinetic model of fission track annealing from Laslett et al. (1987). Although the predictions underestimate the measured values, they refer to an apatite composition that is more easily annealed than the majority of apatites in these samples, and therefore this is expected.

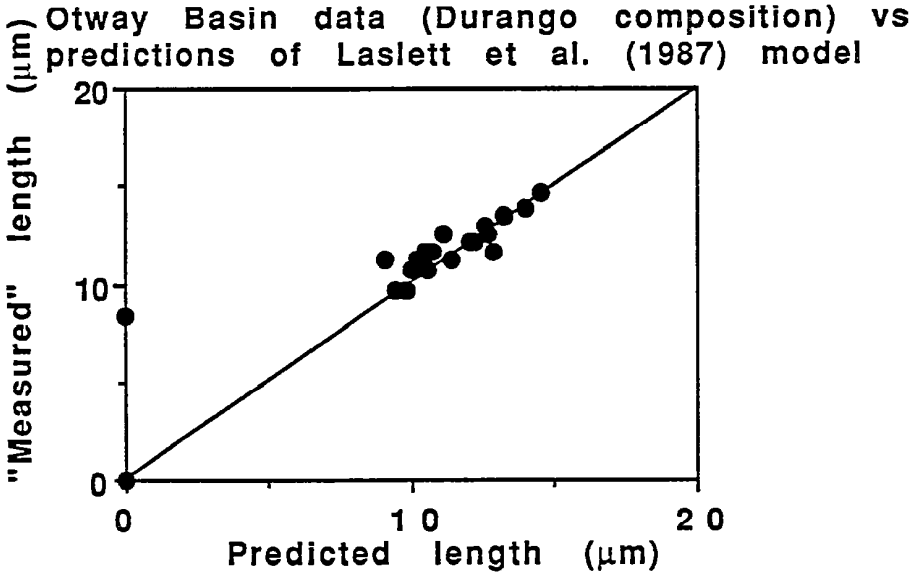


**Figure C.1b** Comparison of the mean track length in apatites of the same Cl content as Durango apatite from the Otway Group samples illustrated in figure C.1a, with values predicted for apatite of the same composition by the model of Laslett et al. (1987). The agreement is clearly very good except possibly at lengths below ~10 µm.

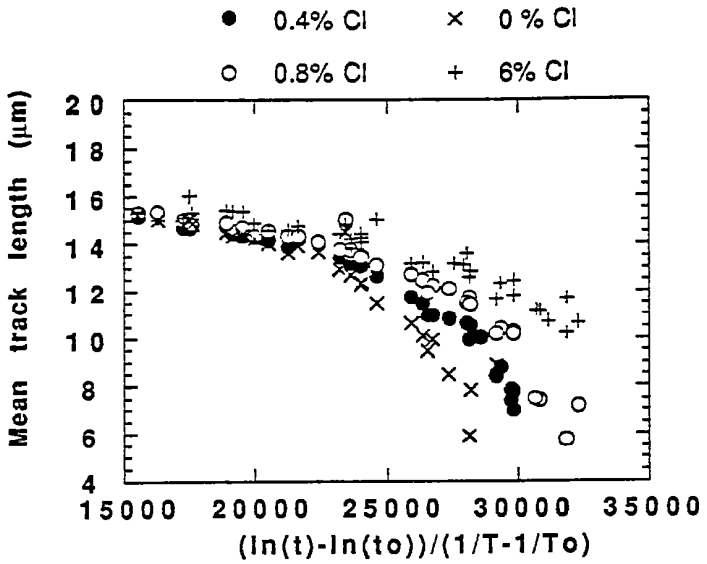


**Figure C.2** Mean track length in apatites with four different chlorine contents, as a combined function of temperature and time, to reduce the data to a single scale. Fluorapatites are more easily annealed than chlorapatites, and the annealing kinetics show a progressive change with increasing Cl content.

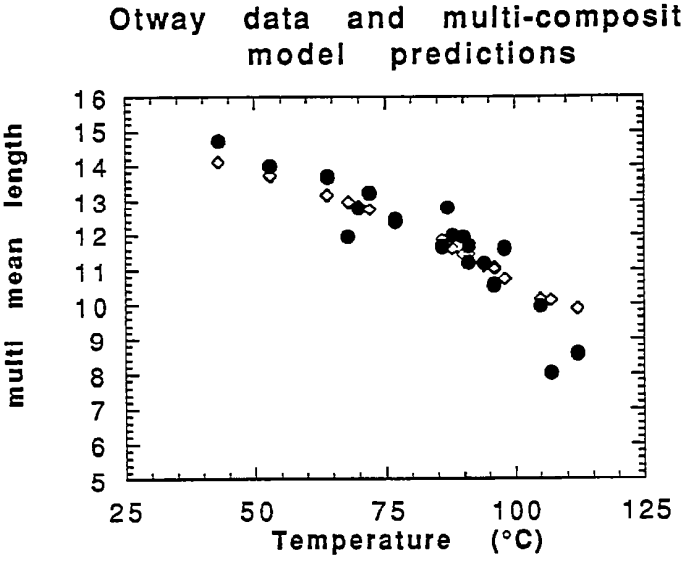


**Figure C.3** Comparison of measured mean track length (solid circles) in samples from four Otway Basin reference wells (from Green et al, 1989a) and predicted mean track lengths (open diamonds) from the new multi-compositional kinetic model of fission track annealing described in Section C.3. This model takes into account the spread of Cl contents in apatites from the Otway Group samples and the influence of Cl content on annealing rate. The agreement is clearly very good over the range of the data.

All samples

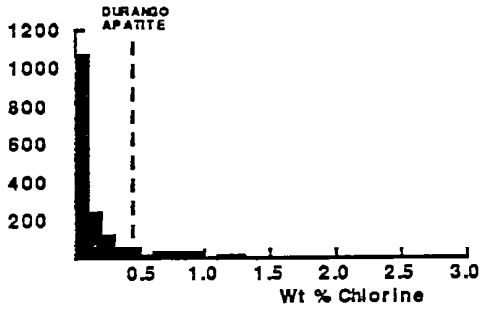


"Normal sandstones"

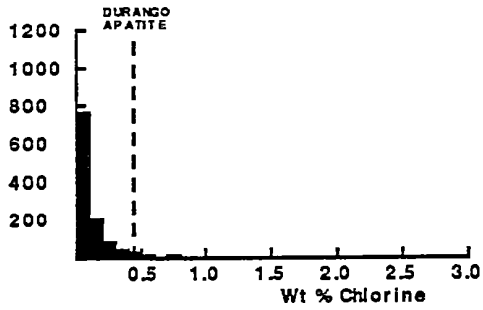


Volcanogenic sandstones

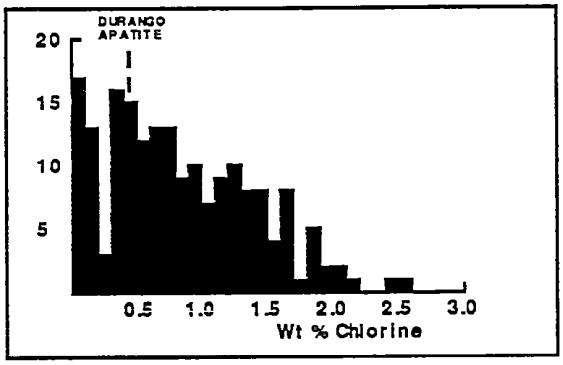


Figure C.4 **a:** Histogram of Cl contents (wt%) in over 1750 apatite grains from over 100 samples of various sedimentary and igneous rocks. Most samples give Cl contents below ~0.5 wt %, while those apatites giving higher Cl contents are characterisitic of volcanogenic sandstones and basic igneous sources.

**b:** Histogram of Cl contents (wt%) in 1168 apatite grains from 61 samples which can loosely be characterised as "normal sandstone". The distribution is similar to that in the upper figure, except for a lower number of grains with Cl contents greater than ~1%.

**c:** Histogram of Cl contents (wt%) in 188 apatite grains from 15 samples of volcanogenic sandstone. The distribution is much flatter than the other two, with much higher proportion of Cl-rich grains.

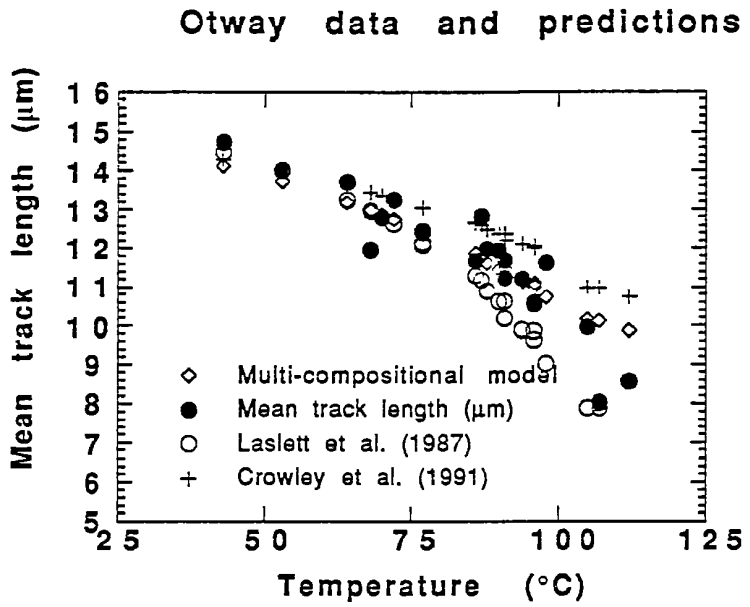


**Figure C.5** Comparison of mean track length in samples from four Otway Basin reference wells (from Green et al, 1989a) and predicted mean track lengths from three kinetic models for fission track annealing. The Crowley et al. (1991) model relates to almost pure Fluorapatite (B-5), yet overpredicts mean lengths in the Otway Group samples which are dominated by Cl-rich apatites. The predictions of that model are therefore not reliable.

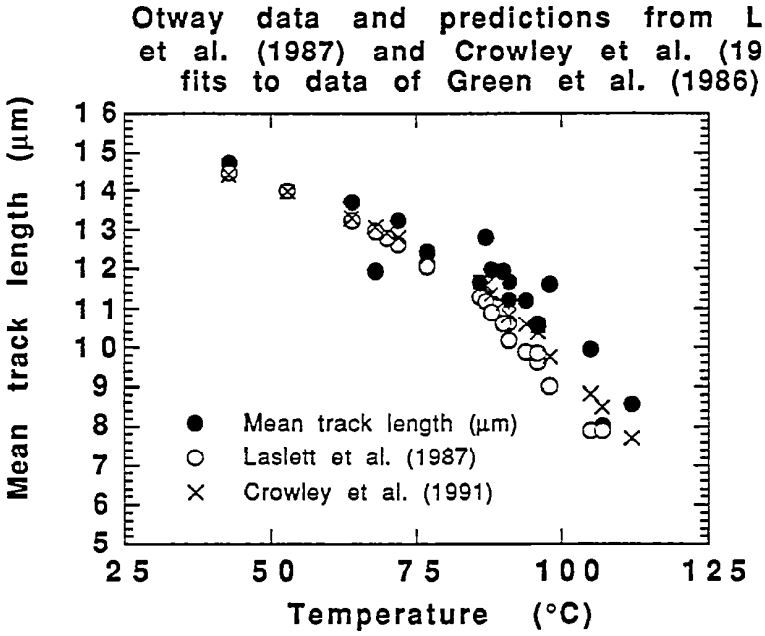


**Figure C.6** Comparison of mean track length in samples from four Otway Basin reference wells with values predicted from Laslett et al. (1987) and the model fitted to the annealing data of Green et al. (1986) by Crowley et al. (1991). The predictions of the two models are not very different.

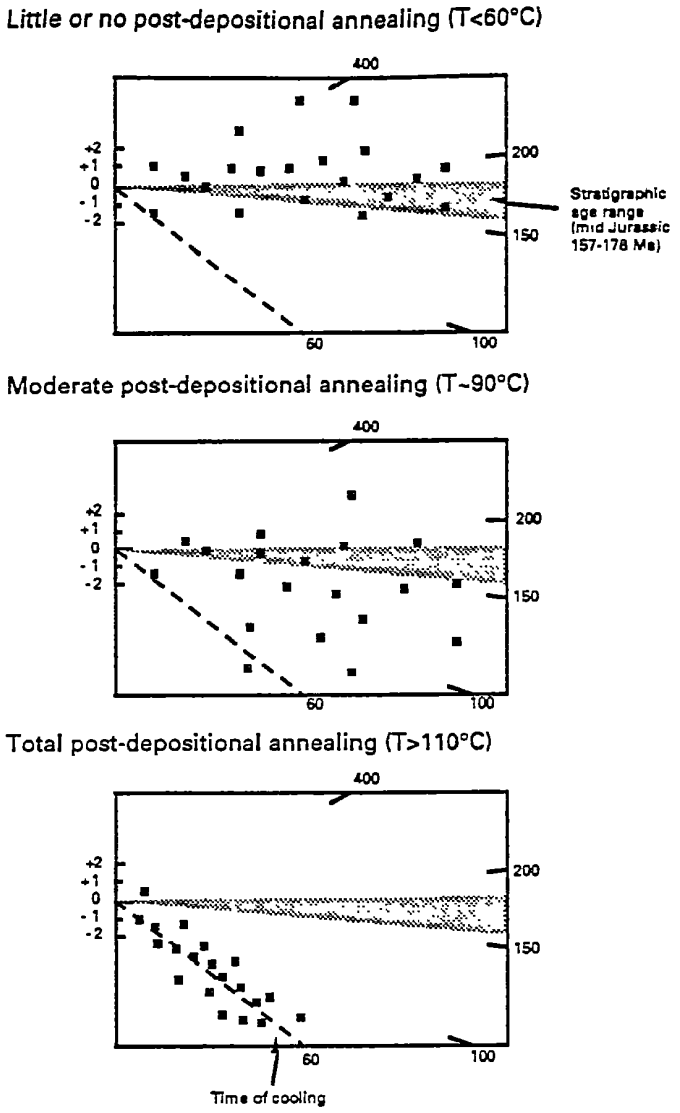


**Figure C.7** Radial plots of single grain age data in three samples of mid-Jurassic sandstone that have been subjected to varying degrees of post-depositional annealing prior to cooling at ~60 Ma. The mid-point of the stratigraphic age range has been taken as the reference value (corresponding to the horizontal).

The upper diagram represents a sample which has remained at paleotemperatures less than ~60°C, and has therefore undergone little or no post-depositional annealing. All single grain ages are either compatible with the stratigraphic age (within $y = \pm 2$ in the radial plot) or older than the stratigraphic age ($y_i > 2$).

The centre diagram represents a sample which has undergone a moderate degree of post-depositional annealing, having reached a maximum paleotemperature of around ~90°C prior to cooling. While some of the individual grain ages are compatible with the stratigraphic age ($-2 < y_i < +2$) and some may be significantly greater than the stratigraphic age ($y_i > 2$), a number of grains give ages which are significantly less than the stratigraphic age ($y < 2$).

The lower diagram represents a sample in which all apatite grains were totally annealed, at paleotemperatures greater than ~110°C, prior to rapid cooling at ~60 Ma. All grains give fission track ages compatible with a fission track age of ~60 Ma (i.e., all data plot within ±2 of the radial line corresponding to an age of ~60 Ma), and most are significantly younger than the stratigraphic age.

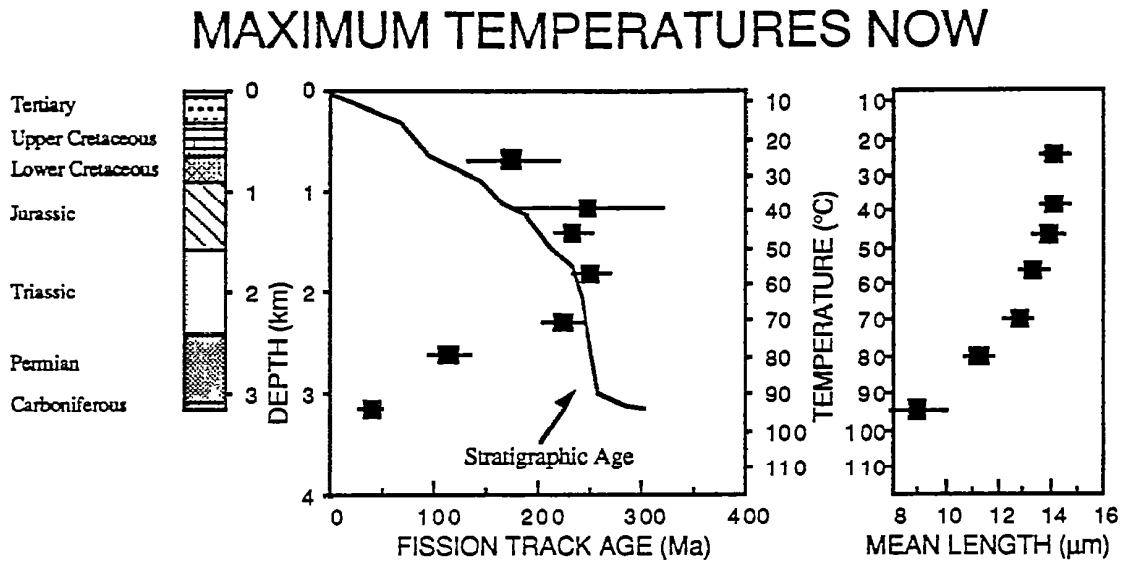


**Figure C.8a** Typical pattern of AFTA parameters in a well in which samples throughout the entire section are currently at their maximum temperatures since deposition. Both the fission track age and mean track length undergo progressive reduction to zero at temperatures of ~100 - 110°C, the actual value depending on the range of apatite compositions present.

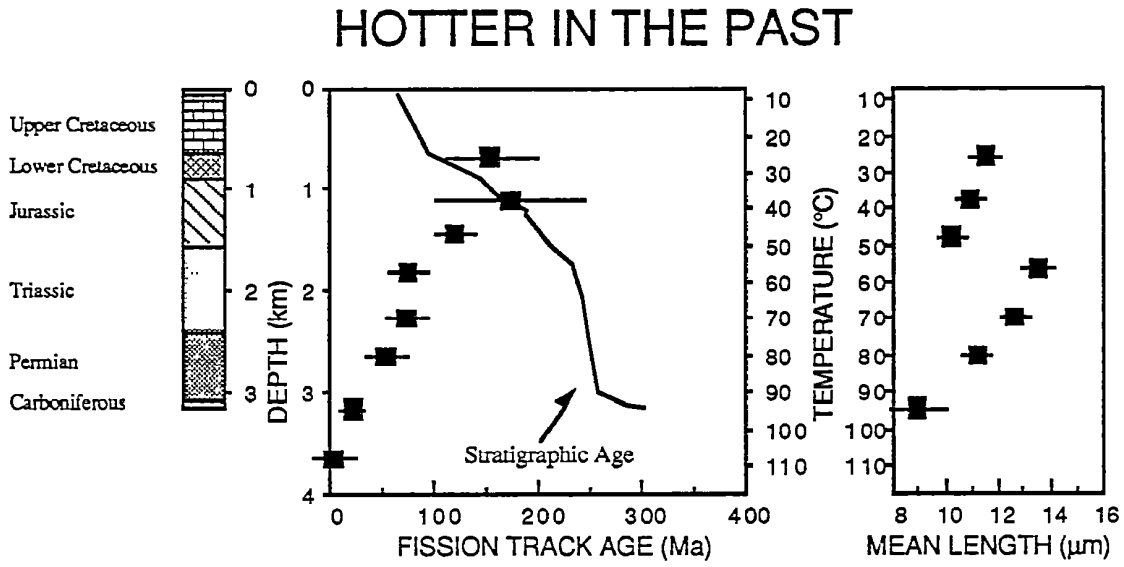


**Figure C.8b** Typical pattern of AFTA parameters in a well in which samples throughout the section were exposed to elevated paleotemperatures after deposition (prior to cooling in the Early Tertiary, in this case). Both the fission track age and mean track length show more reduction at temperatures of ~40 to 50°C than would be expected at such temperatures. At greater depths (higher temperatures), the constancy of fission track age and the increase in track length are both diagnostic of exposure to elevated paleotemperatures. See Appendix C for further discussion

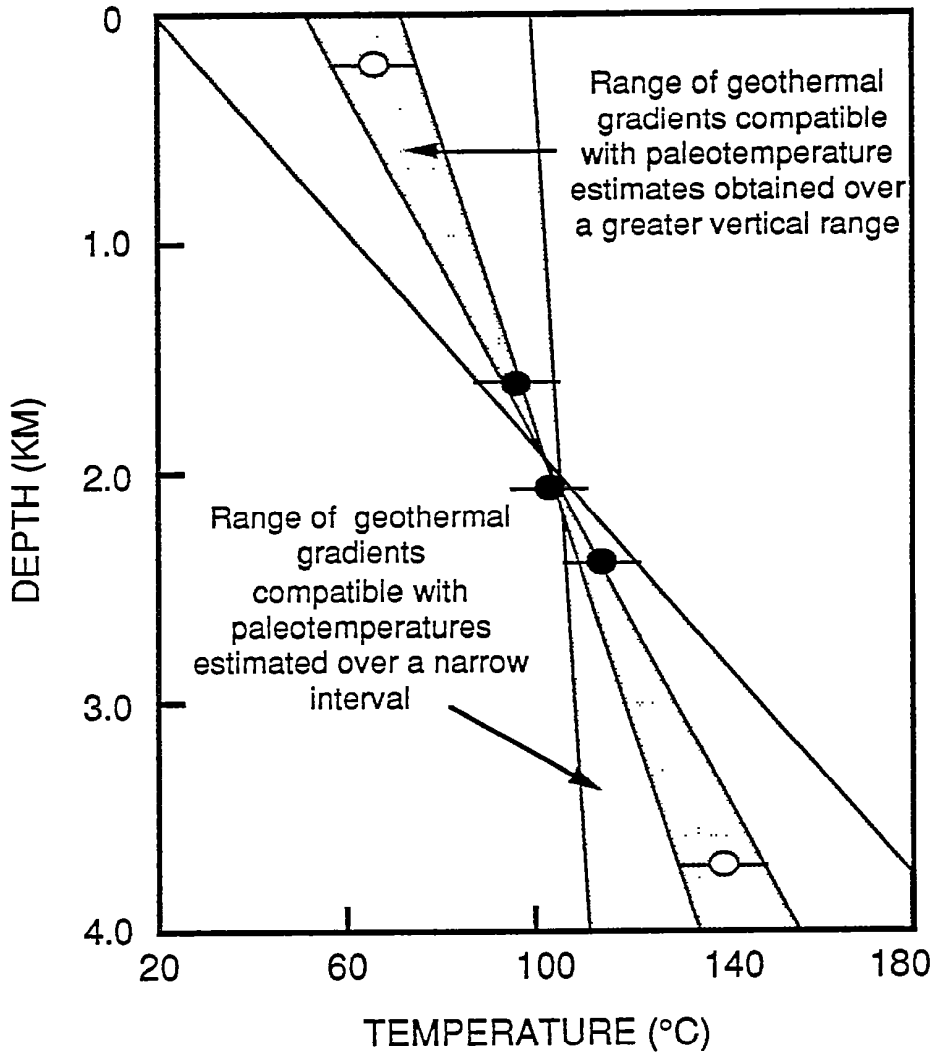


**Figure C.9** It is important to obtain paleotemperature constraints over as great a range of depths as possible in order to provide a reliable estimate of paleogeothermal gradient. If paleotemperatures are only available over a narrow depth range, then the paleogeothermal gradient can only be very loosely constrained.

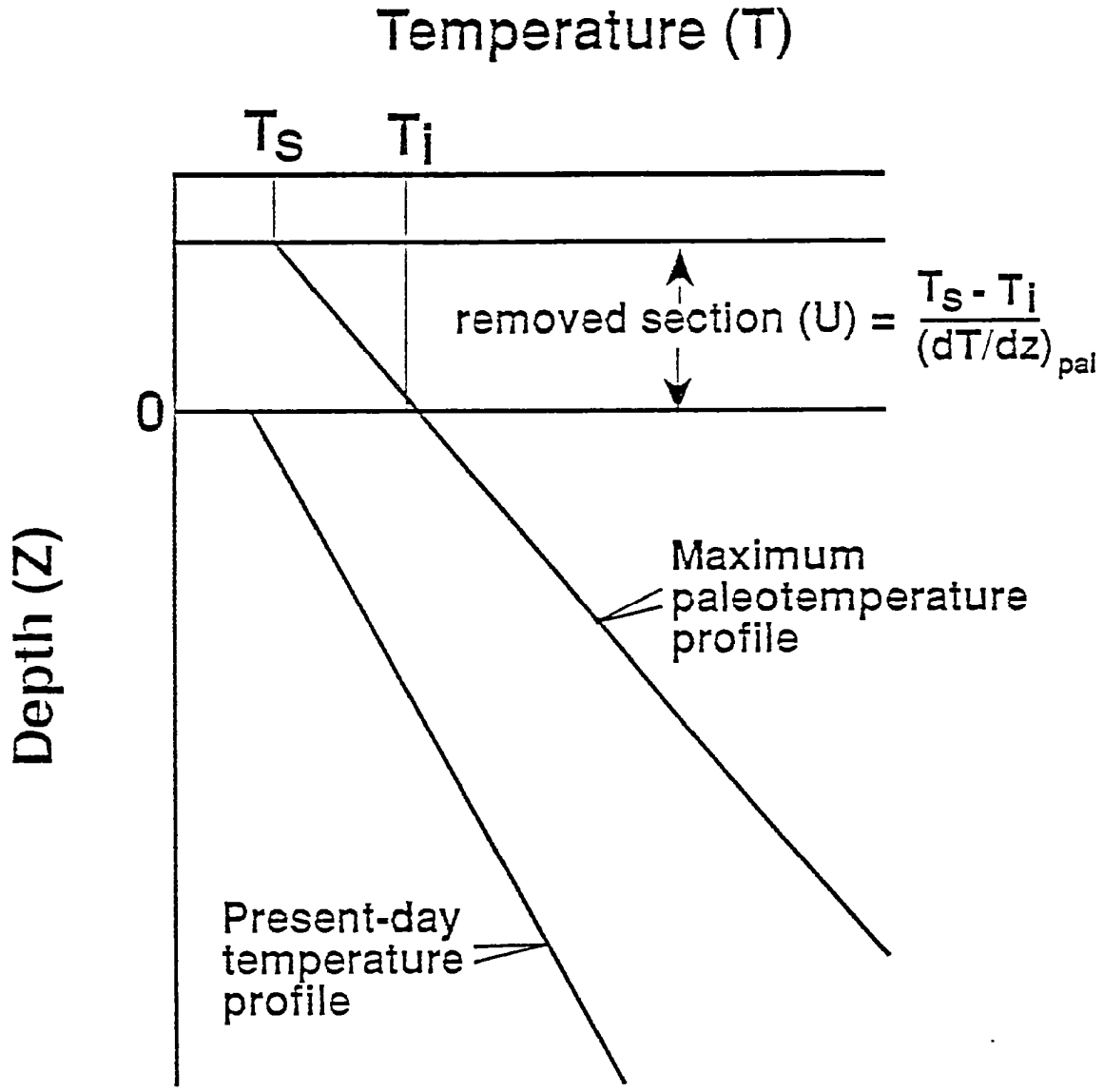


Figure C.10 If the paleogeothermal gradient can be constrained by AFTA and VR, as explained in the text, then for an assumed value of surface temperature, $T_s$, the amount of section removed can be estimated, as shown.

# APPENDIX D

## Vitrinite Reflectance Measurements

### D.1 New vitrinite reflectance determinations

New vitrinite reflectance data were collected as part of this study, with details of determinations described in sections D.1 and D.2 below. In addition, further vitrinite reflectance data were supplied by the client, as summarised in section D.3.

*Samples*

Samples were submitted for vitrinite reflectance determination to Keiraville Konsultants, Australia. Results and sample details are summarised in Table D.2, while supporting data, including maceral descriptions and raw data sheets, are presented in the following pages.

*Equipment*

Leitz MPV1.1 photometer equipped with separate fluorescence illuminator, Swift point counter. Reflectance standards: spinel 0.42%, YAG 0.91%, GGG 1.72%, SiC standard for cokes and masked uranyl glass for measurement of intensity (I) in fluorescence mode. With the Keiraville Konsultants equipment, it is possible to alternate from reflectance to fluorescence mode to check for associated fluorescing liptinite, or importantly with some samples, to check for bitumen impregnation, or the presence, intensity, and source of oil-cut.

*Sample preparation*

Samples are normally mounted in cold setting polyester resin and polished using $Cr_2O_3$ and MgO polishing powders. Epoxy resins or araldite can be used if required. "Whole rock" samples are normally used but demineralisation can be undertaken. Large samples of coals and cokes can be mounted and examined.

*Vitrinite Reflectance measurement*

The procedure used generally follows Australian Standard (AS) 2486, but has been slightly modified for use with dispersed organic matter (DOM). For each sample, a minimum of 25 fields is measured (the number may be less if vitrinite is rare or if a

limited number of particles of vitrinite is supplied, as may be the case with hand-picked samples). If wide dispersal of vitrinite reflectances is found, the number of readings (N) is increased until a stable mean is obtained.

Vitrinite identification is made primarily on textural grounds, and this allows an independent assessment to be made of cavings and re-worked vitrinite populations. Histograms are only used for population definition when a cavings population significantly overlaps the range of the indigenous population. Where such data provides additional information, the mean maximum reflectance of inertinite and/or the mean maximum reflectance of liptinite (exinite) is reported. For each field, the maximum reflectance position is located and the reading recorded. The stage is then rotated by 180° which should give the same reading. In practice, the readings are seldom identical because of stage run-out and slight surface irregularities. If the readings are within ±5% relative, they are accepted. If not, the cause of the difference is sought and the results rejected. The usual source of differences is surface relief. The measurement of both maxima results in a total of 50 measurements being taken for the 25 fields reported. Thus, the 50 readings consist of 25 pairs of closely spaced readings which provide a check on the levelling of the surface and hence additional precision.

As the vitrinite reflectance measurements are being made, the various features of the samples are noted on a check sheet to allow a sample description to be compiled. When the reflectance measurements are complete, a thorough check is made of liptinite fluorescence characteristics. At the same time, organic matter abundance is estimated using a global estimate, a grain count method or point count method as required.

***Data presentation***

Individual sample results are reported in the following format:

| KK No. | Depth (ft) | $\overline{R}_V$max*1 | Range*2 | N*3 |
|---|---|---|---|---|
| x10324 | 3106 | 0.79 | 0.64 - 0.91 | 25 |

*1 Mean of all the maximum reflectance readings obtained.

*2 Lowest Rmax and highest Rmax of the population considered to represent the first generation vitrinite population.

*3 Number of fields measured (Number of measurements = 2N because 2 maximum values are recorded for each field)

*Methods - Organic matter abundance and type.*

After completion of vitrinite reflectance readings, the microscope is switched to fluorescence-mode and an estimate made of the abundance of each liptinite maceral. Fluorescence colours are also noted (BG 3 long UV excitation, TK400 dichroic mirror and a K490 barrier filter). The abundances are estimated using comparison charts. The categories used for liptinite (and other components) are:

| Descriptor | % | Source potential |
|---|---|---|
| Absent | 0 | None |
| Rare | <0.1 | Very poor |
| Sparse | 0.1<x<0.5 | Poor to fair |
| Common | 0.5<x<2.0 | Fair to good |
| Abundant | 2.0<x<10.0 | Good to very good |
| Major | 10.0<x<40.0 | Very good (excellent if algal) |
| Dominant | >40.0 | Excellent |

*Dispersed Organic Matter (DOM) composition*

At the same time as liptinite abundances are estimated, total DOM, vitrinite and inertinite abundances are estimated and reported in the categories listed above. Liptinite (exinite) fluorescence intensity and colour, lithology and a brief description of organic matter type and abundance are also recorded in a further column. Coal is described separately from dispersed organic matter (DOM). These data can be used to estimate the specific yield of the DOM and form a valuable adjunct to TOC data.

*Lithological composition*

The lithological abundances are ranked. For cuttings, these data can be useful in conjunction with geophysical logs in assessing the abundance and nature of cavings. For cores, it provides a record of the lithology examined and of the lithological associations of the organic matter.

*Coal abundance and composition*

Where coals are present, their abundance is recorded and their composition is reported as microlithotypes thus:

Coal major, Vitrinite>Inertinite>Exinite, Clarodurite>vitrite>clarite>inertite.

These data give an approximate maceral composition and information about the organic facies of the coal. Where coal is a major or dominant component, and more precise maceral composition data are required, point count analyses should be requested. However, the precision of the original sampling is commonly a limiting factor in obtaining better quality data.

*Abundance factor analysis*

Especially where cuttings samples are used, abundance factor analyses are used to obtain an assessment of the maceral assemblages in the various lithologies. This can be done by a combination analysis using a point counter, but a large number of categories is required, and the precision is low if DOM is less than about 10%. For an abundance factor analysis (for core, 50 microscope fields of view) we assess the abundance of DOM, coal and shaly coal in 50 grains. The data can be used to plot DOM and coal abundance profiles.

*Analyst/Advisor:* Professor A.C. Cook

Prior to transmittal of final results, all samples are examined and checked by A.C. Cook who has more than 30 years' experience of work on coals, cokes, source rocks and source rock maturation.

## D.3 Integration of vitrinite reflectance data with AFTA

Vitrinite reflectance is a time-temperature indicator governed by a kinetic response in a similar manner to the annealing of fission tracks in apatite as described in Appendix C. In this study, vitrinite reflectance data are interpreted on the basis of the distributed activation energy model describing the evolution of VR with temperature and time described by Burnham and Sweeney (1989), as implemented in the BasinMod™ software package of Platte River Associates. In a considerable number of wells from around the world, in which AFTA has been used to constrain the thermal history, we have found that the Burnham and Sweeney (1989) model gives good agreement between predicted and observed VR data, in a variety of settings.

As in the case of fission track annealing, it is clear from the chemical kinetic description embodied in equation 2 of Burham and Sweeney (1989) that temperature is more important than time in controlling the increase of vitrinite reflectance. If the Burham and Sweeney (1989) distributed activation energy model is expressed in the form of an Arrhenius plot (a plot of the logarithm of time versus inverse absolute temperature), then

the slopes of lines defining contours of equal vitrinite reflectance in such a plot are very similar to those describing the kinetic description of annealing of fission tracks in Durango apatite developed by Laslett et al. (1987), which is used to interpret the AFTA data in this report. This feature of the two quite independent approaches to thermal history analysis means that for a particular sample, a given degree of fission track annealing in apatite of Durango composition will be associated with the same value of vitrinite reflectance regardless of the heating rate experienced by a sample. Thus paleotemperature estimates based on either AFTA or VR data sets should be equivalent, regardless of the duration of heating. As a guide, Table D.1 gives paleotemperature estimates for various values of VR for two different heating times.

One practical consequence of this relationship between AFTA and VR is, for example, that a VR value of 0.7% is associated with total annealing of all fission tracks in apatite of Durango composition, and that total annealing of all fission tracks in apatites of more Chlorine-rich composition is accomplished between VR values of 0.7 and ~0.9%.

Furthermore, because vitrinite reflectance continues to increase progressively with increasing temperature, VR data allow direct estimation of maximum paleotemperatures in the range where fission tracks in apatite are totally annealed (generally above ~110°C) and where therefore AFTA only provides minimum estimates. Maximum paleotemperature estimates based on vitrinite reflectance data from a well in which most AFTA samples were totally annealed will allow constraints on the paleogeothermal gradient that would not be possible from AFTA alone. In such cases the AFTA data should allow tight constraints to be placed on the time of cooling and also the cooling history, since AFTA parameters will be dominated by the effects of tracks formed after cooling from maximum paleotemperatures. Even in situations where AFTA samples were not totally annealed, integration of AFTA and VR can allow paleotemperature control over a greater range of depth, e.g. by combining AFTA from sand-dominated units with VR from other parts of the section, thereby providing tighter constraint on the paleogeothermal gradient.

## D.2 Client-supplied vitrinite reflectance

Vitrinite reflectance and other data (if applicable) supplied by the client is summarised in Table D.3. Unless specified, this vitrinite reflectance data has been treated at face value, as if it were collected in the same manner as described for the new data, because detailed information is usually not available.

## References

Burnham, A.K. and Sweeney, J.J. (1989). A chemical kinetic model of vitrinite reflectance maturation. Geochim. et Cosmochim. Acta, 53, 2649-2657.

Laslett, G.M., Green, P.F., Duddy, I.R. and Gleadow, A.J.W. (1987). Thermal annealing of fission tracks in apatite 2. A quantitative analysis. *Chem. Geol. (Isot. Geosci.Sect.)*, 65, 1-13.

**Table D.1: Paleotemperature - vitrinite reflectance nomogram based on Equation 2 of Burnham and Sweeney (1989)**

| Paleotemperature (°C / °F) | Vitrinite Reflectance (%) 1 Ma Duration of heating | 10 Ma Duration of heating |
|---|---|---|
| 40 / *104* | 0.29 | 0.32 |
| 50 / *122* | 0.31 | 0.35 |
| 60 / *140* | 0.35 | 0.40 |
| 70 / *158* | 0.39 | 0.45 |
| 80 / *176* | 0.43 | 0.52 |
| 90 / *194* | 0.49 | 0.58 |
| 100 / *212* | 0.55 | 0.64 |
| 110 / *230* | 0.61 | 0.70 |
| 120 / *248* | 0.66 | 0.78 |
| 130 / *266* | 0.72 | 0.89 |
| 140 / *284* | 0.81 | 1.04 |
| 150 / *302* | 0.92 | 1.20 |
| 160 / *320* | 1.07 | 1.35 |
| 170 / *338* | 1.23 | 1.55 |
| 180 / *356* | 1.42 | 1.80 |
| 190 / *374* | 1.63 | 2.05 |
| 200 / *392* | 1.86 | 2.33 |
| 210 / *410* | 2.13 | 2.65 |
| 220 / *428* | 2.40 | 2.94 |
| 230 / *446* | 2.70 | 3.23 |

## Table D.2: Vitrinite reflectance sample details and results - well samples from the Duntroon Basin (Geotrack Report #589)

| Sample number | Depth (m) | Sample type | Stratigraphic subdivision | Stratigraphic age (Ma) | Present temperature *1 (°C) | VR (Range) % | N |
|---|---|---|---|---|---|---|---|
| **Platypus-1** | | | | | | | |
| GC589-1.1 | 1597-1600 *(5240'-5250')* | cuttings | Nullabor Lst | 33-0 | 54 | 0.57 | 1 |
| GC589-2.1 | 1798-1801 *(5900'-5910')* | cuttings | Wilsons Bluff | 50-33 | 60 | 0.35 (0.29-0.39) | 18 |
| GC589-3.1 | 1908-1911 *(6260'-6270')* | cuttings | Potoroo | 73-65 | 63 | 0.43 (0.37-0.49) | 16 |
| GC589-4.1 | 2149-2152 *(7050'-7060')* | cuttings | Potoroo | 73-65 | 71 | 0.42 (0.31-0.57) | 26 |
| GC589-5.1 | 2210-2365 *(7250'-7760')* | cuttings | Wigunda | 85-73 | 75 | 0.42 (0.32-0.59) | 26 |
| GC589-6.1 | 2399-2402 *(7870'-7880')* | cuttings | Wigunda | 85-73 | 78 | 0.41 (0.34-0.57) | 17 |
| GC589-7.1 | 2499-2502 *(8200'-8210')* | cuttings | Wigunda | 85-73 | 81 | 0.43 (0.36-0.58) | 28 |
| GC589-8.1 | 2600-2603 *(8530'-8540')* | cuttings | Wigunda | 85-73 | 85 | 0.45 (0.37-0.59) | 28 |
| GC589-9.1 | 2899-2902 *(9510'-9520')* | cuttings | Wigunda | 85-73 | 94 | 0.51 (0.35-0.69) | 30 |
| GC589-10.1 | 3008-3011 *(9870'-9880')* | cuttings | Platypus | 96-85 | 97 | 0.52 (0.41-0.63) | 29 |
| GC589-11.1 | 3197-3200 *(10490'-10500')* | cuttings | Platypus | 96-85 | 103 | 0.55 (0.38-0.70) | 32 |
| GC589-12.1 | 3398-3401 *(11150'-11160')* | cuttings | Ceduna | 100-96 | 109 | 0.62 (0.50-0.77) | 27 |
| GC589-13.1 | 3499-3502 *(11480'-11490')* | cuttings | Ceduna | 100-96 | 112 | 0.55 (0.45-0.67) | 29 |
| GC589-14.1 | 3600-3603 *(11810'-11820')* | cuttings | Ceduna | 100-96 | 115 | 0.55 (0.43-0.65) | 27 |
| GC589-15.1 | 3694-3703 *(12120'-12150')* | cuttings | Ceduna | 100-96 | 118 | 0.58 (0.41-0.71) | 27 |
| GC589-16.1 | 3810-3813 *(12500'-12510')* | cuttings | Upper Borda | 115-100 | 122 | 0.67 (0.53-0.83) | 27 |
| GC589-17.1 | 3886-3889 *(12750'-12760')* | cuttings | Upper Borda | 115-100 | 124 | 0.63 (0.52-0.76) | 26 |

## Table D.2: Continued.

| Sample number | Depth (m) | Sample type | Stratigraphic subdivision | Stratigraphic age (Ma) | Present temperature *1 (°C) | VR (Range) % | N |
|---|---|---|---|---|---|---|---|
| **Duntroon-1** | | | | | | | |
| GC589-18.1 | 1595-1610 *(5233'-5282')* | cuttings | Wilson Bluff | 55-50 | 57 | 0.33 (0.22-0.42) | 6 |
| GC589-19.1 | 1675-1690 *(5496'-5545')* | cuttings | Pidinga | 65-60 | 59 | 0.47 (0.44-0.50) | 2 |
| GC589-20.1 | 1805-1820 *(5922'-5971')* | cuttings | Pidinga | 65-60 | 64 | 0.35 (0.30-0.41) | 3 |
| GC589-21.1 | 1895-1910 *(6217'-6267')* | cuttings | Potoroo | 73-65 | 66 | 0.37 (0.27-0.48) | 25 |
| GC589-22.1 | 2050-2055 *(6726'-6742')* | cuttings | Potoroo | 73-65 | 71 | 0.39 (0.29-0.47) | 25 |
| GC589-23.1 | 2145-2160 *(7038'-7087')* | cuttings | Wigunda | 85-73 | 75 | 0.45 (0.34-0.54) | 22 |
| GC589-24.1 | 2300-2305 *(7546'-7563')* | cuttings | Wigunda | 85-73 | 80 | 0.49 (0.42-0.57) | 25 |
| GC589-25.1 | 2495-2510 *(8186'-8235')* | cuttings | Wigunda | 85-73 | 86 | 0.52 (0.43-0.62) | 26 |
| GC589-26.1 | 2600-2605 *(8531'-8547')* | cuttings | Ceduna | 100-96 | 89 | 0.55 (0.45-0.75) | 27 |
| GC589-27.1 | 2850-2855 *(9351'-9367')* | cuttings | Ceduna | 100-96 | 97 | 0.58 (0.49-0.68) | 28 |
| GC589-28.1 | 2950-2955 *(9679'-9695')* | cuttings | Upper Borda | 119-100 | 101 | 0.56 (0.41-0.76) | 26 |
| GC589-29.1 | 3050-3055 *(10007'-10023')* | cuttings | Upper Borda | 119-100 | 104 | 0.53 (0.37-0.65) | 25 |
| GC589-30.1 | 3350-3355 *(10991'-11008')* | cuttings | Upper Borda | 119-100 | 114 | 0.58 (0.44-0.75) | 25 |
| GC589-31.1 | 3450-3455 *(11319'-11336')* | cuttings | Upper Borda | 119-100 | 117 | 0.66 (0.52-0.79) | 26 |
| GC589-32.1 | 3505-3510 *(11500'-11516')* | cuttings | Upper Borda | 119-100 | 119 | 0.71 (0.60-0.82) | 26 |

Note: Some samples may contain both vitrinite and inertinite.

*1 See Appendix A for discussion of present temperature data.

## Table D.3: Vitrinite reflectance sample details and results - well data supplied by BHP (Geotrack Report #589)

| Depth (m) | Stratigraphic subdivision | Stratigraphic age (Ma) | Present temperature *1 (°C) | VR (Range) % | N |
|---|---|---|---|---|---|
| **Platypus-1** | | | | | |
| 1094 *(3590')* | Nullabor Lst | 33-0 | 38 | 0.27 | - |
| 1207 *(3960')* | Nullabor Lst | 33-0 | 41 | 0.30 | - |
| 1530 *(5020')* | Nullabor Lst | 33-0 | 51 | 0.36 | - |
| 1685 *(5530')* | Nullabor Lst | 33-0 | 56 | 0.35 | - |
| 1829 *(6000')* | Wilsons Bluff | 50-33 | 61 | 0.35 | - |
| 1981 *(6500')* | Potoroo | 73-65 | 65 | 0.35 | - |
| 2133 *(7000')* | Potoroo | 73-65 | 70 | 0.38 | - |
| 2286 *(7500')* | Wigunda | 85-73 | 75 | 0.36 | - |
| 2469 *(8100')* | Wigunda | 85-73 | 80 | 0.40 (0.29-0.49) | 21 |
| 2469 *(8100')* | Wigunda | 85-73 | 80 | 0.41 | - |
| 2594 *(8510')* | Wigunda | 85-73 | 84 | 0.42 | - |
| 2722 *(8930')* | Wigunda | 85-73 | 88 | 0.40 | - |
| 2835 *(9300')* | Wigunda | 85-73 | 92 | 0.47 (0.37-0.55) | 25 |
| 2871 *(9420')* | Wigunda | 85-73 | 93 | 0.49 | - |
| 2899 *(9510')* | Wigunda | 85-73 | 94 | 0.46 | - |
| 2908 *(9540')* | Wigunda | 85-73 | 94 | 0.49 | - |
| 2975 *(9760')* | Platypus | 96-85 | 96 | 0.50 | - |
| 3017 *(9900')* | Platypus | 96-85 | 97 | 0.50 | - |
| 3048 *(10000')* | Platypus | 96-85 | 98 | 0.49 | - |
| 3103 *(10180')* | Platypus | 96-85 | 100 | 0.49 | - |
| 3151 *(10340')* | Platypus | 96-85 | 102 | 0.54 | - |
| 3197 *(10490')* | Platypus | 96-85 | 103 | 0.54 | - |
| 3200 *(10500')* | Platypus | 96-85 | 103 | 0.49 (0.34-0.62) | 30 |
| 3279 *(10760')* | Platypus | 96-85 | 106 | 0.57 | - |
| 3380 *(11090')* | Ceduna | 100-96 | 109 | 0.59 | - |

## Table D.3: Continued.

| Depth (m) | Stratigraphic subdivision | Stratigraphic age (Ma) | Present temperature *1 (°C) | VR (Range) % | N |
|---|---|---|---|---|---|
| **Platypus-1** | | | | | |
| 3447 *(11310')* | Ceduna | 100-96 | 111 | 0.57 | - |
| 3496 *(11470')* | Ceduna | 100-96 | 112 | 0.59 | - |
| 3593 *(11790')* | Ceduna | 100-96 | 115 | 0.55 | - |
| 3724 *(12220')* | Upper Borda | 115-100 | 119 | 0.68 | - |
| 3740 *(12270')* | Upper Borda | 115-100 | 120 | 0.72 | - |
| 3822 *(12540')* | Upper Borda | 115-100 | 122 | 0.71 | - |
| 3877 *(12720')* | Upper Borda | 115-100 | 124 | 0.73 | - |
| 3888 *(12756')* | Upper Borda | 115-100 | 124 | 0.75 (0.61-0.89) | 36 |
| **Duntroon-1** | | | | | |
| 520 *(1706')* | Nullabor Lst | 33-0 | 21 | 0.33 | - |
| 720 *(2362')* | Nullabor Lst | 33-0 | 28 | 0.39 | - |
| 940 *(3084')* | Nullabor Lst | 33-0 | 35 | 0.46 | - |
| 1020 *(3347')* | Nullabor Lst | 33-0 | 38 | 0.45 | - |
| 1220 *(4003')* | Nullabor Lst | 33-0 | 44 | 0.50 | - |
| 1420 *(4659')* | Nullabor Lst | 33-0 | 51 | 0.51 | - |
| 1520 *(4987')* | Wilsons Bluff | 55-50 | 54 | 0.55 | - |
| 1620 *(5315')* | Wilsons Bluff | 55-50 | 57 | 0.44 | - |
| 1686 *(5532')* | Pidinga | 65-60 | 59 | 0.43 | - |
| 1816 *(5958')* | Pidinga | 65-60 | 64 | 0.45 | - |
| 1855 *(6086')* | Potoroo | 73-65 | 65 | 0.60 | - |
| 1870 *(6135')* | Potoroo | 73-65 | 65 | 0.47 | - |
| 1920 *(6300')* | Potoroo | 73-65 | 67 | 0.53 | - |
| 2020 *(6628')* | Potoroo | 73-65 | 70 | 0.42 | - |
| 2065 *(6775')* | Potoroo | 73-65 | 72 | 0.47 (0.38-0.56) | 24 |
| 2125 *(6972')* | Wigunda | 85-73 | 74 | 0.41 | - |

## Table D.3: Continued.

| Depth (m) | Stratigraphic subdivision | Stratigraphic age (Ma) | Present temperature *1 (°C) | VR (Range) % | N |
|---|---|---|---|---|---|
| **Duntroon-1** | | | | | |
| 2134 *(7002')* | Wigunda | 85-73 | 74 | 0.44 | - |
| 2220 *(7284')* | Wigunda | 85-73 | 77 | 0.39 | - |
| 2270 *(7448')* | Wigunda | 85-73 | 78 | 0.51 | - |
| 2310 *(7579')* | Wigunda | 85-73 | 80 | 0.42 | - |
| 2410 *(7907')* | Wigunda | 85-73 | 83 | 0.46 | - |
| 2510 *(8235')* | Wigunda | 85-73 | 86 | 0.42 | - |
| 2615 *(8580')* | Ceduna | 100-96 | 90 | 0.52 | - |
| 2715 *(8908')* | Ceduna | 100-96 | 93 | 0.50 | - |
| 2754 *(9036')* | Ceduna | 100-96 | 94 | 0.39 (0.33-0.46) | 21 |
| 2815 *(9236')* | Ceduna | 100-96 | 96 | 0.43 | - |
| 2905 *(9531')* | Ceduna | 100-96 | 99 | 0.50 | - |
| 3000 *(9843')* | Upper Borda | 119-100 | 102 | 0.36 (0.29-0.47) | 28 |
| 3000 *(9843')* | Upper Borda | 119-100 | 102 | 0.34 | - |
| 3105 *(10188')* | Upper Borda | 119-100 | 106 | 0.58 | - |
| 3200 *(10499')* | Upper Borda | 119-100 | 109 | 0.64 | - |
| 3300 *(10827')* | Upper Borda | 119-100 | 112 | 0.62 | - |
| 3400 *(11155')* | Upper Borda | 119-100 | 115 | 0.67 | - |
| 3500 *(11484')* | Upper Borda | 119-100 | 119 | 0.61 (0.48-0.72) | 41 |

Note: - Indicates data unavailable.

*1 See Appendix A for discussion of present temperature data.

JOB GC589 - AGSO/MESA PLATYPUS-1

| KK/Ref. No. | Depth(ft) Type | $\bar{R}_v$ max | Range | N | Description Including Liptinite (Exinite) Fluorescence |
|---|---|---|---|---|---|
| | | | | | **BASE OF WILSON BLUFF** |
| T1926 1.1 | 5240-250 Ctgs | 0.57 | - | 1 | Rare lamalginite, yellow. Sandstone>>claystone>calcareous claystone. Dom rare, L>I>V. All three maceral groups rare. Mineral fluorescence pervasive, yellow. Glauconite rare. Pyrite sparse. |
| | | | | | **POTOROO** |
| T1927 2.1 | 5900-10 Ctgs | 0.35 | 0.29-0.39 | 18 | Sparse lamalginite and liptodetrinite, greenish yellow to orange. (Siltstone>sandstone>coal. Coal sparse, vitrite. Dom common, L>I>V. All three maceral groups sparse. Mineral fluorescence pervasive, yellow to orange. Igneous rock grains common. Iron oxides sparse. Pyrite abundant). |
| T1928 3.1 | 6260-270 Ctgs | 0.43 | 0.37-0.49 | 16 | Sparse lamalginite, yellow, rare liptodetrinite, yellow. (Siltstone>>claystone. Dom sparse, L>V>I. Liptinite sparse, vitrinite and inertinite rare. Mineral fluorescence patchy, weak yellow. Iron oxides abundant. Pyrite common). |
| T1929 4.1 | 7050-060 Ctgs | 0.42 | 0.31-0.57 | 26 | Rare lamalginite and liptodetrinite, yellow to orange, rare sporinite and cutinite, yellow to orange. (Siltstone>sandstone> carbonate>coal. Coal rare, vitrite. Dom sparse, L>V>I. All three maceral groups sparse. Mineral fluorescence pervasive, yellow to orange in carbonate, weak greenish yellow in siltstone and sandstone. Iron oxides common. Pyrite abundant). |
| | | | | | **WIGUNDA** |
| T1930 5.1 | 7250-260 Ctgs | 0.42 | 0.32-0.59 | 26 | Sparse lamalginite, yellow to orange, rare liptodetrinite, yellow. (Claystone>sandstone>siltstone. Dom sparse, L>I>V. All three maceral groups sparse. Mineral fluorescence pervasive, weak green to yellow. Igneous rocks common. Iron oxides common. Pyrite abundant). |
| T1931 6.1 | 7870-880 Ctgs | 0.41 | 0.34-0.57 | 17 | Rare lamalginite and liptodetrinite, greenish yellow to orange. (Claystone>siltstone. Dom sparse, V>I>L. Vitrinite and inertinite sparse, liptinite rare. Mineral fluorescence pervasive, weak green to yellow. Iron oxides common. Pyrite sparse). |
| T1932 7.1 | 8200-210 Ctgs | 0.43 | 0.36-0.58 | 28 | Rare lamalginite and sporinite, yellow to orange, rare resinite, yellow, rare liptodetrinite, green to yellow, rare cutinite, yellow to orange. (Claystone>siltstone>coal. Coal rare, vitrite>clarite. Dom common, I>V>L. Inertinite common, vitrinite and liptinite sparse. Mineral fluorescence pervasive, weak green to yellow. Iron oxides sparse. Pyrite sparse). |

JOB GC589 - AGSO/MESA PLATYPUS-1

| KK/Ref. No. | Depth(ft) Type | $\bar{R}_v$ max | Range | N | Description Including Liptinite (Exinite) Fluorescence |
|---|---|---|---|---|---|
| | | | | | **WIGUNDA** |
| T1933 8.1 | 8530-540 Ctgs | 0.45 | 0.37-0.59 | 28 | Rare lamalginite, resinite and liptodetrinite, greenish yellow to yellow, rare sporinite and cutinite yellow to dull orange. (Siltstone>>claystone>coal. Coal sparse, vitrite. Dom common, I>V>L. All three maceral groups sparse. Mineral fluorescence pervasive, weak green to yellow. Iron oxides sparse. Pyrite sparse). |
| | | | | | **WOMBAT** |
| T1934 9.1 | 9510-520 Ctgs | 0.51 | 0.35-0.69 | 30 | Sparse lamalginite, liptodetrinite and cutinite, yellow to dull orange, rare sporinite, yellow to dull orange, rare fluorinite, green to orange. (Claystone>sandstone>siltstone>carbonate>coal. Coal and coaly shale abundant, vitrite. Most of liptinite concentrated in coaly shale. Dom common, V>L>I. Vitrinite common, inertinite and liptinite sparse. Oil droplets rare, green to yellow. Mineral fluorescence pervasive, yellow to orange. Pyrite sparse). |
| | | | | | **PLATYPUS** |
| T1935 10.1 | 9870-880 Ctgs | 0.52 | 0.41-0.63 | 29 | Sparse lamalginite, liptodetrinite and resinite, greenish yellow to dull orange, sparse sporinite and cutinite, yellow to brown. (Siltstone>sandstone>carbonate>claystone>coal>igneous rock fragments. Coal sparse, vitrite>clarite. Most of liptinite concentrated in coaly clay. Dom common, L>V>I. Vitrinite and liptinite common, inertinite sparse. Mineral fluorescence pervasive, weak green to orange. Iron oxides sparse. Pyrite common). |
| T1936 11.1 | 10490-500 Ctgs | 0.55 | 0.38-0.70 | 32 | Sparse lamalginite, liptodetrinite, resinite, sporinite and cutinite, yellow to dull orange. (Siltstone>>claystone>>coal> carbonate>shaly coal. Coal abundant, vitrite>clarite. Shaly coal common, vitrite>clarite. Most of liptinite concentrated in coaly clay. Dom common, V>L>I. Vitrinite and liptinite common, inertinite sparse. Oil droplets rare, green to yellow. Mineral fluorescence pervasive, green to orange. Iron oxides sparse. Pyrite sparse). |
| T1937 12.1 | 11150-160 Ctgs | 0.62 | 0.50-0.77 | 27 | Sparse sporinite and lamalginite, yellow to dull orange, sparse resinite, dull orange. (Siltstone>sandstone>claystone>coal. Coal abundant, vitrite>inertite>clarite. Dom common, V>L>I. Vitrinite and liptinite common, inertinite sparse. Mineral fluorescence pervasive, weak yellow. Iron oxides common. Pyrite common). |

JOB GC589 - AGSO/MESA PLATYPUS-1

| KK/Ref. No. | Depth(ft) Type | $\dot{R}_v$ max | Range | N | Description Including Liptinite (Exinite) Fluorescence |
|---|---|---|---|---|---|
| | | | | | **CEDUNA** |
| T1938 13.1 | 11480-490 Ctgs | 0.55 | 0.45-0.67 | 29 | Sparse sporinite, yellow to orange, sparse liptodetrinite yellow to orange, rare resinite yellow to orange, rare ?lamalginite, yellow. (Siltstone>sandstone> coal and shaly coal. Coal and shaly coal rare to sparse, vitrite>clarite, V>L, I not present in coal and shaly coal. Dom common, I>V=L. Inertinite common, vitrinite and liptinite sparse. Much of the vitrinite is partially pyritized. Mineral fluorescence pervasive, moderate to weak dull orange. Pyrite common.) |
| T1939 14.1 | 11810-820 Ctgs | 0.55 | 0.43-0.65 | 27 | Sparse sporinite, yellow to orange, rare liptodetrinite yellow to orange, rare resinite yellow to orange. (Siltstone> sandstone>coal. Coal sparse, vitrite>inertite, V>I, L not present in coal. Dom common, I>V>L. Inertinite common, vitrinite and liptinite sparse. Mineral fluorescence pervasive, moderate to weak dull orange. Pyrite common.) |
| T1940 15.1 | 12120-150 Ctgs | 0.58 | 0.41-0.71 | 27 | Rare sporinite, orange to brown, rare liptodetrinite, yellow to orange. (Siltstone>claystone>sandstone>coal. Coal common, vitrite>clarite, V>L, I not present in coal. Dom sparse, I>V>L. Inertinite and vitrinite sparse, liptinite rare. Mineral fluorescence pervasive, moderate to weak dull orange. Iron oxides rare. Pyrite sparse.) |
| | | | | | **U. BORDA** |
| T1941 16.1 | 12500-510 Ctgs | 0.67 | 0.53-0.83 | 27 | Sparse sporinite, orange to brown, sparse cutinite orange to dull orange. (Sandstone>siltstone>coal>shaly coal. Coal and shaly coal common, vitrite>clarite>clarodurite, V>L>I. Dom sparse, I>V>L. Inertinite and vitrinite sparse, liptinite rare. Mineral fluorescence patchy, moderate to weak dull orange. Pyrite sparse.) |
| T1942 17.1 | 12750-760 Ctgs | 0.63 | 0.52-0.76 | 26 | Sparse sporinite, orange to brown, sparse liptodetrinite yellow to orange. (Siltstone>sandstone>coal>shaly coal. Coal and shaly coal sparse, vitrite>clarite>clarodurite, V>L>I. Dom sparse, I>V>L. All three maceral groups sparse. Mineral fluorescence patchy, bright orange interstitial material in the sandstone, moderate to weak dull orange in the remainder of the sample. Pyrite common.) |

JOB GC589 - AGSO/MESA

DUNTROON-1,

| KK/Ref. No. | Depth(m) Type | $\bar{R}_v$ max | Range | N | Description Including Liptinite (Exinite) Fluorescence |
|---|---|---|---|---|---|
| | | | | | **BASE WILSON BLUFF** |
| T1943 18.1 | 1595-610 Ctgs | 0.33 | 0.22-0.42 | 6 | Rare lamalginite, yellow to orange. (Carbonate>calcareous siltstone>calcareous claystone. Dom rare, I>L>V. All three maceral groups rare. Reworked vitrinite present with reflectances in the range 0.59% to 0.38%, dom rather than coal fragments. Mineral fluorescence pervasive, moderate orange. Pyrite common.) |
| | | | | | **BASE TERTIARY** |
| T1944 19.1 | 1675-690 Ctgs | 0.47 | 0.44-0.50 | 2 | Liptinite absent. (Sandstone>>>siltstone. Dom rare, V only. Vitrinite rare, confined to one grain of fine grained siltstone. Mineral fluorescence absent from sandstone, moderate orange from the siltstone. Iron oxides common. Pyrite rare.) |
| T1945 20.1 | 1805-820 Ctgs | 0.35 | 0.30-0.41 | 3 | Liptinite absent. (Sandstone>>>siderite. Dom rare, V only. Vitrinite rare, confined to interstitial material in some grains of sandstone. Mineral fluorescence weak to absent from sandstone. Iron oxides sparse. Pyrite abundant.) |
| | | | | | **POTOROO** |
| T1946 21.1 | 1895-910 Ctgs | 0.37 | 0.27-0.48 | 25 | Sparse cutinite yellowish orange to orange, rare lamalginite, yellow, rare sporinite orange. (Siltstone>silty sandstone. Dom common, V>I>L. All three maceral groups sparse. Mineral fluorescence patchy, weak orange. Pyrite common to abundant.) |
| T1947 22.1 | 2050-055 Ctgs | 0.39 | 0.29-0.47 | 25 | Sparse liptodetrinite yellow to orange. (Siltstone. Dom common, V>I>L. All three maceral groups sparse. Mineral fluorescence patchy, weak orange. Pyrite abundant.) |
| | | | | | **WIGUNDA** |
| T1948 23.1 | 2145-160 Ctgs | 0.45 | 0.34-0.54 | 22 | Rare cutinite yellowish orange to orange, rare sporinite orange, rare liptodetrinite yellow to orange. (Sandstone>sideritic carbonate>siltstone. Dom sparse, I>V>L. Inertinite sparse, vitrinite and liptinite rare. Mineral fluorescence patchy, weak orange from siltstone, absent from quartz grains in sandstone, bright orange from siderite. Pyrite common.) |
| T1949 24.1 | 2300-305 Ctgs | 0.49 | 0.42-0.57 | 25 | Rare sporinite and ?lamalginite yellow to orange, rare liptodetrinite yellow to orange. (Siltstone>sideritic carbonate. Dom sparse, I>V>L. Inertinite sparse, vitrinite and liptinite rare. Mineral fluorescence patchy, weak orange from siltstone, medium orange from siderite. Pyrite sparse.) |

JOB GC589 - BHP DUNTROON

DUNTROON-1,

| KK/Ref. No. | Depth(m) Type | $\bar{R}_v$ max | Range | N | Description Including Liptinite (Exinite) Fluorescence |
|---|---|---|---|---|---|
| | | | | | **WIGUNDA** |
| T1950 25.1 | 2495-510 Ctgs | 0.52 | 0.43-0.62 | 26 | Sparse cutinite yellow to orange, sparse sporinite yellow to orange, rare liptodetrinite yellow to orange. (Siltstone>sideritic carbonate. Dom common, V>I=L Vitrinite sparse, inertinite and liptinite sparse. Sparse yellow fluorescing oil trapped in interstitial spaces within some grains of carbonate. Mineral fluorescence patchy, moderate orange from siltstone, medium orange from siderite. Pyrite sparse.) |
| | | | | | **CEDUNA** |
| T1951 26.1 | 2600-605 Ctgs | 0.55 | 0.45-0.75 | 27 | Sparse cutinite, within coal and as dom, yellow to orange, rare sporinite, yellow to orange, rare liptodetrinite yellow to orange, rare ?resinite orange to dull orange. (Siltstone>sideritic carbonate>coal. Coal common, vitrite> clarite, V>L, I absent in coal. Dom sparse, I>V=L. Inertinite sparse, vitrinite sparse, liptinite sparse. Abundant coal cavings, R in cavings 0.18% to 0.30%. The coal found within the sample shows a wide range of reflectance. The lower part of the range (0.45 to 0.57%) does not appear to be cavings. The readings above 0.6% could represent reworked coal but the grains occur isolated and textural features are absent that would help determine if reworking was present. Therefore the higher reflectance coals are included within the reported population for vitrinite. Mineral fluorescence patchy, weak dull orange from siltstone, bright orange from sideritic carbonate. Iron oxides common. Pyrite rare.) |
| T1952 27.1 | 2850-855 Ctgs | 0.58 | 0.49-0.68 | 28 | Sparse sporinite, within coal and as dom, yellow to orange, sparse liptodetrinite, yellow to orange, rare resinite yellow. (Siltstone>sandstone>coal. Coal common, vitrite>clarite>duroclarite, V>L,I. Dom sparse, V>L>I. All three maceral groups sparse. Mineral fluorescence patchy, weak dull orange from siltstone. Iron oxides common. Pyrite rare.) |
| | | | | | **U. BORDA** |
| T1953 28.1 | 2950-55 Ctgs | 0.56 | 0.41-0.76 | 26 | Sparse sporinite, largely within coal grains, yellow to orange, rare liptodetrinite yellow to orange, rare resinite yellow to orange. (Sandstone>siltstone>coal and shaly coal. Coal and shaly coal rare to sparse, vitrite>clarite, V>L, I sparse in coal and and shaly coal. Dom sparse, V>I>L. Vitrinite sparse, inertinite sparse, liptinite rare. Abundant coal cavings, R in cavings 0.31 to 0.36%. Mineral fluorescence patchy, moderate to weak dull orange. Pyrite sparse.) |

JOB GC589 - BHP DUNTROON

DUNTROON-1,

| KK/Ref. No. | Depth(m) Type | $\hat{R}_v$ max | Range | N | Description Including Liptinite (Exinite) Fluorescence |
|---|---|---|---|---|---|
| | | | | | U. BORDA |
| T1954 29.1 | 3050-55 Ctgs | 0.53 | 0.37-0.65 | 25 | Rare sporinite and lamalginite, yellow to orange, rare cutinite dull orange, rare liptodetrinite yellow to orange. (Siltstone> sandstone>"coal". "Coal" common, may represent fragments of logs rather than coal beds. Vitrite only. Dom common, V>I=L. Vitrinite sparse, inertinite and liptinite sparse. Some coal and other lithologies cavings. Possible reworked coal with vitrinite reflectance of 0.73%. Mineral fluorescence pervasive, moderate orange to dull orange. Iron oxides sparse, siderite abundant. Pyrite sparse.) |
| T1955 30.1 | 3350-55 Ctgs | 0.58 | 0.44-0.75 | 25 | Sparse sporinite and lamalginite, yellow to orange, sparse cutinite, yellowish orange to orange. (Siltstone>sandstone. Dom sparse to common, L=V>I. Vitrinite and liptinite sparse, inertinite sparse. Abundant coals with vitrinite reflectances in the range 0.28 to 0.34%, either a mud additive or recirculated cuttings. Mineral fluorescence pervasive, moderate to weak dull orange. Pyrite rare.) |
| T1956 31.1 | 3450-55 Ctgs | 0.66 | 0.52-0.79 | 26 | Common sporinite, yellow to dull orange, common cutinite orange to dull orange, sparse liptodetrinite, yellow to orange. (Siltstone>coal>sandstone. Coal major, vitrite>clarite> clarodurite. Dom sparse, I>L>V. Approx maceral composition of coal: vitrinite 85%, inertinite 5%, liptinite 10%. Dom common, inertinite common and liptinite and vitrinite sparse. Moderate green streaming oil cut from some of the coal, both from vitrite and from inertite. Coal cavings present, R in the range 0.2 to 0.44%. It is possible that some of the coal included in the mean value and having reflectances in the range 0.52 to about 0.64% also represents cavings. However, it could also represent a different coal facies from about the same horizon as the higher reflecting vitrinite. Mineral fluorescence patchy, moderate to weak dull orange. Pyrite common.) |
| T1957 32.1 | 3505-10 Ctgs | 0.71 | 0.60-0.82 | 26 | Common sporinite, orange to dull orange, sparse cutinite dull orange. (Siltstone>coal>sandstone. Coal major, vitrite> clarite>clarodurite>inertite. Approx maceral composition of coal: vitrinite 90%, inertinite 5%, liptinite 5%. Dom common, I>V>L. All three maceral groups sparse. Coal cavings abundant, Rv 0.2% to 0.38%. Mineral fluorescence patchy, moderate to weak orange. Pyrite abundant.) |

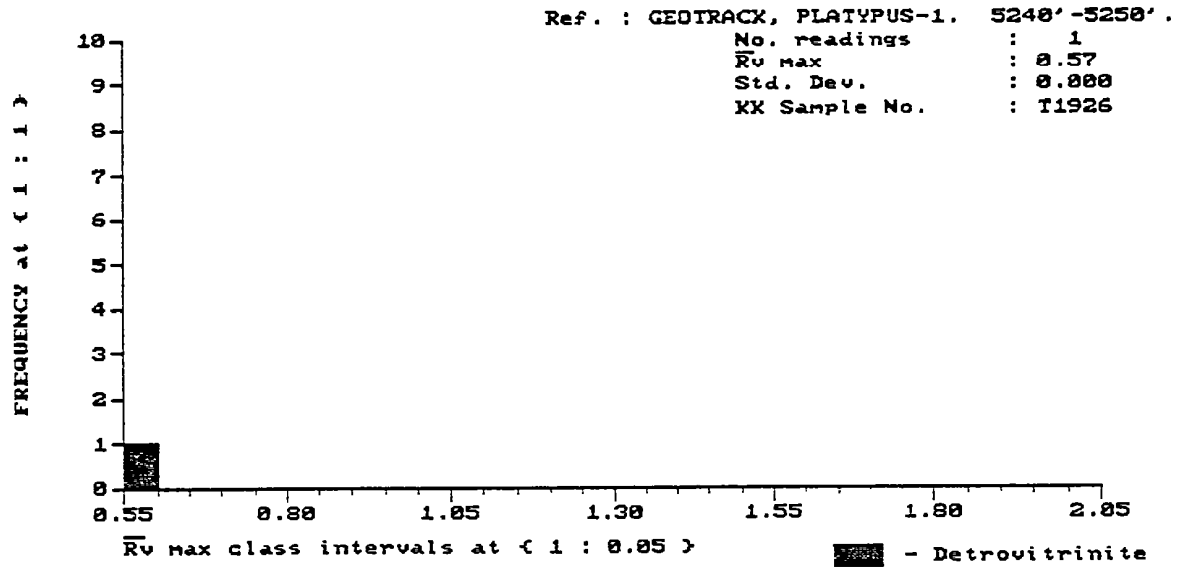


Keiraville Konsultants Pty. Ltd.

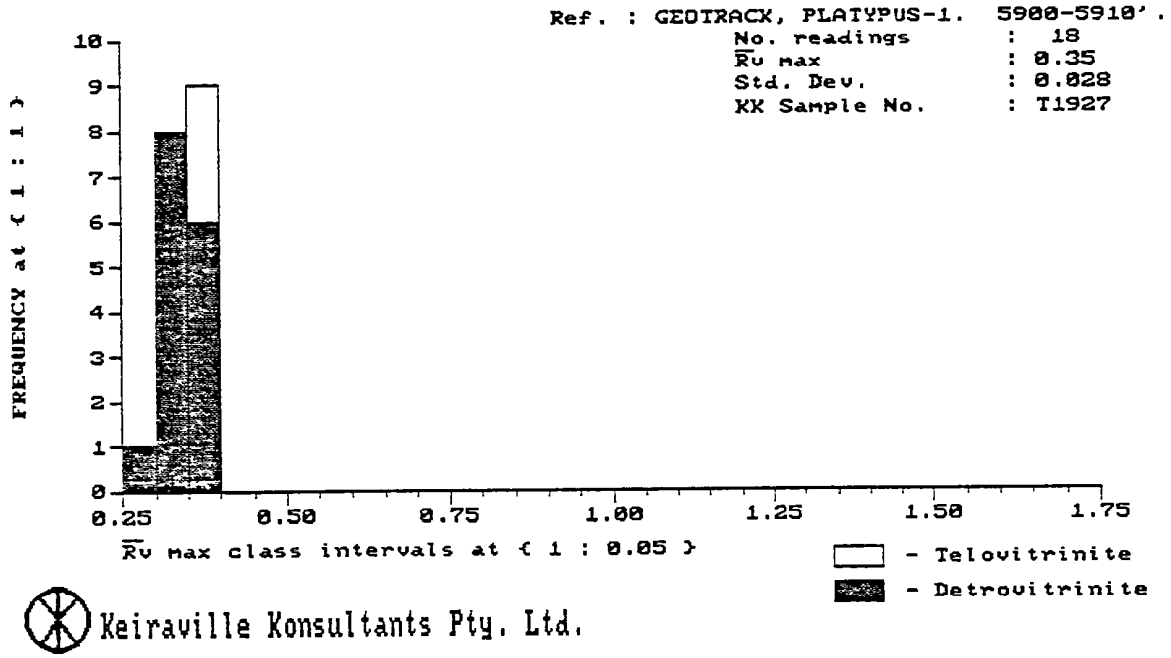


Keiraville Konsultants Pty. Ltd.

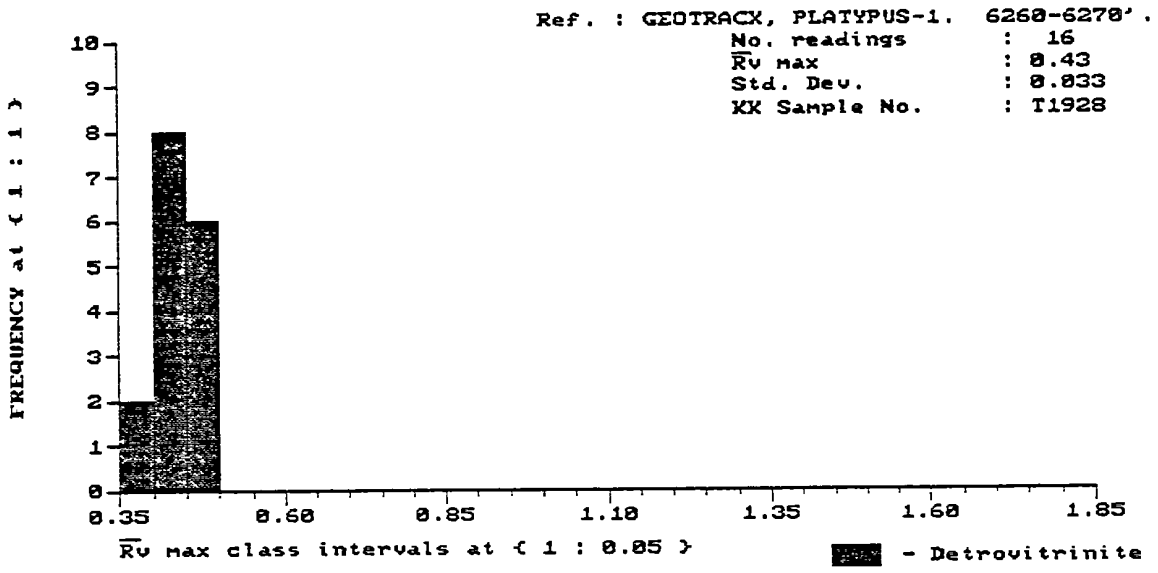


Keiraville Konsultants Pty. Ltd.

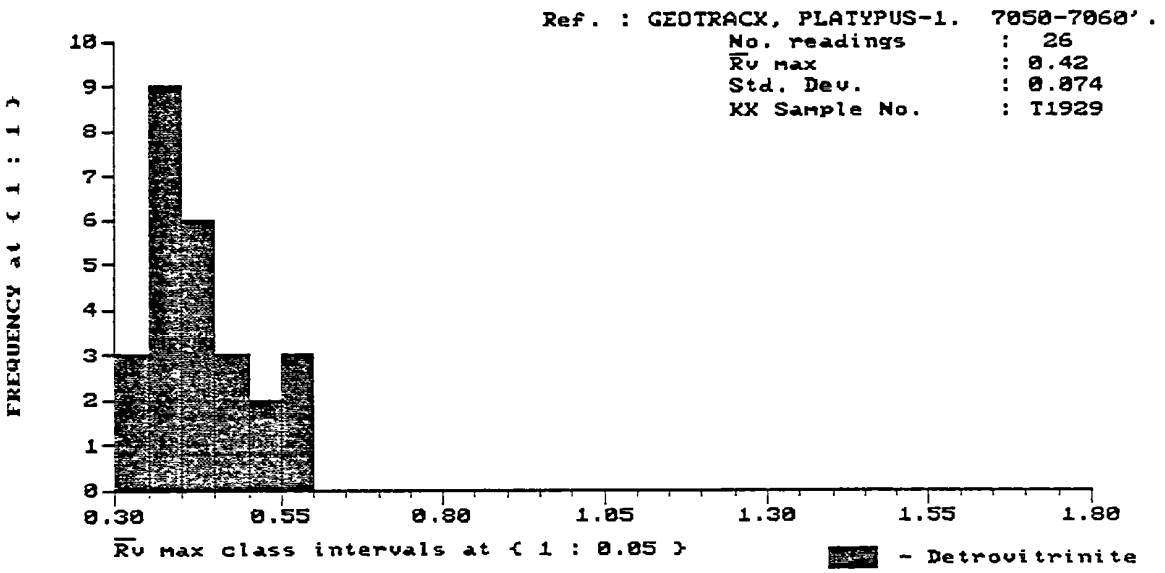


Keiraville Konsultants Pty. Ltd.

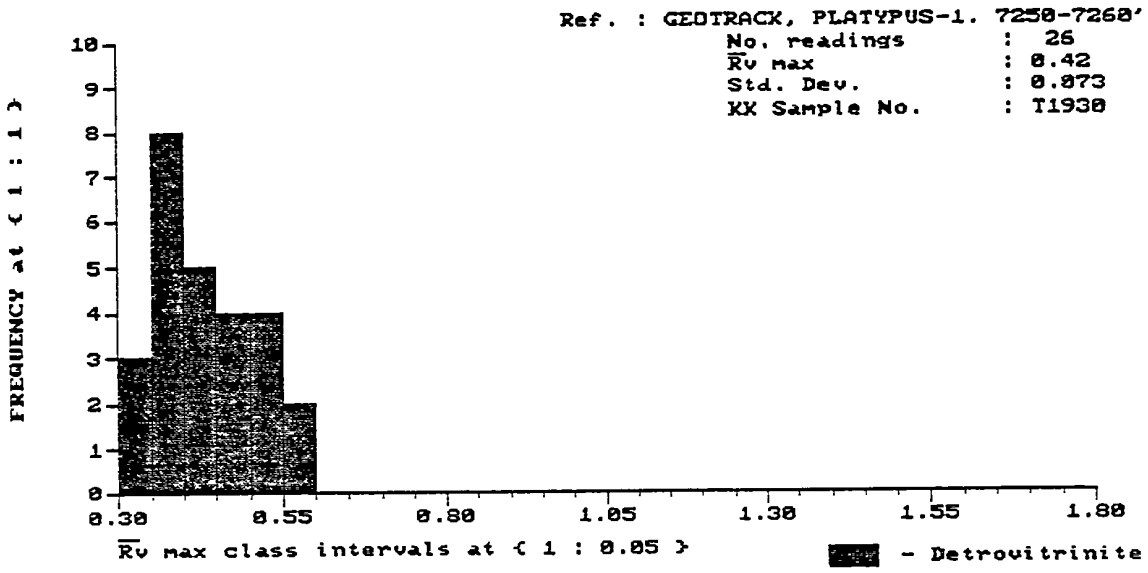


Keiraville Konsultants Pty. Ltd.

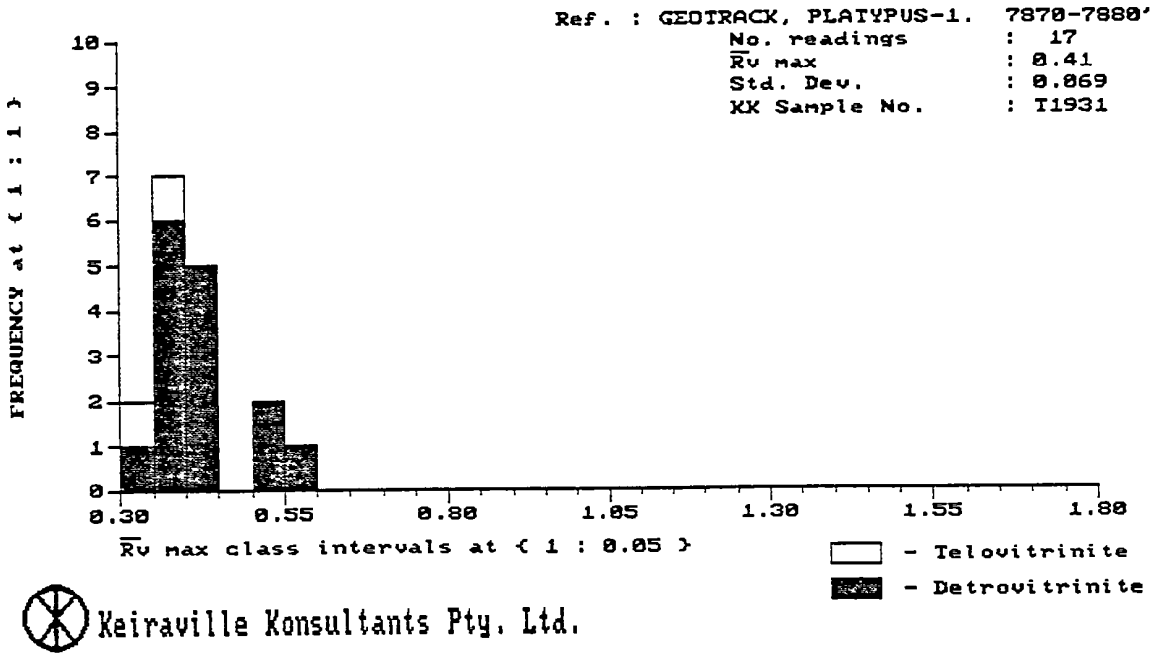


Keiraville Konsultants Pty. Ltd.

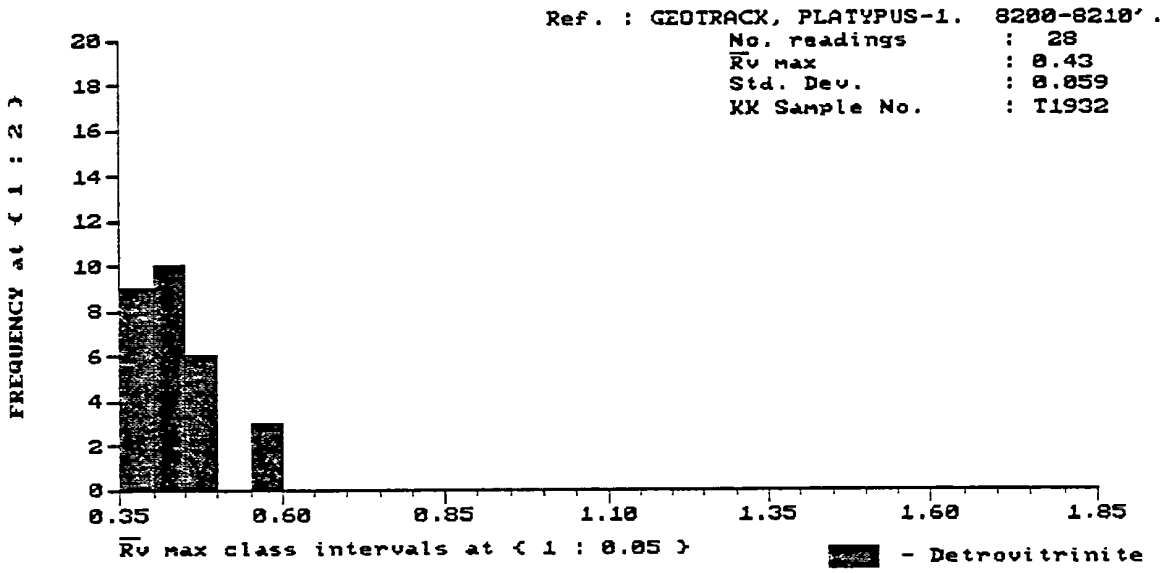


Keiraville Konsultants Pty. Ltd.

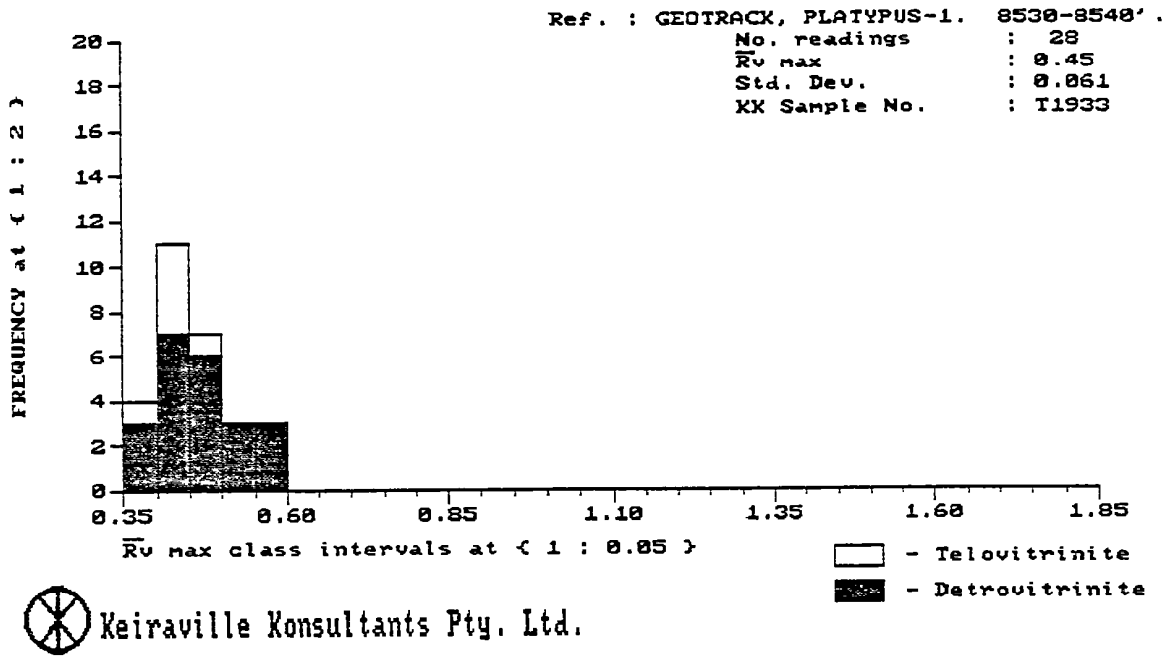


Keiraville Konsultants Pty. Ltd.

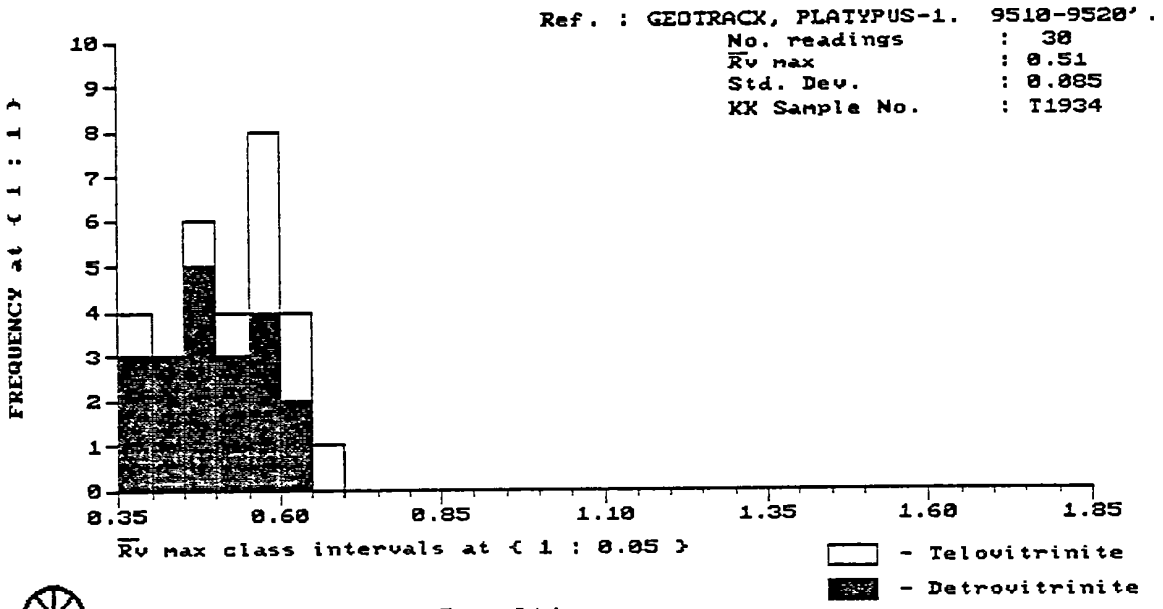


Keiraville Konsultants Pty. Ltd.

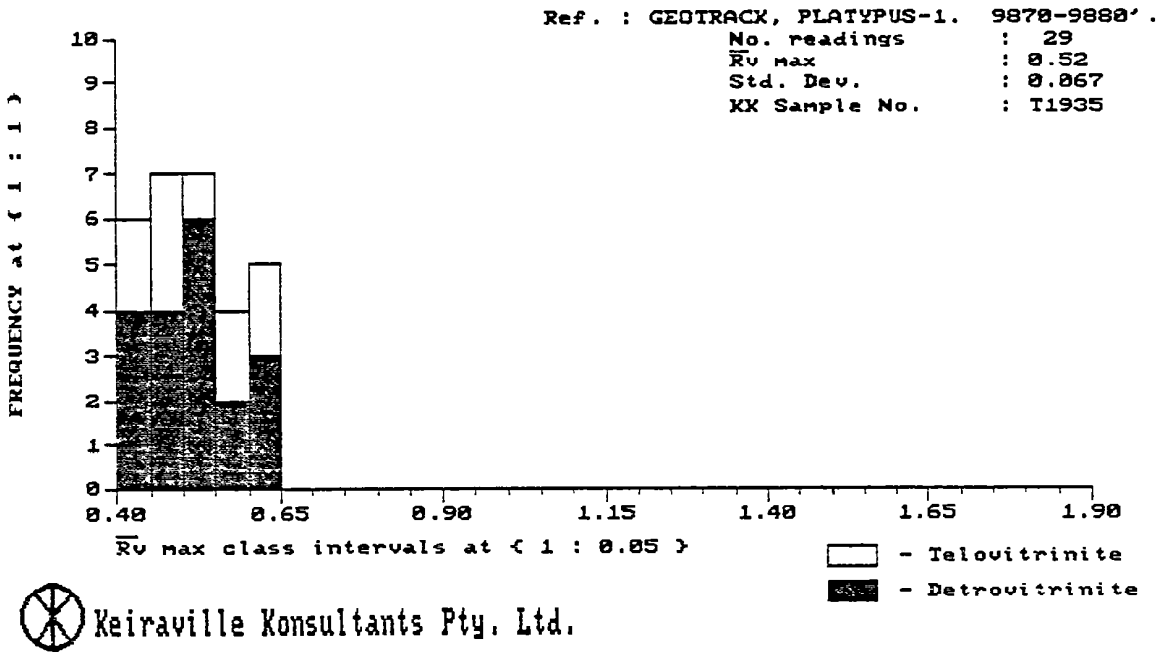


Keiraville Konsultants Pty. Ltd.

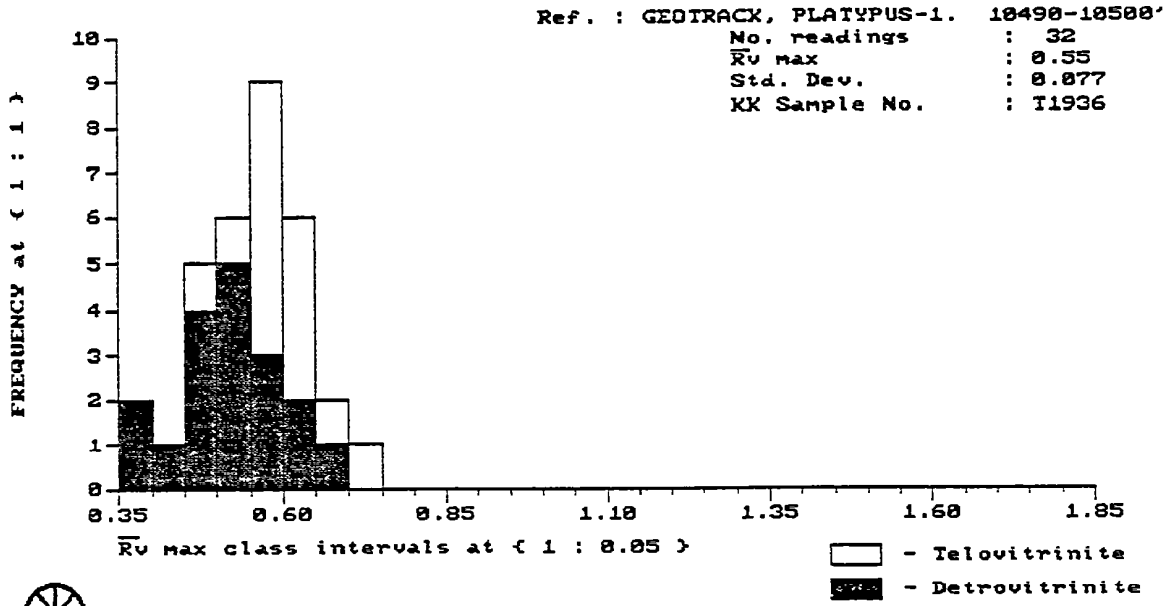


Keiraville Konsultants Pty. Ltd.

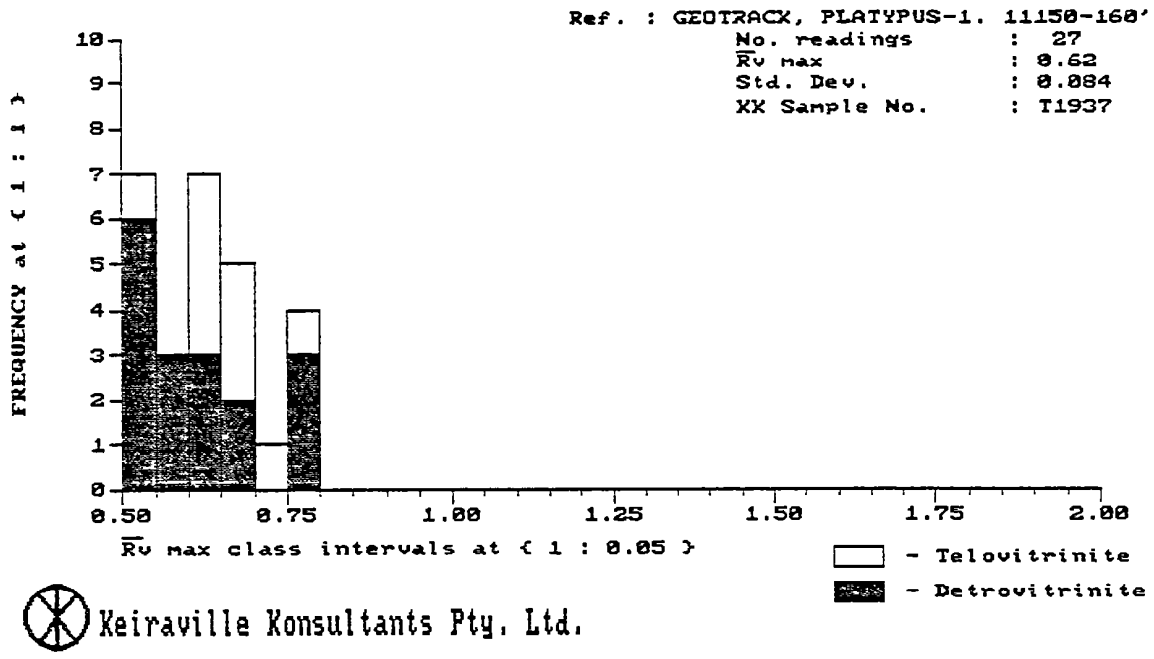


Keiraville Konsultants Pty. Ltd.

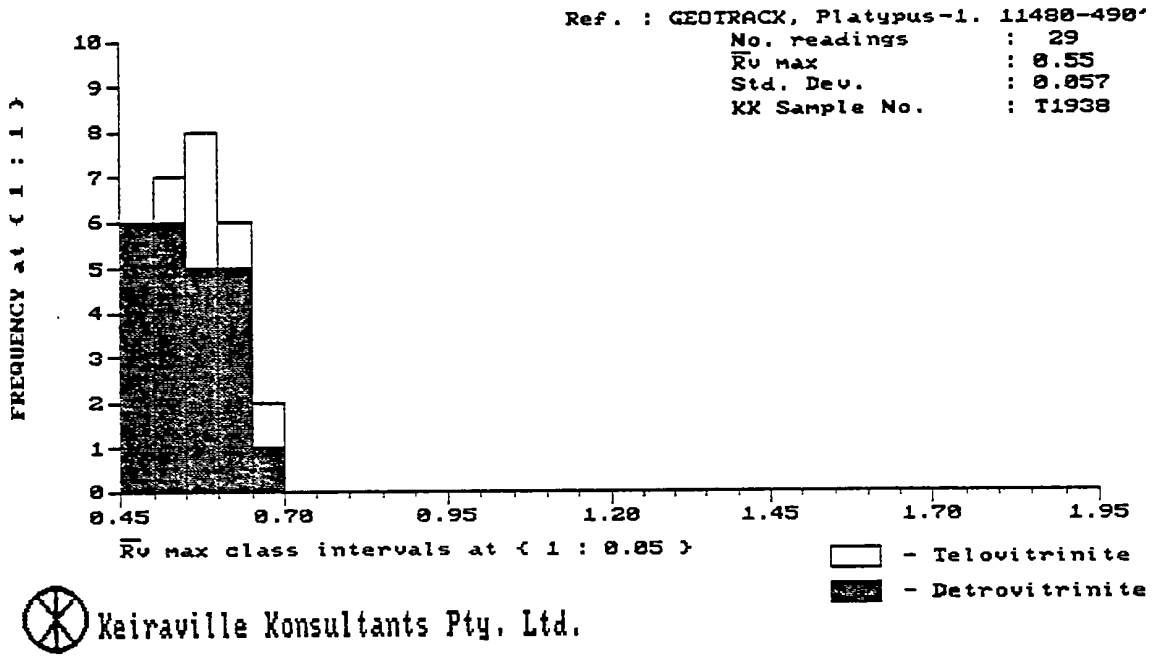


Keiraville Konsultants Pty. Ltd.

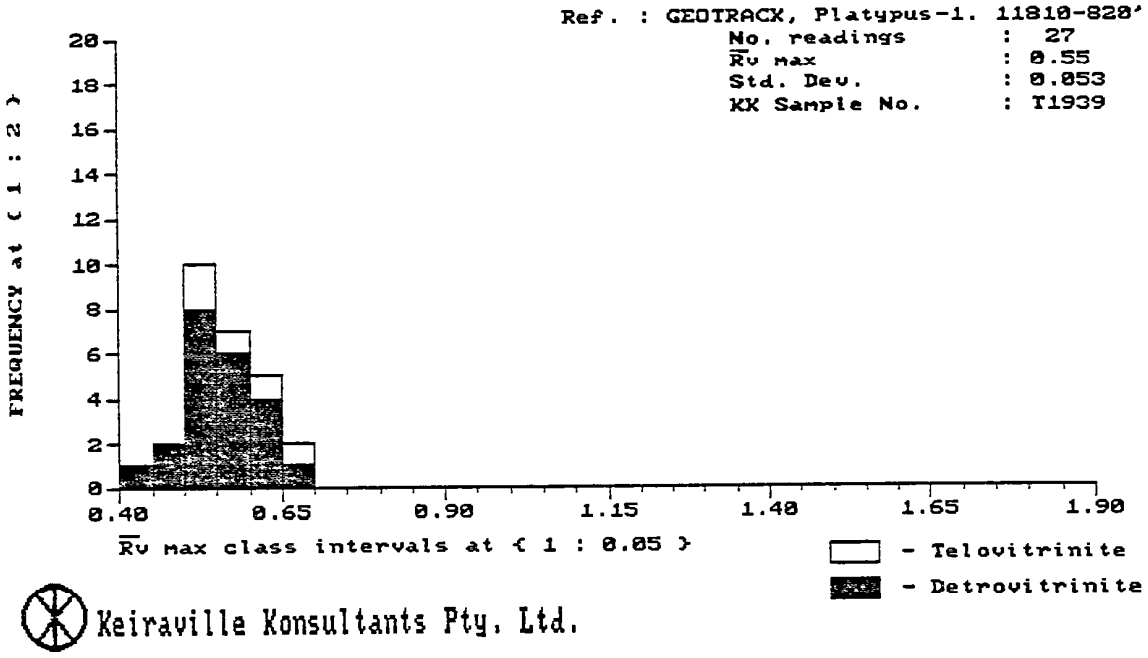


Keiraville Konsultants Pty. Ltd.

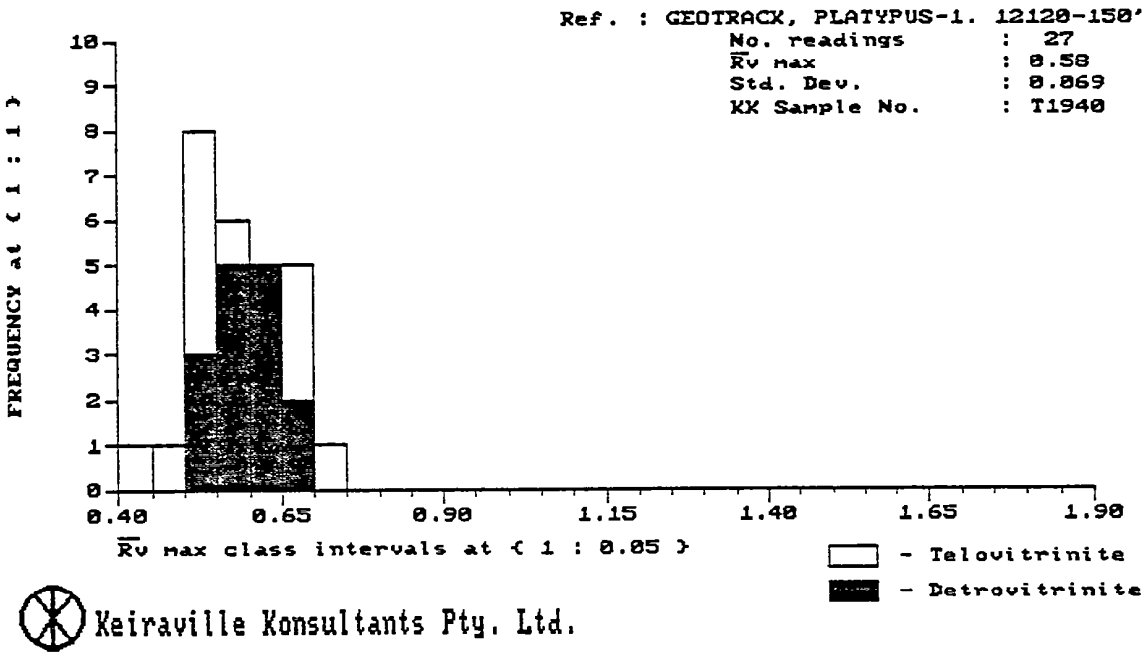


Keiraville Konsultants Pty. Ltd.

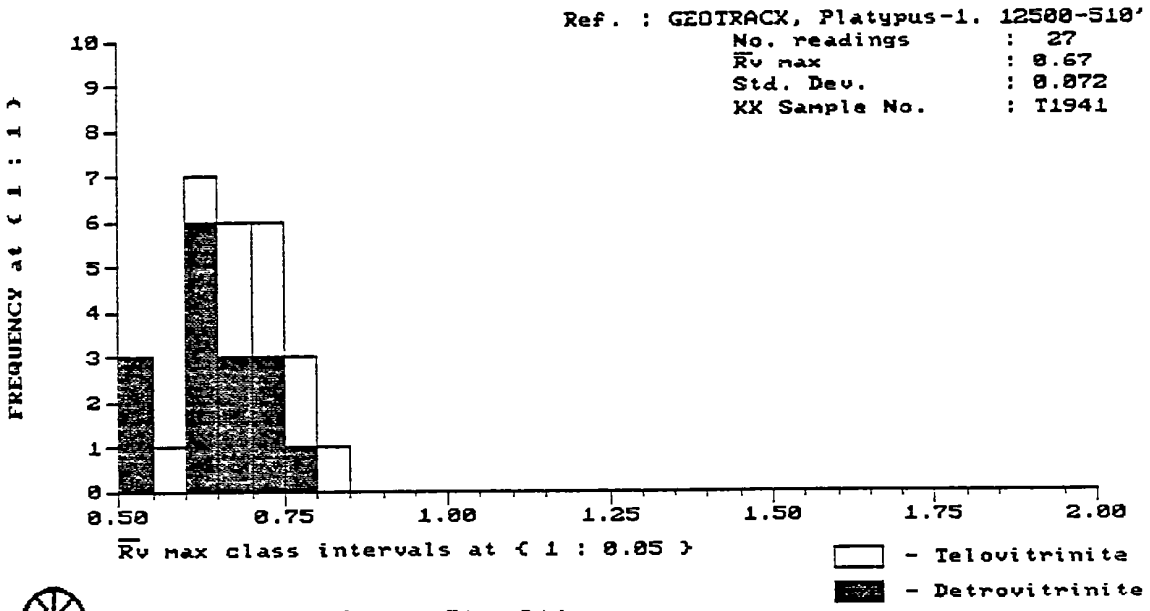


Keiraville Konsultants Pty. Ltd.

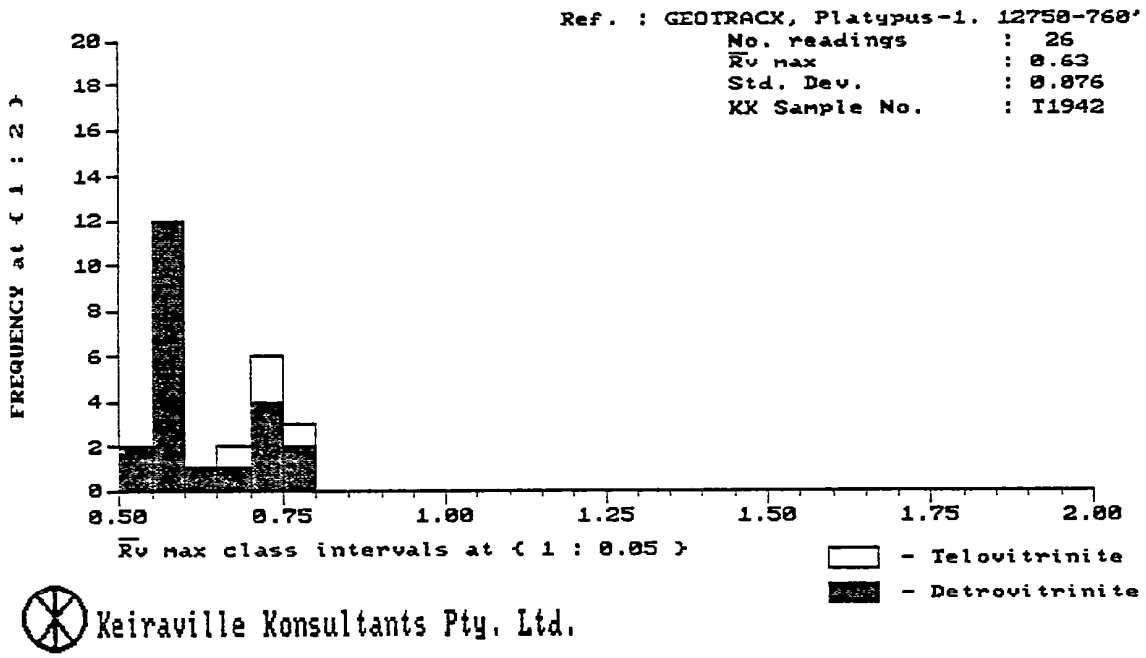


Keiraville Konsultants Pty. Ltd.

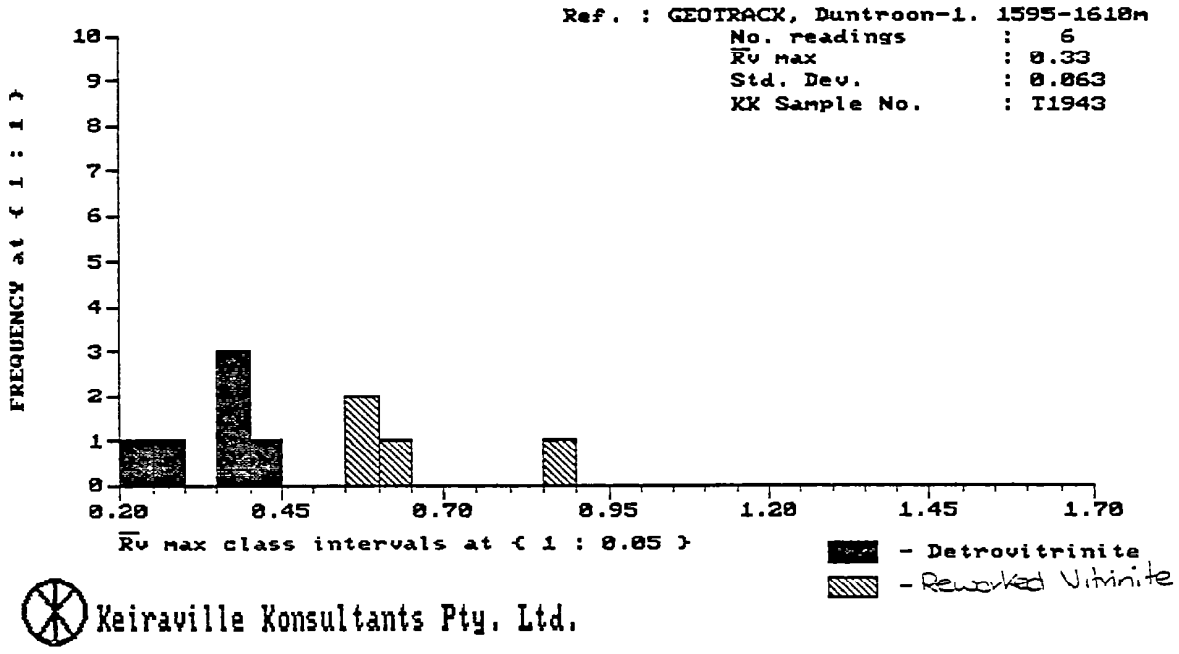


Keiraville Konsultants Pty. Ltd.

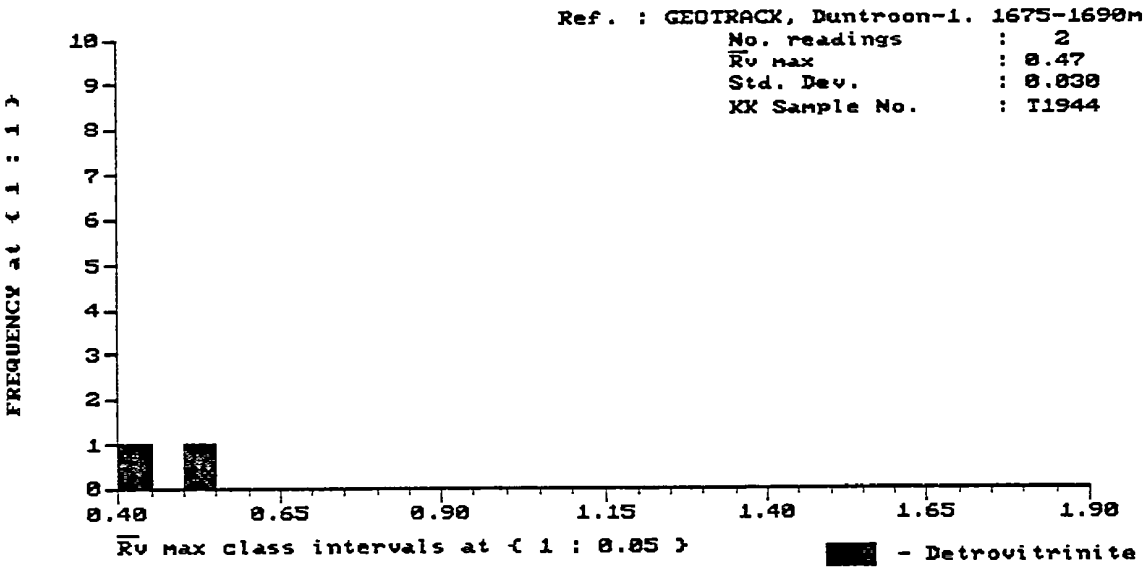


Keiraville Konsultants Pty. Ltd.

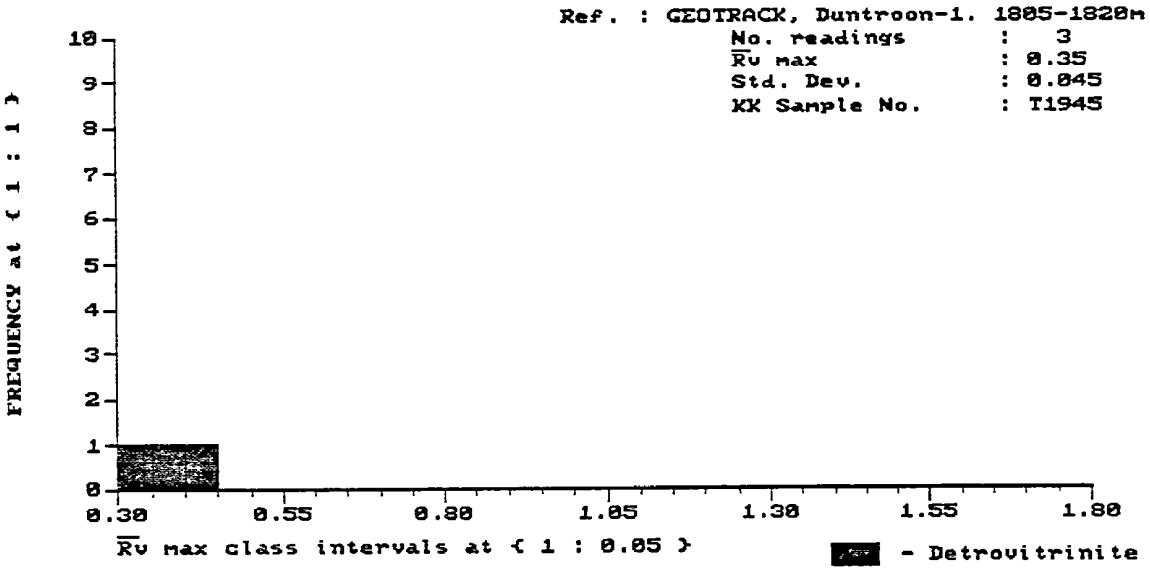


Keiraville Konsultants Pty. Ltd.

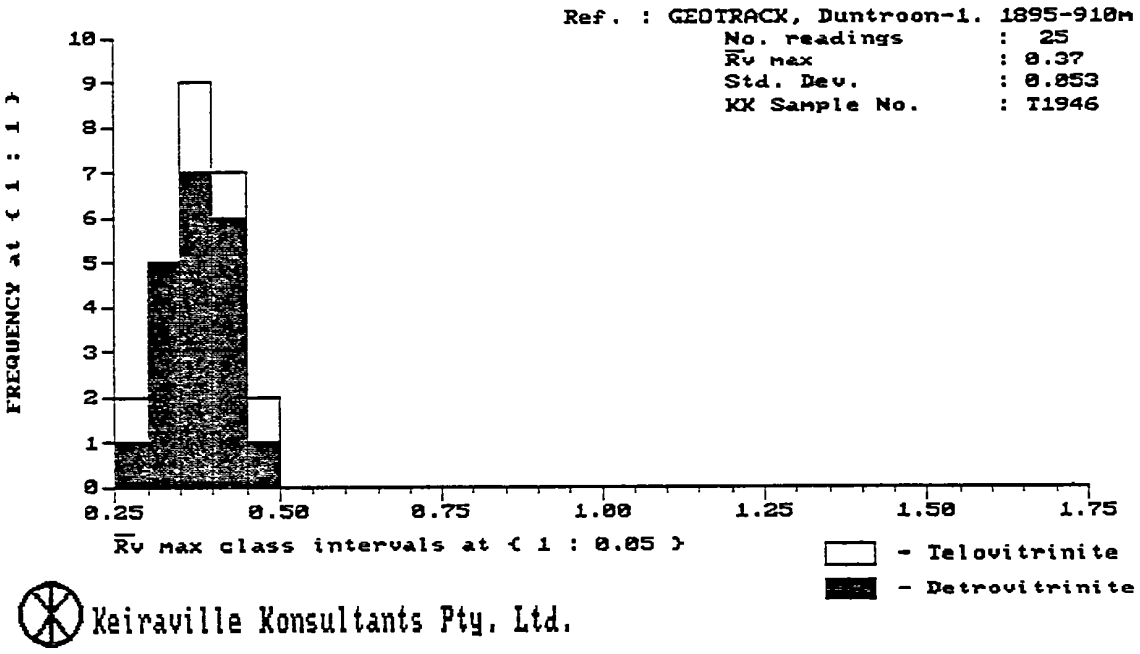


Keiraville Konsultants Pty. Ltd.

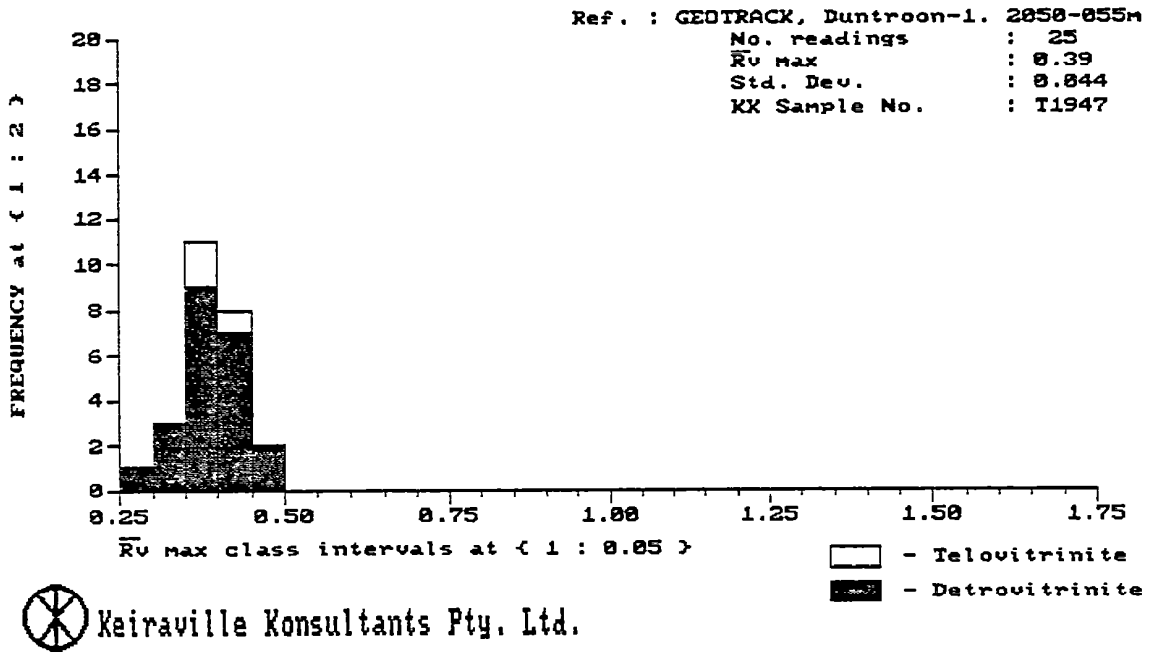


Keiraville Konsultants Pty. Ltd.

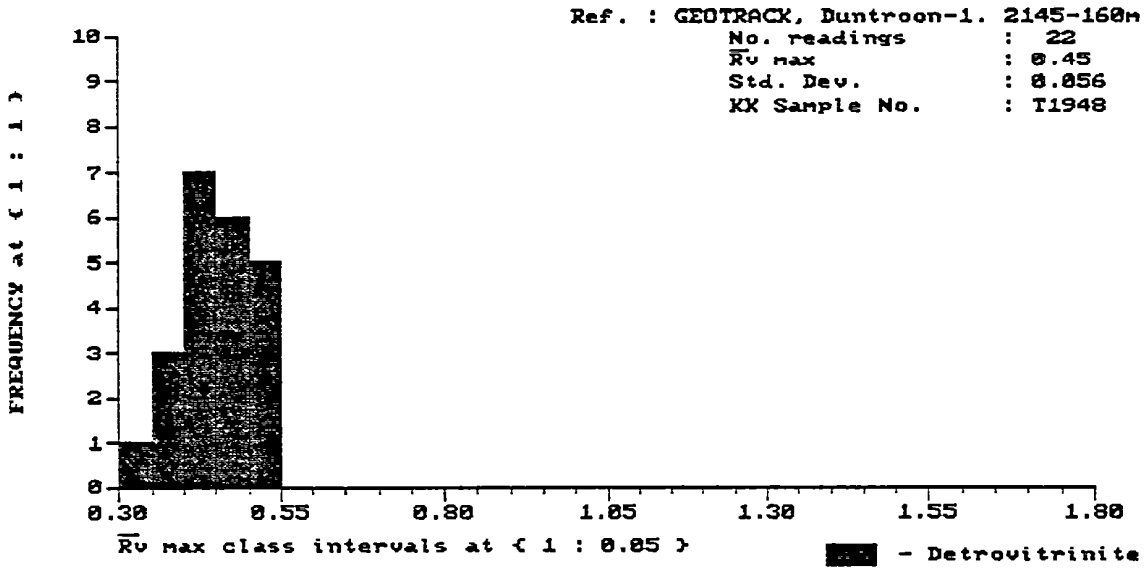


Keiraville Konsultants Pty. Ltd.

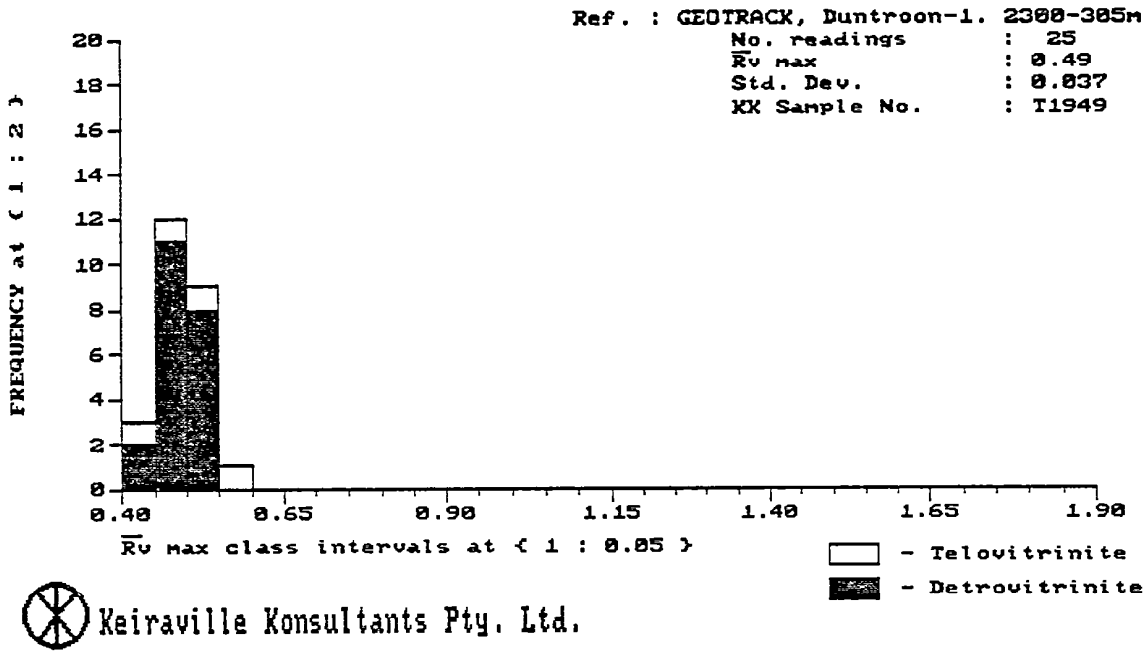


Keiraville Konsultants Pty. Ltd.

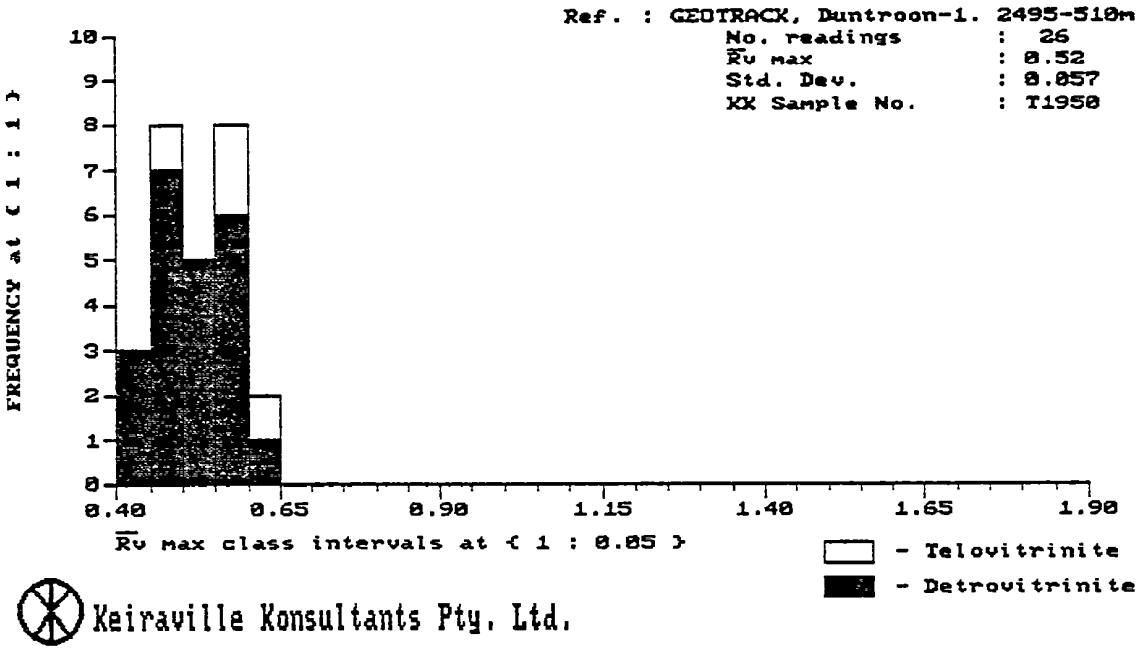


Keiraville Konsultants Pty. Ltd.

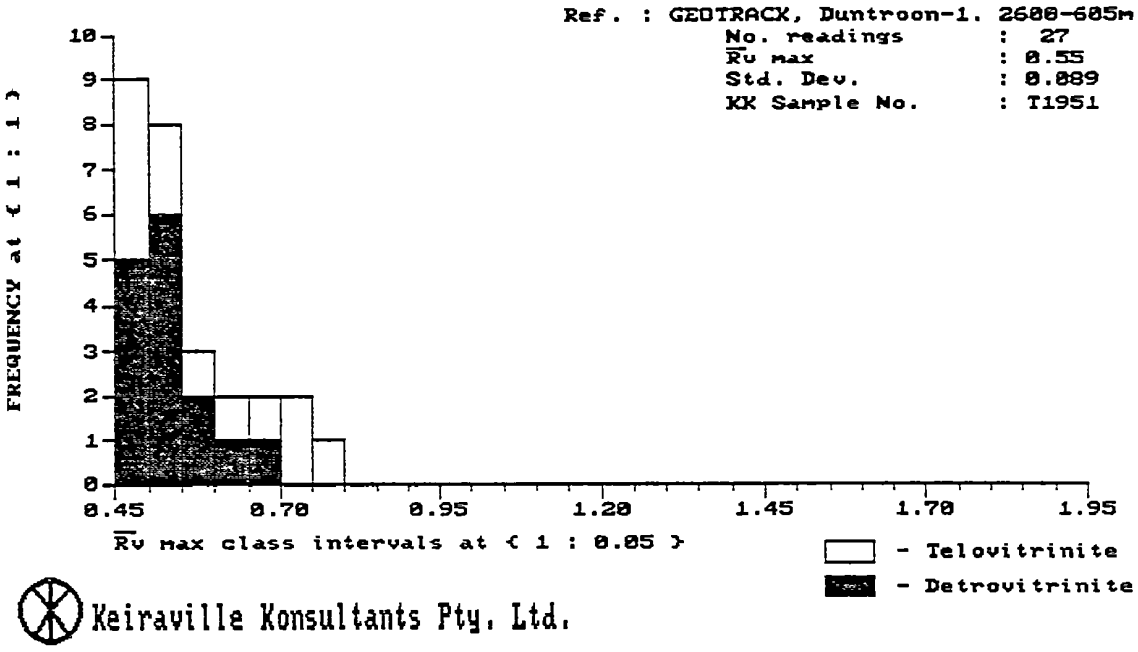


Keiraville Konsultants Pty. Ltd.

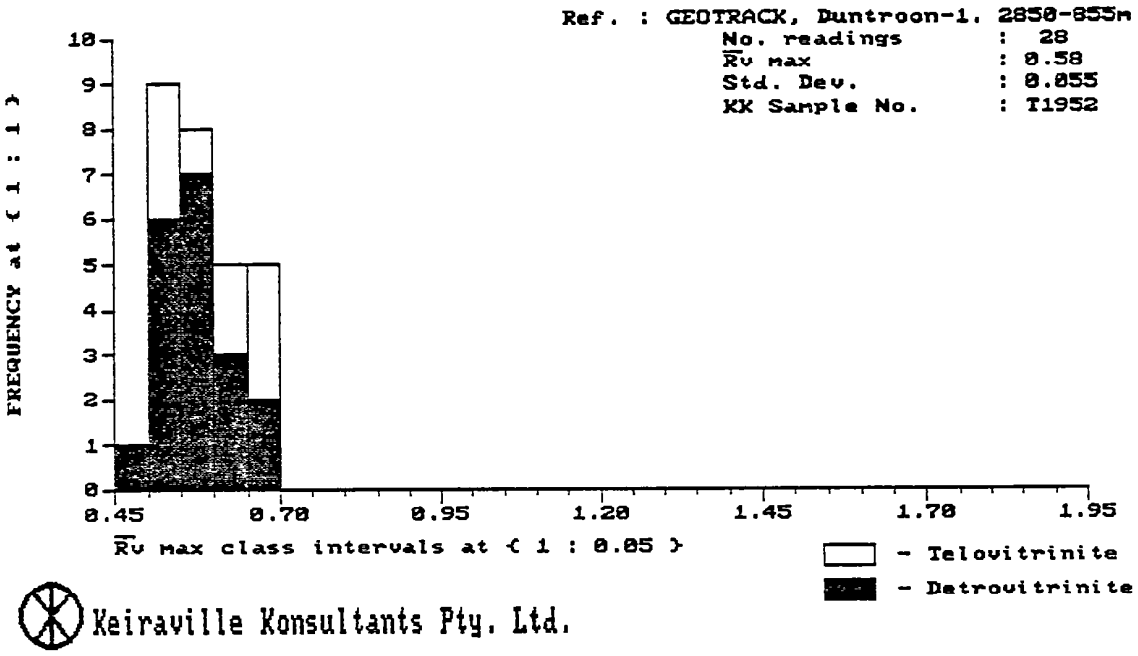


Keiraville Konsultants Pty. Ltd.

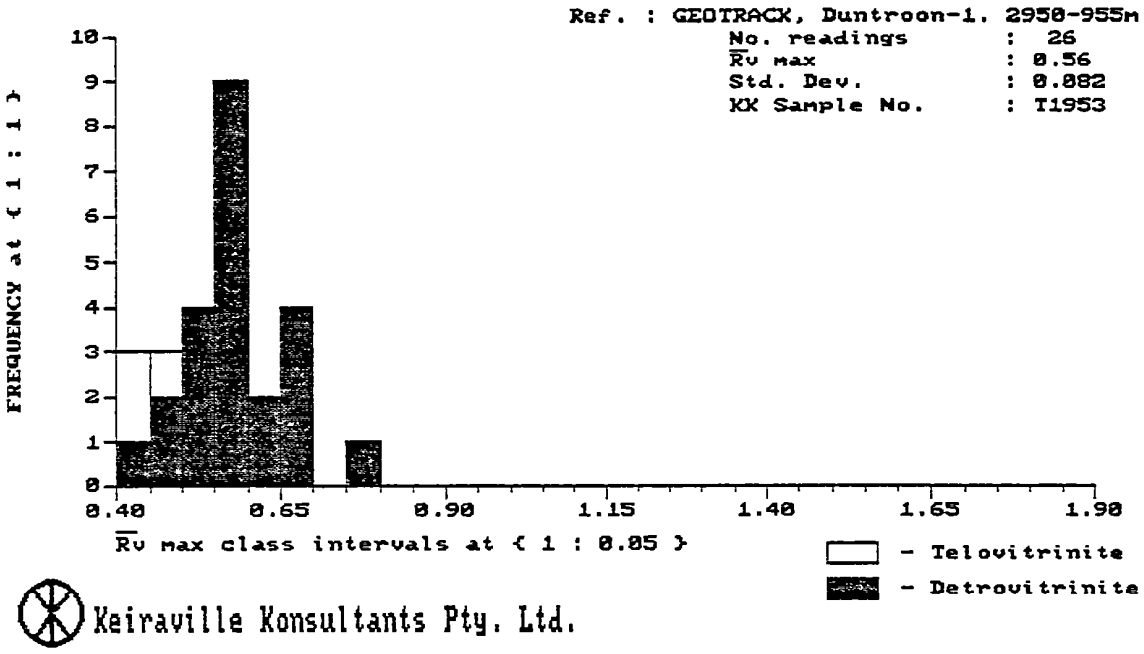


Keiraville Konsultants Pty. Ltd.

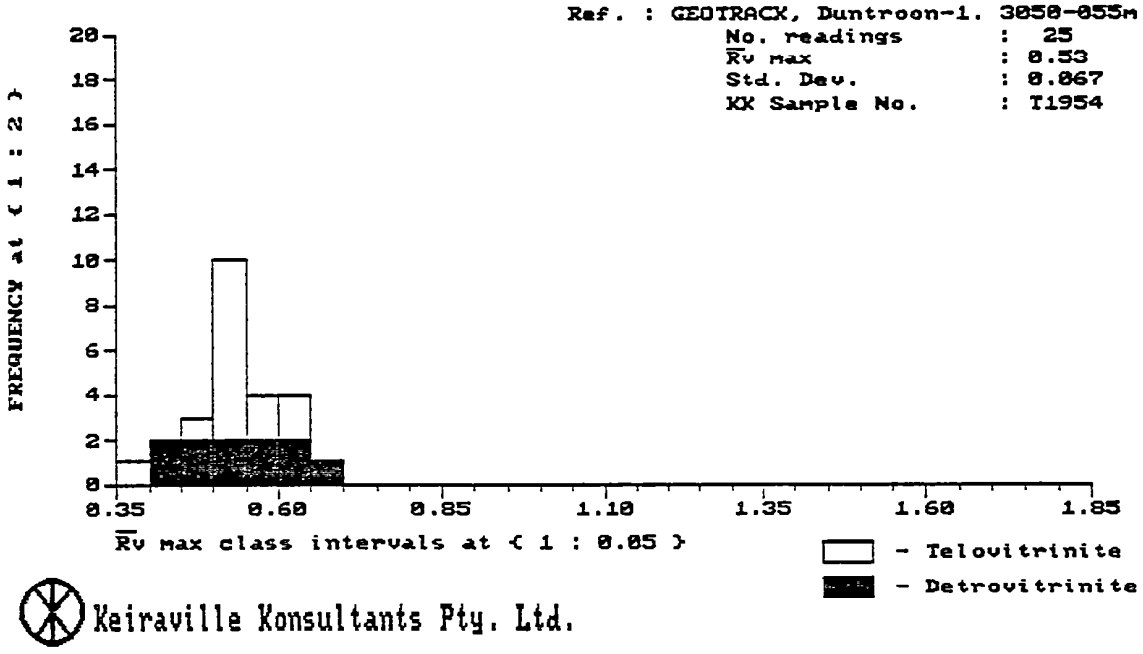


Keiraville Konsultants Pty. Ltd.

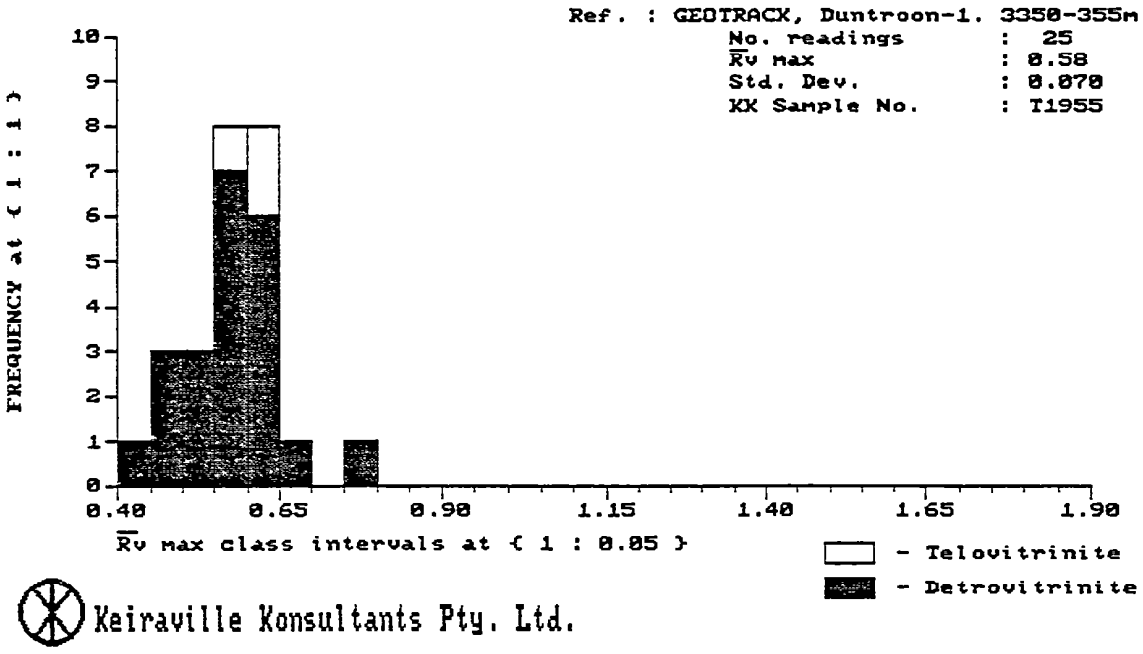
Ref. : GEOTRACK, Duntroon-1. 3350-355m
No. readings : 25
Rv max : 0.58
Std. Dev. : 0.070
KK Sample No. : I1955
FREQUENCY at ( 1 : 1 )
0
1
2
3
4
5
6
7
8
9
10
0.40
0.65
0.90
1.15
1.40
1.65
1.90
Rv max class intervals at ( 1 : 0.05 )
- Telovitrinite
- Detrovitrinite
Keiraville Konsultants Pty. Ltd.

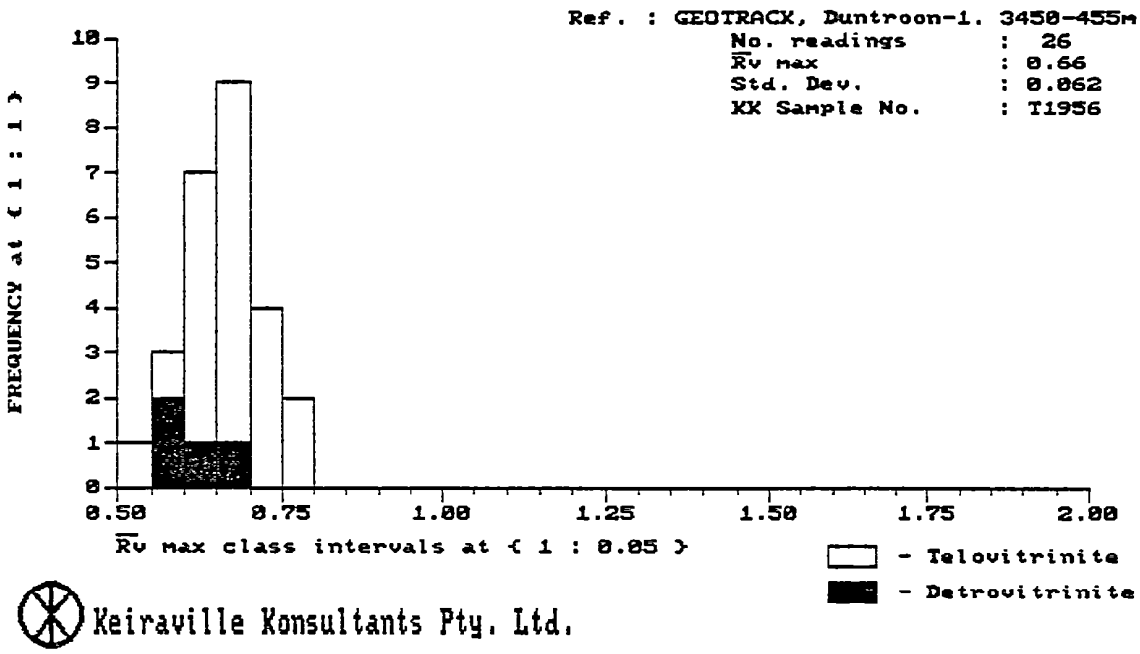


Keiraville Konsultants Pty. Ltd.

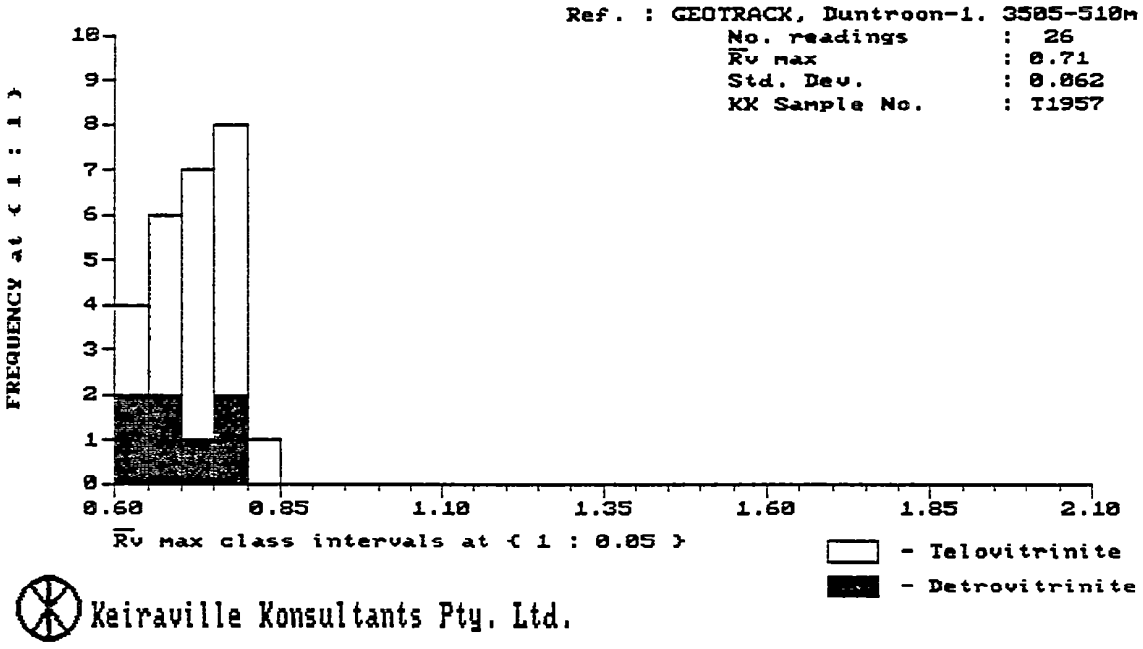


Keiraville Konsultants Pty. Ltd.